UNIVERSIDADE FEDERAL DE MINAS GERAIS

ESCOLA DE ENGENHARIA

PROGRAMA DE PÓS-GRADUAÇÃO EM ENGENHARIA DE ESTRUTURAS

PÉTER LUDVIG

SYNTHESIS AND CHARACTERIZATION OF PORTLAND CEMENT MANUFACTURED WITH CARBON NANOTUBES

DOCTORAL THESIS

SUPERVISOR: Dr. Prof. José Marcio Fonseca Calixto

CO-SUPERVISOR: Dr. Prof. Luiz Orlando Ladeira

BELO HORIZONTE

DECEMBER – 2012

A minha Chérie

AGRADECIMENTOS

À minha esposa Priscila, pelo amor e apoio mesmo nos momentos difíceis, pessoa sem a qual eu nunca teria chegado ao Brasil e nem teria entrado no “mundo da pesquisa”.

Ao meu orientador Prof. Dr. José Marcio Fonseca Calixto, por ter acreditado em mim, pela paciência, apoio e pelo carinho e amizade durante estes quatro anos.

Ao meu co-orientador Prof. Dr. Luiz Orlando Ladeira, pela atenção e motivação, fazendo com que eu me envolvesse no “universo nano”.

À Profa. Dra. Sofia Maria Carrato Diniz, pela participação da banca de defesa de tese e de projeto de tese e pelas críticas construtivas.

Ao Prof. Dr. Marcos Assunção Pimenta, pela constante atenção, pela participação na banca de defesa de tese e de projeto de tese e pelas críticas construtivas.

Ao Prof. Dr. Philippe Jean Paul Gleize, pela participação na banca de defesa de tese e de projeto de tese e pelas críticas construtivas.

Ao Prof. Dr. Valder Nogueira Freire, pela participação na banca de defesa de tese e pelas críticas construtivas.

Ao Prof. Dr. Paulo Roberto Gomes Brandão, pela consultoria sobre os métodos de investigação dos materiais.

À minha colega Júnia Nunes de Paula, pela simpatia e pelas discussões sobre a nanotecnologia do cimento.

À Profa. Dra. Elizabeth Vieira Maia, pelas conversas e pela alegria.

Ao Prof. Dr. Francisco Carlos Rodrigues e ao Prof. Dr. Rodrigo Barreto Caldas, pela disponibilidade e aos técnicos do Laboratório de Análise Experimental de Estruturas da UFMG, pela ajuda na realização dos ensaios.

Aos colegas do Laboratório de Nanomateriais da UFMG, especialmente Daiana, Edelma, Erick, Eudes, Samuel, Sérgio, Viviany, pela boa convivência e pelas contribuições ao meu trabalho.

Aos membros do Centro de Microscopia pelo fornecimento de excelentes imagens para este trabalho.

À equipe do Laboratório de Microanálise da UFMG pela disponibilidade e pela ajuda na análise dos materiais.

Ao Laboratório de Cristalografia da UFMG, especialmente ao Alexandre de Melo Moreira, pela realização das análises envolvendo difração de raios X.

Ao Mateus Justino da Silva do CEFET pela ajuda emergencial.

Aos membros do Laboratório de Química de Nanoestruturas da CDTN, especialmente à Profa. Dra. Adelina Pinheiro Santos, à Profa. Dra. Clascídia Aparecida Furtado, ao Sérgio Carneiro dos Reis, à Carla Onara e à Sirlaine Diniz, pela disponibilidade para realizar as análises de termogravimetria, BET e picnometria.

Aos meus estagiários Ivan, Julia e Tainá, pela ajuda e pela boa vontade.

Aos funcionários da Oficina Mecânica do ICEx, pela ajuda na fabricação e conserto de vários equipamentos.

À Intercement Brasil SA (extensivo aos funcionários), pela disposição, pelo auxílio na realização dos ensaios e pelo apoio financeiro ao projeto.

Ao Centro de Pesquisa e de Desenvolvimento da Magnesita Refratários SA pelo grande apoio na realização da parte experimental.

Ao Eng. Adriano Gamallo da BASF AS pelas consultas e pelo fornecimento de materiais para os experimentos.

Ao Eng. Silvio de Paula Pereira da RheoSet por fornecer materiais para os experimentos

Ao Eng. Célio Monteiro da Sika AS Brasil pelo fornecimento de materiais para os experimentos.

Ao INCT de Nanomateriais de Carbono pelo apoio financeiro para a realização deste trabalho.

À FAPEMIG pelo apoio financeiro durante a realização deste trabalho.

Enfim, a todos que, de alguma forma, contribuíram durante estes quatro anos para o desenvolvimento deste trabalho.

KÖSZÖNETNYÍLVÁNÍTÁS

Köszönettel tartozom Szüleimnek és Öcsémnek amiért akkora távolságból is velem voltak és támogattak egy új élet kezdetén.

Köszönöm volt tanáromnak, Dr. Nédli Péternek a doktori tanulmányok folytatásához nyújtott támogatását.

REMERCIEMENTS

Je tiens à remercier M. Dr. Mohammed Hjiaj de son support pour que je puisse continuer mes études à niveau doctorat.

ACKNOWLEDGEMENTS

I would like to acknowledge the help of Noah Lozada during his stay in Belo Horizonte that was very important for the advance of my work.

RESUMO

O cimento Portland (PC) é um dos produtos mais consumidos no mundo. Seus derivados (concreto, argamassa, pasta) apresentam características satisfatórias quanto à compressão, entretanto o mesmo não ocorre com relação à tração. Os nanotubos de carbono (NTCs) possuem elevada resistência à tração, sendo deste modo candidatos para reforçar estruturalmente materiais cimentícicos. Várias tentativas foram realizadas no mundo para desenvolver processos envolvendo a produção de compósitos a partir da mistura física de cimento e de nanotubos de alta qualidade. Atualmente estes processos são ainda inviáveis para produzir material de construção em grande escala. Os problemas a isto associados estão relacionados à escala e custo de produção, além da dispersão e ligação dos nanotubos na matriz de cimento. Para tentar resolver estes problemas, neste trabalho foi desenvolvido um processo de síntese *in-situ* de nanotubos e nanofibras de carbono em clínquer e sílica ativa. Além disso, resíduos da siderurgia como carepa de laminação de aço e pó de aciaria foram utilizados para melhorara as características dos produtos. Os produtos da síntese foram caracterizados por microscopia eletrônica de varredura, por análise termogravimétrica e por resíduo por queima. Estes produtos apresentaram grande heterogeneidade em morfologia. Foi desenvolvido também um processo de funcionalização *in-situ* dos nanotubos via amônia. Os materiais nano-estruturados foram adicionados aos cimentos CP-III e CP-V em uma concentração de 0,3 % para realização de análises físico-químicas convencionais de cimento. O tempo de pega apresentou um leve aumento no cimento CP-V, mas os demais parâmetros não sofreram alterações significativas pela adição de clínquer nano-estruturado. Argamassas foram preparadas para testar as resistências à compressão e à tração dos compósitos, este último por flexão ou por compressão diametral. Aumentos nas resistências à compressão e à tração foram observados em argamassas preparados com 0,3 % de nanotubos em relação ao peso do cimento, e com aditivos plastificantes a base de policarboxilato e polinaftaleno além de lignosulfonato. Resultados promissores também foram obtidos com o uso de peróxido de hidrogênio como agente de funcionalização. A adição de sílica ativa nano-estruturada também provocou aumento de resistência mecânica dos compósitos. Análises por BET e por picnometria a hélio mostraram aumento da área superficial específica e redução dos diâmetros dos poros dos compósitos.

Palavras chave: *cimento, nanotubos de carbono, nanofibras de carbono, síntese, caracterização, ensaios mecânicos*

ABSTRACT

Portland cement (PC) is one of the most consumed products of the world. Its derivates (concrete, mortar, paste) have good compressive characteristics, but on the other hand have poor tensile behavior. Carbon nanotubes have exceptionally high tensile strength and are therefore candidates for structural reinforcement of cement materials. Many tentative have been reported to develop composites with the physical mixture of high quality nanotubes and cement. These processes today are still unviable for large scale production of construction material. The problems are linked to the scale and costs of production and the dispersion and bond of the nanotubes to the cement matrix. In order to solve these problems in present work an *in-situ* synthesis process was developed to produce nanotubes and nanofibers on clinker and silica fume particles. Steelmaking by-products, such as steel mill scale and converter dust were also added to improve product characteristics. The synthesis products were characterized by scanning electron microscopy, thermogravimetric analysis and loss on ignition. The products showed highly heterogeneous morphology. An *in-situ* functionalization process was also developed based on ammonia. The nano-structured materials were added to Brazilian CP-III and CP-V type cements in 0.3 % concentration to perform common physical and chemical cement analysis. Setting time of CP-V suffered a slight delay, but other characteristics were not altered significantly after the addition of nano-structured clinker. Mortars were prepared in order to determine compressive and flexural or splitting tensile strength of the composites. Gains in the compressive and tensile strengths were observed of mortars incorporating 0.3 % nanotubes prepared with a combined polycarboxylate and polynaphtalene and a lignosulfonate based plasticizer. Positive results were also observed with the use of hydrogen peroxide as functionalizing agent. The addition of nano-structured silica fume also resulted in increase of the mechanical strength of the composites. BET and helium pycnometry analysis of the mortars showed an increase in specific surface area and reduction of mean pore diameter of the composites.

Keywords: *cement, carbon nanotubes, carbon nanofibers, synthesis, characterization, mechanical tests*

TABLE OF CONTENTS

1 Introduction 1

1.1 Initial considerations 1

1.2 Justification 2

1.3 Objective 4

1.4 Scope of this study 4

2 Literature review 6

2.1 Portland cement 6

2.1.1 Production 6

2.1.2 Cement hydration 8

2.1.3 Admixtures for cement paste, mortars and concrete 12

2.2 Carbon nanotubes 14

2.2.1 Synthesis 16

2.2.2 Functionalization 19

2.2.3 Mechanical characteristics 21

2.3 Composites 22

2.3.1 Portland cement composites 22

2.3.2 Portland cement-carbon nanotube composites 25

2.4 Synthesis of literature 34

3 Synthesis and characterization of nano-structured materials 37

3.1 Introduction 37

3.2 Characterization of the materials used for synthesis 38

3.2.1 Electron probe microanalysis 38

3.2.2 Analysis procedures 38

3.2.3 Support materials 39

3.2.4 Catalyst particles 40
3.3 Synthesis procedures 43
3.3.1 Catalyst preparation 43
3.3.2 CVD reactor 43
3.3.3 Synthesis based on clinker 44
3.3.4 Synthesis based on silica fume 45
3.4 Characterization of synthesis products 45
3.4.1 Thermogravimetry 45
3.4.2 Scanning electron microscopy 46
3.4.3 Procedures for characterization of synthesis products 47
3.4.4 Nano-structured clinker 47
3.4.5 Nano-structured silica fume 61
3.4.6 Comparison of the results of nano-structured clinker and silica fume 63
3.5 Characterization of nano-structured cement 64
3.5.1 Procedures 64
3.5.2 Nano-structured Brazilian CP-V type cement 64
3.5.3 Nano-structured Brazilian CP-III type cement 66
3.5.4 Comparative analysis of the results of nano-structured CP-V and CP-III cements 68
4 Characterization of mortar nano-composites 69
4.1 Materials and methods for characterization of mortar nano-composites 69
4.2 Behavior of mortar nano-composites 72
4.2.1 Behavior of mortars made with Portland cement manufactured with carbon nanotubes 72
4.2.2 Behavior of mortars made with Portland cement and nano-structured silica fume 83
4.2.3 Covalent functionalization: hydrogen peroxide as functionalizing agent 86
4.2.4 Comparative analysis of the results of mechanical strength tests 89

4.3 Pore structure and density of CNT/CNF-cement mortar composites 92
5 Conclusions 98
5.1 Synthesis 98
5.2 Characterization of nano-structured mortars 99
5.3 Propositions for future investigations 100
6 References 102
7 Appendix 116
8 Annexes 123
A.1 – Introduction 124
A.2 – Methodology 126
A.3 – X-ray diffractograms 127
C.1 – Gas adsorption porosimetry 137
C.3 – BET results 139
C.3 – Helium pycnometry 189
C.4 – Helium pycnometry results 190

LIST OF FIGURES

Figure 1.1 – Comparison of the gains for the compressive and tensile strength of CNT-cement based composites.....3

Figure 2.1– Evolution of heat liberation during cement hydration. Source: Bentz *et al.*, 1994.....9

Figure 2.2– Nature of bonds between *C-S-H* lamellae. Source: Ramachandran and Feldman, 1996.....11

Figure 2.3– Different CNT chiralities according to the direction of rolling of the graphene sheet with possible chirality vector coordinates. Y axis is the direction of the CNT axis and X axis is the direction in which the graphene sheet is rolled. Source: Dresselhaus *et al.*, 1995.....15

Figure 2.4– Schematic comparison of structure and diameter of carbon nanotubes, nanofibers and fibers. Based on Mori and Suzuki (2010).....16

Figure 2.5– Growth mechanisms of CNTs. Source: Daenen *et al.* (2003).....17

Figure 2.6– Schematic view of a CVD reactor. The gases used in this case are argon and acetylene.....18

Figure 2.7– Rotary CVD furnace for continuous CNT synthesis. Source: Couteau *et al.* (2003).....19

Figure 2.8– Typical Young's modulus values vs. disorder of CNT walls. Source: Salvetat *et al.* (1999).....21

Figure 2.9– Fiber dispersion below the percolation threshold: (a) poor dispersion; (b) good dispersion. Source: Chung (2005).....24

Figure 2.10 – SEM images of CNTs bridging cracks in a cement matrix. Source: Makar *et al.* (2005).....26

Figure 2.11 – SEM image of cement grain covered by CNTs and CNFs. Source: Cwirzen *et al.* (2009).....33

Figure 3.1– The CVD reactor used during the investigations.....44

Figure 3.2– SEM image of curly CNTs and CNFs grown on pure clinker.....50

Figure 3.3– SEM image of curly CNTs and CNFs with high dispersion of size grown on CO-5 catalyst.....51

Figure 3.4 – SEM image of straight CNTs and CNFs grown on CS-5 catalyst 51
Figure 3.5 – SEM image of straight CNTs and CNFs grown on CD-5 catalyst.....52
Figure 3.6– TGA and DTG curves of synthesis products grown on clinker-steel mill scale catalyst (CS-5) 53
Figure 3.7 – SEM image of CNTs/CNFs grown on CD-1 catalyst 54
Figure 3.8– SEM image of well distributed CNTs and CNFs on clinker particles (CD-2.5 catalyst).....55
Figure 3.9 – SEM image of CNTs/CNFs synthesized on CD-5 catalsyt.....55
Figure 3.10– SEM image of synthesis products grown on high Fe-content clinker based catalyst (CD-10) 56
Figure 3.11 – Histogram of the diameters of CNTs/CNFs grown on clinker with 2.5 % iron addition (converter dust) measured on SEM images 56
Figure 3.12– TGA and DTG curves of synthesis products grown on clinker-converter dust catalyst (CD-2.5).....57
Figure 3.13 – SEM image of CNTs/CNFs synthesized on clinker and functionalized with ammonia 59
Figure 3.14 – SEM image of CNTs/CNFs synthesized on clinker and functionalized with ammonia 59
Figure 3.15 – Histogram of the diameters of CNTs/CNFs grown on clinker with ammonia treatment 60
Figure 3.16 – TGA results of nano-structured clinker treated with ammonia.....60
Figure 3.17 – TGA (in black) and DTGA (in blue) curves of CNTs/CNFs synthesized on silica fume based catalyst with 2.5 % iron addition 61
Figure 3.18 – SEM image of CNTs grown on silica fume under high magnification..62
Figure 3.19 – SEM image of CNTs grown on silica fume 62
Figure 3.20 – Histogram of the diameters of CNTs/CNFs grown on silica fume measured on SEM images 63
Figure 4.1– Experimental setup for three-point bending test 70
Figure 4.2 – Experimental setup for splitting tensile strength tests.....71
Figure 4.3 – Results of flexural tensile strength tests at ages of 7 and 28 days of mortar specimens prepared with different CNT/binder ratios 74
Figure 4.4– Flexural tensile strength of mortar specimens prepared with different admixtures at 7 and 28 days. 77

Figure 4.5– Compressive strength of test specimens prepared with different admixtures at 28 days. 78

Figure 4.6– Compressive strength of mortars prepared with different mixing process at the ages of 7 and 28 days 80

Figure 4.7– Splitting tensile strength of mortars prepared with 0, 0.1 and 0.3 % of ammonia functionalized CNTs/CNFs 82

Figure 4.8– Compressive strength of mortars prepared with 0, 0.1 and 0.3 % of ammonia functionalized CNTs/CNFs 83

Figure 4.9– Flexural strength of test specimens for investigation of the behavior of mortars incorporating nano-structured silica fume 85

Figure 4.10– Compressive strength of test specimens for comparison of the behavior of mortars incorporating nano-structured silica fume. 86

Figure 4.11– Flexural tensile strength of test specimens for evaluation of the addition of nano-structured clinker treated by hydrogen peroxide 88

Figure 4.12– Compressive strength of test specimens for evaluation of the addition of nano-structured clinker treated by hydrogen peroxide 89

Figure 7.1– Transmission electron micrograph of nanotubes grown on *MgO-FeO* catalyst a) without ammonia, b) with ammonia. Arrows indicate the bamboo-like structure. 119

Figure 7.2– Histograms of the diameters of CNTs grown on *MgO-FeO* catalyst measured on SEM images. a) without ammonia; b) with ammonia 119

Figure 7.3 – Raman spectra of purified CNTs grown on *MgO-FeO* catalyst without ammonia. Intensity is represented with arbitrary units 120

Figure 7.4 – Raman spectra of purified CNTs grown on *MgO-FeO* catalyst with ammonia. Intensity is represented with arbitrary units 120

Figure 7.5– TGA and DTG curves of purified CNTs grown on *MgO-FeO* catalyst without ammonia. Black color represents TGA and red color represents DTG curves 121

Figure 7.6 – TGA and DTG curves of purified CNTs grown on *MgO-FeO* catalyst with ammonia. Black color represents TGA and red color represents DTG curves 121

Figure 8.1– Classification of isotherms (I-VI) according to pore size and distribution, with the monolayer saturation point (B). II and IV follow BET model. Vertical axis represents gas volume and horizontal axis P/P_0 ratio. Source: Sing *et al.*(1985) 137

LIST OF TABLES

Table 2.1 –Comparison of the results of some works for cementitious composites made by covalently functionalized CNTs 29

Table 2.2– Comparison of the results of some works for cementitious composites made by surfactant assisted CNT dispersions 30

Table 3.1 – Chemical composition of Portland cement clinker determined by electron microprobe analysis. The compound annotations refer to any type of oxides of that type of element. 39

Table 3.2– Chemical composition of silica fume as given by the provider..... 40

Table 3.3 – Chemical composition of iron ore determined by electron microprobe analysis. The compound annotations refer to any type of oxides of that type of element. 41

Table 3.4 – Chemical composition of steel mill scale determined by electron microprobe analysis. The compound annotations refer to any type of oxides of that type of element. 41

Table 3.5 – Chemical composition of converter dust based on an EDS study (mass %) 42

Table 3.6– Iron content of the catalyst particles 42

Table 3.7– Fe crystallite size of catalyst particles as determined by X-ray diffraction 43

Table 3.8– Composition of the clinker based catalysts for nano-structured material synthesis 45

Table 3.9– Composition of the silica fume based catalysts for nano-structured material synthesis 45

Table 3.10 – Effect of synthesis time changes on the efficiency of the CNT/CNF synthesis on pure clinker 48

Table 3.11 – Effect of carbon source gas flow rate on the efficiency of CNT/CNF synthesis on pure clinker 48

Table 3.12 – Effect of temperature on the efficiency of CNT/CNF synthesis on pure clinker 49

Table 3.13 – Effect of the addition of different iron oxide sources to clinker on the efficiency of CNT/CNF synthesis 49

Table 3.14– Effect of the quantity of iron (converter dust) added to clinker on the efficiency of CNT/CNF synthesis 53
Table 3.15– Efficiency of synthesis on silica fume based catalyst 61
Table 3.16– Chemical composition of pure CP-V cement and its blend with 0.3 % of CNTs/CNFs as a result of an X-ray spectroscopy analysis 65
Table 3.17 – Setting times of cement pastes prepared with Brazilian CP-V type cement 66
Table 3.18– Chemical composition of pure CP-III cement and its' blend with 0.3 % of CNTs/CNFs as a result of an X-ray spectroscopy analysis 67
Table 3.19 – Setting times of cement pastes prepared with Brazilian CP-III type cement 67
Table 4.1– Mortar compositions for optimal nanotube/cement ratio determination tests 73
Table 4.2– Detailing of the mix proportions for chemical admixture comparison tests 75
Table 4.3 – Detailing of the mixing proportions for investigation of the effect of mixing order 79
Table 4.4 – Detailing of the mixing proportions of mortars prepared with ammonia treated nano-structured clinker 81
Table 4.5 –Mix details of mortars prepared with PVP and lignosulfonate dispersing agents and nano-structured silica fume 84
Table 4.6 – Details of mortars prepared with H_2O_2 treated nano-structured clinker 87
Table 4.7 – Comparison of the gains obtained in flexural tensile and compressive strength of mortars prepared with nano-structured materials with different supports without covalent functionalization 90
Table 4.8 – Comparison of the gains obtained in flexural tensile and compressive strength of mortars prepared with nano-structured clinker with different functionalization methods 91
Table 4.9 – Comparison of percentage gains in compressive and tensile strength of CNT-cement mortars prepared with surfactants obtained during present and previous investigations 91
Table 4.10 – Comparison of percentage gains in compressive and tensile strength of CNT-cement mortars prepared with covalently functionalized nanotubes obtained during present and previous investigations 92

Table 4.11 – Details of specimens analyzed by gas adsorption porosimetry and *He* pycnometry 93

Table 4.12 – Results of the pore structure analysis of mortars incorporating CNTs/CNFs synthesized on clinker and silica fume with different surface treatments and in different amounts 94

Table 4.13 – Comparison of the pore structure analysis results of mortars made with Brazilian CP-III and CP-V type cements and with nano-structured clinker or silica fume 95

Table 4.14 – Comparison of the pore structure analysis results of mortars made with Brazilian CP-III type cement and with ammonia or H_2O_2 treated nano-structured clinker 96

Table 8.1 – Details of specimens analyzed by gas adsorption porosimetry and *He* pycnometry 138

LIST OF ABBREVIATIONS

Å	Ångström
AFm	Alumino-ferrite monosulfate
AFt	Alumino-ferrite trisulfate, ettringite
Al	Aluminium
Ar	Argon
C	Calcium oxide (cement chemist notation)
C-S-H	Calcium silicate hydrate (cement chemist notation)
C_2S	Dicalcium silicate (belite, cement chemist notation)
C_3A	Tricalcium aluminate (cement chemist notation)
C_3S	Tricalcium silicate (alite, cement chemist notation)
C_4AF	Tetracalcium aluminoferrite (cement chemist notation)
Ca	Calcium
CaO	Calcium oxide
CHH	Cement hedgehog composite
Co	Cobalt
CO_2	Carbon dioxide
CNF	Carbon nanofiber
CNT	Carbon nanotube
CVD	Chemical vapor deposition
DTG	Derivative thermogravimetric analysis
EAFD	Electric arc furnace dust
EDS	Energy dispersive spectroscopy

Fe	Iron
Fe_2O_3	Hematite
FeO	Wüstite
FRC	Fiber reinforced concrete
FTIR	Fourier transform infrared (spectroscopy)
GPa	Gigapascal
H	Water (cement chemist notation)
HCl	Hydrochloric acid
He	Helium
H_2O_2	Hydrogen peroxide
Mg	Magnesium
MgO	Magnesium oxide
NBR	Brazilian standard (Norma Brasileira)
N_2	Nitrogen
Ni	Nickel
nm	Nanometer (10^{-9} m)
MWCNT	Multi walled carbon nanotube
PC	Portland cement
PVC	Polyvinylchloride
PVP	Polivinylpirrolydone
S	Silicon dioxide (cement chemist notation)
sccm	Standard cubic centimeters per minute
SEM	Scanning electron microscopy
SiC	Silicon carbide
SiO_2	Silicon dioxide (silica)
SWCNT	Single walled carbon nanotube

TEM	Transmission electron microscopy
TGA	Thermogravimetric analysis
TPa	Terapascal
w/c	Water to cement ratio
WDS	Wavelength dispersive spectroscopy
XPS	X-ray photoelectron spectroscopy
XRD	X-ray diffraction
μm	Micron (10^{-6} m)

1

INTRODUCTION

1.1 Initial considerations

Humanity has always been interested in better understanding the surrounding world. This surrounding world in the scale comparable to human size is relatively well known nowadays. The center of researchers' interest has turned to the world of both smaller and bigger scale.

Nanometer (10^{-9} meter) is the scale of atoms and molecules. At the end of the 20^{th} century the technological development made possible the investigation of nano-size matter and the science called nanotechnology was born. In fact, nanotechnology is not only a science, but the application of the recently discovered correlations at molecular scale to the classic fields of sciences. At this scale, materials have very different behavior from their macroscopic characteristics. Nanotechnology is the tool to get acquainted with and to exploit these "nano-characteristics" in the development of civilization.

Nanomaterials are modern materials developed by the nanotechnology containing nano-sized particles in a controlled manner. These materials have remarkably different characteristics: higher thermal and/or electric conductivity, enhanced mechanical properties, catalysis of different chemical reactions and self-healing properties. These characteristics of the material at macro-size are inherited of the nanoparticles. And this is the main challenge in the development of nanomaterials: to incorporate these particles into a matrix while keeping their extraordinary characteristics.

Nanotechnology is one of today's most active research and development fields, with high sum of funds allocated to it. Meanwhile compared to other main fields of industry, the impact of nanotechnology in construction industry is still little exploited. The possible reasons for this, according to Bartos (2008), are: (1) construction industry is not a field that produces new technologies, but it rather uses the benefits of technologies developed in other areas; (2) construction industry has historically low level of investments in research and development and (3) the necessity of very high initial capital investment required in nano-related research and development. The same study states that the employment of nanotechnology in construction industry will lead in the near future to buildings with zero environmental impact, since new, smart, high performance materials with characteristics such as self-cleaning and –healing and self-monitoring will be used.

With focus on sustainability, the nanotechnology applied to construction industry has to satisfy health, environmental, social and economic conditions. New materials with improved or new characteristics will certainly have economic benefits if the necessary improvements in production technology are accomplished. Health and environmental effects are subjects of ongoing research parallel to investigations on applications. The nanoparticles may represent various risks as their size permits to cross cell membranes. The most difficult thing is to foresee possible social effects of applied nanotechnology. It is not known for example whether a product labeled "nano" would sell better, but certainly there will be threats regarding them with or without any logical explanation.

The nano-related research and development of ordinary Portland cement and concrete composites today has several areas of focus. These areas include the better understanding and engineering the process of cement hydration and the hydration products themselves at nano-scale level, incorporation of nano-particles such as nano-silica, carbon black, carbon nanotubes (CNTs) in cement matrix in order to improve concrete performance and durability or to develop micrometer-thick coatings, and nano-sensors in order to achieve a smart concrete (BALAGURU and CHONG, 2008).

1.2 Justification

The development of a composite made with Portland cement produced with CNTs could lead to a new high performance material. The CNTs would act as bridges across cracks and voids and thus strengthen significantly the matrix in tension. As it has been reported in recent

studies, cement composites incorporating CNTs in the amount of 0.3 to 0.5 % of the mass of binder show 19-34 % better tensile strength to the reference specimens (LI *et al.*, 2004a; MELO, 2009; MUSSO *et al.*, 2009; XU *et al.*, 2009). Figure 1.1 shows a comparison of some published results on the compressive and tensile strength of CNT/cement-based composites. The gains presented are very modest in comparison to the potential of individual CNTs' mechanical properties, but it can be foreseen, that if the issues of dispersing nanotubes in the matrix and assuring strong bond between CNTs and cement particles are solved, the results should be much more favorable. In addition to better strength, characteristics such as shrinkage and ductility are expected to show better performance, and the appearance and propagation of micro-cracks could be controlled. These enhancements besides having an impact on the structural performance of cement-based materials would also allow the concrete industry become more sustainable. The desired characteristics would provide significantly longer service life of concrete structures. Less and smaller cracks can also reduce corrosive agents to penetrate into the concrete and consequently damage the steel rebars.

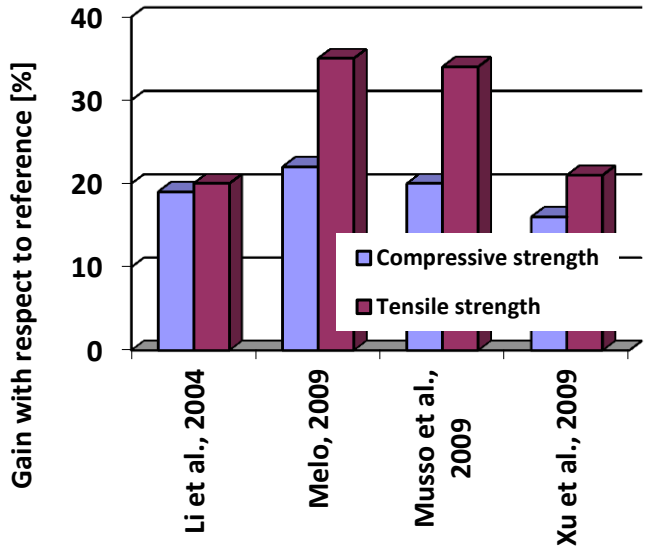

Figure 1.1 – Comparison of the gains for the compressive and tensile strength of CNT-cement based composites

Compared to most of the investigations in the literature, which involve the physical mixture of nanotubes and cement paste or mortar, the in-situ synthesis of these particles can resolve many of the dispersion and bonding problems. The research group based at the Nanomaterials Laboratory of UFMG developed a method to produce nano-structured clinker with *in-situ* synthesis of CNTs (LADEIRA *et al.*, 2008). This technique involves industrial by-products as catalyst materials, which probably has not been reported elsewhere.

1.3 Objective

The primary objective of this research project is to create a viable method of producing CNT reinforced cement matrices through *in-situ* chemical vapor deposition (CVD) synthesis of multiwalled carbon nanotubes (MWCNTs) on clinker particles or other Portland cement-compatible materials. The *in-situ* synthesis is expected to radically improve the dispersion and the bond between nanotubes and the binding material. Also continuous process production can be more efficient due to the removal of startup conditions in batch processes.

The study covers the whole process from CNT synthesis by CVD to the determination of mechanical properties of CNT-reinforced cement test specimens. There is an important focus on the development of an economically viable production process including CNT synthesis. Attempts are going to be made to reduce production costs by using residual materials as catalysts and carbon source gas and optimizing the CNT yield of the process. At the same time, laboratory CNT synthesis is needed to be up-scaled in order to produce enough material to perform strength tests and to reduce production costs. Nanotube synthesis in greater amount will allow stepping toward the industrial scale production.

This doctoral work's objective is to investigate the influences between the process parameters and the micro- and macrostructure of CNT-reinforced cement paste, with principal focus on tensile strength. The characteristics of the new material are to be compared with standard Portland cement in order to prove its significance as a construction material.

1.4 Scope of this study

The second chapter presents the literature review with results about cement hydration and nanostructure of cement hydration products, information on the synthesis of carbon nanotubes and their main characteristics. Test results of Portland cement composites are presented next. Finally the current state-of-art of composites prepared with cement and carbon nanotubes is reviewed in details.

The third chapter describes the materials and methods used during the synthesis of carbon nanotubes and nanofibers on clinker particles and other materials. The characterization of the produced nano-structured cement is shown in the second part of this chapter.

The materials and methods involved during the preparation and testing of mortars containing the nano-structured cement are presented in the fourth chapter. The results of these tests are also described and analyzed.

The conclusion of the investigations is described in chapter five. Some propositions are made concerning future research.

The work is completed with a list of references and an appendix. The annexes show details of the performed tests and respective analysis as well as a list of publications involving this doctoral study.

2

LITERATURE REVIEW

2.1 Portland cement

2.1.1 Production

The origin of Portland cement (PC) is linked to Louis Vicat, a French engineer who published a work on the calcination of limestone and clays that makes a material that hardens after mixing with water (VICAT, 1818). However, it was after the patent of Joseph Aspdin, a British bricklayer, in 1824, that Portland cement got his name (of the Portland peninsula from where the prime materials were extracted).

Portland cement is the product of the heating of limestone, clays and other corrective minerals (ex. iron ore or bauxite) to approximately 1400 °C sintering temperature in a cement kiln. First all ingredients are dosed in the correct composition and ground. The resulting powder is called raw mixture. This raw mixture is then heated progressively first in cyclones using residual heat, then in the cement kiln. In the first phase of the clinker formation process free water evaporates at 100 °C. At 340 °C dolomite decomposes to *MgO* and CO_2:

$$MgCO_3 \rightarrow MgO + CO_2. \qquad (2.1)^1$$

After further heating, at 800-900 °C calcium carbonate is decomposed following the equation:

[1] Mehta and Monteiro, 1994

$$CaCO_3 \rightarrow CaO + CO_2. \qquad (2.2)^2$$

Most of the decarbonation process occurs before the material enters the cement kiln. At temperatures over 550 °C clay minerals lose their combined water and form tricalcium aluminate (cement chemist notation C_3A) and tetracalcium aluminoferrite (C_4AF) with free *CaO*. At 900 °C belite (dicalcium silicate, C_2S) phase begins to form catalyzed by present *Al* and *Fe*:

$$2CaO + SiO_2 \rightarrow 2CaO.SiO_2. \qquad (2.3)^3$$

At 1250-1280 °C part of the material melts (this phenomenon is called sintering) that helps chemical reactions occur. When the material reaches 1400-1450 °C alite (tricalcium silicate, C_3S) phase forms:

$$2CaO.SiO_2 + CaO \rightarrow 3CaO.SiO_2. \qquad (2.4)^4$$

During the cooling process, part of the C_3S phase decomposes in C_2S liberating free *CaO*, in function of the speed of cooling. If the cooling is too slow, a greater part of C_3S decomposes which results in a lower quality cement. The cooled material agglomerates in nodules of approximately 5 to 25 mm. The obtained clinker is then ground together with gypsum to adjust cement setting time and quality. Blast furnace slag and other pozzolanic materials can also be added. The different cement types and their composition are regulated in Brazil by the NBR 5732 (CP I – normal Portland cement), NBR 11578 (CP II – composite cement), NBR 5735 (CP III – slag cement), NBR 5736 (CP IV – pozzolanic cement) and NBR 5733 (CP V ARI – high initial strength cement) standards. The typical chemical composition of the Portland cement is 50-70 % C_3S, 15-30 % C_2S, 5-10 % C_3A, 5-15 % C_4AF and 3-8 % of other additives or minerals (such as free *CaO* and *MgO*).

Cement production, especially the clinker formation process is considered to have high environmental impact. This impact includes a significant CO_2 release that represents approximately 5 % of global CO_2 emission (WBCSD-IEA, 2009). This emission is composed principally of decarbonation of limestone and cement kiln fuel combustion. There is high demand to reduce this emission. When comparing the environmental impact of reinforced

[2] Mehta and Monteiro, 1994
[3] Mehta and Monteiro, 1994
[4] Mehta and Monteiro, 1994

concrete and steel buildings, it can be seen that a reinforced concrete beam results in less air and water pollution and less energy consumption than a steel beam, even using more than the double of resources. The only parameter in which the reinforced concrete beam appears to have higher environmental impact is the greenhouse-effect gas emission (STRUBLE and GODFREY, 2004). According to Mehta (2009), the reduction of this emission could be achieved using three tools: (1) consume less concrete using innovative architectural concepts, structural design and high durability concrete, (2) consume less cement in concrete mixtures considering 56 to 90 day compressive strength instead of 28 days and using the newest generation admixtures and (3) consume less clinker in cement incorporating fly ash, blast furnace slag, rice husk ash or silica fume which ingredients does not additionally emit CO_2.On the other hand, due to high temperature and oxidative environment in cement kilns, it is possible to incinerate some hazardous wastes effectively.

2.1.2 Cement hydration

One of the most actively researched fields of cement science is the hydration and formation of hydrated compounds. When Portland cement is mixed with water (*H*), many different types of hydrated compounds will form. These compounds are mainly ettringite, monosulfate, calcium silicate hydrate and calcium hydroxide.

After the mixture with water, first gypsum (calcium sulfate) dissolves in its ionic compounds followed by the calcium and aluminate ions of C_3A. This solution gets rapidly saturated and some materials precipitate. The formation of the hydration products is a function of the composition of these dissolved materials and thus of the initial composition of the cement paste mixture. The most active C_3A phase reacts with the dissolved sulfates to form rod-like ettringite (*AFt*) crystals (stage 1 on Figure 2.1). This reaction is highly exothermic.

After that the heat liberation is reduced during the so-called induction or dormant period (stage 2 on Figure 2.1). Two or three hours after the mixing with water alite (C_3S) and belite (C_2S) start to react and form calcium silicate hydrate (*C-S-H*) and calcium hydroxide (*CH*) crystals. *C-S-H* is often called gel. The grains react from their surface inwards and the hydration reactions goes on as long as not hydrated cement grain cores are available. Since each cement grain is composed of the different cement phases, again all types of hydration products can form as the cement grain hydration goes on and the water penetrates into the

grain. The formation of *C-S-H* in this phase (stage 3 and 4 in Figure 2.1) is mainly responsible for the strength of hydrated cement.

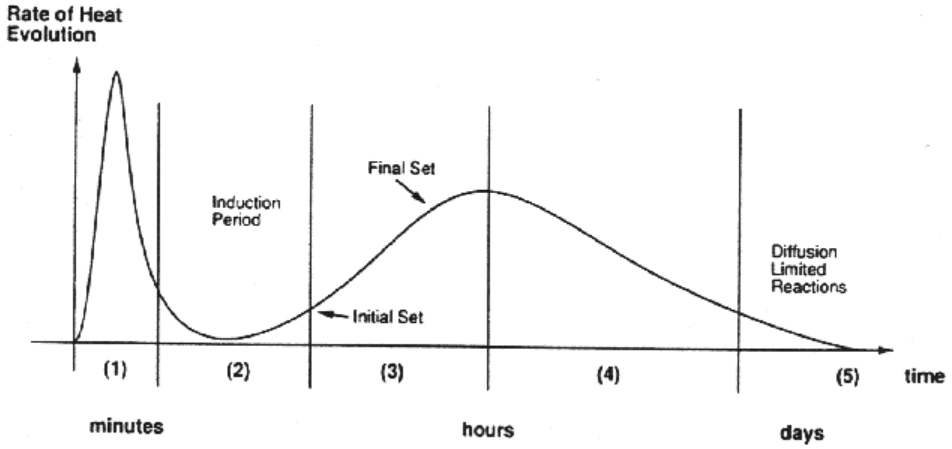

Figure 2.1– Evolution of heat liberation during cement hydration. Source: Bentz *et al.*, 1994

The hydration of calcium silicates occurs following these equations (MEHTA and MONTEIRO, 1994):

$$2C_3S + 6H \rightarrow C_3S_2H_3 + 3CH; \qquad (2.5)^5$$

$$2C_2S + 4H \rightarrow C_3S_2H_3 + CH. \qquad (2.6)^6$$

It is seen, that C_3S generates more *CH* than C_2S. C_3S hydrates more rapidly and thus contributes to the early age (2-3 h to 14 days) strength; meanwhile C_2S hydrates slower and contributes to the strength after one or two weeks. Their hydration product, *C-S-H* forms lamellas bonded covalently or non-covalently – by van der Waals forces or by adsorbed water on the surface – between each other. The appearance of the *C-S-H* is highly influenced by the *C/S* relation of the cement.

It is seen also, that the hydration of both types of calcium silicates liberates calcium ions which concentration will increase. Because of the relationship between the concentration of sulfate and calcium ions, and also the aluminate ions liberated by the hydrating C_4AF phase, monosulfate (*AFm*) will be more stable than ettringite. The calcium and aluminate ions will interact with the still present sulfate ions and also partly with ettringite to slowly form monosulfate (POURCHET *et al.*, 2006).

[5] Mehta and Monteiro, 1994
[6] Mehta and Monteiro, 1994

Calcium silicate hydrates being formed do not have a specific stoichiometric ratio and have generally poorly crystalline structure. Some 44 different natural minerals and their varieties have been already identified as possible forms for calcium silicate hydrates amongst them the most relevant ones are tobermorite, jennite and jaffeite types (RICHARDSON, 2008). The resulting type of C-S-H is influenced mostly by the initial composition of cement, but also depends on the presence of admixtures and on the curing time and conditions. The tensile brittle behavior of *C-S-H* is due to the inherent characteristics of its constituents. Jennings *et al.* (2007) used a nanoindentation technique to identify two different types of *C-S-H* in cement phase by mechanical characteristics. According to the moduli measured from several indentations two peaks, corresponding to the two – low-density and high-density – *C-S-H*, were clearly identified. It is not well known which parameters (cement composition, cure conditions) are responsible for the formation of each type of *C-S-H*.

The general form of *C-S-H* is an agglomerate of nearly amorphous lamellae. Each lamella is formed by a double layer of *CaO* crystals with silicate ions linked on both sides, as shown in Figure 2.2. The space between the lamellae is filled with water and dissolved ions. Water in the hardened cement matrix is classified in four groups: (1) capillary water, that is present in the greater cavities, where the distance between the *C-S-H* sheets is bigger than some tens of nanometers; (2) fisically adsorbed water on the surface of lamellae, where the distance between the sheets is in the order of some tens of nanometers; (3) interlaminar water, which participates in the link between lamellae at some nanometers distance; and (4) water of the crystals which is chemically linked to the hydration products. The loss of the capillary water has low influence on the volume of the hardened paste. The remove of the adsorbed water causes drying shrinkage or creep, if the loss of water is due to mechanical loading. The loss of interlaminar water occurs by intensive drying and results in massive volume loss of *C-S-H*. The water of crystals can only be removed by calcination at high temperatures and decomposition of hydration products.(MEHTA and MONTEIRO, 1994)

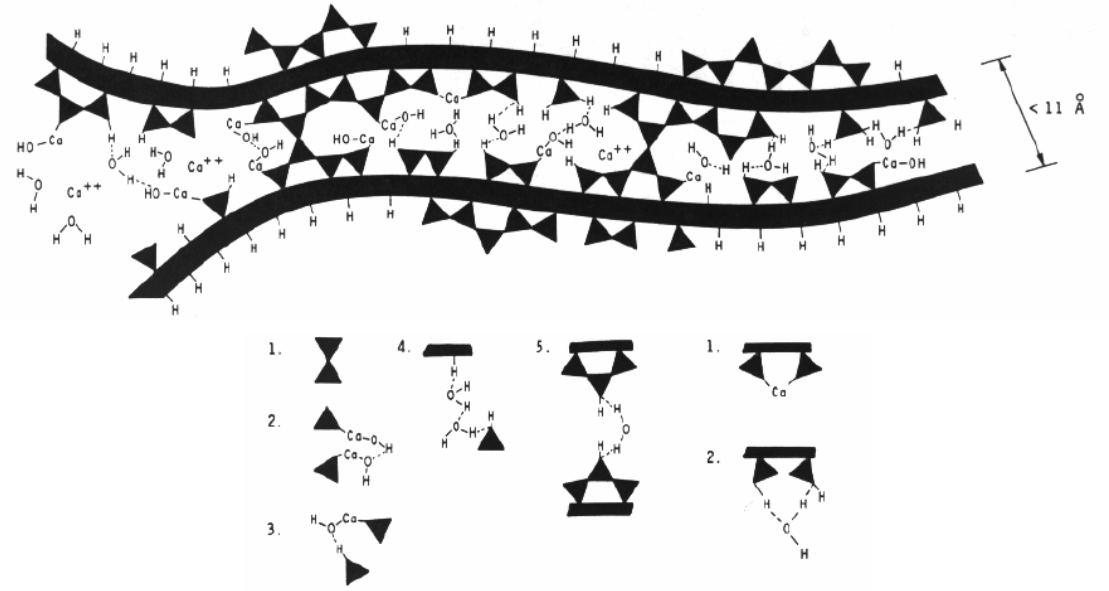

Figure 2.2– Nature of bonds between *C-S-H* lamellae. Source: Ramachandran and Feldman, 1996

The position of C-S-H lamellae is aleatory with some parts linked between each other. These links may occur directly between the silicates of the lamellae, or through other molecules or ions (hidroxyl, calcium hydroxide, see Figure 2.2). The nature of these bonds is principally ionic or covalent, but can be also by hydrogen bridge or by van der Waals attraction. (PELLENQ *et al.*, 2008)

The hardened cement paste is porous even after the most efficient compacting. This occurs because the formed crystals occupy less volume than the sum of cement and mixing water. These pores are in the region of macro-, mezo- and micro pores. The pores of the smallest diameter are capillaries between the agglomerates of *C-S-H* or other hydration products.

C-S-H lamellae form particles of the size of tens of nanometers. These particles make agglomerates of the size of microns. The set of these agglomerates form centimeter size minerals.

To enhance cohesion of *C-S-H* and mechanical behavior of hardened paste, Gleize (2008) suggests two main strategies:

- Control of the nanoporosity of *C-S-H* and the interlaminary distance, in order to assure the continuity and uniformity of bonds;
- Reinforcement of the bonds between lamellae, possibly with the incorporation of fibers or other materials (polymers) that give ductility to the composite.

It is important to know, that meanwhile standard concrete or mortar strength is achieved at 28 days, hydrated cement never stops to continue hydrating and – depending on the climatic conditions which the structure is exposed to – continues gaining strength.

The ratio of the cement's constituents influences the strength achieved at different ages of the concrete and other characteristics. The set time depends on the C_3S/C_2S ratio, with faster setting at higher C_3S contents. Higher C_4AF content slows hydration. Sulfate resistant cements contain less C_3A. Another important factor on cement hydration speed is the fineness: smaller grains are easier to hydrate. Cement hydration is a highly exothermal reaction. With higher hydration speed more heat will be generated that can damage concrete if exceeds a certain limit. Also the amount of heat liberated can cause a differential drying of the concrete structure causing cracks. The hydrated cement has *pH* between 12 and 13. This gives a protection to steel reinforcing bars. If the *pH* lowers, the protection ceases its effects.

2.1.3 Admixtures for cement paste, mortars and concrete

Organic admixtures such as milk, blood or eggs were used already by antique Romans and also in the middle ages to enhance water resistance of concrete or for tinting. It was later discovered, that water to cement (w/c) ratio of the mix highly influences the final strength of concrete. Although the amount of water necessary to totally hydrate the cement is approximately 30 % of the cement mass (JOLICOEUR and SIMARD, 1998), the amount of mixing water used is generally higher in order to secure good workability and casting characteristics to the fresh concrete. This additional water will not compose hydrates with the cement, thus it will leave pores in the hardened matrix after evaporation. These pores are imperfections of the matrix and will be possibly the origin of cracks.

In order to reduce the amount of water used in a concrete mix, special surfactant agents as modern concrete admixtures have been developed to assure workability while reducing w/c ratio. Besides water reducing, some admixtures have effects also on other characteristics of fresh or hardened cement paste, such as retarding or acceleration of setting and hardening, air-entraining, etc. These characteristics also help to achieve a concrete/mortar/cement paste with the desired behavior at fresh or hardened state (ACI E-701, 2003).

The first generation water reducing admixtures were based on salts of lignosulfonic acids, a by-product of the paper industry. Its main effect is called electrostatic repulsion and consists of fixing charged particles (in the case of lignosulfonates positively charged) on the

surface of cement grains so that they will repel each other and assure more fluidity to the mix. Lignosulfonate based plasticizers can reduce the amount of water needed by approximately 5 %. They tend to entrain air and have set retarding effect due to their polysaccharide content.

Second generation water reducing admixtures were already designed to avoid such fact. They were mainly ionic (both cationic and anionic) surfactants, giving a charge to the cement particles to create repelling and dispersing effects between them. Some typical chemical compositions of these admixtures are sulfonates of (poly)naphthalene or melamine.

The newest generation of water reducing admixtures is based on polycarboxylate-ethers. They can reduce the amount of water necessary for the same consistence by up to 40 %. Their effect is based rather on steric repulsion of cement particles. The polycarboxilates are composed of a comb-like structure with a primary chain and lateral ether chains. It is the carboxylate groups of the main chain that assure adsorption to the cement particles, while the side chains provide the steric hindrance effect. The behavior of the polycarboxylate thus depends on its structure. The number of carboxylate groups and the length of the main chain affect the adsorption and the length and the number of ether side chains influence the dispersive ability (YOSHIOKA *et al.*, 1997). The comb-like superplasticizers may have a longer duration as the graft chains of the adsorbed molecule can remain active until the hydration products have incorporated them (FLATT and HOUST, 2001).

Since the behavior of concrete admixtures depends on various factors such as cement and aggregate type and composition, it is advisable to perform trial mixtures in order to determine the correct type and dosage of the admixture, with respect to the needed fresh state or hardened characteristics.

Flatt and Houst (2001) state that admixtures can interact with cement particles in three ways. They can be adsorbed on the cement grain surface, may be consumed by intercalation, coprecipitation or micellization forming an organo-mineral phase, or can remain in solution. Adsorption characteristics of admixtures on cement are generally related with their efficiency, but some care should be taken when performing adsorption tests. Adsorption and plasticizer efficiency measurements should be performed by saturated (high concentration) admixture solutions; otherwise the consumption of the surfactant in the organo-mineral phase will be more important. When wetting cement particles, a so-called double Stern layer is created around them. The positive *Ca* and *Mg* ions enter into solution leaving a negatively charged core composed of mainly silicates. Therefore the inner Stern layer is composed of positive ions and water meanwhile the outer Stern layer is composed of negative ions and water. If the

admixture is anionic, it will thus be adsorbed in the outer Stern layer. At the same time, a cationic molecule will be adsorbed in the inner Stern layer, which is slightly more difficult, since the admixture molecule have to cross the outer layer first (ZHANG *et al.*, 2001). The adsorption characteristics of the same admixture on different cement mineral phases may be different, as it was demonstrated by Yoshioka *et al.* (2002).

The organo-mineral phase is composed by the admixture molecules and dissolved ions from cement. Complexes formed by sulfates and admixture consume more sulfate and thus will favor *AFm* formation rather than *AFt* in the hardened paste. Complexes formed by admixture molecules and calcium or *C-S-H* have also been observed (UCHIKAWA *et al.*, 1995; FLATT and HOUST, 2001).

Puertas *et al.* (2005) found that water reducing or superplasticizer admixtures generally cause delay in early hydration and retardation of setting. This phenomenon may be explained by the competitiveness between admixture molecules and dissolved ions of cement particles to form hydration products or organo-mineral phase. Admixture molecules adsorbed to the cement particle surface block the way for ions of the cement particle to enter in solution. The presence of admixtures during cement hydration also limits the dissolvable ion quantity as the mixing water already contains a dissolved phase (the admixture) and becomes saturated more rapidly. At early hydration ages a difference in the pore structure of hardened paste was observed by Puertas *et al.* (2005) when applying admixtures, but no difference was shown in the mineralogical composition and morphology of hydration products.

2.2 Carbon nanotubes

Carbon nanotubes (CNTs) are a special form of carbon. They were already used – although involuntarily – to reinforce Damascus steel in the 17th century. The modern era discovery of CNTs is discussed by Monthioux and Kuznetsov (2006), but it was without any doubt after the work published by Iijima (1991) that CNT research gained focus, most probably because of the extraordinary mechanical, thermal optical, chemical and electric characteristics of CNTs. These features allowed already the use of CNTs in some commercial applications (polymer composite bicycle components, hydrogen sensors), but many further applications are subject of ongoing research. The possible applications of CNTs are in the fields of molecular electronics, energy storage, nanomechanic devices, biotechnology and composite materials (DAENEN *et al.*, 2003).Today one of the main obstacles in the

development of new CNT based materials and devices are the costs of production, purification and functionalization. Also, there is little experience in the up-scaling production from laboratorial size to industrial.

CNTs are long, rolled graphene sheets. According to the number of sheets, single walled carbon nanotubes (only one sheet, SWCNTs) and multi walled carbon nanotubes (more than one sheet, MWCNTs) can be differentiated. The number of walls can be up to 40 or 50. The chirality – the direction in which the grapheme sheet is rolled – is a characteristic of every single nanotube wall. According to the chirality of the SWCNTs, they can be classified as armchair, zig-zag or chiral structure (Figure 2.3). Chirality is characterized by a vector (*n*,*m*), where *n* and *m* are the unit vectors on an imaginary infinite grapheme sheet. These structural differences may result in different mechanical, electric or thermal behavior. It remains still a challenge to have a total control on CNT chirality during the synthesis (especially for MWCNTs).Nowadays there are only some theoretical studies on the comparison of the mechanical properties of SWCNTs with different chiralities. It is supposed that zig-zag type CNTs have slightly lower tensile strength than armchair structure CNTs because of the parallel position of some of the covalent links between carbon atoms to the axis of the nanotube and loading (NATSUKI *et al.*, 2004; RANJBARTOREH and WANG, 2010).

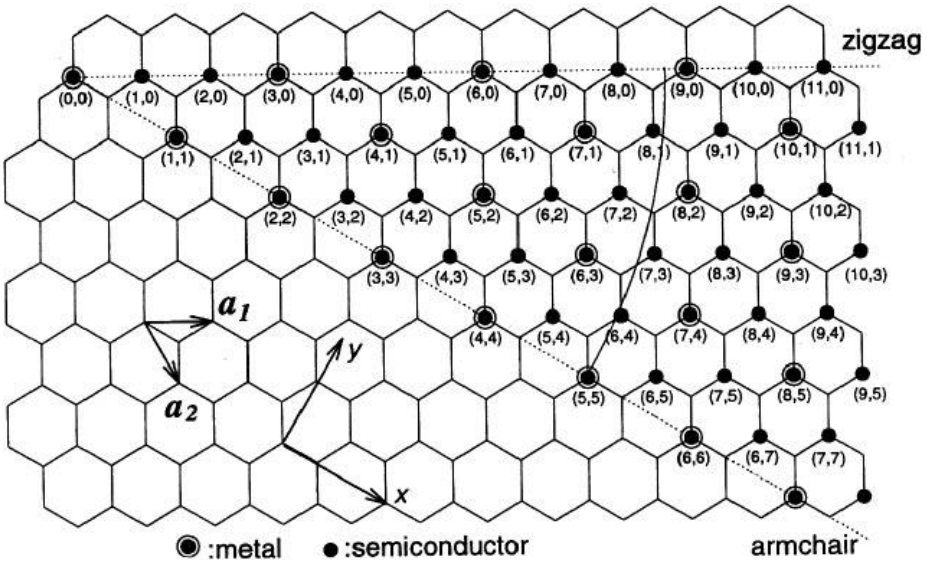

Figure 2.3– Different CNT chiralities according to the direction of rolling of the graphene sheet with possible chirality vector coordinates. Y axis is the direction of the CNT axis and X axis is the direction in which the graphene sheet is rolled. Source: Dresselhaus *et al.*, 1995

In practice, CNT structures are not perfect: they show defects and deformations. These defects show up where a hexagon in the graphene sheet is replaced by a pentagon or heptagon, or can be a result of the presence of impurities. Also, different materials and particles can be built inside the CNT. These points of defect bring other important characteristics to CNTs and thus are often introduced in a controlled way. These imperfections and functional groups linked to them are an important factor in functionalizing (preparing to use) CNTs, because pristine nanotubes are hydrophobic, have low reactivity and tend to stay together due to the attraction of van der Waals forces.

The so-called carbon nanofibers (CNFs) are different from conventional carbon fibers. Nanofibers have significantly smaller diameter (10-200 nm in comparison with fiber's 7-15 μm diameter) and have a different, tube-like structure. CNFs are also different from CNTs, which have even smaller diameter and are formed by ordered graphene layers along with the axis; while the orientation of the layers of a CNF is at an angle to the axis (Figure 2.4).

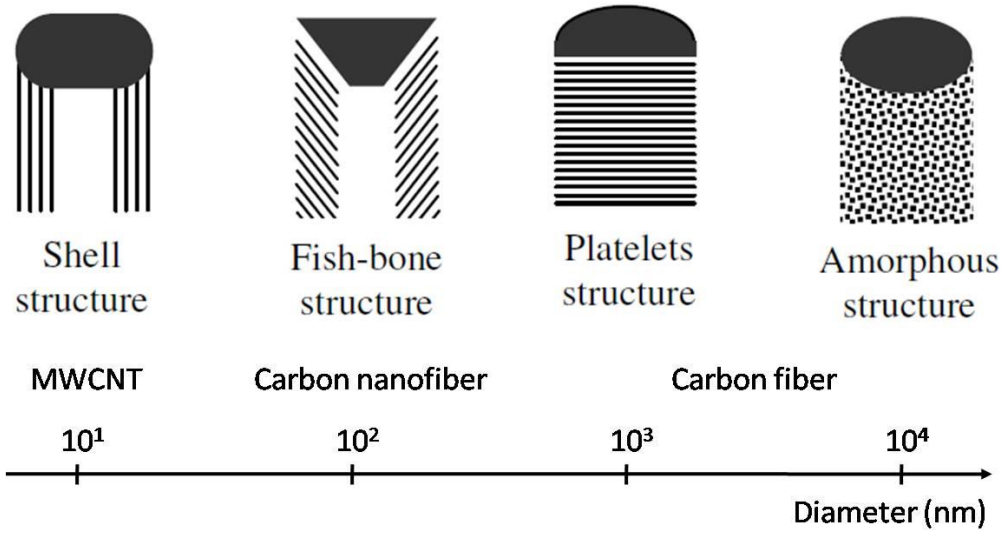

Figure 2.4– Schematic comparison of structure and diameter of carbon nanotubes, nanofibers and fibers. Based on Mori and Suzuki (2010)

2.2.1 Synthesis

The growth mechanism of CNTs is still an object of ongoing research. Current synthesis methods are based on applying energy on a carbon feedstock to liberate carbon atoms that will self-assembly in nanotubes in the presence of a catalyst. The two main CNT growth theories are the root growth and the tip growth theory (Figure 2.5).

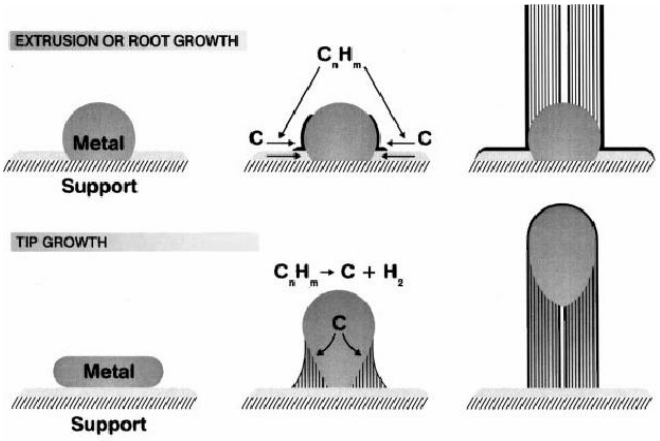

Figure 2.5– Growth mechanisms of CNTs. Source: Daenen *et al.* (2003)

The main CNT synthesis methods used are arc discharge, laser ablation, flame synthesis and chemical vapor deposition (CVD). Even in a simple paraffin wax candle's flame CNT formation was observed (LI and HSIEH, 2007), which demonstrates that any combustion of carbonaceous material may synthesize CNTs. The soot in the air we breathe in contemporary urban ambiance can contain CNTs (MURR *et al.*, 2004) and there is some evidence, that nanotubes were present in prehistoric atmosphere also (ESQUIVEL and MURR, 2004).

In arc discharge, carbon vapor is created between two carbon electrodes, and nanotubes form from this vapor. CNTs grown by arc discharge have high impurity but their size is highly controllable.

Laser ablation technique uses a high power laser beam to decompose a carbon feedstock (hydrocarbon gas) in its constituents in order to form CNTs. The product of laser ablation is of high purity but the method is not too productive.

The CVD is the pyrolysis of hydrocarbons at temperatures generally between 500-1000 °C over transition metal catalysts supported on a stable material (Figure 2.6), and it is proved to be a promising method for large scale production of CNTs. The product is of high purity and the technique is relatively economic. Numerous catalyst-support combinations, carbon source and carrier gas and synthesis conditions (temperature, process duration and gas flow rate) have been tested to grow CNTs. Vesselényi *et al.*, (2001) compared the catalytic activity of the binary combinations of cobalt, nickel, iron and vanadium catalysts and two types of zeolite and alumina supports using acetylene as carbon source; Songsasen and Pairgreethaves (2001) used liquefied petroleum gas and zeolite supported nickel. On the other hand Gournis *et al.*, (2002) managed to grow CNTs on clay minerals with acetylene. The

catalytic activity of different support-catalyst combinations and the product morphology was compared in the work of Kathayini *et al.* (2004). The authors prepared the combinations of *Fe*, *Co* and *Fe*/*Co* particles as catalyst and *Ca* and *Mg* oxides, hydroxides and carbonates as support, and these catalysts showed significant differences in the carbon yield and morphology using the same synthesis parameters. They successfully identified some support-catalyst combinations that proved to be efficient in CNT synthesis. Recently, Nasibulin *et al.* (2009) and Mudimela *et al.* (2009) used Portland cement clinker and silica fume, respectively, to grow CNTs and carbon nanofibres (CNFs). Yasui *et al.* (2009) and Dunens *et al.* (2009) reported independently the growth of MWCNTs and CNFs on fly ash with or without further iron addition.

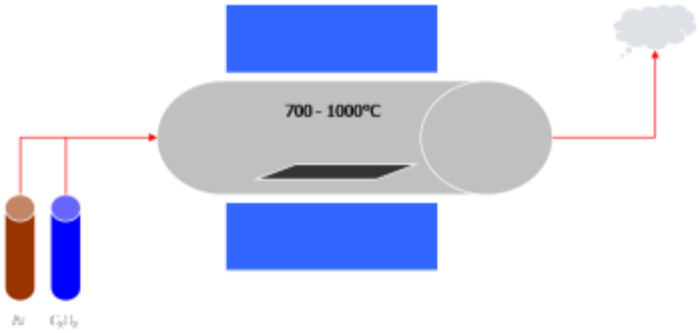

Figure 2.6– Schematic view of a CVD reactor. The gases used in this case are argon and acetylene.

An important value to evaluate CNT growth efficiency of a catalyst-support combination at given synthesis conditions is carbon yield (*Y*):

$$Y = \frac{w_3 - (w_1 - w_2)}{w_1 - w_2} \times 100, \qquad (2.7)^7$$

where w_1 is the catalyst's initial weight, w_2 is the weight loss of the catalyst at the reaction temperature and w_3 is the total weight of the carbon deposit and the catalyst (COUTEAU *et al.*, 2003).

Other important properties of CNTs are size, aspect ratio, number of walls and morphology. These properties are mainly influenced by catalyst preparation and catalyst particle size (RÜMMELI *et al.*, 2007). The size of the catalyst crystallite has a great influence on the diameter of the nanotube to be grown (KHASSIN *et al.*, 1997). Theoretically any combination of a transition metal catalyst and a support material that remains stable at the

[7] Couteau *et al.*, 2003

process temperature can be used for CVD CNT synthesis, but *Fe*, *Ni* and *Co* are the most used catalysts on a high surface area support.

The gases used as carrier for CVD process are mainly N_2 and noble gases as *Ar*. The carbon source used is mainly a hydrocarbon gas (methane, ethylene, acetylene etc.), but carbon monoxide or heavier hydrocarbons are also an alternative.

Carbon yield and product quality are dependent of catalyst type and preparation method, type and flow of gases and process temperature and time.

The price of CNTs is still high, but falling, due to the high capacity of CNT production facilities being installed. Couteau *et al.* (2003) developed a continuous, large scale CNT-production CVD method using a rotary-tube oven (Figure 2.7). The application of such a continuous production line would raise significantly the production capacity and thus, reduce prices.

Figure 2.7– Rotary CVD furnace for continuous CNT synthesis. Source: Couteau *et al.* (2003)

2.2.2 Functionalization

Functionalization of CNTs is the surface treatment process that gives them special properties to enable them to be used for specific applications. As CNTs have a perfect carbon structure and are highly hydrophobic, it is essential to use surface treatments to make them applicable in composite materials such as Portland cement (PC) paste. The aim of these treatments is to attach some specific functional groups on the surface of CNT to change their characteristics and also to remove amorphous carbon, catalyst particles or any other impurities. The functional groups are mainly attached to nanotube caps or local defect spots. Some of these processes use oxidation of the carbon material of the nanotubes to attach

functional groups; other methods involve the – covalent or non-covalent – attachment of a specific molecule.

Many methods and materials have been tested to functionalize CNTs. Shaffer *et al.* (1998) present a method based on aqueous nitric and sulfuric acid treatment of MWCNTs to attach oxygen containing functional groups on their surface. Using FTIR spectroscopy the authors observed the presence of carboxyl groups. The so-treated nanotubes dispersed in water with ease. Datsyuk *et al.* (2008) compared some different CNT-functionalization treatments. The used nanotubes were multiwalled. The compared methods were based on hydrochloric acid, nitric acid, piranha solution (a mixture of sulfuric acid and hydrogen peroxide) and ammonium and hydrogen peroxide treatments. When evaluating the aqueous dispersion, the authors found that the mentioned functionalization methods were efficient with the exception of hydrochloric acid treatment. A functionalization method based on ozone treatment in hydrogen peroxide was developed by Naeimi *et al.* (2009). XPS studies showed the attachment of carboxyl groups on the MWCNTs. The ozone treatment is much milder than the above mentioned acid treatments, and so damages less the CNT structure. Furthermore, ozone can be generated and used for treatment under much simpler conditions than acids. Meanwhile, it is still able to attach carboxyl groups to CNTs, as it was found in the comparative study of Sulong *et al.* (2009).

The injection of ammonia during the synthesis process incorporates nitrogen atoms into the CNT structure. The alterations caused by this incorporation are bamboo-shape structure and amino functional groups on the surface of the nanotubes (MI *et al.*, 2005; ŢIRPIGAN *et al.*, 2007).

The above mentioned methods introduce functional groups covalently bonded to CNTs. Besides this, non-covalently bonded surfactant molecules can also change CNTs' characteristics including better dispersion in water. Twenty-four different surfactants and polymers were tested by Moore *et al.* (2003) to disperse nanotubes in water. Earlier, Bandyopadhyaya *et al.* (2002) achieved a good aqueous CNT dispersion using a natural polymer: gum arabic. Liu et al. (2007) dispersed MWCNTs in water that were previously grinded together with sodium lignosulfonate, which is considered a mild treatment method. The amount of sodium lignosulfonate was 1 g for 0.1 g of MWCNTs.

2.2.3 Mechanical characteristics

Although it is very difficult to directly measure mechanical characteristics of CNTs such as axial and flexural strength, strain at ultimate and Young's modulus, many tests have been performed on single CNTs to determine their mechanical characteristics. The obtained values are one of the highest among all known materials. Demczyk *et al.* (2002) measured directly the tensile and flexural behavior of MWCNTs. The obtained tensile strength of 12.5 nm diameter nanotubes was 0.15 TPa. They reported also the flexural robustness of CNTs, as the nanotube was bent over itself during a flexural test in atomic force microscopy. The calculated elastic modulus was 0.91 TPa. Earlier Falvo *et al.* (1997) observed MWCNTs under bending and reported the nanotubes sustaining local strain up to 16 %. Yu *et al.* (2000) tested 19 MWCNTs under tensile loading and measured strengths between 11 and 63 GPa and elastic modulus between 270 and 950 GPa. The Young's modulus of CNTs with different structures was compared by Salvetat *et al.* (1999). The authors concluded, that the more ordered the tube walls are, the higher its Young's modulus will be. In Figure 2.8 typical modulus values are presented in the case of perfect, wavy and bamboo-like nanotube wall structure. When CNT's are agglomerated, these properties are significantly reduced. Even though, Li *et al.* (2000) performed tensile tests on macroscopic ropes of roughly aligned SWCNTs impregnated by PVC resin. The mean value of 3.6 GPa of tensile strength is similar to that of commercial carbon fibers.

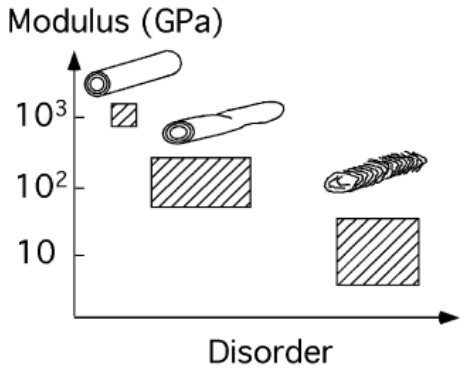

Figure 2.8– Typical Young's modulus values vs. disorder of CNT walls. Source: Salvetat *et al.* (1999)

Experiences show that MWCNT shells are able to slip telescopically, at a relatively low load level (CUMMINGS and ZETTL, 2000). It was also reported, that a failure in the outermost layer of a MWCNT would lead to the pull-out and the total failure of the nanotubes in case of tensile loading (YU *et al.*, 2000).

As it was observed by Lu *et al.* (1996), ultrasound may cause damages on the CNTs breaking and stripping the outermost graphitic layers. When the treatment of the nanotubes involves sonication care should be taken in order to avoid the deterioration of the nanotube structure.

2.3 Composites

2.3.1 Portland cement composites

Portland cement concrete is the second most used product in the world after water. There are two main directions in which concrete developed: (1) a compacter, less permeable concrete with the addition of fine materials and (2) the addition of fibers to enhance tensile characteristics that would affect permeability too, because of limited cracks.

In order to make concrete more resistant to climate and corrosive effects some fine aggregates were added to achieve higher density, less porosity and higher impermeability. For these purposes, materials with smaller particle size than those of the Portland cement particles can be used. As price is an important factor, many industrial by-products have been incorporated and tested in concrete to attain better performance. Many of these materials have pozzolanic effects or help the formation of cement hydration products. Nowadays fly ash, silica fume, blast furnace slag and rice husk ash are used in industrial scale to achieve a better performing concrete or simply to reduce production costs.

Blast furnace slag is a steel-making byproduct that contains mainly impurities of the produced steel. These impurities are mainly calcium and silica, the same materials that constitute Portland cement. In order to be used in conventional cement, the slag has to be ground to the fineness of cement particles. Slag cements have slower hydration speed and higher set time than conventional Portland cement.

Fly ash is produced in huge amounts in power plants during the combustion of coal. It is a fine powder containing pozzolanic materials, such as SiO_2, CaO and Fe and Al oxides. The use of fly ash in concrete leads to a higher final strength and durability at lower hydration speed.

Silica fume is today's most used mineral admixture of high strength concrete. It consists of amorphous SiO_2 particles of high fineness and surface area. Silica fume is a byproduct of silicon and ferrosilicon production and is a highly pozzolanic material. An

addition of silica fume up to 10 % of the binder content enhances the final strength and durability of concrete. At the same time, the small particles of silica increase water demand/reduce workability, increase pozzolanic activity, accelerate the cement hydration process and reduce setting time (CHENG-YI and FELDMAN, 1985; DE ROJAS and FRÍAS, 1996; BHANJA and SENGUPTA, 2005; ACI 234R-06, 2006).

After the combustion of rice husk, nearly 20 % of the material remains as ash. The ash is 92 to 95 % silica, lightweight, highly porous and has a very high surface area. The characteristics of concretes containing rice husk ash are similar to those which contain silica fume: higher setting speed, higher water demand, higher final strength and higher durability (HWANG and CHANDRA, 1997).

It is clearly seen that the smaller the particle size of these auxiliary materials is the better they can fill in the pores of the concrete. But it is clear too that the smaller the particle size is the more complicated will be the handling and application of these additional materials.

Li *et al.* (2004b) studied the effect of the addition of SiO_2 and Fe_2O_3 nanoparticles on cement mortars. With the incorporation of these particles in the rate between 3 and 5 % of the binder content gains up to 26.0 and 27.1 % in compressive and flexural strength respectively have been achieved. This gain in strength was due to filling in pores and by the catalysis of cement hydration product formation by the nanoparticles. This fact was also analyzed in the work of Li (2004) in which tests performed on Portland cement concrete made with fly ash and nano-SiO_2. The results showed higher heat liberation through the early stages of hydration of the concrete due to the addition of SiO_2 nanoparticles averaging 10 nm in size. Change in the concrete weight during the cure was also observed: specimens containing 4 % nano-$SiO_2$with respect to the binder content had a significant mass gain at early ages when cured in saturated lime solution. Qing *et al.* (2007) also witnessed higher compressive strength of mortars incorporating nano-SiO_2 than plain cement mortar reference. Other effects observed were higher pozzolanic activity and higher bond strength between cement paste and aggregates.

Electric arc furnace dust (EAFD) is a steel industry by-product and considered hazardous waste as it has toxic heavy metal content. It consists mainly of fine, nanoparticle fume. EAFD was tested by Flores-Velez and Dominguez (2002) in Portland cement paste composites. Its use was found to have a positive effect on the compressive strength at rates up to 10% of the cement. In order to resolve some other industrial waste disposal issues, Al-Otaibi (2008) studied the effect of steel mill scale as fine aggregate in Portland cement

mortar. He observed the best enhancement in cement mortar compressive and flexural strength with the addition of steel mill scale at the ratio of 40 % of the fine aggregate. The durability of such composites was not analyzed neither in the work of Flores-Velez and Dominguez nor in that of Al-Otaibi.

The other way to improve concrete performance is to add fiber-like materials that have high tensile strength and can bridge cracks and prevent them from opening. In fiber-reinforced concrete (FRC) steel, glass, synthetic and natural fibers are used. Typical fiber content of a FRC is between 0.1 and 3 % of the binder content. Today's commercially used fibers enhance a little the flexural strength of concrete: they are used mainly for cracking control and to help to achieve higher durability. Normally the flexural strength gain is not considered at the strength of the structure itself. The main reason for this is that there is not a known, reliable procedure to evaluate the efficiency of fiber dispersion, which is a key issue in the mechanical behavior of these composites. Carbon microfiber dispersion in Portland cement composites was investigated by Chung (2005). The issues of fiber dispersion and bonding between the fibers and the cement matrix were carefully analyzed. The results showed that microscopy does not give correct information about the degree of fiber dispersion. For composites with conductive fibers in a content below the percolation threshold, the electrical conductivity may indicate the degree of dispersion, as better dispersed fibers reduce the electrical resistance of the composite (Figure 2.9). To improve the dispersion silica fume was used: the silica size is similar to the fibers' which allow them enter between the fibers and open the bundles. This fact was confirmed by the reduction of the composite's resistivity. Commercially available surfactants were also employed to achieve better fiber dispersion. The addition of polymer dispersants resulted in lower composite resistivity and higher tensile strength.

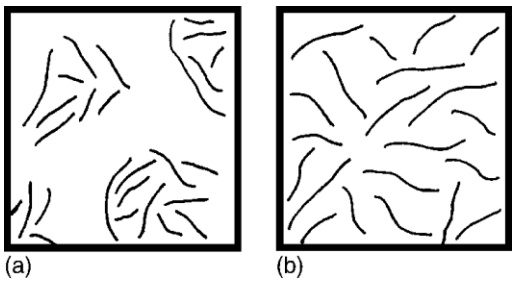

Figure 2.9– Fiber dispersion below the percolation threshold: (a) poor dispersion; (b) good dispersion. Source: Chung (2005)

Surface treatment of the fibers is also a powerful tool to help dispersion and to improve bond to the matrix. The use of ozone treatment (FU and CHUNG, 1998) or silane treatment (XU and CHUNG, 1999) on pristine fibers resulted in 14 and 56 % gain in tensile strength of the cement composite respectively. Furthermore, Young's modulus and ductility of the composites were significantly enhanced.

The positive effect of silica fume on carbon fiber dispersion was confirmed by Sanchez and Ince (2009). A pore refinement phenomenon in carbon fiber-cement composites was observed when incorporating silica fume. The volume of pores in the diameter range of 6 to 200 nm increased as a result of the creation of an inter-fiber pore mesh. On the other hand, no gain in tensile or compressive strength was achieved.

Chung (2001) compared the reinforcing effect of CNFs to that of conventional carbon fibers in cement based composites. CNFs were not found to be as efficient to reinforce cement-based composite materials as carbon fibers were, but still provided some enhancement in the tensile properties of the concrete.

2.3.2 Portland cement-carbon nanotube composites

As mentioned by Baughman *et al.* (2002), the most important challenges of a CNT-composite are uniform dispersion and CNT-matrix bond allowing efficient stress transfer. Because of the costs involved, most of the accessible works published by now analyze the behavior of composites in small specimens, made by the physical mixture of CNTs in the cement matrix – plain cement paste or cement mortar. Both destructive and non-destructive test were used to evaluate the behavior.

The destructive strength tests generally are performed on plain cement paste or mortar specimens with sizes up to 40 mm × 40 mm × 160 mm with maximum concentrations of CNTs in the order of 1 % of the binder content (MAKAR and CHAN, 2009; CHAIPANICH *et al.*, 2010 and KUMAR *et al.*, 2012).Although this 1 % limit seems to be due to economical reason, there should be an upper limit also of the CNT concentration in cement matrices which provide positive effects. Makar and Beaudoin (2003) suggests this upper limit between 2 and 10 %;on the other hand Melo (2009), Collins *et al.* (2012) and Kumar *et al.* (2012) observed reductions in strength with CNT concentrations above 0.5 % with respect to the binder content. Higher CNT concentrations will not disperse well and will form clumps that can be the origin of cracks, thus weakening the composite.

Non-destructive methods include Vickers hardness measurement and nanoindentation. Using Vickers hardness tests, Makar *et al.* (2005) analyzed the effect of CNT addition to cement pastes: no enhancement was found, but CNTs bridging cracks were observed (Figure 2.10) in the scanning electron microscopy (SEM) images. Ibarra *et al.* (2006) measured the hardness of cement pastes containing SWCNTs and MWCNTs by atomic force microscope (AFM): the effect of CNT addition was found to be negative, probably due to dispersion issues. When clumps of agglomerated CNTs exist in cement matrix, they act more like imperfections and possible origins of cracks rather than nano-reinforcement. With the use of nanoindentation, Konsta-Gdoutos *et al.* (2010b) reported a 45 % gain in Young's modulus of cement pastes with addition of 0.08 % of CNTs. A higher quantity of high stiffness *C-S-H* was also presented in the cement pastes with CNT addition (KONSTA-GDOUTOS *et al.* 2010a).

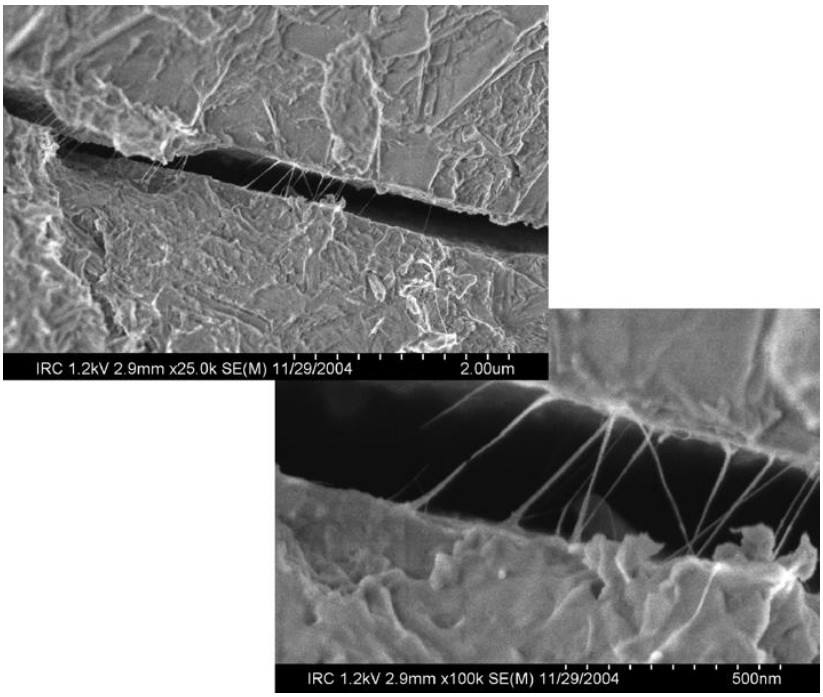

Figure 2.10 – SEM images of CNTs bridging cracks in a cement matrix. Source: Makar *et al.* (2005)

Two basic methods have been developed by researchers to disperse CNTs in the cement matrix. One involves the dispersion of the nanotubes prior to mixing with cement, generally using dispersing agents (surfactants) and sonication, possibly covalent functionalization. The other method tries to disperse nanotubes on the cement particles using a non-aqueous medium (MAKAR and BEAUDOIN, 2003) or growing the nanotubes directly on the cement grains (NASIBULIN *et al.*, 2009).

In the first method the nanotubes need to be surface treated to provide compatibility with water based composites. Different nanotube functionalization methods were tested including covalent and non-covalent types in order to permit incorporation in aqueous media and to provide a good dispersion.

Covalent functionalization of CNTs for application in cement based composites involves mostly carboxyle groups (*–COOH*). Musso *et al.* (2009) obtained smaller compressive and flexural strength using *–COOH* functionalized CNTs in cement mortars with respect to ordinary ones. Even using pristine CNTs, the results were better than with functionalized ones, but not in respect to reference. Following the authors' explanation, the functionalized CNTs may have become so hydrophilic that they adsorbed water and did not let the cement hydrate. Xu *et al.* (2009) also witnessed worse behavior of functionalized CNTs than not functionalized ones in both compressive and flexural strength experiments, although both mortars incorporating nanotubes had enhanced strength with respect to ordinary mortar. At the same time, Li *et al.* (2004a), Batiston *et al.* (2008) and Melo *et al.* (2011) obtained significant gains in compressive and flexural strengths of mortars. In all cases, CNT dispersion was assisted by surfactants (water reducer or superplasticizer admixtures).

Batiston (2012) prepared cement paste composites incorporating carboxylated CNTs in the proportion of 0.05 to 0.10 % of cement mass after treatment with $Ca(OH)_2$. Mechanical strength of such composites did not show any enhancement. Cwirzen *et al.* (2008) compared the effect of the addition of *–COOH* functionalized and not functionalized CNTs on mechanical strength of cement pastes. CNTs with no functionalization had no effect on compressive or flexural strength of the specimens; meanwhile the functionalized ones caused nearly 50 % gain in compressive strength. Flexural strength remained unchanged when comparing with ordinary cement paste. In a later work, Cwirzen *et al.*(2009) suggest that the polyacrylic acid polymer based admixture – that was used in all cases to enhance CNT dispersion – did not provide a strong bond between CNTs and the cement matrix. Xu *et al.* (2009) had the same conclusion and supposed that the effect of CNT addition is rather micro-filling, than real fiber reinforcement. At the same time Makar *et al.* (2005) observed single and bundles of CNTs bridging cracks of approximately 300 nm in cement matrix (Figure 2.9) and proposed as an evidence of reinforcing effect of nanotubes. Table 2.1 presents a summary of these results on the behavior of Portland cement pastes and mortars incorporating covalently functionalized CNTs.

Besides covalent functionalization of CNTs, many different surfactants have been tested to enhance nanotube dispersion. These surfactants include commercially available concrete admixtures of all types and other anionic, cationic and non-ionic dispersants.

Luo *et al.* (2009) analyzed the effect of some surfactants – sodium dodecyl benzene sulfonate, sodium deoxycholate, Triton X-100, gum arabic and cetyltrimethyil ammonium bromide – to disperse CNTs in water and in cement pastes. Significant improvements of compressive and flexural strength of cement paste were obtained. On the other hand, no clear correlation between the stability of aqueous nanotube suspension and cement paste strength was found. Chan and Andrawes (2010) used polyvinylpyrrolidone (PVP) and a long sonication process (40 hours) to disperse CNTs in water prior to casting paste specimens. Flexural strength improved 47 % and a 25 % gain in toughness was achieved. Comparing the effects of gum Arabic and the polyacrylic acid polymer, Cwirzen *et al.* (2008) concluded that gum Arabic has incompatibility problems with concrete and slowed down the cement hydration resulting in lower compressive strength. Yazdanbakhsh *et al.* (2009) studied the dispersion of carbon nanofibers (CNFs) in cement matrix. CNFs' surface areas are smaller compared to CNTs', thus they are easier to disperse. The authors used a method involving sonication and two commercially available surfactants: a nonionic difunctional block copolymer and a polycarboxylate based water reducing agent. Transmission electron microscopy (TEM) and scanning electron microscopy (SEM) images showed poor CNF dispersion in cement matrix with respect to water. This fact indicates that a surfactant that effectively disperses CNTs or CNFs in water sometimes has negative effects on cement hydration and consequently is incompatible with cement composites. Xu *et al.* (2009) suggested that the effect of the addition of CNTs assisted by surfactants is more micro filling rather than fiber reinforcing mechanism. The absence of strong bond between cement matrix and CNTs can be an explanation to this fact (CHAN and ANDRAWES, 2010). The results of these experiments are summarized in Table 2.2.

Like many other nano-sized materials, the addition of CNTs has effects on the pore structure of cement matrix. Li *et al.* (2004a) observed a 64 % reduction of total pore volume and a refinement of pore size due to the addition of CNTs to cement mortars. Metaxa *et al.* (2009) also observed lower pore volume. The reduction of pore size was reported by Yakovlev *et al.* (2006) and Melo *et al.* (2011). Yakovlev *et al.* also observed a reduction of pore percolation in foam cement concrete blocks reinforced with CNTs.

Table 2.1 –Comparison of the results of some works for cementitious composites made by covalently functionalized CNTs

Author	Type of functionalization	CNT content	CNT aspect ratio	Results
Batiston *et al.*, 2008	Carboxyled	0.25-0.5 %	8.3-375	22 % increase in compressive strength of PC mortars
Batiston, 2012	Carboxyled and treated with $Ca(OH)_2$	0.05-0.10 %	17-1500	No enhancement of compressive and flexural strength of PC pastes
Cwirzen *et al.*, 2008	Carboxyled	0.042-0.15 %	200-400	50 % increase in compressive strength of PC pastes
Li *et al.*, 2004a	Carboxyled	0.5 %	16.7-50000	19 and 25 % increase in compressive and flexural strength of PC mortars
Melo *et al.*, 2011	Carboxyled	0.3-0.75 %	8000-90000	12 and 34 % increase in compressive and flexural strength of PC mortars
Musso *et al.*, 2009	Carboxyled	0.5 %	5-1000	Losses in flexural and compressive strength of PC mortars

Table 2.2– Comparison of the results of some works for cementitious composites made by surfactant assisted CNT dispersions

Author	Surfactant used	CNT content	CNT aspect ratio	Results
Chan and Andrawes, 2010	PVP	0.25 %	Not given	47 % increase in flexural strength of PC pastes
Cwirzen *et al.*, 2008	PAA	0.006-0.15 %	1000	No enhancement of compressive and flexural strength of PC pastes
Luo *et al.*, 2009	SDBS, NaDC, TX-100, GA, CTAB	0.2 %	125-750	29 and 21 % increase in flexural and compressive strength of PC pastes
Musso *et al.*, 2009	MAP	0.5 %	500-25000	34 % increase in compressive strength of PC mortars

PVP – polivynilpyrrolidone
PAA – polyacrylic acid polymer
SDBS – sodium dodecyl benzene sulfonate
NaDC – sodium deoxycholate
CTAB – cetyltrimethyl ammonium bromide
DBC – difunctional block copolymer
MAP – modified acrylic polymer

According to Batiston *et al.*, (2008), autogenous shrinkage is not influenced by nanotube addition in the cement matrix. At the same time, Konsta-Gdoutos *et al.* (2010a) observed a slight decrease in the shrinkage of cement pastes prepared with CNT addition in amounts between 0.025 and 0.08 % with respect to cement weight.

CNTs have also effects on cement setting and hydration. Adding a high surface area material to a medium where chemical reactions occur can cause both retardation and acceleration of processes, depending on the nature of the surface of that material. Hydrophilic, functionalized CNTs can capture water molecules or calcium ions and thus cause setting retardation and inhibition of hydration product formation. But when adding not functionalized CNTs, they can act as nucleation sites of hydration product formation accelerating setting and hardening (BATISTON *et al.*, 2010; MAKAR and CHAN, 2009).

The morphology and size of CNTs may have also an influence on the behavior of cement composites. Konsta-Gdoutos *et al.* (2010a) compared two types of commercially available MWCNTs: a short and a long one, with aspect ratios of 700 and 1600 respectively and diameters of 20-40 nm. The amount of CNTs used was between 0.025 and 0.1 % with respect to binder content. The results of flexural tensile strength tests showed increase in comparison to the reference cement paste in all cases. Maximum enhancement occurred with 0.08 % of short CNT and 0.048 % long CNT content. Thus longer CNTs act better as reinforcement in such composites.

Some attempts have been made to computationally model such composites. As many issues are still to be discovered (the nature and the strength of the link between the CNTs and the cement matrix, behavior at different levels of stress), finite element modeling (FEM) can be a powerful tool in these investigations. Rouainia and Djeghaba (2008) used a 3D FEM to determine the Young-modulus of a SWCNT reinforced concrete composite. They analyzed the flexural behavior of a cantilever nano-beam including only one and multiple long and aligned SWCNTs in contents between 1 and 3 % with respect to the volume of the composite. CNT material properties were based on experimental data. A perfect bond between CNTs and cement matrix was assumed. The results revealed a 33 %increase in Young's modulus of the composite when 1 % of SWCNTs was incorporated into the matrix. Further CNT addition resulted in a non-linear behavior with decreasing gains in the composite properties.

A parametric FEM study on the behavior of single MWCNT embedded in cement matrix showed significant influence of the nanotube's elastic modulus on the mechanical behavior of the composite. Increasing the CNT modulus from 500 GPa to 2 TPa resulted in an

increase of the composite compressive strength by 100 %, while the ultimate strain was reduced by 49 % (CHAN and ANDRAWES, 2009).

Although the assumption of a perfect bond between CNTs and cement matrix remains a dream for researchers, it is important to know better the interaction of the two components and the effect of this interaction on the structural behavior of the composite. A recent FEM study showed a raise of the bond shear strength from 6.5 MPa to 20 MPa – due to a better functionalization of the CNTs for example – would lead to significant enhancement in the composite mechanical behavior: 141 % increase in flexural strength, 259 % in ductility and 1976 % in toughness (CHAN and ANDRAWES, 2010).

In order to determine the possible bond strength between a graphitic surface such as carbon nanotubes and *C-S-H*, Sanchez and Zhang (2008) compared the effect of the type and number of functional groups in a molecular dynamics simulation. The functional groups used were *–NH_2*, *=O*, *–OH*, protonated and deprotonated *–COOH* (*–COO^-* with *Ca^{2+}* ions). An increase in the interaction energy with increasing polarity of the functional groups was observed. The values were compared with the interaction energy between pristine graphitic surface and *C-S-H*. The values using *–NH_2*, *=O*, *–OH* and protonated *–COOH* functional groups were 41 to 135 % higher, increasing in this order. Deprotonation of *–COOH* resulted in an increase in the interaction energy with more than an order of magnitude. The nature of attractive forces was purely van der Waals in the case of pristine graphitic surface and had an increasing proportion of electrostatic forces with increasing polarity.

CNT-cement composites show piezoresistivity properties. The addition of CNTs significantly lowers the resistivity of cement based composites (LUO *et al.*, 2009). Besides, the conductivity of such composites changes with the intensity of the applied stresses. Conductivity increases with increasing compressive stresses, and decreases with increasing tensile stresses. Some studies have shown interesting results on the piezoresistivity behavior of composites (LI *et al.*, 2007; GONG *et al.*, 2011; HAN *et al.*, 2011; ANDRAWES and CHAN, 2012), including a direct application as sensors for traffic monitoring (HAN *et al.*, 2009; YU and KWON, 2009). Han *et al.* (2011) found the existence of an optimal CNT content in the composite in order to have the highest conductivity response. This response was observed higher with increasing w/c ratio.

In all previously mentioned investigations high purity and high quality CNTs grown in laboratory were employed. They were added to the cement mix mostly in the form of an aqueous suspension obtained by sonication and/or by the use of surfactants and

functionalization. Nasibulin *et al.* (2009) reported the growth of CNTs and CNFs directly on Portland cement in a continuous process, using the *Fe* content of the clinker as catalyst (Figure 2.11). The authors called the as-received hybrid material carbon-hedgehog composite (CHH). The way CNTs and CNFs are distributed on the cement grains itself could lead to a better dispersion in the matrix. It is worth mentioning that, during the synthesis of the material, the gypsum content of the cement was decomposed, which was confirmed by X-ray diffraction analysis. The strength results of cement paste samples with different CNT-CNF-clinker composite content and made with CHH of different synthesis processes showed a reduction of flexural tensile strength with increasing amount of CNT-CNF. The CNT-CNF-clinker addition to cement paste resulted in more than 100 % gain in compressive strength. The presence of CNT-CNF in the cement paste led to significantly higher values of electrical conductivity in all cases.

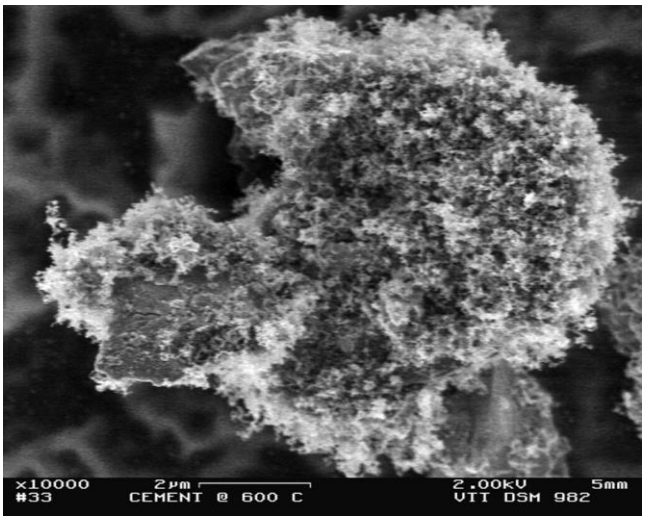

Figure 2.11 – SEM image of cement grain covered by CNTs and CNFs. Source: Cwirzen *et al.* (2009)

This high compressive strength gain was confirmed by Cwirzen *et al.* (2009), who compared the mechanical behavior of cement pastes made with differently processed composite materials in different concentrations. Cement pastes made with 100 % of the composite material showed nearly 100 % increase of the compressive strength. Meanwhile, the flexural tensile strength of cement pastes including different proportions of the above mentioned material showed decreasing values with increasing CHH content. According to the authors, this fact was due to the lower degree of hydration of cement particles. The presence of carbon could lead to higher water demand and lower hydration rate – as it was observed at the addition of some other carbon-containing materials (for example fly ash) to concrete (JOZIĆ and ZELIĆ, 2006). Hlavacek *et al.* (2011) used the same CHH material to produce

mortar and cement paste specimens. Meanwhile paste specimens incorporating CNTs and CNFs presented gains in both compressive strength and fracture energy, no improvement was shown in mortars produced with the same material.

2.4 Synthesis of literature

Nanotechnology offers many tools to bring new and enhanced characteristics to existing building materials. One of the first applications is the formation of a nano-composite made with a classic material and nano-sized particles. Cement based composites – besides having centuries of powerful utilities – have many negative characteristics that can be meliorated by the application of nanomaterials. Carbon nanotubes, for example are a good candidate to enhance tensile behavior.

Cement based materials compose a multi-component system. During hydration, this multi-component system dissociates in ions and forms other products. The characterization of these processes is still subject of ongoing research, since there is not a stoichiometric composition of each compound involved. Furthermore, the addition of any other material may have impacts in these processes. Aggregates create a weak interfacial transition zone around them in the cement matrix, admixtures adsorb on the surface of cement minerals preventing them to interact with other components, or form organo-mineral compounds that cause alterations of the hardened paste's characteristics. The introduction of a nano-sized material such as CNTs thus has complex impacts on the behavior of cement based composites. These effects include modifications in setting and hardening speed (may be both acceleration and retardation) besides the desired effect of creating a reinforcement at nano-level of *C-S-H*.

CNTs synthesis methods are becoming better known and controlled. Nanotubes have been synthesized on many different supports. The growth of CNTs by CVD on clinker particles or other cement-compatible materials is viable as it was shown in various investigations (NASIBULIN *et al.*, 2009, MUDIMELA *et al.*, 2009; DUNENS *et al.*, 2009).The use of raw materials with relatively low level of composition and morphology control result in low level of control of the synthesized nanoparticles and in a lower synthesis efficiency. On the other hand, the use of such materials can significantly reduce the costs of the production when comparing with the use of high purity catalysts.

The key factor to create cement-CNT composites is the dispersion and bond of nanotubes in the matrix. Special surface treatments called functionalization is necessary to

allow the incorporation of highly hydrophobic CNTs in aqueous media like cement paste. These functionalization methods vary from the linking of functional groups by aggressive acid treatments to the simple mixture with surfactants, which create repulsion forces between the nanotubes. Following the published results, the quantity of surfactants necessary to achieve a good dispersion in water would cause negative effects on cement hydration if CNTs are to be employed in a concentration around 0.1 % of cement mass.

Improvements have been observed in the behavior of both fresh and hardened cement pastes and mortars as an effect of CNT addition, in comparison with ordinary cement pastes or mortars. The highest values of enhancement in compressive and tensile strength and elastic modulus are in the order of 30-40 % (LI *et al.*, 2004a; CWIRZEN *et al.*, 2008; BATISTON *et al.*, 2008; XU *et al.*, 2009; METAXA *et al.*, 2009; MELO *et al.*, 2011; MORSY *et al.*, 2011), besides reporting better pore structure (YAKOVLEV *et al.*, 2006; METAXA *et al.*, 2009; MELO *et al.*, 2011).The use of *in-situ* synthesized CNTs/CNFs on cement particles did not have significantly different results of mechanical strength in comparison with high purity CNTs (NASIBULIN *et al.*, 2009).

The methods that seem to give reliable results on mechanical properties of these composites at hardened state include classical compressive, flexural (fracture energy) and splitting tensile tests, nanoindentation and hardness measurements. At the same time SEM imaging of CNT dispersions in hardened cement paste seem to give contradictory impressions. Makar *et al.* (2005) suggested that the visible CNTs bridging a crack of the cement paste would be a proof of the reinforcing effect. Meanwhile other researchers (CWIRZEN *et al.*, 2009; XU *et al.*, 2009) suggest that the CNTs did not enhance the mechanical behavior of their composites so much because the loss of bond between the nanotubes and the matrix. It seems reasonable, that if CNTs can be easily identified on SEM micrographs, it is because of poor dispersion or poor bonding to cement matrix. The absence of visible CNTs on the images could be due to that the hydration products covered completely them and created a strong link.

One of the objectives of present work, the synthesis of CNTs/CNFs on clinker particles using industrial by-products as catalyst particles has not been reported before. The synthesis products are to be characterized quantitatively and qualitatively. An important factor when applying a new material to the construction industry is the compatibility with existing methods or equipment for production and characterization. Nano-structured cement therefore should be analyzed by common investigation techniques used to characterize ordinary

Portland cement. The mechanical strength of Portland cements are determined by tests on mortar specimens according to NBR 7215 (1996) Brazilian standard. In order to evaluate the effect of CNT/CNF addition on the mechanical behavior of Portland cement, mortars are to be prepared with standard composition containing nano-structured material and compared with reference mortars with the same composition except the CNT/CNF content. BET and *He* pycnometry are adequate tools to characterize the pore structure and density of hardened cement composites. Melo (2009) used these techniques to evaluate the changes in the pore structure of mortar samples due to the incorporation of high quality CNTs. The effect of nano-structured material addition should also be analyzed by these techniques.

3

SYNTHESIS AND CHARACTERIZATION OF NANO-STRUCTURED MATERIALS

3.1 Introduction

The first step in the production of cement-based composites made with nanotubes was the synthesis of nano-structured materials. The synthesis was performed on low cost (compared to other materials used for CNT synthesis) cement-compatible materials: Portland cement clinker and silica fume with the addition of steel-making byproducts such as ground iron ore, steel mill scale and converter dust. The objective of the investigations was to determine optimal synthesis parameters and catalyst composition. Comparative investigations were performed with different catalyst preparations and different synthesis temperatures, duration and carbon source gas concentrations. The main points of the evaluation were the efficiency and the morphology of the synthesized products.

A characterization of the nano-structured cement was conducted to obtain typical cement properties like setting time, composition and Blaine fineness. These results are compared to conventional Portland cement data.

3.2 Characterization of the materials used for synthesis

3.2.1 Electron probe microanalysis

Electron probe microanalysis is a non-destructive analytical method used to obtain detailed composition data of a sample material. It is a combination of the SEM and XRD techniques. The sample is hit by an electron beam. The instrument is equipped by SE or BSE detectors to help aiming of the beam. The electron beam also generates X-ray radiation of the sample that is characteristic of the material. When wavelength dispersive X-ray spectroscopy (WDS) is used, this radiation passes through a collimator, then hits a crystal with known diffraction parameters and finally is intercepted by a counter – all mounted on a goniometer that permits to position the elements according to the characteristic radiation of each (excepting very light) chemical element. The diffraction at the crystal occurs according to the above mentioned Bragg's law. WDS technique counts the photon impacts of a single radiation wavelength at once; meanwhile energy dispersive X-ray spectroscopy (EDS) gives a general view of the chemical composition of a sample analyzing the entire spectrum. Thus WDS analysis is more precise but is slower than EDS. The sample for microprobe analysis has to be compacted and polished to obtain a leveled surface and is maintained at vacuum. Modern microprobe analyzers are equipped by 3 to 5 or more WDS systems to analyze the same number of elements at a time. The resolution of the X-ray spectroscopy is limited to the volume of the material that is emitting characteristic X-radiation. To yield chemical composition several points of the sample have to be mapped. (SKOOG and LEARY, 1992)

3.2.2 Analysis procedures

The catalysts used during the synthesis were composed of a support material and metallic catalyst particles.

The quantitative composition of the support materials and metallic catalyst particles – when not informed by the provider – was determined by a JEOL JXA-8900R type electron microprobe located at the Laboratory of Microanalysis, UFMG. The samples for this analysis were compacted in a pellet of approximately 1 mm height. The results were calculated for each sample as the average of the composition of 10 points analyzed.

The composition of the metallic catalyst particles was analyzed qualitatively at the Laboratory of Cristallography, UFMG, by XRD in a Rigaku Geigerflex 2037 type instrument equipped with copper or cobalt X-ray tubes, as specified. This technique was also used to

determine iron crystallite size of the catalysts based on the Scherrer equation. The standard used in all cases was silica. The detector was moved at steps of 0.1° for phase identification of iron oxide and 0.02° for crystallite size analysis.

3.2.3 Support materials

Catalyst support materials used during the investigations included Portland cement clinker and silica fume. All of these materials were produced at high temperatures and thus have stable characteristics at typical carbon nanotube synthesis temperatures by CVD (600 to 800 °C).The materials were provided by Intercement Brasil SA.

Clinker

Portland cement clinker was received ground to the fineness of Brazilian type CP-I cement. The composition, determined by electron microprobe analysis, is presented in Table 3.1.

Table 3.1 – Chemical composition of Portland cement clinker determined by electron microprobe analysis. The compound annotations refer to any type of oxides of that type of element.

Compound	Percentage
MgO	2.12
SO_3	0.55
MnO	0.05
Al_2O_3	3.94
K_2O	1.33
Fe_2O_3	3.08
SiO_2	17.17
CaO	54.67

Silica fume

Silica fume produced by Silmix was used as received. The composition of the silica fume was given by the providers and is presented in Table 3.2.

Table 3.2– Chemical composition of silica fume as given by the provider

Compound	Percentage
Fe_2O_3	0.04
CaO	0.20
Al_2O_3	0.08
MgO	0.63
Na_2O	0.15
K_2O	0.40
SiO_2	96.47
H_2O	0.61

3.2.4 Catalyst particles

Metal catalyst materials included steel mill scale, ground iron ore and converter dust. For CNT synthesis an important parameter of the catalyst particles is the mean crystallite size, as it serves as a template for the nanotube diameter. Iron oxide phases were identified and the crystallite size was calculated using XRD. Detailed difractograms of every catalyst particle are presented in Annex A.

Ground iron ore

Ground iron ore was received from Vale. The main composition was identified to be hematite (Fe_2O_3) by XRD. The purity was 77 %, based on electron microprobe analysis (Table 3.3). The mean hematite crystallite size was 210 nm, as determined by the Scherrer method (see chapter 3.2.1).

Table 3.3 – Chemical composition of iron ore determined by electron microprobe analysis. The compound annotations refer to any type of oxides of that type of element.

Compound	Percentage
MgO	0.03
SO_3	0.02
MnO	1.48
Al_2O_3	2.41
K_2O	0.02
Fe_2O_3	77.32
SiO_2	1.74
CaO	0.06

Steel mill scale

Steel mill scale was received in the form of a rough powder and was ground using a ball mill. The composition is presented in Table 3.4. XRD analysis identified the iron-containing phase as wüstite (*FeO*). The mean crystallite size was 80 nm.

Table 3.4 – Chemical composition of steel mill scale determined by electron microprobe analysis. The compound annotations refer to any type of oxides of that type of element.

Compound	Percentage
MgO	0.04
SO_3	0.01
MnO	1.00
Al_2O_3	0.27
K_2O	0.01
FeO	85.45
SiO_2	1.10
CaO	0.06

Converter dust

The converter dust, given by Arcelor Mittal in the form of a fine powder, was used also as-received. The composition of the furnace dust, determined by EDS analysis, was given by the provider and is presented in Table 3.5. Iron content of converter dust was identified as hematite (Fe_2O_3). Mean crystallite diameter was 106 nm.

Table 3.5 – Chemical composition of converter dust based on an EDS study (mass %)

Element	Percentage
C	3.01
O	32.47
Mg	3.22
Si	0.74
Ca	6.80
Fe	55.76

Clinker

Clinker contains approximately 3 % of iron oxide (of C_4AF phase), as presented above (Table 3.1). The form of iron oxide in this case was hematite (Fe_2O_3). Mean crystallite size was 122 nm.

Conclusion of the catalyst particle analysis

Iron oxide was present in clinker, ground iron ore and converter dust in the form of hematite (Fe_2O_3). Steel mill scale was composed of wüstite (FeO). Iron content was determined based on the chemical formula of iron oxide present and its percentage of the material composition. The weight ratio of iron as element for every catalyst particle is given in Table 3.6.

Table 3.6– Iron content of the catalyst particles

Catalyst particle	Fe content [%]
Clinker	2.15
Ground iron ore	54.08
Steel mill scale	66.42
Converter dust	55.76

The crystallite size of the catalyst particles are presented in Table 3.7. It can be seen, that ground iron ore has the larger *Fe* crystallites; meanwhile the smaller crystallites of clinker, steel mill scale and converter dust are closer to typical CNT diameters thus are probably better for CNT synthesis.

Table 3.7– Fe crystallite size of catalyst particles as determined by X-ray diffraction

Catalyst particle	Crystallite size [nm]
Clinker	122
Ground iron ore	210
Steel mill scale	80
Converter dust	106

3.3 Synthesis procedures

3.3.1 Catalyst preparation

Catalysts were prepared as a mixture of support material and catalyst particles. The iron content of the catalyst particle was considered as given in Table 3.6. The catalyst components were mixed in a ball mill during at least 24 hours.

3.3.2 CVD reactor

Every synthesis process of CNTs was carried out in a CVD reactor with three controllable zones of 100 cm total length (Figure 3.1). The reactor tube was made of silicon carbide (*SiC*) and had an inner diameter of 120 mm. Before each process the catalyst material was weighed and placed in *SiC* boats. Each batch process was done using 30 to 300 g of catalyst material. The mass of the different types of catalyst materials was determined in order to get a similar bulk volume. Synthesis was performed under controlled flow with argon (1500 sccm flow) as carrier gas and as carbon source gas acetylene or ethylene, as specified. During the heating up and cooling argon flow was maintained to ensure inert atmosphere.

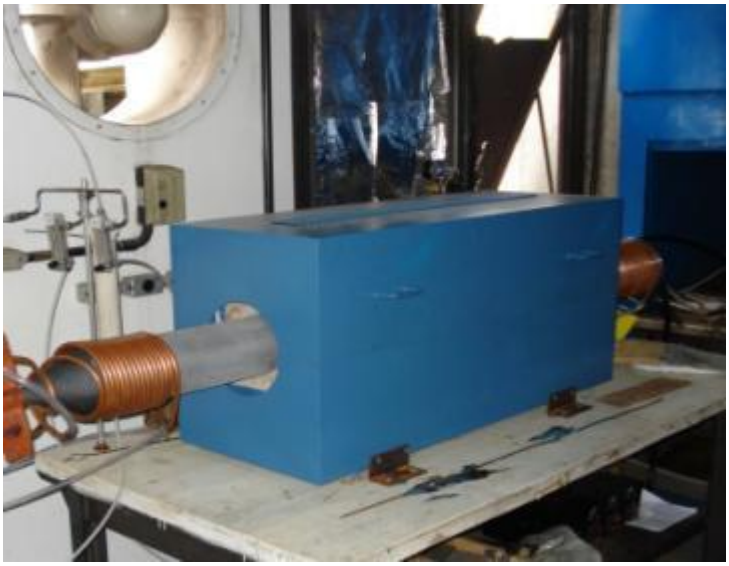

Figure 3.1– The CVD reactor used during the investigations

3.3.3 Synthesis based on clinker

Pure clinker, clinker with different quantity of steel mill scale, ground iron ore or converter dust additions were prepared and used as catalyst for nanotube synthesis. Investigations were performed to determine optimum synthesis parameters such as catalyst iron addition, process duration, temperature and gas flow rates. Table 3.8 shows the catalysts compositions investigated. The amount of added iron catalyst particles were between 0 and 10 % of the clinker mass. Synthesis temperature varied between 775 and 850 °C. Synthesis duration varied between 30 and 120 minutes. The acetylene or ethylene gas flow varied between 300 and 600 sccm.

An in-situ functionalization method linked to the synthesis of nano-structured clinker was developed (Appendix 1). The method involves ammonia gas that was passed through the reactor together with the other gases during the synthesis process. The objective of this functionalization was to create nitrogen containing functional groups on the surface of the nanotubes and nanofibers.

Table 3.8– Composition of the clinker based catalysts for nano-structured material synthesis

Catalyst	Support	Catalyst particles	Total Fe content [%]
C-0	clinker	-	2.15
CO-5	clinker	iron ore	7.15
CS-5	clinker	steel mill scale	7.15
CD-1	clinker	converter dust	3.15
CD-2.5	clinker	converter dust	4.65
CD-5	clinker	converter dust	7.15
CD-10	clinker	converter dust	12.15

3.3.4 Synthesis based on silica fume

Nanotubes were also synthesized on silica fume with 2.5 % iron addition. The added iron was converter dust. Table 3.9 shows the composition of the silica fume based catalyst. The parameters of the synthesis were 500 sccm acetylene flow, 750 °C temperature and 30 minutes processing time.

Table 3.9– Composition of the silica fume based catalysts for nano-structured material synthesis

Catalyst	Support	Catalyst particles	Total Fe content [%]
FS-2.5	silica fume	converter dust	2.50

3.4 Characterization of synthesis products

3.4.1 Thermogravimetry

Thermogravimetry is a powerful tool to determine the quantity (mass) of different substances and/or reaction products of a material. The mass of a sample is continuously analyzed as function of time or temperature as the temperature of the sample is raised following a predefined heating rate, under controlled atmosphere. An instrument of thermogravimetry consists of a sensitive analytical scale, a furnace, a gas feeding system and a control and data acquisition and display unit. The capacity of the scale generally is ranging between 1 mg and 100 g in modern instruments. It is thermally isolated of the furnace but the

sample holder is housed in it. The temperature range of most furnaces is between room temperature and 1500 °C. Heating and cooling rates of the furnace can be selected to as high as 200 °C/min. Evidently, the slower the heat ramp is, the more precise the results will be.

The mass or mass percent versus temperature or time plot is called thermogram. Generally the first derivate of this graph is also plotted, the differential thermogram. The derivative curve may reveal details (peaks) that are not detectible in the original thermogram curve and also gives more precisely the temperature peaks corresponding to the highest mass loss or gain rate. (SKOOG and LEARY, 1992)

3.4.2 Scanning electron microscopy

When an electron beam hits a target surface, different types of radiations are emitted. These radiations are characteristic of the upper few nanometer of the target material under the area of the electron beam. The more focused the electron beam is and the smaller the area of the electron beam as it hits the target, the higher the resolution will be of any image obtained of the characteristic radiations.

In scanning electron microscopy (SEM), the surface of the solid sample is swept by an electron beam in a raster pattern. The electrons are emitted by an electron gun. The electron beam which is accelerated by a voltage between generally 1-20 kV passes through a system of magnetic condenser and objective lenses and hits the target at a spot of 3 to 100 nm diameter area. Two electromagnetic coils deflect the beam in *x* and *y* directions which allow the scanning of the surface. Two of the signals produced by the electron beam hitting the surface are secondary electrons (SE) and backscattered electrons (BSE). SE and BSE signals are used in SEM to make images of the sample. The magnification of the image can be changed increasing or decreasing the width of a single scan line across the sample. Modern scanning electron microscopes allow a magnification from 10× up to ~1,000,000×. To allow imaging of the sample, it has to be electric and thermal conductive. If the sample is not conductive itself, a few nanometer carbon or gold coating is applied. The sample holder can be moved in all *x*, *y* and *z* directions and rotated about each axis, so the surfaces of the samples can be viewed in almost every perspective. To enhance the quality of imaging, higher voltage is applied and high vacuum (10^{-6} Pa) is created in the sample chamber. (SKOOG and LEARY, 1992)

3.4.3 Procedures for characterization of synthesis products

After the processes the products were collected and were characterized. The carbon yield was determined by TGA, using a TA Instruments SDT-2960 (CDTN) or Shimadzu DTG-60H (Nanomaterials Laboratory) equipment and by the combustion of the carbon material at 800 °C in an oven. The amount of nano-structured material used for combustion varied from 200 mg to 1 g. Due to the smaller quantity of sample used for TGA (approx. 3 mg) the nanotube content values obtained by combustion were considered more representative. TGA results were used to evaluate purity and proportion of the synthesized CNTs and CNFs. Combustion temperature is influenced by the degree of CNT structural perfection: higher temperatures may correspond to a lower quantity of defects (TRIGUEIRO *et al.*, 2007).

Characterization also included SEM imaging in a JEOL JSM-840A (Laboratory of Microanalysis, UFMG) or Quanta 200 – FEG – FEI – 2006 (Center of Microscopy, UFMG) equipment with magnification up to 200,000×. In order to assure sample conductivity, 1 to 2 nm gold coating was used.

3.4.4 Nano-structured clinker

The more efficient synthesis parameters were investigated focusing on the synthesis duration and temperature, carbon source gas flow rate and different types of iron addition.

The objective of the first analysis was to determine optimal synthesis time in order to achieve highest carbon deposit rate. Pure clinker was used as catalyst. The durations of the processes were 30, 60 and 120 minutes. Acetylene or ethylene was used as carbon feedstock; the other parameters were maintained constant: 300 sccm gas flow and 775 °C temperature. The results of the three processes can be compared in Table 3.10. Higher carbon deposit rates were achieved with longer processes. At the same time the increase in efficiency with the increase of process duration from 30 to 60 minutes was higher (from 3.03 to 5.08 %) than that achieved by increasing from 60 to 120 minutes (from 5.08 to 6.33 %).

Table 3.10 – Effect of synthesis time changes on the efficiency of the CNT/CNF synthesis on pure clinker

Catalyst identification	Carbon source	Gas flow [sccm]	Synthesis temperature [°C]	Synthesis duration [min]	Mass loss at 800°C [%]
C-0	ethylene	300	775	30	3.03
C-0	acetylene	300	775	60	5.08
C-0	ethylene	300	775	120	6.33

The optimal quantity of carbon disposable to form CNTs and CNFs was determined by comparing different acetylene flow rates: 300, 500 and 600 sccm. Other parameters were kept constant: 775 °C temperature and 60 minutes synthesis duration. Pure clinker was used as catalyst. The efficiencies obtained are shown in Table 3.11. Acetylene flow equal to 500 sccm resulted in higher efficiency (6.50 %) than the processes when lower or higher gas flow rates were employed (both 5.08 %).

Table 3.11 – Effect of carbon source gas flow rate on the efficiency of CNT/CNF synthesis on pure clinker

Catalyst identification	Carbon source	Gas flow [sccm]	Synthesis temperature [°C]	Synthesis duration [min]	Mass loss at 800°C [%]
C-0	acetylene	300	775	60	5.08
C-0	acetylene	500	775	60	6.50
C-0	acetylene	600	775	60	5.08

The effect of temperature on the synthesis efficiency was investigated next. Two processing temperatures were studied: 775 and 850 °C. Other parameters were kept constant: 500 sccm acetylene flow and 60 minutes process time. Pure clinker was used as catalyst. These results are shown in Table 3.12. It can be seen, that higher temperature resulted in a lower carbon deposit rate. The decrease was from 6.50 to 5.70 %.

Table 3.12 – Effect of temperature on the efficiency of CNT/CNF synthesis on pure clinker

Catalyst identification	Carbon source	Gas flow [sccm]	Synthesis temperature [°C]	Synthesis duration [min]	Mass loss at 800°C [%]
C-0	acetylene	500	775	60	6.50
C-0	acetylene	500	850	60	5.70

The effect of the addition of different iron sources on the synthesis efficiency was also investigated. The amount of 5 % of iron was added to the clinker of the following sources: ground iron ore, steel mill scale and converter dust. This 5 % addition corresponded to the iron element content of the material, according to Table 3.6. The synthesis parameters were 500 sccm acetylene flow and 60 minutes of process duration. Temperature of the synthesis was 775 or 850 °C. It should be noted that these investigations were performed partially before the results of the effect of the higher temperature was concluded. The results of production are shown in Table 3.13. Clinker with steel mill scale addition had similar efficiency (6.29 %) as pure clinker (6.50 %). On the other hand, ground iron ore and converter dust addition resulted in lower carbon deposit rates (2.40 and 3.89 %, respectively).

Table 3.13 – Effect of the addition of different iron oxide sources to clinker on the efficiency of CNT/CNF synthesis

Catalyst identification	Source of additional iron	Total Fe content [%]	Synthesis temperature [°C]	Mass loss at 800°C [%]
C-0	-	2.15	850	5.70
C-0	-	2.15	775	6.50
CO-5	Ground iron ore	7.15	775	2.40
CS-5	Steel mill scale	7.15	775	6.29
CD-5	Converter dust	7.15	850	3.89

The synthesis products were analyzed by SEM and the presence of fiber-like structures was confirmed in all cases (Figures 3.2 to 3.5). The diameter of these products ranged within typical carbon nanotube and nanofiber values. The size and morphology of the product varied with respect to the catalyst preparation. Pure clinker and clinker with ground iron ore addition produced CNTs and CNFs with a curly structure, meanwhile steel mill scale and converter dust addition resulted in straight CNTs/CNFs. Maximum length of the products was in all

cases in the order of tens of microns. Mean diameter of nanotubes and nanofibers was between 80 and 120 nm in the case of pure clinker and clinker with ground iron ore catalysts. Smaller mean diameters between 50 and 80 nm were found for products synthesized on clinker with steel mill scale and converter dust addition.

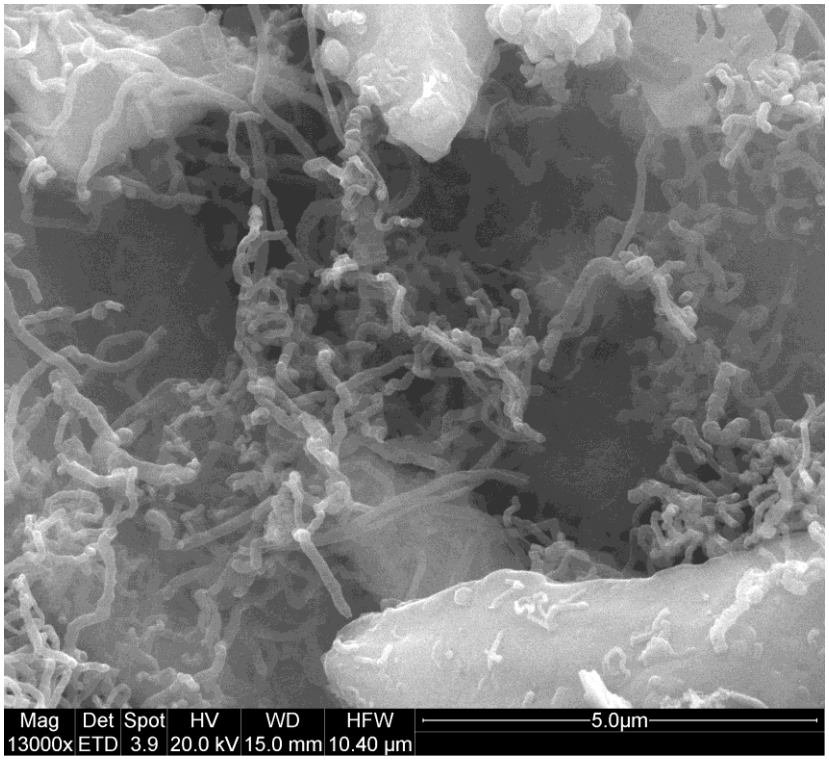

Figure 3.2– SEM image of curly CNTs and CNFs grown on pure clinker

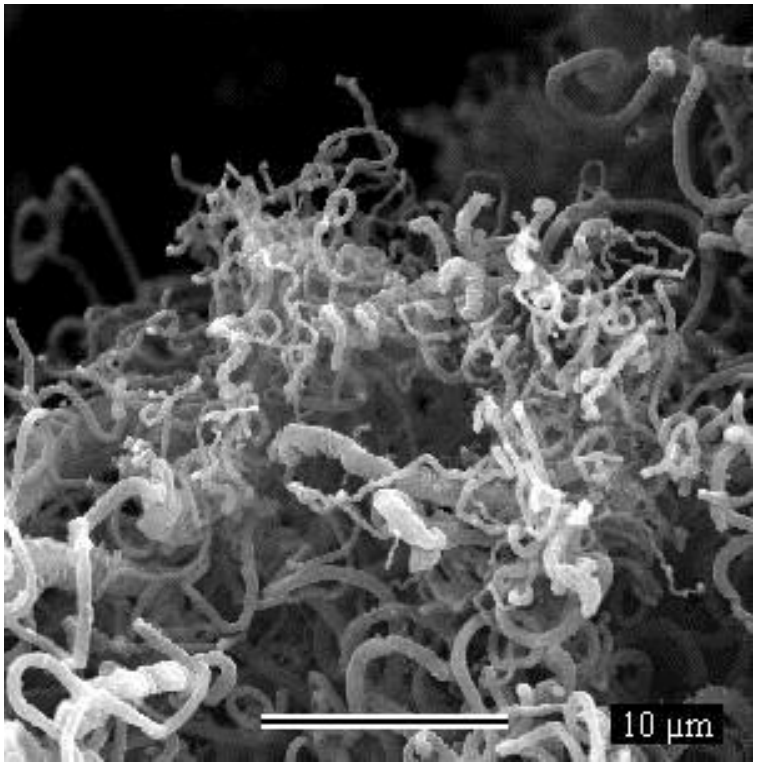

Figure 3.3– SEM image of curly CNTs and CNFs with high dispersion of size grown on CO-5 catalyst

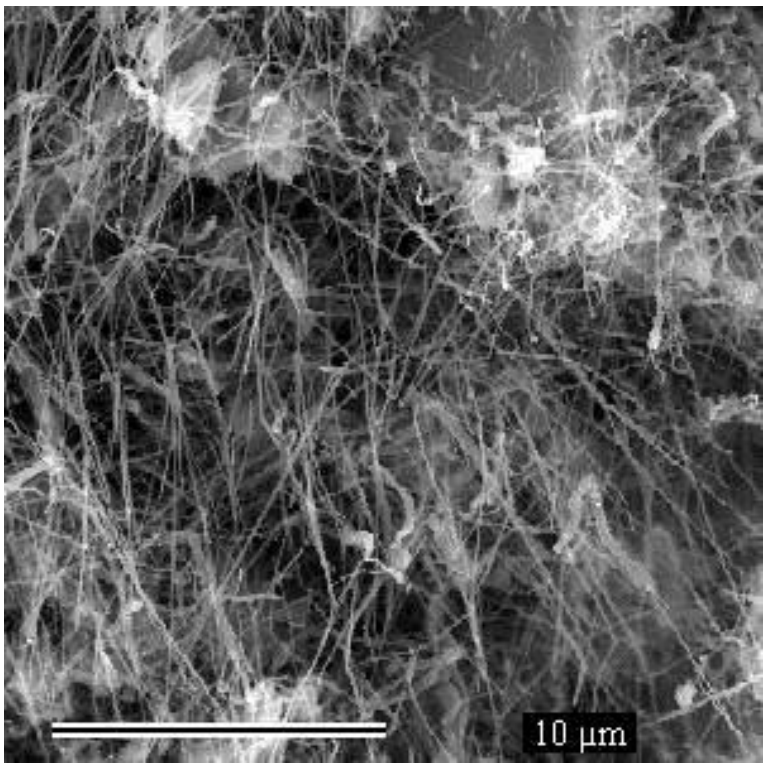

Figure 3.4 – SEM image of straight CNTs and CNFs grown on CS-5 catalyst

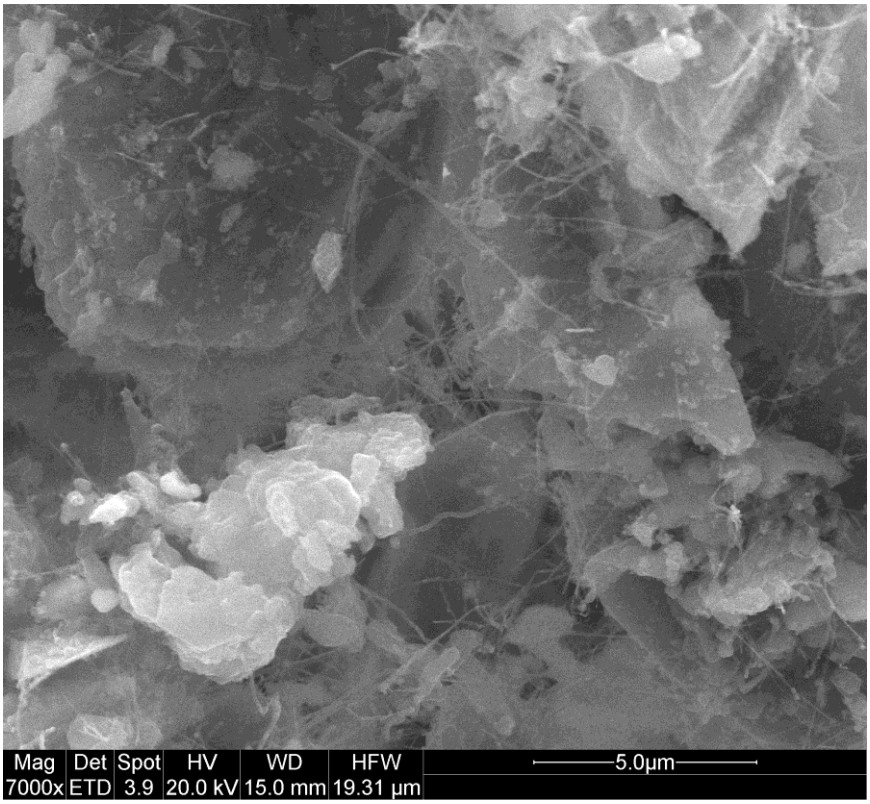

Figure 3.5 – SEM image of straight CNTs and CNFs grown on CD-5 catalyst

Thermogravimetric analysis of the products grown on clinker with steel mill scale addition shows two mass loss peaks, probably corresponding to two main types of CNTs/CNFs formed. The temperatures corresponding to these peaks were 572°C and 623 °C (Figure 3.6). One can see that a higher mass loss was observed for the first peak with respect to the second.

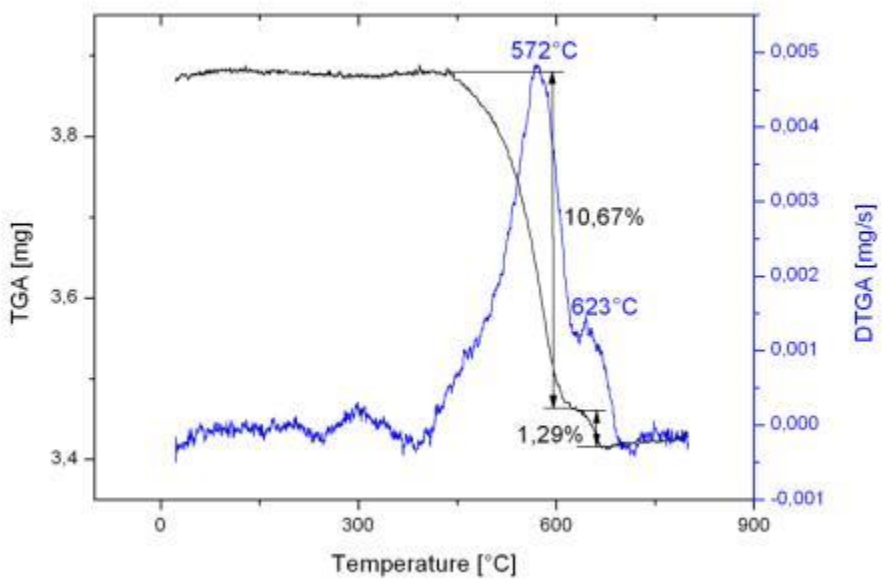

Figure 3.6– TGA and DTG curves of synthesis products grown on clinker-steel mill scale catalyst (CS-5)

Clinker with different percentages of iron addition was prepared and the efficiency of these catalysts was investigated. The iron addition varied from 1 to 10 % in mass. The used iron source was converter dust. The synthesis parameters were 500 sccm acetylene flow, 850 °C temperature and 60 minutes process duration. The results are presented in Table 3.14. Efficiency increased with increasing iron addition up to 2.5 % content (6.14 %). Further iron addition resulted in lower efficiency.

Table 3.14– Effect of the quantity of iron (converter dust) added to clinker on the efficiency of CNT/CNF synthesis

Catalyst identification	Total Fe content [%]	Carbon source	Synthesis temperature [°C]	Synthesis duration [min]	Mass loss at 800°C [%]
C-0	2.15	acetylene	850	60	5.70
CD-1	3.15	acetylene	850	60	4.76
CD-2.5	4.65	acetylene	850	60	6.14
CD-5	7.15	acetylene	850	60	3.89
CD-10	12.15	acetylene	850	60	1.20

SEM images of the samples of CNTs/CNFs grown on clinker with different iron addition ratios revealed some influence of this ratio on the product morphology (Figures 3.7 to 3.10). Iron addition up to 5 % of clinker mass resulted in nanotubes and nanofibers with similar appearance, length and diameter. On the other hand, the products grown on the CD-10 catalyst showed more curly structure and higher dispersion of size.

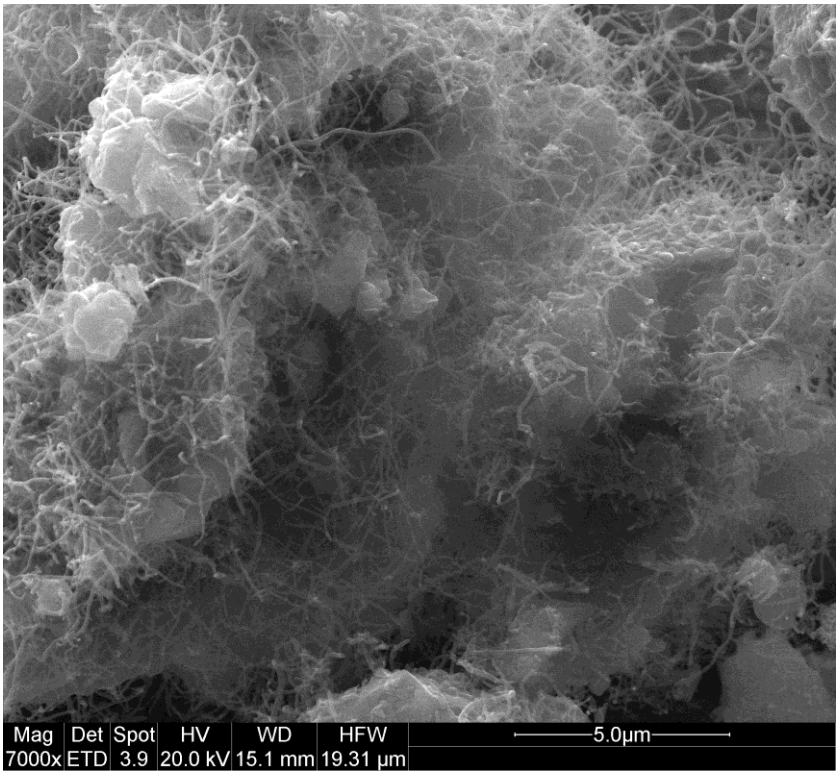

Figure 3.7 – SEM image of CNTs/CNFs grown on CD-1 catalyst

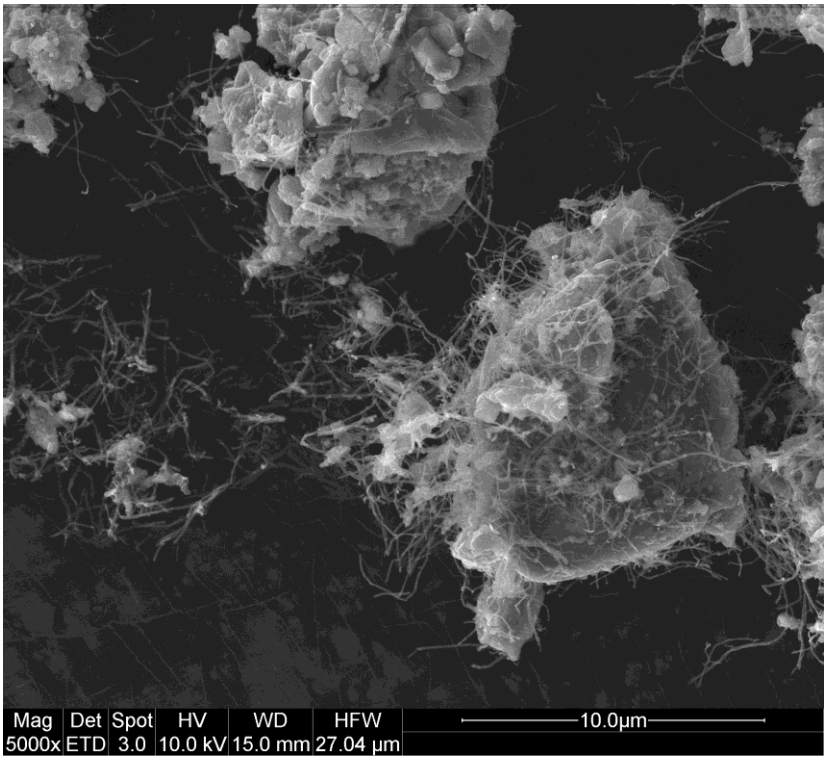

Figure 3.8– SEM image of well distributed CNTs and CNFs on clinker particles (CD-2.5 catalyst)

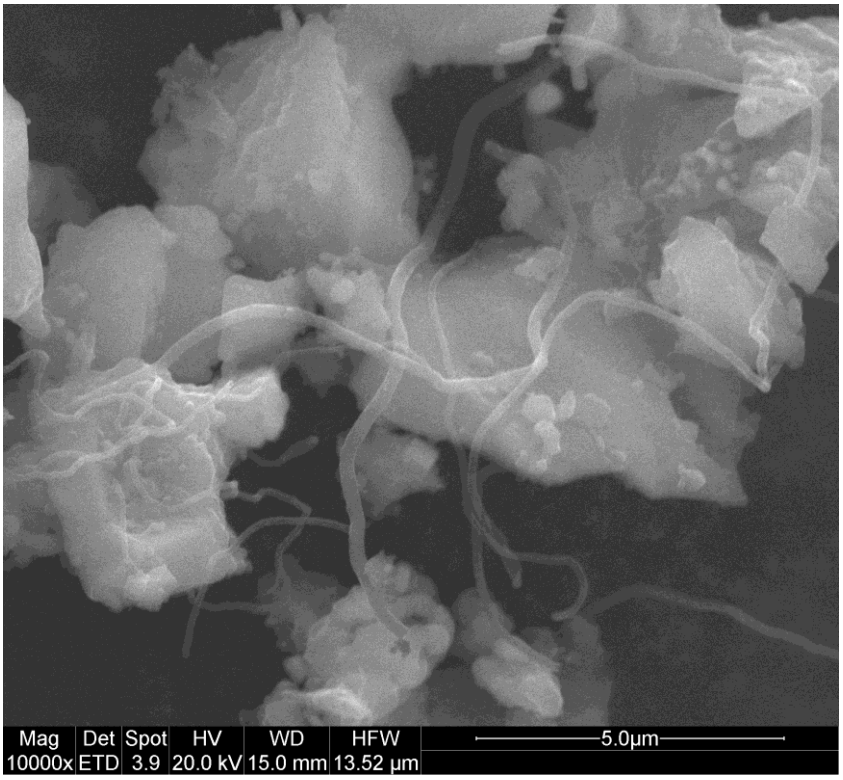

Figure 3.9 – SEM image of CNTs/CNFs synthesized on CD-5 catalsyt

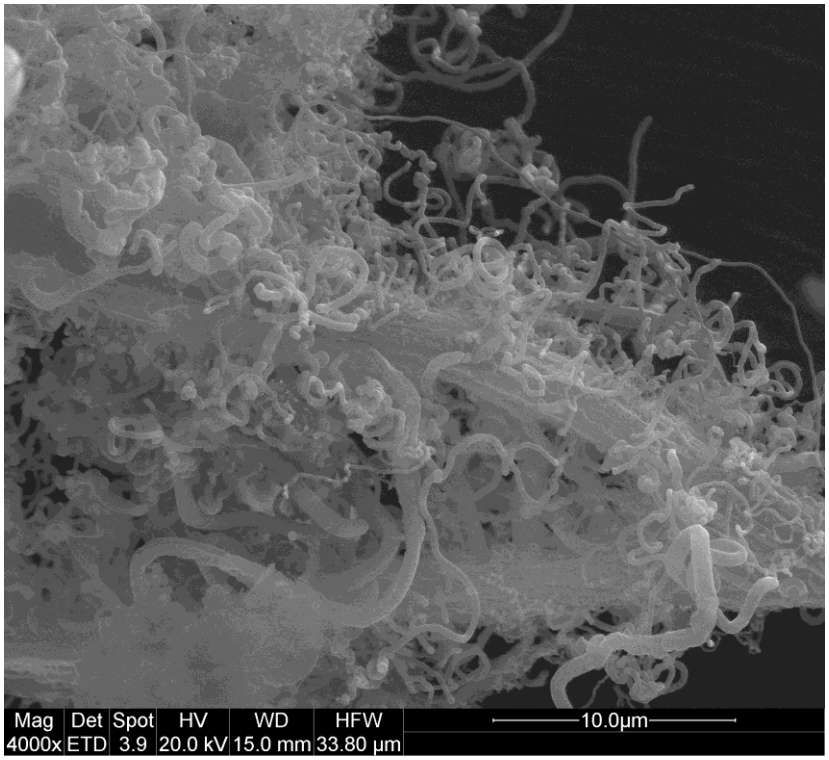

Figure 3.10– SEM image of synthesis products grown on high Fe-content clinker based catalyst (CD-10)

Figure 3.11 shows the histogram of the diameter values measured on SEM images of CNTs/CNFs grown on CD-2.5 catalyst. The values are dispersed, and show two diameter ranges of greater occurrence: between 40 and 50 nm and between 60 and 80 nm.

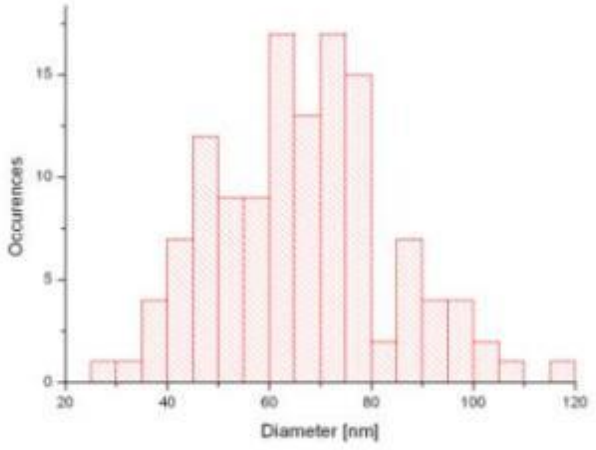

Figure 3.11 – Histogram of the diameters of CNTs/CNFs grown on clinker with 2.5 % iron addition (converter dust) measured on SEM images

Thermogravimetric analysis of the products grown on CD-2.5 catalyst also shows two mass loss peaks. In this case, the temperatures corresponding to these peaks were 525°C and 620 °C (Figure 3.12). A higher mass loss was also observed for the first peak with respect to the second.

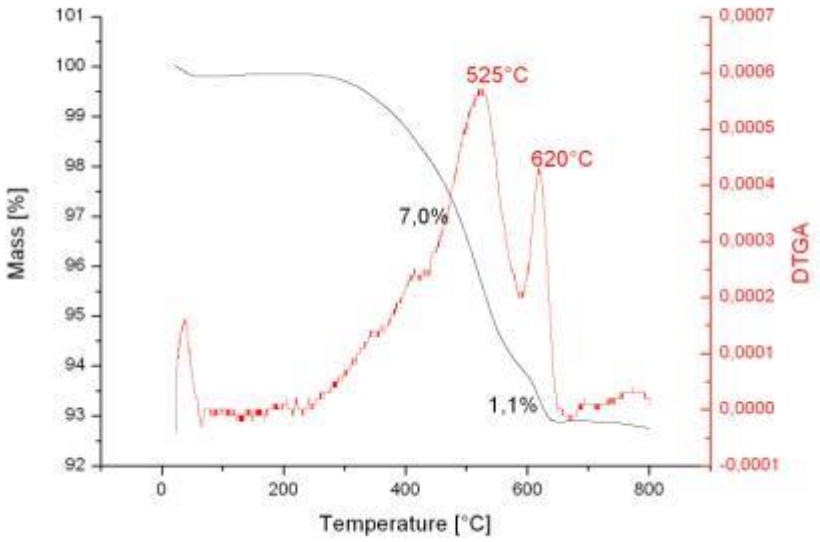

Figure 3.12– TGA and DTG curves of synthesis products grown on clinker-converter dust catalyst (CD-2.5)

According to the production results presented before, the following synthesis parameters were approved to be the best, using pure clinker catalyst: 60 minutes of process duration, 500 sccm of acetylene/ethylene flow and 775 °C temperature.

The main points for interpreting SEM images were product morphology and nanotube/nanofiber diameter. For structural reinforcement CNTs and CNFs with straight form and smaller diameter may have better performance. Longer and straighter nanotubes can attach cement particles of a longer distance. Smaller diameter may indicate a structure with less defects and a shape closer to a perfect CNT and consequently with better tensile behavior (SALVETAT *et al.*, 1999). Therefore straighter and longer nanotubes and nanofibers with smaller diameters were considered as better option for incorporation in cement mortars.

Pure clinker produced short, curly fibers. This morphology suggests that the CNTs/CNFs are of poorer tensile behavior (SALVETAT *et al.*, 1999).

Additional iron sources added to the clinker modified the production of the synthesis. Meanwhile ground iron ore did not have positive effects on production, steel mill scale and converter dust addition had good production with respect to pure clinker. The optimum addition was found to be 2.5 % of iron with respect to clinker mass in the case of converter dust.

Ground iron ore addition also produced CNTs/CNFs with curly structure. Meanwhile with the addition of converter dust or steel mill scale the products were more straight and with smaller diameter. The diameter of the nanotubes depended mostly on the type of catalyst particle used during the synthesis. According to the crystallite size determined by XRD, the smaller crystallites of converter dust and steel mill scale produced nanotubes and nanofibers with smaller diameter. At the same time high variability of the synthesized products could be seen in all cases as a result of the employed raw materials with low quality and composition control.

DTGA diagrams of nanostructured clinker show two peaks. In the case of clinker with steel mill scale addition as catalyst the two peaks were found to be at 572 and 623 °C. The converter dust addition modified the position of the first peak to 525 °C. The lower temperature of ignition of the products may indicate a nanotube structure with more defects. On the other hand, the ratio of mass loss between the higher and lower peaks in the case of steel mill scale catalyst is lower (1.29 to 10.69 = 0.12) than in the case of converter dust addition (1.1 to 7.0 = 0.16). Thus converter dust produces more nanotubes which have higher ignition temperature and consequently a more perfect structure.

Covalent functionalization of nano-structured clinker through ammonia treatment

A process to *in-situ* synthesize ammonia functionalized nanotubes has been developed (Appendix 1). The used catalyst was composed of clinker with 2.5 % iron addition in the form of converter dust. The synthesis was carried out at 750 °C using acetylene and ammonia gases with flows of 300 and 150 sccm respectively. The process duration was 30 minutes. These process parameters were chosen based on the results obtained with silica fume as catalyst support (see Chapter 3.4.3).

Figures 3.13 and 3.14 show SEM images of the ammonia functionalized nano-structured clinker. Diameters of the CNTs/CNFs had an average of 68.5 nm (see histogram in

Figure 3.15), which is practically equal to that of the nanotubes synthesized without ammonia (66.5 nm, see histogram in Figure 3.11).

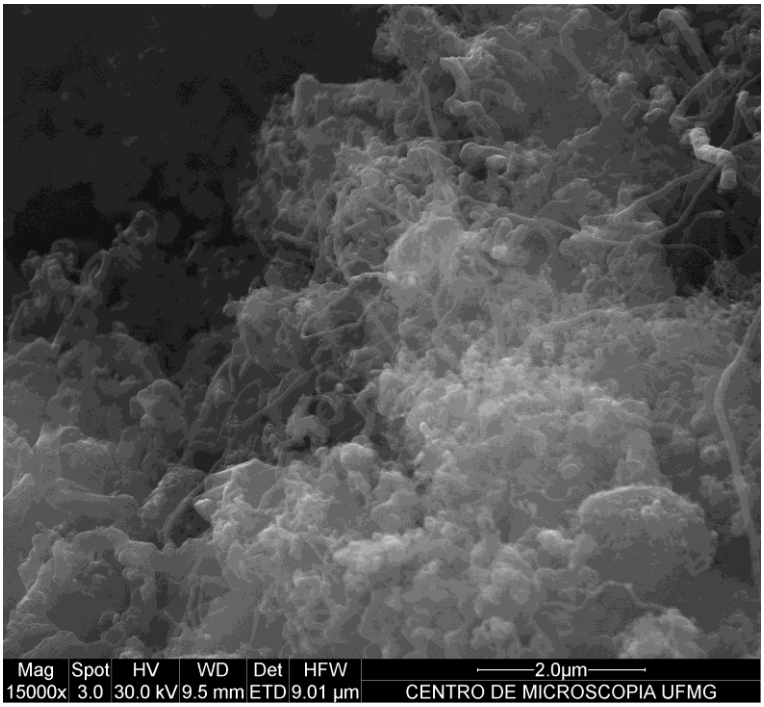

Figure 3.13 – SEM image of CNTs/CNFs synthesized on clinker and functionalized with ammonia

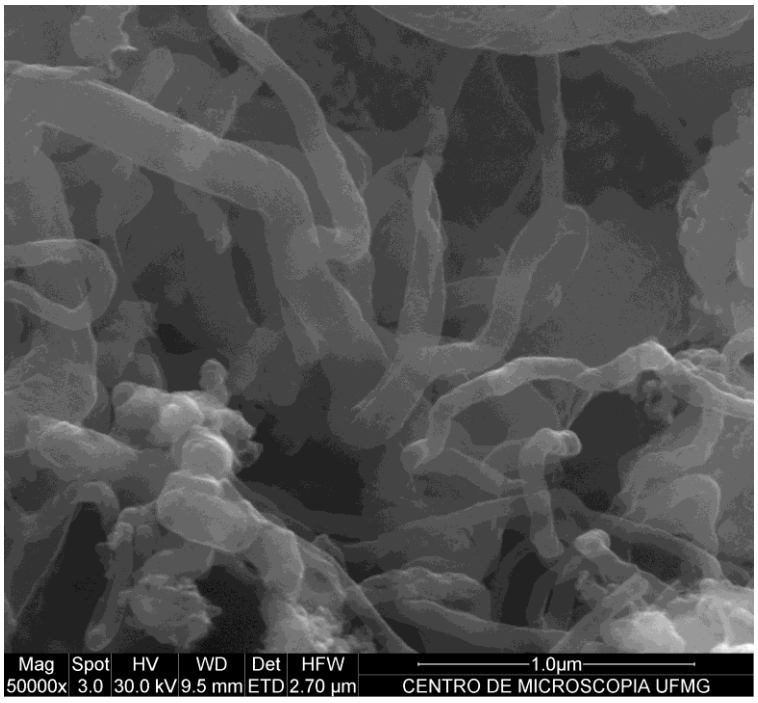

Figure 3.14 – SEM image of CNTs/CNFs synthesized on clinker and functionalized with ammonia

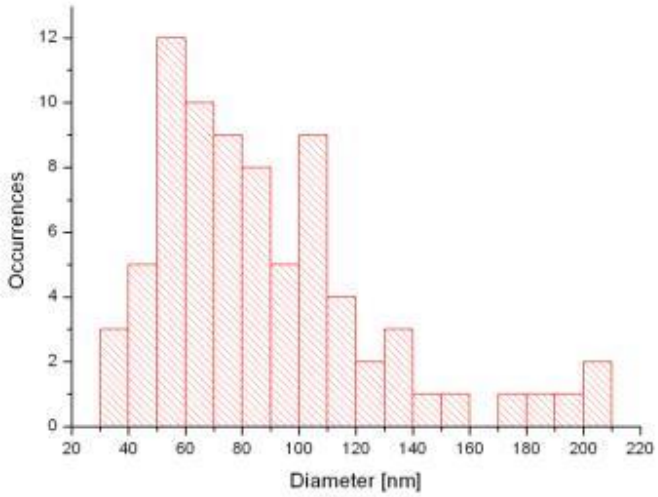

Figure 3.15 – Histogram of the diameters of CNTs/CNFs grown on clinker with ammonia treatment

Figure 3.16 shows the TGA results of the ammonia treated nano-structured clinker. Only one mass loss peak appeared. The highest mass loss was observed at 569 °C, which is between the two peak temperatures of the DTGA curve of nano-structured clinker without ammonia functionalization (525 and 620 °C, see Figure 3.12). Mass loss obtained by combustion at 800 °C was 26.1 %.

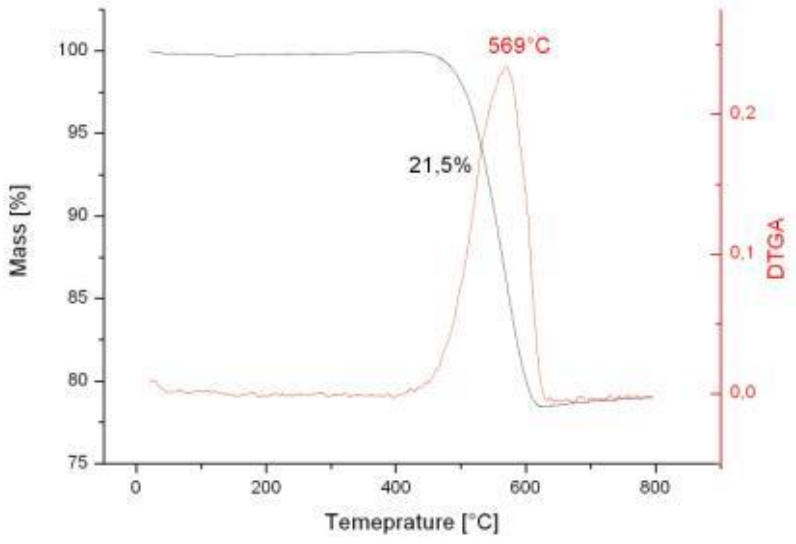

Figure 3.16 – TGA results of nano-structured clinker treated with ammonia

The application of ammonia during the synthesis process resulted in some alterations of the nano-structured clinker characteristics: the products synthesized with ammonia showed only one DTGA peak instead of two. This alteration suggests the incorporation of nitrogen containing functional groups in the nanotubes structure as shown by the results in Appendix 1. At the same time production was increased from values varying from 5 to 7 % to approximately 26 %.

3.4.5 Nano-structured silica fume

The silica fume catalyst had about 25 % of carbon yield, as it can be seen in Table 3.15. The thermogravimetric analysis of the products indicates the presence of two types of CNTs/CNFs corresponding to the two peaks of mass loss: at 615 and at 666 °C (Figure 3.17).

Table 3.15– Efficiency of synthesis on silica fume based catalyst

Catalyst identification	Carbon source	Gas flow [sccm]	Synthesis temperature [°C]	Synthesis time [min]	Mass loss at 800°C [%]
FS-2.5	acetylene	500	750	30	25

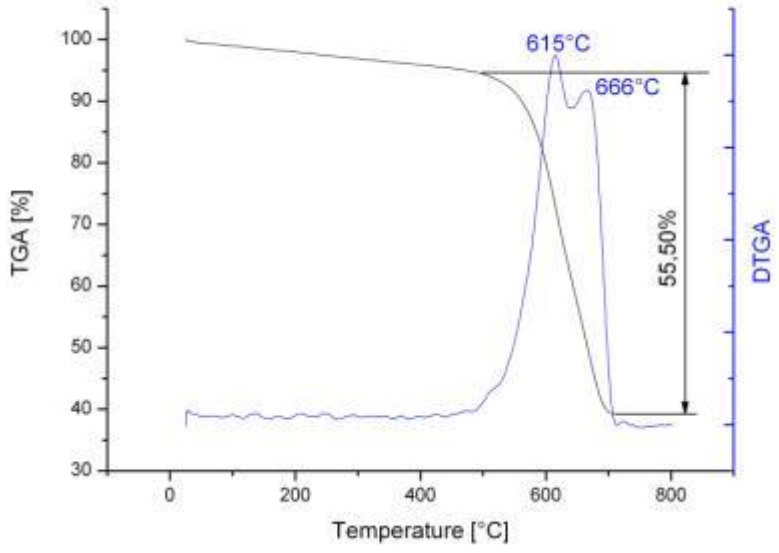

Figure 3.17 – TGA (in black) and DTGA (in blue) curves of CNTs/CNFs synthesized on silica fume based catalyst with 2.5 % iron addition

Synthesis on silica fume resulted in CNTs and CNFs, as can be seen in Figures 3.18 and 3.19. Histogram of the diameter distribution for nanotubes grown on silica fume is shown in Figure 3.20.Theaverage diameter of the CNTs/CNFs was about 30 to 50 nm.

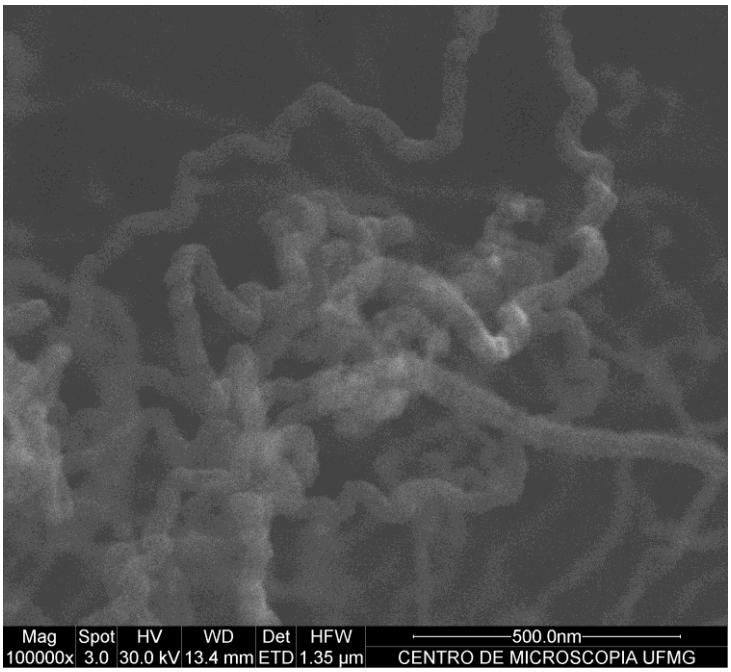

Figure 3.18 – SEM image of CNTs grown on silica fume under high magnification

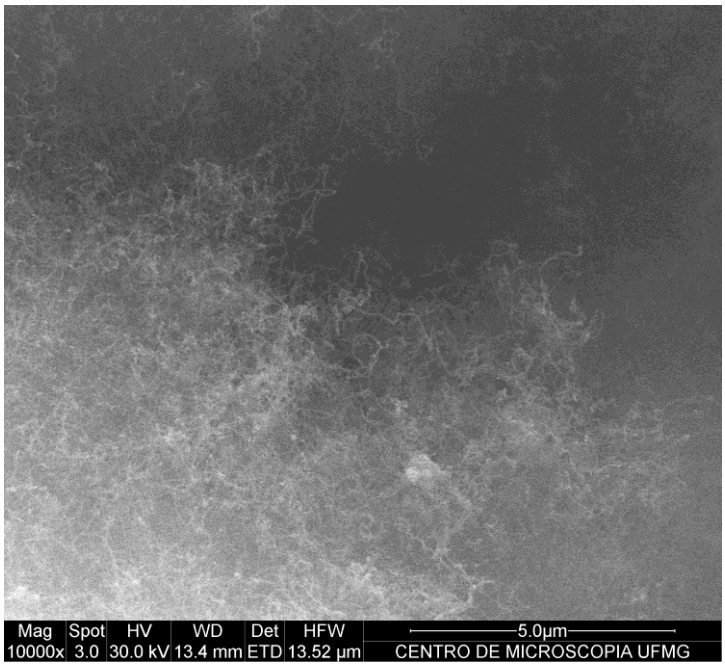

Figure 3.19 – SEM image of CNTs grown on silica fume

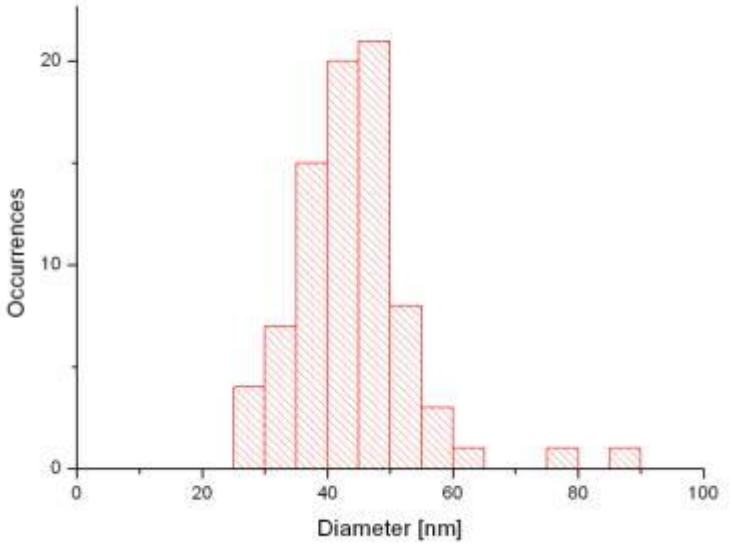

Figure 3.20 – Histogram of the diameters of CNTs/CNFs grown on silica fume measured on SEM images

To investigate the reinforcing effect of the nano-structured silica fume on mortars via mechanical strength tests, the product of the FS-2.5 catalyst using a 30 min process at 750 °C was used as standard.

3.4.6 Comparison of the results of nano-structured clinker and silica fume

Efficiency of the synthesis processes was evaluated by ignition at 800 °C as it was possible to characterize a more relevant quantity of material. Highest efficiency was achieved with silica fume. The value of 25 % is significantly higher than carbon yield obtained with catalysts based on clinker (in the order of 3 to 7 %). The difference can be explained by the higher surface area of silica fume which allows a better distribution of the catalyst particles and thus the optimization of carbon deposit.

Both types of supports produced nanotubes and nanofibers, as it was confirmed on SEM images. At the same time there were some differences in product morphology. Diameters of CNTs/CNFs synthesized on silica fume were smaller than of those synthesized on clinker: typical values ranged between 40 and 60 nm instead of 40 and 80 nm.

Both catalysts based on clinker and silica fume with converter dust addition produced CNTs/CNFs with two DTGA peaks. The peaks were situated at higher temperatures in the

case of silica fume based catalyst with respect to clinker based ones. The temperatures corresponding to the peaks were at 615 and 666 °C for silica fume and at 525 and 620 °C for clinker based catalyst. The higher ignition temperature in the case of nano-structured silica fume indicates the presence of nanotubes and nanofibers with fewer structural defects (TRIGUEIRO *et al.*, 2007).

3.5 Characterization of nano-structured cement

3.5.1 Procedures

Physico-chemical investigations were performed on the mixture of nano-structured clinker with Brazilian CP-III or CP-V type cement. The product of the CD-2.5 catalyst was used. The mixture incorporating 0.3 % CNTs/CNFs of the cement mass was initially homogenized in a plastic bag with agitation. For both types of cement, Blaine fineness was measured according to NBR NM76 (1998) standard. Their chemical compositions were determined by X-ray spectrometer and compared with that of pure CP-III or CP-V cement. Loss on ignition was also measured using an oven at 1000 °C (NBR NM18, 2012). Water content for normal consistency was determined by a method based on a Vicat instrument (NBR NM43, 2002). The initial and final setting times were evaluated for both plain cement pastes and for the mixtures with CNTs/CNFs according to NBR NM65 (2003) standard. Insoluble solid content was determined according to NBR NM15 (2012) standard. All physico-chemical investigations were performed at the laboratory of Intercement SA in Pedro Leopoldo.

3.5.2 Nano-structured Brazilian CP-V type cement

Blaine fineness of pure Brazilian CP-V type cement was 4653 cm^2/g, meanwhile with the inclusion of CNTs/CNFs it changed to4752 cm^2/g. A slight increase of CP-V cement fineness was revealed as an influence of nanotube addition.

Composition of pure Brazilian CP-V type cement and of its blend with nanotubes is shown in Table 3.16. Nano-structured clinker addition did not influence the chemical composition of CP-V cement.

Table 3.16– Chemical composition of pure CP-V cement and its blend with 0.3 % of CNTs/CNFs as a result of an X-ray spectroscopy analysis

Compound	Pure Brazilian CP-V type cement [%]	Brazilian CP-V type cement with 0.3 % CNTs/CNFs [%]
SiO_2	21.03	20.89
Al_2O_3	5.12	5.07
Fe_2O_3	2.56	2.63
CaO	61.00	60.94
MgO	2.61	2.60
SO_3	3.31	3.24
Na_2O	0.28	0.28
K_2O	0.74	0.73

Water content for normal consistency of plain Brazilian CP-V type cement paste was 0.297 with respect to cement weight. The same characteristic of CP-V paste containing 0.3 % nanotubes with respect to cement weight was 0.302. The analysis showed minimal influence of nano-structured addition on the water demand of cement paste. The presence of nanotubes caused a small increase in water demand. At the same time this alteration is within the normal variability of water demand of Brazilian CP-V type cement.

The results of setting time investigations on CP-V cement pastes are shown in Table 3.17. The values of initial and final setting times of both samples were higher than that of ordinary CP-V type cement pastes without admixtures (start of setting at 140 minutes and finish of setting at 220 minutes). The use of the lignosulfonate and polysaccharide based plasticizer caused partly the delay of the setting. The cement paste prepared with nanotubes suffered additional delay due to this inclusion. Initial setting of CP-V cement paste was retarded by 35 minutes due to the addition of CNTs/CNFs. There was less difference between the final setting times: the paste prepared with nanotubes occurred only 15 minutes later than the reference. The difference between the initial and final setting times changed slightly: from 100 minutes it decreased to 80 as an effect of CNT/CNF addition. Both initial and final setting respected the time limits of NBR 5733 (1991) norm established for CP-V type cement: minimum of 60 minutes for the start and maximum of 600 minutes for final setting.

Table 3.17 – Setting times of cement pastes prepared with Brazilian CP-V type cement

Sample	Start of setting	End of setting	Setting time
CP-V reference	205 min	305 min	100 min
CP-V with nano-structured clinker	240 min	320 min	80 min

Loss on ignition of CP-V cement containing 0.3 % CNTs/CNFs was 1.24 %. This value remains below the 4.5 % limit defined by NBR5733 (1991) standard. Plain CP-V cement showed 3.72 % of loss on ignition.

Insoluble solid content of nano-structured CP-V cement with 0.3 % nanotube content as well as pure CP-V cement was 1.12 %. Both values were beyond the limit of 1.0 % established by NBR5733 (1991) standard.

These results show that the addition of 0.3 % of nanotubes to Brazilian CP-V type cement did not alter significantly the fineness, the chemical composition, the water demand and the insoluble solid content with respect to the normal variability of the parameters of the CP-V type cement. It also respected the limits defined by Brazilian standards. On the other hand, initial and final setting times were slightly delayed as an effect of nano-structured clinker addition. The loss on ignition showed some alteration due to this addition, but remained below the limits defined by the Brazilian standard.

3.5.3 Nano-structured Brazilian CP-III type cement

Blaine fineness of pure Brazilian CP-III type cement was 4199 cm^2/g. With 0.3 % of CNTs/CNFs addition it changed to4209 cm^2/g. Thus no significant influence was revealed with nanotube addition to CP-III cement fineness.

Composition of pure Brazilian CP-III type cement and of its blend with 0.3 % nanotubes is shown in Table 3.18. Nano-structured clinker addition did not influence the chemical composition of CP-III cement.

Table 3.18– Chemical composition of pure CP-III cement and its' blend with 0.3 % of CNTs/CNFs as a result of an X-ray spectroscopy analysis

Compound	Pure Brazilian CP-III type cement [%]	Brazilian CP-III type cement with 0.3 % CNTs/CNFs [%]
SiO_2	25,89	25,60
Al_2O_3	6,64	6,56
Fe_2O_3	2,09	2,22
CaO	56,31	56,46
MgO	3,60	3,59
SO_3	2,38	2,32
Na_2O	0,28	0,30
K_2O	0,59	0,58

Water content for normal consistency of plain Brazilian CP-III type cement paste was 0.280 with respect to cement weight. The same characteristic of CP-III paste containing 0.3 % nanotubes with respect to cement weight was 0.286. The analysis showed a slight increase of water demand of cement paste as an influence of nano-structured clinker addition. This change is within the normal variability of water demand of Brazilian CP-III type cement.

The results of setting time investigations on CP-III cement pastes are shown in Table 3.19. As an effect of the lignosulfonate and polysaccharide based admixture the values were higher than for ordinary CP-III type cement pastes (initial setting at 190 minutes and final setting at 290 minutes). Setting time of CP-III cement paste was not influenced significantly by the addition of CNTs/CNFs. Both initial and final of setting times respect the criteria established by Brazilian standard NBR 5735 (1991) for CP-III cement: minimum of 60 minutes for the initial and maximum of 720 minutes for final setting.

Table 3.19 – Setting times of cement pastes prepared with Brazilian CP-III type cement

Sample	Start of setting	End of setting	Setting time
CP-III reference	475 min	550 min	75 min
CP-III with nano-structured clinker	485 min	565 min	80 min

Loss on ignition of nano-structured Brazilian CP-III type cement with 0.3 % CNTs/CNFs was 2.74 %. The result for pure CP-III cement was 2.69 %. Both values are below the 4.5 % limit defined by NBR 5735 (1991) standard. Loss on ignition of CP-III cement was not affected by the addition of nanotubes.

The nano-structured CP-III cement with 0.3 % nanotubes had an insoluble solid content equal to 1.66 %.The result obtained for plain CP-III cement was 1.61 %. Both values are slightly beyond the limit of 1.5 % defined by NBR 5735 (1991) standard. Insoluble solid content of CP-III cement was not affected by the addition of nanotubes.

It can be concluded that the addition of 0.3 % of nanotubes to Brazilian CP-III type cement did not alter significantly the investigated characteristics with respect to the normal variability of the parameters of the CP-III type cement. The measured values were within the limits of the respective Brazilian standards, with the exception of insoluble solid content. The measured values for this parameter were slightly above the limits in the case of plain CP-III cement as well as of its blend with CNTs/CNFs.

3.5.4 Comparative analysis of the results of nano-structured CP-V and CP-III cements

The addition of nano-structured clinker did not result in significant alterations to the investigated physical or chemical properties of CP-III or CP-V type cements. Blain fineness was influenced neither in the case of CP-III nor in the case of higher surface area CP-V type cement. Chemical composition also remained the same after adding 0.3 % of CNTs/CNFs with respect to cement mass. The water demand of CP-V cement was slightly higher than that of CP-III cement due to the higher surface area. Both cements had the water demand slightly increased after nano-structured clinker addition. Initial and final setting times were more influenced by the presence of chemical admixture than by the addition of nanotubes for both types of cements. Meanwhile initial and final setting times of nano-structured CP-V type cement increased, no significant influence was found on CP-III type cement with the addition of CNTs/CNFs. Loss on ignition of both cements incorporating CNTs/CNFs was within the limits of the respective Brazilian standards. The values were also similar to those obtained for ordinary cement. Insoluble solid content of the two cements was not influenced significantly by the nanotubes addition.

4

CHARACTERIZATION OF MORTAR NANO-COMPOSITES

4.1 Materials and methods for characterization of mortar nano-composites

Portland cement mortars were made with standard composition, according to Brazilian standard NBR 7215 (1996). Equal amounts of natural sand of 0.15, 0.30, 0.60 and 1.20 mm in size were used. The binder to aggregate ratio was 1:3 in all cases and cement content was equal to 530 kg/m^3. Water to cement (w/c) ratio varied: the employed value is indicated with the results of each test. The materials were placed in a mortar blender: first the dry materials were mixed together followed by the gradually addition of water with the chemical admixtures. Powder admixtures were first dissolved in the mixing water.

Initially for every composition prismatic specimens were cast: 25 × 25 × 150 mm^3 or 40 × 40 × 160 mm^3 beams for the flexural tensile strength tests and 40 × 40 × 40 mm^3 cubes for compression strength tests. These specimens were compacted using a vibrating table. Test specimens were cured in water after de-molding until the day of testing. The testing ages are specified with the results of each test.

A 30 kN servo-hydraulic Kratos machine was employed for the evaluation of the flexural tensile strength (Figure 4.1). The three-point bending tests were performed in a constant displacement mode of 0.50 mm/min. The span used for these tests was 80 mm in the case of the 25 × 25 × 150 mm^3 specimens and 100 mm for the 40 × 40 × 160 mm^3 ones. The flexural strength f_c^{flex} of the specimens was determined according to the following equation:

$$f_c^{flex} = \frac{3}{2}\frac{Fl}{h^2 b}, \qquad (4.1)^{8}$$

where F is the maximum load, l is the span, h is the height and b is the width of the specimen cross-section.

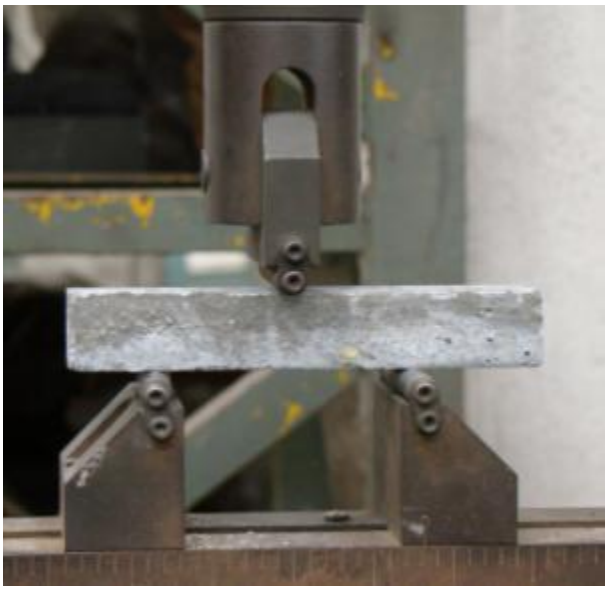

Figure 4.1– Experimental setup for three-point bending test

The compressive strength tests of the mortars were performed on a 1000 kN servo-hydraulic Kratos machine in a constant stress mode. Besides the 40 × 40 × 40 mm^3 cube specimens, the remaining ends of the 40 × 40 × 160 mm^3 beams were also used. In this later case two 40 × 40 mm^2 steel plates were fit on the lower and upper side of the specimens to assure uniform load distribution under a constant area of 1600 mm^2.

In the second part of this investigation experiments were performed using cylindrical specimens of 50 mm diameter and 100 mm height. The mixing procedure was the same as presented previously. The casting was done in four equal layers, with 30 hits on each layer to achieve a good compaction. These specimens were removed from the molds 24 hours after casting and kept in lime-saturated water until the day of testing.

Testing of the cylindrical specimens was performed using an MTS universal system with actuators of 100 and 250 kN of capacity. For compressive tests the mortar specimens

[8] NBR 12142, 1991

were capped with sulfur on both sides. Tensile strength was determined by splitting tests using the same type of specimen (Figure 4.2). The tensile strength σ_t was calculated using the following equation:

$$\sigma_t = \frac{2P}{\pi DL}, \qquad (4.2)^9$$

where P is the compressive force, D is the diameter and L is the length of the cylinder.

Figure 4.2 – Experimental setup for splitting tensile strength tests

The preparation of mortar specimens as well as the strength tests were performed partly at the Center of Research and Development of Magnesita SA and partly in the LAEEs at the UFMG.

The test results for each mix proportion and age, to be presented next, correspond to the mean value of 3 to 8 specimens. In order to correctly evaluate the effect of CNT addition,

[9] NBR 7222, 1994

for every mortar composition prepared with CNTs/CNFs a reference batch with exactly the same composition but without nanotubes was also cast.

4.2 Behavior of mortar nano-composites

4.2.1 Behavior of mortars made with Portland cement manufactured with carbon nanotubes

Optimal nanotube/cement ratio

The amount of CNTs used in the previously described investigations varied between 0.05 and 1.0 % with respect to binder content. The first reason for this is the cost of CNTs, which would make concrete very expensive with the use of high-quality and -purity nanotubes. The other and more important reason is the issue of dispersion. A CNT content up to 1.0 % seems to be dispersible in cement matrix when the adequate methods are used. Some investigations showed decreasing composite strength with increasing CNT content (NASIBULIN *et al.*, 2009; MELO *et al.*, 2011; COLLINS *et al.*, 2012). Thus, the first strength tests had the objective to verify the validity of this phenomenon. For these tests the nano-composites of CNTs/CNFs grown on PC clinker with 2.5 % steel mill scale were used. These mortars were identified by the label CL.

Brazilian CP-V type Portland cement was used with water cement ratio (w/c) of 0.48. To allow better dispersion and bond of nanotubes to the cement matrix, a combination of two commercial concrete admixtures was used: a polycarboxylate based superplasticizer in 0.8 % of binder content (Chryso Premia 180) and a sulfonated polynaphtalene based plasticizer, also in 0.8 % of binder content (Chryso Plast 850), as described by Melo (2009). In the mortar identification NP represents this combination of concrete admixtures. Seven mix proportions were made with different CNT contents, whose compositions are given in Table 4.1. The CNT/CNF content of the composites varied between 0.05 and 4.90% of the binder weight. The suffixes N05 to N245 in the mortar identification represent these CNT contents. A mortar without nano-structured clinker but with the same mixing proportions was also cast (CL-NP).

Table 4.1– Mortar compositions for optimal nanotube/cement ratio determination tests

Mortar identification	CNT content* [%]
CL-NP	0
CL-NP-N05	0.05
CL-NP-N25	0.25
CL-NP-N50	0.5
CL-NP-N100	1.0
CL-NP-N125	1.25
CL-NP-N245	2.45
CL-NP-N490	4.90

* - with respect to binder content

Prismatic specimens (25 × 25 ×150 mm^3in size) were cast in steel molds. Mortars with more than 1.0 % of nanotubes (CL-NP-N100, -N125, -N245 and -N490) were apparently drier than the mortars with lower CNT content. Clusters of clinker with nanotubes (black spots) were also visible indicating an inefficient dispersion of the nanotubes. In the case of CNT/CNF content smaller than 1.0 % the workability was similar for all mortars and practically no clusters could be seen.

The flexural tensile strength was determined at the ages of 7 and 28 days.CL-NP-N245 mortar did not harden and it was impossible to perform the tests. Six specimens of every other mortar were used at every age. The results are presented in Figure 4.3.

It is worth to mention that the composition with more than 0.5 % CNT content with respect to cement apparently hardened slower than other compositions. Specimens with CNT content above 0.25 % appeared to be weaker than the reference. The highest flexural tensile strength with respect to the reference was achieved with 0.05 % of CNTs (CL-NP-N05). Flexural tensile strength of this mortar was higher or equal to that of plain cement mortar at 7 and 28 days. These results confirmed that nanotube content above 0.5 % with respect to binder mass may cause loss in the strength of mortars. The reason may be the difficulties in the dispersion of a higher quantity of nanotubes. For further tests CNT/CNF contents below 0.3 % were chosen in order to have a common basis for comparison with previous results obtained by the physical mixture of high quality CNTs in cement mortars (MELO *et al.*, 2011).

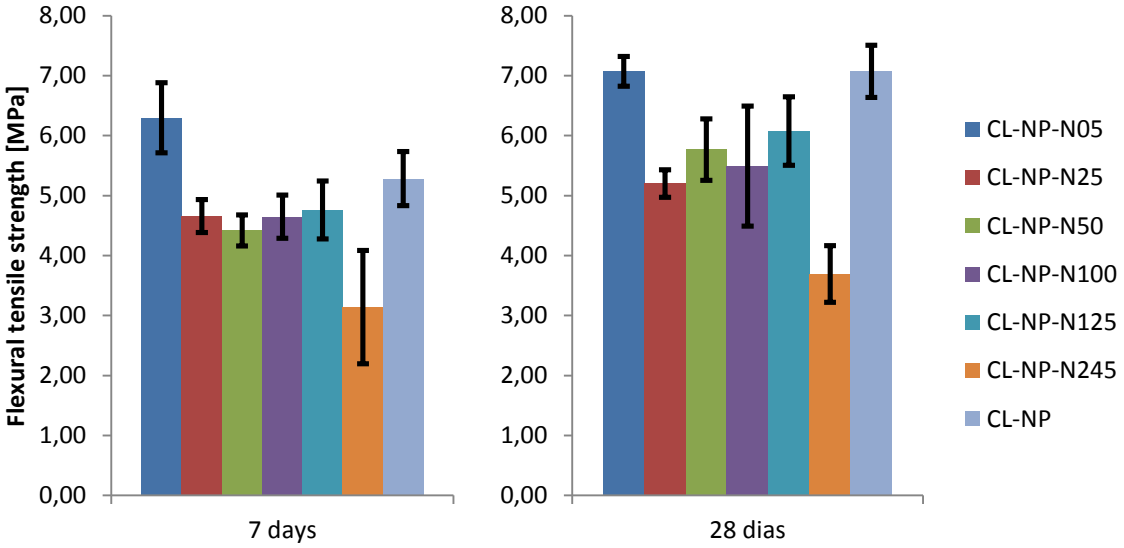

Mortar identification	Flexural tensile strength			
	7 days		28 days	
	Mean [MPa]	Coefficient of variation [%]	Mean [MPa]	Coefficient of variation [%]
CL-NP	5.28	8.53	7.07	6.18
CL-NP-N05	6.30	9.25	7.07	3.52
CL-NP-N25	4.66	5.92	5.20	4.43
CL-NP-N50	4.42	5.85	5.77	8.91
CL-NP-N100	4.65	7.73	5.49	5.99
CL-NP-N125	4.76	10.15	6.08	9.42
CL-NP-N245	3.14	30.11	3.69	12.75

Figure 4.3 – Results of flexural tensile strength tests at ages of 7 and 28 days of mortar specimens prepared with different CNT/binder ratios

Chemical admixture comparison

As it was mentioned before, the main problems of the application of CNTs in cement composites are dispersion and bond. The objective of the next tests was to evaluate the performance of some commercially available concrete chemical admixtures with respect to the dispersion and bond of CNTs in the cement matrixes through the preparation and testing of mortar specimens. CNTs grown on clinker with 2.5 % iron addition (converter dust) in 0.3

% of the binder content were used, based also on the results of Melo *et al.* (2011).These mortars were identified by the label CL.

Brazilian CP-V type cement was also used in this case. The w/c ratio was equal to 0.43. Four different types of admixtures or their combination were employed: the same combination of polycarboxylate and polynaphtalene used previously (label NP in the mortar identification), a lignosulfonate and polysaccharide based – RheoSet TecMult 850 (label LS in the mortar identification) – and a sulphonated melamine based – Basf Melment F10X (label SM in the mortar identification). The sulphonated melamine based admixture comes in the form of a powder; meanwhile all other admixtures used are already dissolved. In order to maintain a similar solid content of the admixtures, the dosage of the sulphonated melamine admixture was equal to 0.5 % of binder content, while the total addition of the other admixtures was kept between 1.5 and 1.6 % with respect to the binder content. The mix proportions are shown in Table 4.2.

Table 4.2– Detailing of the mix proportions for chemical admixture comparison tests

Mortar identification	**Admixture composition**	**Admixture content* [%]**	**CNT content* [%]**
CL-NP	polycarboxylate + sulphonated polynaphtalene	0.8 + 0.8	0
CL-NP-N30	polycarboxylate + sulphonated polynaphtalene	0.8 + 0.8	0.3
CL-LS	lignosulfonate and polysaccharide	1.5	0
CL-LS-N30	lignosulfonate and polysaccharide	1.5	0.3
CL-SM	sulphonated melamine	0.5	0
CL-SM-N30	sulphonated melamine	0.5	0.3

* - with respect to binder content

There was no significant difference between the workability of the mortars, nor could clusters of clinker with CNTs be identified during the mixing.

Beams 25 × 25 × 150 mm^3 in size were used for three-point bending tests (span equal to 80 mm) at the ages of 7 and 28 days after casting. Six specimens of every composition were tested at each age. Due to the quantity of material mixed in each batch, compressive strength was evaluated only at 28 days. Cubic specimens (40 × 40 × 40 mm^3) were used in this case. The strength test results are presented in Figures 4.4 and 4.5.

Specimens made with polysaccharide based plasticizer did not harden and tests could not be performed in all cases. The compressive strength tests of reference mortar prepared with sulphonated melamine were performed only on two specimens due to the failure of the specimens prior to testing; therefore its results were discarded. With the exemption of these two mortars, compressive strength of mortars with CNTs showed enhancement in performance with respect to the corresponding reference. On the other hand, gains in the flexural tensile strength for mortars CL-NP-N30 and CL-SM-N30 with respect to reference ones were marginal, if any. Mortar CL-LS-N30 prepared with lignosulfonate showed the best performance with respect to flexural strength (14.9 % gain at 28 days). For compressive strength, mortar CL-NP-N30 had the highest gain: 43.1 % gain at 28 days. Since the principal objective was to enhance tensile behavior of mortars, the lignosulfonate admixture was chosen as the main dispersing agent to be used for further testing in order to reduce the number of variables.

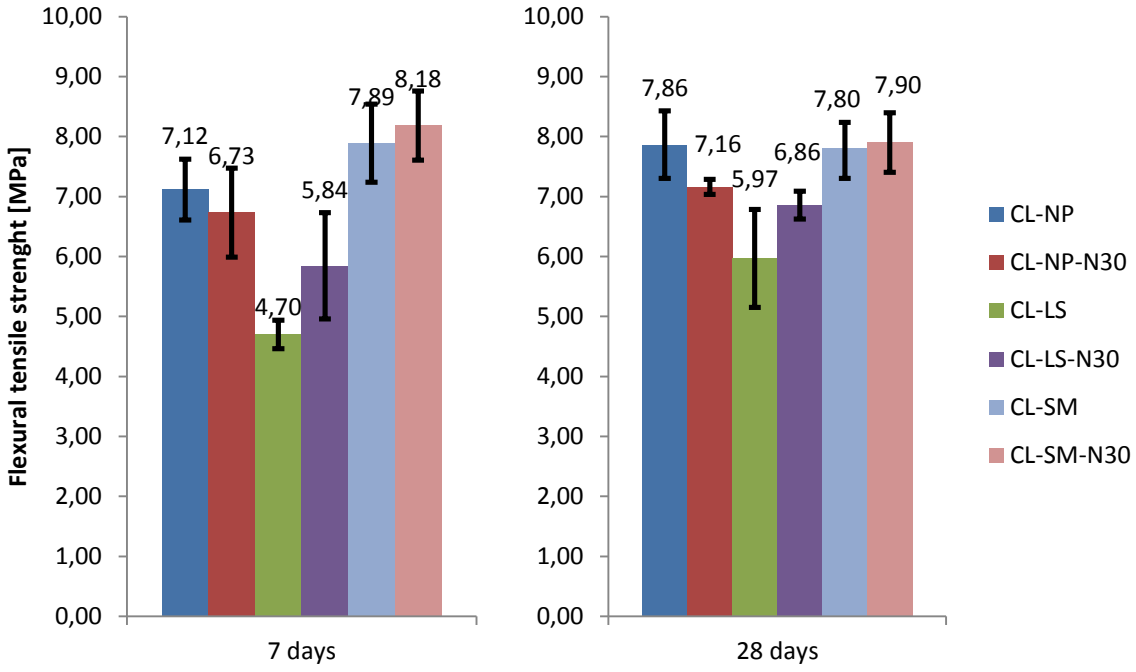

Mortar identification	Flexural tensile strength			
	7 days		28 days	
	Mean [MPa]	Coefficient of variation [%]	Mean [MPa]	Coefficient of variation [%]
CL-NP	7.12	7.13	7.86	7.18
CL-NP-N30	6.73	11.01	7.16	1.74
CL-LS	4.70	5.07	5.97	13.66
CL-LS-N30	5.84	15.16	6.86	3.39
CL-SM	7.89	8.25	7.80	5.62
CL-SM-N30	8.18	7.03	7.90	6.29

CL-NP – reference mortar prepared with polycarboxylate and polynaphtalene admixtures;
CL-NP-N30 – mortar prepared with polycarboxylate and polynaphtalene admixtures and 0.3 % CNTs/CNFs;
CL-LS – reference mortar prepared with lignosulfonate admixture;
CL-LS-N30 – mortar prepared with lignosulfonate admixture and 0.3 % CNTs/CNFs;
CL-SM – reference mortar prepared with sulfonated melamine admixture;
CL-SM-N30 –mortar prepared with sulfonated melamine admixture and 0.3 % CNTs/CNFs

Figure 4.4– Flexural tensile strength of mortar specimens prepared with different admixtures at 7 and 28 days.

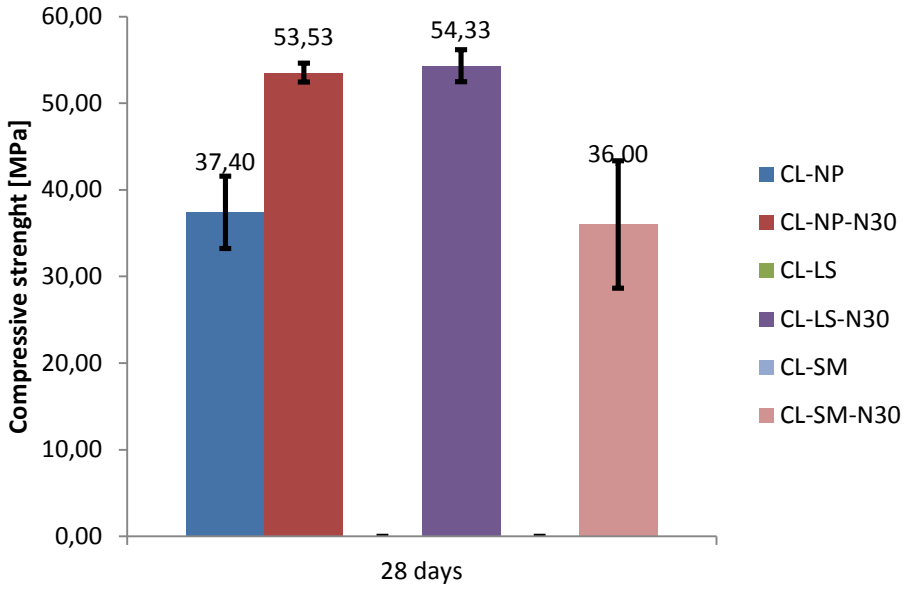

Mortar identification	Compressive strength	
	28 days	
	Mean [MPa]	Coefficient of variation [%]
CL-NP	37.40	11.13
CL-NP-N30	53.53	2.03
CL-LS	-*	-*
CL-LS-N30	54.33	3.40
CL-SM	55.00**	8.49**
CL-SM-N30	36.00	20.47

* - tests could not be performed due to inefficient hardening of mortar
** - only two results

CL-NP – reference mortar prepared with polycarboxylate and polynaphtalene admixtures;
CL-NP-N30 – mortar prepared with polycarboxylate and polynaphtalene admixtures and 0.3 % CNTs/CNFs;
CL-LS – reference mortar prepared with lignosulfonate admixture;
CL-LS-N30 – mortar prepared with lignosulfonate admixture and 0.3 % CNTs/CNFs;
CL-SM – reference mortar prepared with sulfonated melamine admixture;
CL-SM-N30 –mortar prepared with sulfonated melamine admixture and 0.3 % CNTs/CNFs

Figure 4.5– Compressive strength of test specimens prepared with different admixtures at 28 days.

Effect of batching procedure

When nano-sized particles are added to a cementitious composite, the preparation processes are of extreme importance in order to ensure a good dispersion. Three different mortars were produced to investigate the effects of changes in the mixing order of the composite components. Nano-structured clinker (labeled CL in the mortar identification) made with 2.5 % converter dust addition was used in this case. The w/c ratio and the CNT/CNF content was 0.48 and 0.1% respectively. Brazilian CP-V type cement was used. Lignosulfonate and polysaccharide based plasticizer was used at 0.5 % of cement weight (labeled LS05). The CNTs/CNFs in an aqueous dispersion may react first with plasticizer molecules without competing with other particles and a better dispersion could be achieved. The mortar CL-LS05-DM-N10 was prepared by first mixing the nano-structured clinker with the cement; then the sand aggregates were added. Finally the plasticizer dissolved in water was placed over. The second mortar (CL-LS05-WM-N10) was prepared by mixing first the nano-structured clinker to water and plasticizer and then pouring it to the dry mix of cement and sand. Besides these mortars incorporating nano-structured clinker, a plain reference one (CL-LS05) was prepared with the same amount of plasticizer. Details about the mixing proportions are shown in Table 4.3.

Table 4.3 – Detailing of the mixing proportions for investigation of the effect of mixing order

Mortar identification	CNT/CNF content*	Observations
CL-LS05	0	-
CL-LS05-DM-N10	0.1 %	CNTs/CNFs added to cement
CL-LS05-WM-N10	0.1 %	CNTs/CNFs added to mixing water

* - with respect to binder content

No apparent inhomogeneities or difference in workability could be visualized during the mixing.

Compressive strength was determined at the ages of 7 and 28 days on cylindrical specimens. These experiments were performed at the laboratory of Intercement SA. at Pedro Leopoldo, Minas Gerais. Test results are presented in Figure 4.6.

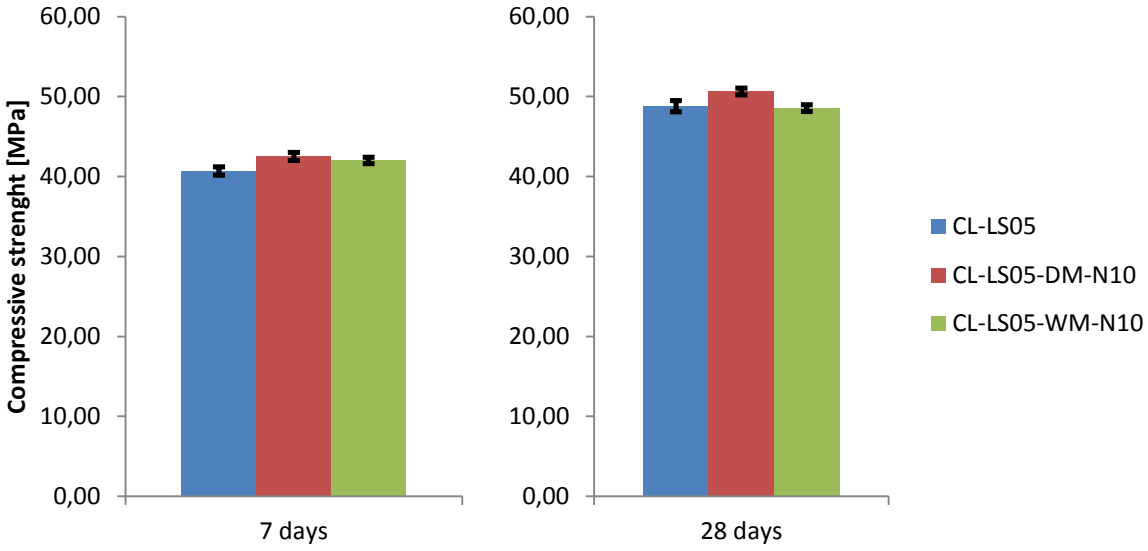

Mortar identification	Compressive strength			
	7 days		28 days	
	Mean [MPa]	Coefficient of variation [%]	Mean [MPa]	Coefficient of variation [%]
CL-LS05	40.70	1.28	48.80	1.43
CL-LS05-DM-N10	42.50	1.18	50.63	0.80
CL-LS05-WM-N10	42.00	0.95	48.57	0.86

CL-LS05 – reference;
CL-LS05-DM-N10 – mortar with 0.1 CNTs/CNFs dry mixed with cement;
CL-LS05-WM-N10 – mortar with 0.1 % CNTs/CNFs added with mixing water

Figure 4.6– Compressive strength of mortars prepared with different mixing process at the ages of 7 and 28 days

Both mortars incorporating nano-structured clinker had practically equal compressive strength at the ages of 7 and 28 days. The differences were less than 5 %.There was also no significant difference (≤ 5 %) with respect to the reference mortar. These results show that at these conditions there is practically no importance whether the CNTs/CNFs are dry mixed with cement or added together with mixing water. The supposed better functionalization of the nanotubes added with mixing water did not result in higher compressive strength of the composite.

Covalent functionalization: performance of ammonia functionalized nano-structured clinker

CNTs and CNFs with modified structure were successfully synthesized using ammonia on clinker with 2.5 % iron addition in the form of converter dust (labeled CL-NH in the mortar identification). In order to evaluate the reinforcing effect of these functionalized nanotubes cylindrical mortar specimens were cast and tested in axial compression and tensile splitting. Brazilian CP-III type cement was used and the w/c ratio of these mortars was 0.375. Lignosulfonate and polysaccharide based plasticizer and polycarboxylate based superplasticizer were used at 0.8 % both of the binder (labeled LP in the mortar identification). Three compositions were prepared: CL-NH-LP without nanotubes, CL-NH-LP-N10 with 0.1 % and CL-NH-LP-N30 with 0.3 % of CNTs/CNFs with respect to the binder content. Details about the three mortar compositions are given in Table 4.4.

Table 4.4 – Detailing of the mixing proportions of mortars prepared with ammonia treated nano-structured clinker

Mortar identification	CNT/CNF content*
CL-NH-LP	0
CL-NH-LP-N10	0.1 %
CL-NH-LP-N30	0.3 %

* - with respect to binder content

There was no significant difference between the workability of the three mortars and no clusters of clinker with CNTs/CNFs were identified during the mixing.

The tests were performed at the ages of 7 and 28 days on four specimens of each composition and type of test. Test results are shown in Figures 4.7 and 4.8.

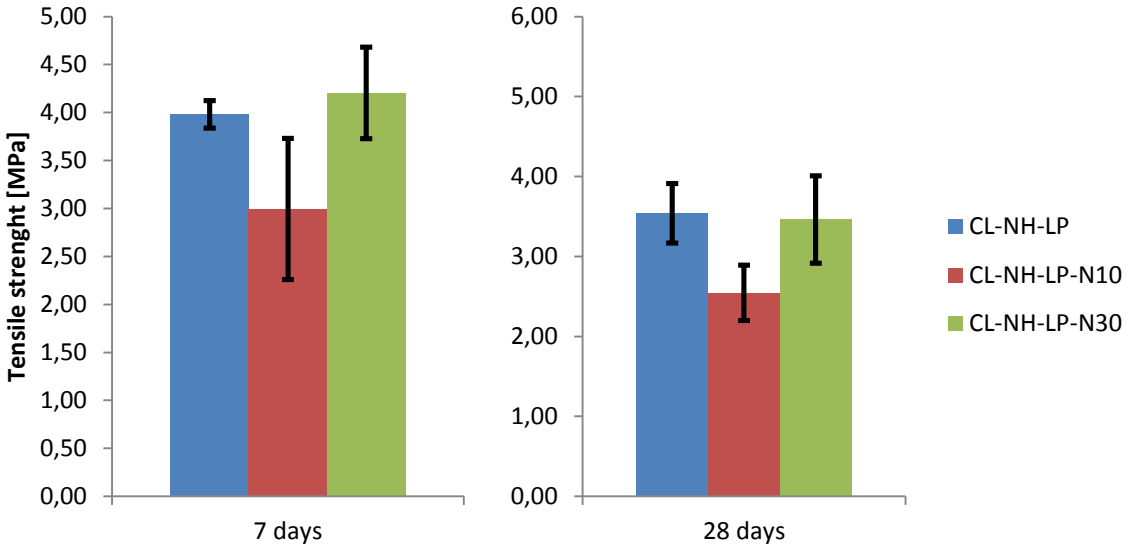

Mortar identification	Splitting tensile strength			
	7 days		28 days	
	Mean [MPa]	Coefficient of variation [%]	Mean [MPa]	Coefficient of variation [%]
CL-NH-LP	3.98	3.62	3.54	10.53
CL-NH-LP-N10	3.00	24.52	2.55	13.66
CL-NH-LP-N30	4.21	11.33	3.46	15.79

CL-NH-LP – reference;
CL-NH-LP-N10 – prepared with 0.1 % CNTs/CNFs;
CL-NH-LP-N30 – prepared with 0.3 % CNTs/CNFs.

Figure 4.7– Splitting tensile strength of mortars prepared with 0, 0.1 and 0.3 % of ammonia functionalized CNTs/CNFs

Splitting tensile strength tests did not show significant enhancement of mortars prepared with ammonia functionalized nanotubes. The mortar containing 0.3 % CNTs/CNFs had higher tensile strength than the other containing 0.1 % but remained lower than the reference at the ages of 7 and 28 days.

The values obtained during splitting tensile tests of mortars incorporating ammonia treated nano-structured clinker showed high variability. The scattering of the results indicate an inhomogeneous mortar due to inefficient dispersion of the nanotubes.

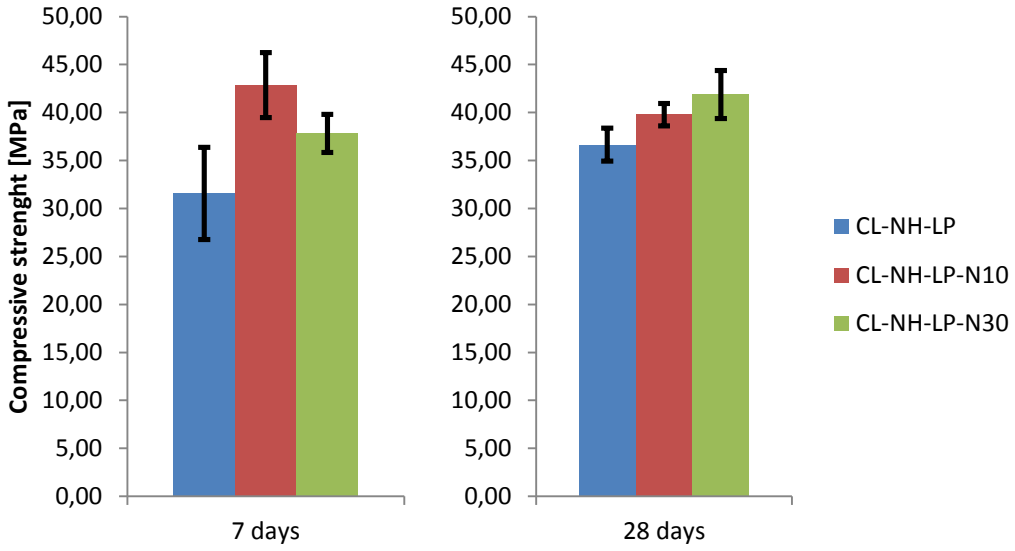

Mortar identification	Compressive strength			
	7 days		28 days	
	Mean [MPa]	Coefficient of variation [%]	Mean [MPa]	Coefficient of variation [%]
CL-NH-LP	31.57	15.26	36.65	4.71
CL-NH-LP-N10	42.85	7.90	39.78	2.95
CL-NH-LP-N30	37.82	5.22	41.88	5.99

CL-NH-LP – reference;
CL-NH-LP-N10 – prepared with 0.1 % CNTs/CNFs;
CL-NH-LP-N30 – prepared with 0.3 % CNTs/CNFs.

Figure 4.8– Compressive strength of mortars prepared with 0, 0.1 and 0.3 % of ammonia functionalized CNTs/CNFs

Compressive strength of mortars containing nano-structured clinker treated with ammonia was higher than the reference at the investigated ages. The gains with respect to reference were 8.5 and 14.3 % for CL-NH-LP-N10 and CL-NH-LP-N30 mortars respectively at 28 days.

4.2.2 Behavior of mortars made with Portland cement and nano-structured silica fume

CNTs and CNFs were successfully synthesized on silica fume support with converter dust (representing additional 2.5 % *Fe*). The effect of the addition of this nano-structured silica fume (0.3 % of nanotubes of the mass of binder, labeled SF in the mortar identification)

on the flexural tensile and compressive strength of cement mortar was investigated using 40 ×40 × 160 mm^3prismatic specimens. The surfactants used were the previously standardized lignosulfonate and polysaccharide based plasticizer (LS) and polivinylpyrrolidone (PVP) at 1.5 % and 1.0 % of binder respectively. PVP comes in the form of pure powder therefore its dosage was reduced with respect to that of the dissolved LS admixture. Brazilian CP-III type cement was used. The water to binder ratio was 0.40. The silica fume content in all cases was 10 % of the cement mass. Composition details of the mortar specimens are presented in Table 4.5.

Table 4.5 –Mix details of mortars prepared with PVP and lignosulfonate dispersing agents and nano-structured silica fume

Mortar identification	CNT/CNF content*	Admixture type
SF-PVP	0	PVP
SF-PVP- N30	0.3 %	PVP
SF-LS	0	Lignosulfonate-polisaccharide based
SF-LS-N30	0.3 %	Lignosulfonate-polisaccharide based

* - with respect to binder content

The consistency of mortars prepared with PVP was apparently drier. No significant indications of inhomogeneities could be visually identified during mixing.

Testing ages were 7 and 28 days. Flexural tensile and compressive tests were performed on the same specimens using steel plates as described previously. The results are presented in Figures 4.9 and 4.10.

The results of the flexural tensile and compressive strength of CNT-containing mortar prepared with lignosulfonate admixture show some enhancement with respect to the reference one at the age of 28 days. The gains were 9.4 % and 39.6 % in flexural tensile and compressive strength respectively.

On the other hand, CNT/CNF addition to mortar prepared with PVP surfactant had negative effect on the flexural tensile strength at both investigated ages. Compressive strength was not influenced by CNT/CNF addition at 7 days; meanwhile a 15 % gain was achieved at 28 days.

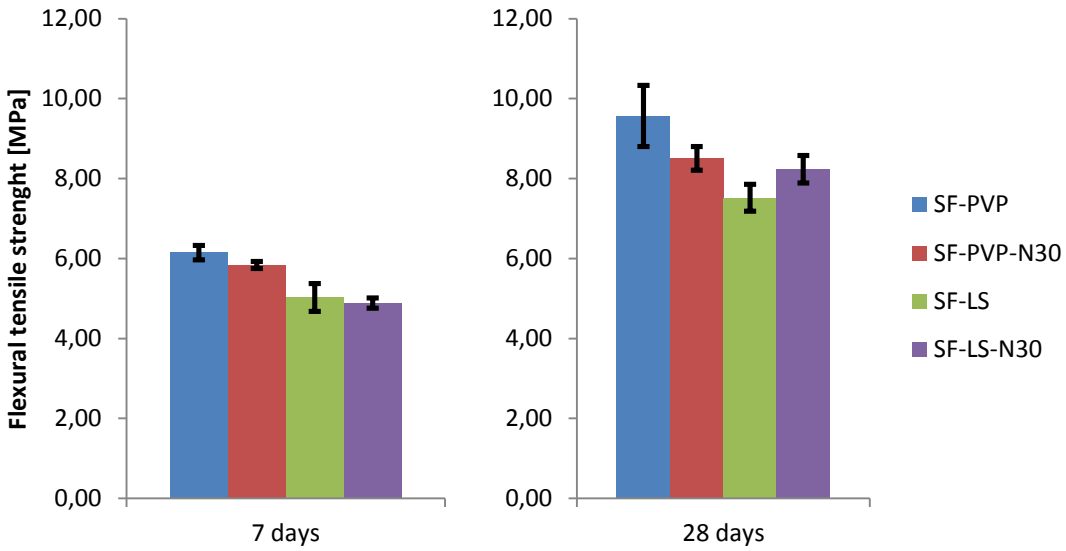

Mortar identification	Flexural tensile strength			
	7 days		28 days	
	Mean [MPa]	Coefficient of variation [%]	Mean [MPa]	Coefficient of variation [%]
SF-PVP	6.15	2.93	9.57	8.00
SF-PVP-N30	5.84	1.51	8.50	3.51
SF-LS	5.03	6.89	7.52	4.48
SF-LS-N30	4.89	2.61	8.23	4.15

SF-PVP – reference without CNTs with PVP;
SF-PVP-N30 – with CNTs and with PVP;
SF-LS – reference without CNTs and with lignosulfonate based plasticizer;
SF-LS-N30 – with CNTs and with lignosulfonate based plasticizer.

Figure 4.9– Flexural strength of test specimens for investigation of the behavior of mortars incorporating nano-structured silica fume

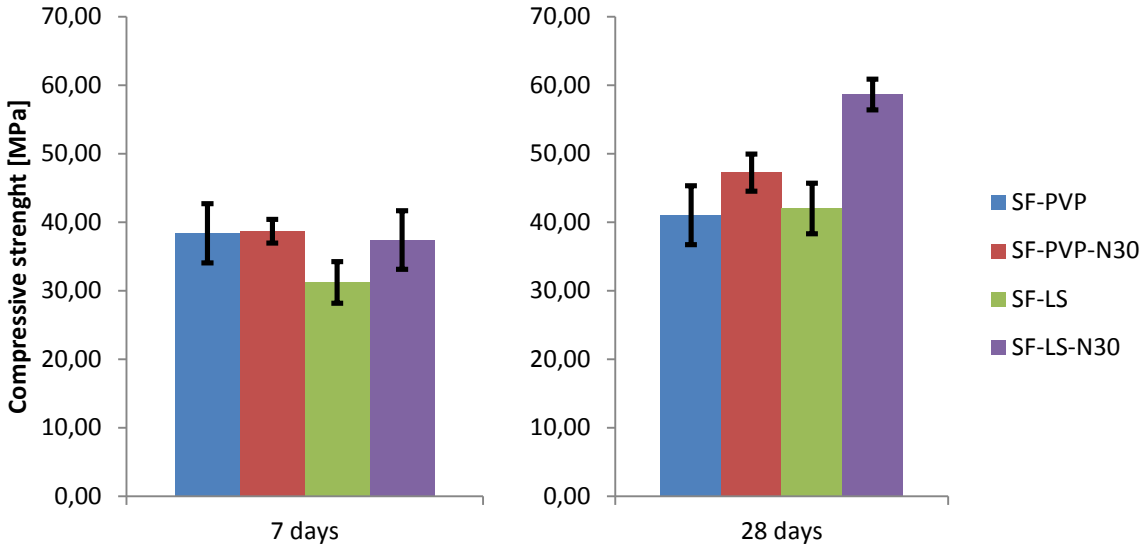

Mortar identification	Compressive strength			
	7 days		28 days	
	Mean [MPa]	Coefficient of variation [%]	Mean [MPa]	Coefficient of variation [%]
SF-PVP	38.38	11.22	41.00	10.48
SF-PVP-N30	38.668	4.46	47.22	5.76
SF-LS	31.23	9.70	42.00	8.76
SF-LS-N30	37.40	11.43	58.63	3.82

SF-PVP – reference without CNTs with PVP;
SF-PVP-N30 – with CNTs and with PVP;
SF-LS – reference without CNTs and with lignosulfonate based plasticizer;
SF-LS-N30 – with CNTs and with lignosulfonate based plasticizer.

Figure 4.10– Compressive strength of test specimens for comparison of the behavior of mortars incorporating nano-structured silica fume.

4.2.3 Covalent functionalization: hydrogen peroxide as functionalizing agent

As presented in the literature review, CNT bonding in the cement matrix is an important aspect in the reinforcing mechanism of nanotubes. To improve this bonding, hydrogen peroxide (H_2O_2) was employed as a functionalizing agent for the nanotubes. Since it is commonly used as air-entraining admixture in concrete, there is no compatibility problem with Portland cement. CNTs/CNFs grown on clinker with 2.5 % Fe addition (in the form of converter dust) were employed. The functionalization process was performed as follows. Some 80 ml of H_2O_2 was applied to 50 g of CNT-clinker composite. The quantity of H_2O_2

was determined by adding it to the clinker gradually until the total amount ceased to evaporate as a result of the highly exothermic reaction. The preparation was dried at 105 °C immediately after the reaction stopped, in order to minimize clinker hydration. The w/c ratio this time was 0.41, Brazilian CP-III type cement was used and 1.5 % (with respect to binder weight) lignosulfonate and polysaccharide based plasticizer (LS) was added to help CNT dispersion. The CNT content remained 0.3 % of binder weight. Details of these mortar mix proportions are shown in Table 4.6.

Table 4.6 – Details of mortars prepared with H_2O_2 treated nano-structured clinker

Mortar identification	CNT/CNF content*
CL-POX-LS	0
CL-POX-LS-N30	0.3 %

* - with respect to binder content

There was no visible difference between the workability of the two mortars. No clusters of clinker with nanotubes could be visually identified during the mixing of CL-POX-LS-N30 mortar.

Prismatic specimens 40 × 40 × 160 mm^3 in size were cast in which flexural tensile strength tests and compression tests were subsequently performed as described previously. Because of some problems with scheduling the tests, they were performed at the ages of 10, and 28 days. Test results are presented in Figures 4.11 and 4.12.

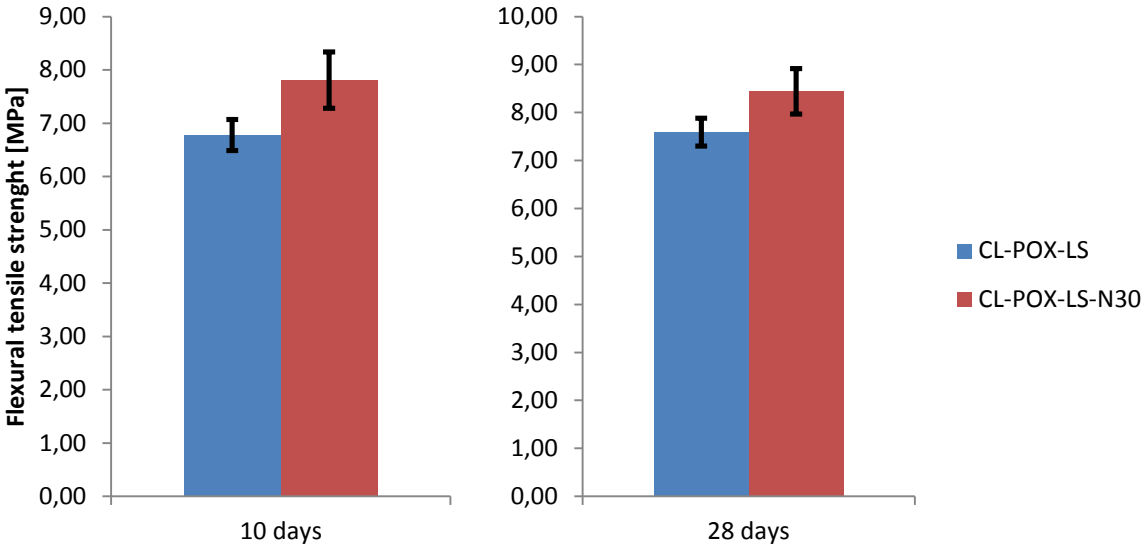

Mortar identification	Flexural tensile strength			
	10 days		28 days	
	Mean [MPa]	Coefficient of variation [%]	Mean [MPa]	Coefficient of variation [%]
CL-POX-LS	6.78	4.28	7.59	3.81
CL-POX-LS-N30	7.81	0.53	8.44	5.62

CL-POX-LS – reference plain cement mortar;
CL-POX-LS-N30 – mortar with hydrogen peroxide treated CNTs.

Figure 4.11– Flexural tensile strength of test specimens for evaluation of the addition of nano-structured clinker treated by hydrogen peroxide

As it can be seen, the addition of H_2O_2 treated CNTs to the mortar resulted in slightly higher compressive and flexural tensile strengths. The gains of flexural tensile and compressive strength were 15.2 % and 14.3 % at 10 days and 11.2 % and 26.0 % at 28 days respectively.

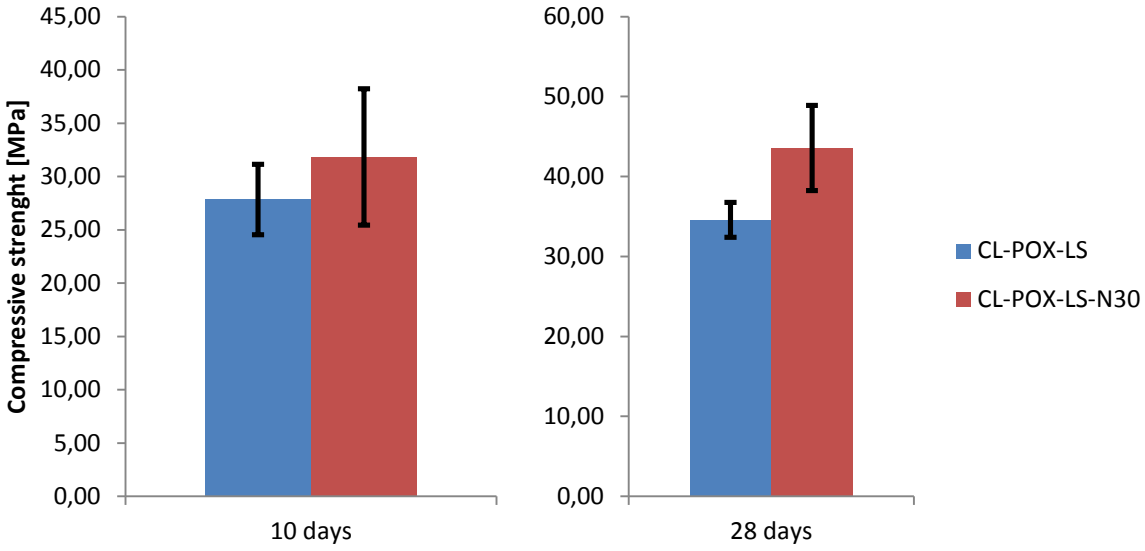

Mortar identification	Compressive strength			
	10 days		28 days	
	Mean [MPa]	Coefficient of variation [%]	Mean [MPa]	Coefficient of variation [%]
CL-POX-LS	27.85	11.87	34.58	6.29
CL-POX-LS-N30	31.83	20.09	43.58	12.24

CL-POX-LS – reference plain cement mortar;
CL-POX-LS-N30 – mortar with hydrogen peroxide treated CNTs.

Figure 4.12– Compressive strength of test specimens for evaluation of the addition of nano-structured clinker treated by hydrogen peroxide

4.2.4 Comparative analysis of the results of mechanical strength tests

The addition of CNTs and CNFs grown on all three types of materials (clinker, blast furnace slag and silica fume) to cement mortars had some positive effect on both compressive and tensile strengths. The amount of nanotubes that provide efficient reinforcement was between 0.1 and 0.3 % with respect to binder content. The result of the comparison of tensile strength of mortars produced with different surfactants as dispersing agents for the CNTs and CNFs showed that the lignosulfonate and polysaccharide based first generation plasticizer admixture had the best effect. However, the high dosage necessary in order to achieve a good dispersion may have negative effects on the hydration of cement. Setting and the evolution of strength were retarded as an effect of this admixture.

The best results achieved by nano-structured clinker were 14.9 % enhancement of flexural tensile (using lignosulfonate based plasticizer) and 43.1 % increase of compressive strength (using polynaphtalene and polycarboxylate plasticizers) at 28 days with respect to the reference without nanotubes (Table 4.7). The highest gains achieved with nano-structured silica fume were 9.4 % in flexural tensile strength and 39.6 %in compressive strength, also at 28 days.

Table 4.7 – Comparison of the gains obtained in flexural tensile and compressive strength of mortars prepared with nano-structured materials with different supports without covalent functionalization

Type of nano-structured material	**Maximum percentage gain achieved with respect to reference at 28 days**	
	Tensile strength	**Compressive strength**
Nano-structured clinker (CL-LS-N30)	14.9 %	-
Nano-structured clinker (CL-NP-N30)	-	43.1 %
Nano structured silica fume (SF-LS-N30)	9.4 %	39.6 %

Mortars incorporating nanotubes functionalized by ammonia during the synthesis showed only small increase in tensile and compressive strength than the reference, if any. At the same time the nano-structured clinker treated by hydrogen peroxide resulted in 11.2 % and 26.0 % higher flexural tensile and compressive strength respectively at 28 days (Table 4.8). This difference was theoretically foreseen by Sanchez and Zhang (2008) using molecular dynamics simulation. Hydrogen peroxide is an inexpensive material and is a commonly used air entrainer admixture for concrete thus there is no known incompatibility issues with cement based materials. The method developed during the investigations to functionalize the nanotubes is much easier to conduct with respect to conventional treatments to create covalently bonded functional groups (DATSYUK *et al.*, 2008; MELO, 2009; BATISTON, 2012): the material is inexpensive and easy to handle and the process can be adapted to existing concrete production chain.

Table 4.8 – Comparison of the gains obtained in flexural tensile and compressive strength of mortars prepared with nano-structured clinker with different functionalization methods

Covalent functionalization method	Maximum percentage gain achieved with respect to reference at 28 days	
	Tensile strength	Compressive strength
Ammonia treatment (CL-NH-LP-N30)	-	14.3 %
Hydrogen peroxide treatment (CL-POX-LP-N30)	11.2 %	26.0 %

When comparing the presented results with others found in the literature it can be seen, that there was a significant increase of gains in strength of mortars prepared with the *in-situ* synthesized nano-structured materials with respect to the ones prepared with the physical mixture of high quality CNTs, with probably higher tensile strength and without covalent functionalization (Table 4.9).

Table 4.9 – Comparison of percentage gains in compressive and tensile strength of CNT-cement mortars prepared with surfactants obtained during present and previous investigations

Author	CNT content	Results	
		Tensile strength	Compressive strength
Cwirzen *et al.*, 2009	0.006-0.15 %	0	0
Musso *et al.*, 2009	0.5 %	-	34 %
Ludvig (this study)	0.3 %	14.9 %	43.1 %

The same comparison of gains of both compressive and tensile strengths of mortars prepared with nano-structured clinker treated with hydrogen peroxide show similar results to those of mortars prepared with covalently functionalized high quality CNTs (Table 4.10). However the functionalization process presented in this study is considerably simpler than those used for high quality CNTs.

Gains in tensile strength in all cases remained lower than that of compressive strength. This phenomenon may be caused by poor dispersion and bond of CNTs in the hardened cement matrix. The nanotube addition in this case can have two effects: they may fill in

smaller pores and/or they may act as nucleating sites for the formation of hydration products (MAKAR and CHAN, 2009).At the same time the bond between the carbon material and the hydration products is weak, therefore the better results in the compressive behavior of such composites than in the tensile characteristics.

Table 4.10 – Comparison of percentage gains in compressive and tensile strength of CNT-cement mortars prepared with covalently functionalized nanotubes obtained during present and previous investigations

Author	CNT content	Results	
		Tensile strength	Compressive strength
Li *et al.*, 2005	0.5 %	19 %*	25 %
Batiston *et al.*, 2008	0.5 %	-	22 %
Cwirzen *et al.*, 2008	0.045 %	-	50 %
Musso *et al.*, 2009	0.5 %	0*	0
Melo *et al.*, 2011	0.3 %	34 %**	12 %
Ludvig (this study)	0.3 %	11.2 %*	26.0 %

* – flexural tensile strength
** – splitting tensile strength

4.3 Pore structure and density of CNT/CNF-cement mortar composites

Pore structure and density of mortars were analyzed by nitrogen adsorption and helium pycnometry. For these two investigations pieces of mortar specimens were cut instead of grounding (MELO, 2009) in order to minimize damage to the pore structure. On the other hand, pores without contact with the outer surface of the samples possibly were not considered by the investigations. The specimens in all cases were those previously tested at 28 days of age. Mix proportions and other details are given in Table 4.11. All mortars were prepared using lignosulfonate and polysaccharide based admixture. The approximate size of the samples was 5 × 5 × 20 mm^3. The samples were dried at 60°C during one week. The

drying at this temperature was found to be relatively effective in sample preparation for mercury porosimetry analysis (GALLÉ, 2001). The samples were degasified after the drying process and analyzed on a Quantachrome Instruments Nova 2200 instrument in the Laboratory of the Chemistry of Nanostructures at the Development Center of Nuclear Technology (CDTN – Centro de Desenvolvimento da Tecnologia Nuclear). Helium pycnometry measurements were performed on the same specimens using a Quantachrome Instruments Ultrapycnometer 1000 equipment in the same laboratory.

Table 4.11 – Details of specimens analyzed by gas adsorption porosimetry and *He* pycnometry

Sample name	**CNT/CNF content* [%]**	**W/C ratio**
CPIII-CL-LS[1]	0	0.43
CPIII-CL-LS-N30[1,3]	0.3	0.43
CP-III-CL-POX-LS-N30[1,5]	0.3	0.43
CPV-CL-LS[2]	0	0.43
CPV-CL-LS-N30[2,3]	0.3	0.43
CPIII-SF-LS[1]	0	0.40
CPIII-SF-LS-N30[1,4]	0.3	0.40
CPIII-CL-NH-LP[1]	0	0.375
CPIII-CL-NH-LP-N10[1,6]	0.1	0.375
CPIII-CL-NH-LP-N30[1,6]	0.3	0.375

* – with respect to binder content
[1] – CP-III cement
[2] – CP-V cement
[3] – with nano-structured clinker
[4] –with nano-structured silica fume
[5] – with H_2O_2 treated nano-structured clinker
[6] – with ammonia treated nano-structured clinker

Results of the gas adsorption porosimetry and *He* pycnometry are presented in Table 4.12. Specific surface area was determined by both multipoint and single point method. The average pore diameter was determined based on the adsorption and desorption data. For density analysis 20 measurements were done by the pycnometer and the average of the last three values was considered. Detailed data of the gas adsorption porosimetry by BET and *He* pycnometry can be found in Annex C.

Table 4.12 – Results of the pore structure analysis of mortars incorporating CNTs/CNFs synthesized on clinker and silica fume with different surface treatments and in different amounts

Sample name	Multipoint specific surface area [m^2/g]	Single point specific surface area [m^2/g]	Average pore diameter [nm]	Density [g/cm^3]
CPIII-CL-LS	1.56	1.60	15.8	2.63
CPIII-CL-LS-N30	2.21	2.21	12.7	2.68
CP-III-CL-POX-LS-N30	2.27	2.31	14.3	2.71
CPV-CL-LS	1.59	1.61	14.0	2.67
CPV-CL-LS-N30	1.79	1.81	12.8	2.65
CPIII-SF-LS	2.23	2.26	17.7	2.55
CPIII-SF-LS-N30	2.76	2.74	14.1	2.61
CPIII-CL-NH-LP	1.81	1.82	15.4	2.66
CPIII-CL-NH-LP-N10	2.30	2.30	11.5	2.68
CPIII-CL-NH-LP-N30	2.12	2.15	13.5	2.67

The specific surface areas of the same samples measured with the two methods – multi point and single point – presented only small differences. Thus the results of any of the two methods could be considered for discussion. Pore diameters of the mortar specimens had an average between 10 and 15 nm. The parameter less affected by the incorporation of nano-structured material was the density determined by helium pycnometry with 3 % maximum alteration.

Specific surface area of mortars prepared with nano-structured clinker and CP-III cement was higher than that of ordinary cement mortar by approximately 40 % (Table 4.13). In the case of CP-V mortars the presence of nano-structured clinker resulted in less, about 12 % of increase of specific surface area. The mortars containing nano-structured silica fume had approximately 23 % increase of the specific surface area.

Table 4.13 – Comparison of the pore structure analysis results of mortars made with Brazilian CP-III and CP-V type cements and with nano-structured clinker or silica fume

Sample identification	Reference sample identification	Multipoint specific surface area	Average pore diameter	Density
CPIII-CL-LS-N30	CPIII-CL-LS	+41.7 %	-19.6 %	+1.9 %
CPV-CL-LS-N30	CPV-CL-LS	+12.6 %	-8.6 %	-0.7 %
CPIII-SF-LS-N30	CPIII-SF-LS	+23.8 %	-20.3 %	+2.4 %

The average pore diameter of the CP-III mortar decreased as an effect of nano-structured clinker addition in the amount of 0.3 % of CNTs/CNFs with respect to binder content (Table 4.13). The decrease was 19.6 %. Brazilian CP-V type cement mortars presented similar characteristics: the inclusion of the same amount of nano-structured clinker resulted in 8.6 % decrease of the mean pore diameter. The addition of nano-structured silica fume caused a decrease of the pore diameter of the CP-III mortar by 20.3 %.

The density of Brazilian CP-III type cement mortar incorporating nano-structured clinker was higher than plain cement mortar as determined by *He* pycnometry (Table 4.12). The increase was from 2.63 to 2.68 g/cm^3. The mortars prepared with CP-V cement did not show similar behavior. The measured density of plain cement mortar was 2.67 g/cm^3, meanwhile that of the sample containing nano-structured clinker was 2.65 g/cm^3. The addition of nano-structured silica fume increased the density of the mortar from 2.55 to 2.61 g/cm^3. All investigated parameters presented higher alterations when using CP-III cement, than in the case of CP-V type. At the same time there was no significant difference between the effect of nano-structured clinker and nano-structured silica fume addition to CP-III mortar.

The incorporation of ammonia treated nanotubes grown on clinker had also a similar effect on the mortars. However, mortars incorporating 0.1 % of CNT/CNF of the binder content showed a higher increase of the specific surface area with respect to ordinary cement mortars than the ones incorporating 0.3 %. The increases were about 27 % and 17 % respectively (Table 4.14). The addition of 0.3 % of CNTs/CNFs treated with hydrogen peroxide increased the specific surface area of the Brazilian CP-III type cement mortar by 45 %. This effect of H_2O_2 treated nanotube addition is significantly higher than that of the addition of ammonia treated ones.

Table 4.14 – Comparison of the pore structure analysis results of mortars made with Brazilian CP-III type cement and with ammonia or H_2O_2 treated nano-structured clinker

Sample identification	Reference sample identification	Multipoint specific surface area	Average pore diameter	Density
CPIII-CL-POX-LS-N30	CPIII-CL-POX-LS	+45.5 %	-9.5 %	+3.0 %
CPIII-CL-NH-LP-N10	CPIII-CL-NH-LP	+27.1 %	-25.3 %	+0.8 %
CPIII-CL-NH-LP-N30	CPIII-CL-NH-LP	+17.1 %	-12.3 %	+0.4 %

The pore diameter was also smaller after adding CNTs/CNFs treated with ammonia: 25.3 % for mortars incorporating 0.1 % of this type of nanotubes and 12.3 % in the case of mortars with 0.3 % of CNTs/CNFs (Table 4.14). The addition of hydrogen peroxide treated nanotubes caused the reduction of the mean pore diameter of mortars. The decrease was 9.5 %.

The addition of ammonia treated nanotubes did not influence significantly the mortar density. The values were 2.66, 2.68 and 2.67 g/cm^3 for mortars incorporating 0, 0.1 and 0.3 % of nanotubes respectively. At the same time, the addition of hydrogen peroxide treated nanotubes increased the density of Brazilian CP-III type cement mortar from 2.63 to 2.71 g/cm^3 (Table 4.12).

Among the investigated parameters the more influenced by the addition of hydrogen peroxide treated nanotubes than by ammonia treated ones were the specific surface area and the density. On the other hand, mean pore size suffered higher influence when ammonia treated nano-structured clinker was employed. Pore structure of mortars prepared with lower ammonia treated CNT/CNF content presented higher alterations than the other prepared with higher CNT/CNF content. A better dispersion of fewer nanotubes may explain this difference.

The small increase of the density may indicate a denser cement matrix as a result of the addition of nanomaterials. The nanotubes may act as nucleating sites for hydration product formation, as it can be concluded from the BET results: higher surface area and smaller pores indicate that CNTs and CNFs filled some pores and divided them into smaller ones. This phenomenon causes the increase of specific surface area. Since practically no change was observed in the density of the mortars, the same volume of pores are distributed in smaller ones with higher specific surface area.

The increase of specific surface area and the decrease of pore diameter were also witnessed by Melo *et al.* (2011) on cement mortars incorporating CNTs in contents between 0.3 and 0.75 % of binder mass. The mortars with 0.3 % CNT content showed the highest alterations of these parameters with respect to the reference: specific surface area was increased by 58.7 % and pore diameter was decreased by 31.3 %. The higher nominal values obtained by Melo *et al.* can be explained by the higher w/c ratio of 0.48 against values between 0.375 and 0.43 used in present investigations. Helium pycnometry results of Melo *et al.* showed also marginal influence of CNT addition on the density of the mortars.

The increase of specific surface area (13 to 45 % increase) and decrease of mean pore diameter (9 to 25 % decrease) indicates a better packing of cement hydration products even with the same mortar density values. The better packing can explain the better compressive behavior of the mortars containing CNTs/CNFs.

5

CONCLUSIONS

5.1 Synthesis

CNTs and CNFs were successfully synthesized on Portland cement clinker and silica fume using CVD method. The catalysts of the CNT/CNF synthesis were prepared using the clinker or silica fume as support and or the iron content of the support itself, or the addition of industrial wastes containing iron as catalyst particles. Silica fume with converter dust and clinker with steel mill scale or converter dust addition produced CNTs and CNFs in best quantity and quality. Scanning electron microscopy and thermogravimetric analysis approved to be effective tools for the qualitative characterization of the products. The synthesis efficiency at the same time was determined by the mass loss at 800 °C as the increased amount of sample analyzed reduced the effect of inhomogenity.

The optimal synthesis parameters were determined using pure clinker as catalyst. The parameters that resulted in the highest production were: 30 minutes of process duration, 500 sccm acetylene or ethylene flow and 775 ºC temperature. The addition of industrial wastes such as steel mill scale and converter dust to clinker resulted in the growth of CNTs/CNFs with better morphology. Highest production was achieved using as catalyst clinker mixed with 2.5 % additional iron.

The highest production was achieved by silica fume as catalyst support, due to the higher surface area of this support than that of ground clinker. At the same time the products have high dispersion of size and morphology when comparing with high quality and high

purity CNT growth processes. The use of raw materials with low quality control probably caused the apparent deterioration of the nanotubes. On the other hand, the synthesis process of CNTs/CNFs on clinker or silica fume is much less complex and much less expensive than that of high quality synthesis.

Simple processes for functionalization of these nanotubes were developed. When ammonia was introduced during the synthesis process, CNTs suffered an alteration in their structure. This alteration may indicate a successful nitrogen functionalization. The functionalization process consists of the use of an additional gas during the synthesis which gives various advantages with respect to other common functionalization processes based on acids (DATSYUK *et al.*, 2008, MELO, 2009). Functionalization with hydrogen peroxide also occurs under milder conditions which do not interfere with the reactivity of clinker.

The produced nano-structured clinker was subjected to comparative physic-chemical investigations. The results showed no significant alteration in Blaine fineness, chemical composition and setting times of Brazilian CP-III and CP-V type cement when nano-structured clinker was added at 0.3 % nanotube concentration.

5.2 Characterization of nano-structured mortars

The optimal CNT/CNF content of cement mortars was found to be in the range of 0.1 to 0.3 % of binder weight. Higher amount of nanotubes do not disperse well and tend to form clusters which weaken the matrix. Some commercial concrete admixtures worked well to disperse the nano-structured material. The best tensile test results were achieved by a lignosulfonate based plasticizer (14 % enhancement). With respect to compressive strength, a combination of polynaphtalene and polycarboxylate admixtures led to 43 % gain.

The treatment of the nanotubes with ammonia caused modifications on their structure, but compressive or tensile strengths of the mortars prepared with such nano-structured clinker did not show enhancement. At the same time, positive results were obtained by nano-structured clinker treated by hydrogen peroxide. Gains were observed in both tensile and compressive strength of mortars prepared with H_2O_2 treated nanotubes, which indicate a possibly stronger bond of these nanotubes to the cement paste.

With respect to published mechanical property results of mortars prepared with physical mixture of high quality and high purity CNTs, it can be concluded that the addition of nano-structured clinker or silica fume to cement mortars can provide similar or better

enhancement in these properties. This fact strongly suggests that issues of dispersion and bond to the cement paste matrix are more relevant at this level than the mechanical strength of the nanotubes themselves.

Pore structure of the mortars was analyzed by gas adsorption and *He* pycnometry. The incorporation of CNTs/CNFs caused an increase of specific surface area of the mortars, meanwhile reducing the mean pore diameter. The addition of these nanomaterials resulted in a finer pore structure. The smaller pores have higher surface area, which explains the observed increase of this parameter. At the same time the nano-structured clinker or silica fume addition caused a small increase of the density. The incorporation of nanotubes and nanofibers resulted in a more compact matrix probably by filling in pores and by serving as catalysts for the formation of cement hydration products. The same observations were made by Melo (2009) on the pore structure of mortars prepared with the physical mixture of CNTs. These observations suggest that the addition of CNTs/CNFs results in a better compaction of hardened cement pastes, causing also an increase of compressive strength of these composites.

5.3 Propositions for future investigations

As a new material, there are several fields that remain to be investigated with respect to the synthesis and characterization of nano-structured materials. Based on the findings of present study further research should focus on the following fields:

- Development of a continuous production process based on a rotating CVD reactor in order to increase production and homogeneity of the material as well as to reduce costs. Further characterization will also be necessary.
- Tests of other gas sources in order to reduce production costs and/or improve synthesis efficiency and product quality. The use of nitrogen as carrier gas instead of argon has already been reported (MALGAS *et al.*, 2008) and could significantly reduce costs of CNT synthesis. The use of cheaper carbon source gases (methane or natural gas) may also reduce production costs. The use of nitrogen as carrier gas may cause alteration of the nanotube structure (TANG *et al.*, 2004) and may be a simple functionalization method linked to the synthesis process which may enhance the bond between nanotubes and the cement matrix.

- Evaluation of the dispersion of the CNTs/CNFs in the cement matrix. A possible method may be developed based on electrical resistivity of the composites. Because of the high conductivity of the nanotubes, a better dispersion would result in the reduction of resistivity of the composite.
- Investigation of the interaction between the nano-structured material and surfactants in order to optimize the dispersing effect on the nanotubes. The quantity of the surfactant adsorbed on the nano-structured material surface may characterize the dispersive agent efficiency (ZHANG *et al.*, 2001; WANG *et al.*, 2007).
- Theoretic study (possibly by molecular dynamics) of the interaction between CNTs and cement matrix in order to achieve information about the ideal dosage, size, morphology and functionalization of the nanotubes.
- Continue the investigation based on the promising results of mortars prepared with hydrogen peroxide. Another mild functionalization process may be developed based on ozone treatment.
- Investigations on other cement-based, nano-structured materials: concrete and paste.
- Investigation of the possibility to use blast furnace slag as catalyst support for CNT/CNF synthesis.
- Evaluation of the strength at the ages after 28 days in order to characterize the effect of CNT/CNF addition on the whole hydration process of Portland cement. The strength values at more advanced ages may be used as final strength and may result in material (cement) saving which can reduce the environmental impact of structures made with nano-structured cement.

6

REFERENCES

AMERICAN CONCRETE INSTITUTE (ACI) COMMITTEE E-701 MATERIALS FOR CONCRETE CONSTRUCTION. Chemical admixtures for concrete. In: Education Bulletin E4-03. American Concrete Institute, 2003.

_____ ACI 234R-06. Guide to the use of silica fume in concrete. Report. American Concrete Institute, 2006.

AL-OTAIBI, S. Recycling steel mill scale as fine aggregate in cement mortars. *European Journal of Scientific Research*, v. 24, p. 332-338, 2008.

AMARAL, E. C.; BOTELHO, R. A.; LAMEIRAS, F. S.; REIS, S. C.; TOLENTINO, E. O efeito do tratamento térmico a 300 °C na conectividade da estrutura de poros de argamassas de cimento Portland reforçadas por fibras de polipropileno. *Cerâmica*, v. 58, p. 262-269, 2012.

ANDRAWES, B.; CHAN, L. Y. Compression and tension stress-sensing of carbon nanotube-reinforced cement. *Magazine of Concrete Research*, v. 64, p. 253-258, 2012.

ASSOCIAÇÃO BRASILEIRA DE NORMAS TÉCNICAS. NBR 5733 – Cimento Portland de alta resistência inicial. Rio de Janeiro, 1991.

_____. NBR 5735 – Cimento Portland de alto-forno. Rio de Janeiro, 1991.

_____. NBR 7215 – Cimento Portland – Determinação da resistência á compressão. Rio de Janeiro, 1996.

_____. NBR 7222 – Argamassa e Concreto – Determinação da resistência à tração por compressão diametral de corpos-de-prova cilíndricos. Rio de Janeiro, 1994.

_____. NBR 12142 – Concreto – Determinação da resistência à tração na flexão em corpos-de-prova prismáticos. Rio de Janeiro, 1991.

_____. NBR NM15: Cimento Portland – Análise química – Determinação de resíduo insolúvel. Rio de Janeiro, 2012.

_____. NBR NM18: Cimento Portland – Análise química – Determinação de perda ao fogo. Rio de Janeiro, 2012.

_____. NBR NM43: Cimento Portland – Determinação da água de consistência normal no estado fresco. Rio de Janeiro, 2002.

_____. NBR NM65: Cimento Portland – Determinação do tempo de pega. Rio de Janeiro, 2003.

_____. NBR NM76: Cimento Portland – Determinação da finura pelo método de permeabilidade ao ar (método Blaine). Rio de Janeiro, 1998.

BALAGURU, P.; CHONG, K. Nanotechnology and concrete: Research opportunities. In: SOBOLEV, K. and SHAH, S. P. (Ed.) *Nanotechnology of Concrete: Recent Developments and Future Perspectives.* Farmington Hills, MI: American Concrete Institute, p. 15-28, 2008.

BANDYOPADHYAYA, R.; NATIV-ROTH, E.; REGEV, O.; YERUSHALMI-ROZEN, R. Stabilization of individual carbon nanotubes in aqueous solutions. *Nano Letters*, v. 2, p. 25-28, 2002.

BARTOS, P. J. M. Nanotechnology in construction: A roadmap for development. In: SOBOLEV, K. and SHAH, S. P. (Ed.) *Nanotechnology of Concrete: Recent Developments and Future Perspectives.* Farmington Hills, MI: American Concrete Institute, p. 1-14, 2008.

BATISTON, E. R. *Incorporação de nanotubos de carbono em matriz de cimento Portland*. 2012. 136p. PhD Thesis in civil engineering. Federal University of Santa Catarina, Florianópolis.

BATISTON, E. R.; GLEIZE, P. J. P.; GOMEZ, L. A. Estudo exploratório dos efeitos de nanotubos de carbono em matrizes de cimento Portland. In: 50º Congresso Brasileiro do Concreto. *Anais*. Salvador, BA: Associação Brasileira de Concreto, 2008.

BATISTON, E. R.; HAMPINELLI, D. H.; DE OLIVEIRA, R. C.; GLEIZE, P. J. P. Funcionalização e efeito da incorporação de nanotubos de carbono na cinética de hidratação em matrizes cimentíceas. In: 52º Congresso Brasileiro do Concreto. *Anais*. Fortaleza, CE: Associação Brasileira do Concreto, 2010.

BAUGHMAN, R. H.; ZAKHIDOV, A. A.; DE HEER, W. A. Carbon nanotubes – The route toward applications. *Science*, v. 297, p. 787-792, 2002.

BENTZ, D. P.; COVENEY, P. V.; GARBOCZI, E. J.; KLEYN, M. F., STUTZMAN P. E. Cellular automaton simulations of cement hydration and microstructure development. *Modeling and Simulation in Materials Science and Engineering*, v. 2, p. 783-808, 1994.

BHANJA, S.; SENGUPTA, B. Influence of silica fume on the tensile strength of concrete. *Cement and Concrete Research*, v. 35, p. 743-747, 2005.

CHAIPANICH, A.; NOCHAIYA, T.; WONGKEO, W.; TORKITTIKUL, P. Compressive strength and microstructure of carbon nanotubes-fly ash cement composites. *Materials Science and Engineering A*, v. 527, p. 1063-1067, 2010.

CHAN, L. Y.; ANDRAWES, B. Characterization of the uncertainties in the constitutive behavior of carbon nanotube/cement composites. *Science and Technology of Advanced Materials*, v. 10, p. 1-13, 2009.

CHAN, L. Y.; ANDRAWES, B. Finite element analysis of carbon nanotube/cement composite with degraded bond strength. *Computational Materials Science*, v. 47, p. 994-1004, 2010.

CHENG-YI, H.; FELDMAN, R. F. Influence of silica fume on the microstructural development in cement mortars. *Cement and Concrete Research*, v. 15, p. 285-294, 1985.

CHUNG, D. L. L. Comparison of submicron-diameter carbon filaments and conventional carbon fibers as fillers in composite materials. *Carbon*, v. 39, p. 1119-1125, 2001.

CHUNG, D. L. L. Dispersion of short fibers in cement. *Journal of Materials in Civil Engineering*, v. 17, p. 379-383, 2005.

COLLINS, F.; LAMBERT, J.; DUAN, W. H. The influences of admixtures on the dispersion, workability and strength of carbon nanotube-OPC paste mixtures. *Cement & Concrete Composites*, v. 34, p. 201-207, 2012.

COUTEAU, E.; HERNADI, K.; SEO, J. W.; THIÊN-NGA, L.; MIKÓ, CS.; GAÁL, R.; FORRÓ, L. CVD synthesis of high-purity multiwalled carbon nanotubes using $CaCO_3$ catalyst support for large-scale production. *Chemical Physics Letters*, v. 378, p. 9-17, 2003.

CULLITY, B. D. *Elements of X-ray diffraction*. 2nd ed. Reading, MA: Addison-Wesley Publishing Company Inc. 555 p., 1978.

CUMMINGS, J.; ZETTL, A. Low-friction nanoscale linear bearing realized from multiwall carbon nanotubes. *Science*, v. 289, p. 602-604, 2000.

CWIRZEN, A.; HABERMEHL-CWIRZEN, K.; PENTTALA, V. Surface decoration of carbon nanotubes and mechanical properties of cement/carbon nanotube composites. *Advances in Cement Research*, v. 20, p. 65-73, 2008.

CWIRZEN, A.; HABERMEHL-CWIRZEN, K.; SHANDAKOV, D.; NASIBULINA, L. I.; NASIBULIN, A. G.; MUDIMELA, P. R.; KAUPPINEN, E. I.; PENTTALA V. Properties of high yield synthesized carbon nanofibres/Portland cement composite. *Advances in Cement Research*, v. 21, p. 141-146, 2009.

DAENEN, M.; DE FOUW, R. D.; HAMERS, B.; JANSSEN, P. G. A.; SCHOUTEDEN, K.; VELD, M. A. J. The wondrous world of carbon nanotubes. 'A review of current carbon nanotube technologies'. 2003. 93 p. Multidisciplinair project – Eindhoven University of Technology, Eindhoven, 2003.

DATSYUK, V.; KALYVA, M.; PAPAGELIS, K.; PARTHENIOS, J.; TASIS, D.; SIOKOU, A.; KALLITSIS, I.; GALIOTIS, C. Chemical oxidation of multiwalled carbon nanotubes. *Carbon*, v. 46, p. 833-840, 2008.

DE ROJAS, M. I. S.; FRÍAS, M. The pozzolanic activity of different materials, its influence on the hydration heat of mortars. *Cement and Concrete Research*, v. 26, p. 203-213, 1996.

DEMCZYK, B. G.; WANG, Y. M.; CUMINGS, J.; HETMAN, M.; HAN, W.; ZETTL, A.; RITCHIE, R. O. Direct mechanical measurement of the tensile strength and elastic modulus of multiwalled carbon nanotubes. *Materials Science and Engineering A*, v. 334, p. 173-178, 2002.

DRESSELHAUS, M. S.; DRESSELHAUS, G.; SAITO, R. Physics of carbon nanotubes. *Carbon*, v. 33, p. 883-891, 1995.

DRESSELHAUS, M. S.; DRESSELHAUS, G.; SAITO, R. JORIO, A. Raman spectroscopy of carbon nanotubes. Physics reports, v. 409, p. 47-99, 2005.

DUNENS, O. M.; MACKENZIE, K. J.; HARRIS, A. T. Synthesis of multiwalled carbon nanotubes on fly ash derived catalysts. *Environmental Science & Technology*, v. 43, p. 7889-7894, 2009.

ESQUIVEL, E. V.; MURR, L. E. A TEM analysis of nanoparticles in Polar ice core. *Materials Characterization*, v. 52, p. 15-25, 2004.

FALVO, M. R.; CLARY, G. J.; TAYLOR II, R. M.; CHI, V.; BROOKS JR, F. P.; WASHBURN, S.; SUPERFINE, R. Bending and buckling of carbon nanotubes under large strain. *Nature*, v. 389, p. 582-584, 1997.

FLATT, R. J.; HOUST, Y. F. A simplified view on chemical effects perturbing the action of superplasticizers. *Cement and Concrete Research*, v. 31, p. 1169-1176, 2001.

FLORES-VELEZ, L. M.; DOMINGUEZ, O. Characterization and properties of Portland cement composites incorporating zinc-iron oxide nanoparticles. *Journal of Materials Science*, v. 37, p. 938-988, 2002.

FU, X.; CHUNG, D. L. L. Submicron-diameter-carbon-filament cement-matrix composites. *Carbon*, v. 36, p. 459-462, 1998.

GALLÉ, C. Effect of drying on cement-based materials pore structure as identified by Mercury intrusion porosimetry: A comparative study between oven-, vacuum-, and freeze-drying. *Cement and Concrete Research*, v. 31, p. 1467-1477, 2001.

GLEIZE, P. J. P. Nanotecnologia e concreto. In: IV Simpósio Internacional sobre Concretos Especiais - SINCO 2008, 2008, Fortaleza - CE. IV Simpósio Internacional sobre Concretos Especiais. SINCO 2008. Sobral - CE : Universidade Estadual Vale do Acaraú - UVA, 2008.

GONG, H.; ZHANG, Y.; QUAN, J.; CHE, S. Preparation and properties of cement based piezoelectric composites modified by CNTs. *Current Applied Physics*, v. 11, p. 653-656, 2011.

GOURNIS, D.; KARAKASSIDES, M. A.; BAKAS, T.; BOUKOS, N.; PETRIDIS, D. Catalytic synthesis of carbon nanotubes on clay minerals. *Carbon*, v. 40, p. 2641-2646, 2002.

HAN, B.; YU, X.; KWON, E. A self-sensing carbon nanotube/cement composite for traffic monitoring. *Nanotechnology*, v. 20, p. 1-5, 2009.

HAN, B.; YU, X.; KWON, E.; OU, J. Effects of CNT concentration level and water/cement ratio on the piezoresistivity of CNT/cement composites. *Journal of Composite Materials*, v. 46, p. 19-25, 2011.

HLAVACEK, P.; SMILAUER, V.; PADEVET, P.; NASIBULINA, L.; NASIBULIN, A. G. Cement grains with surface-synthetized carbon nanofibres: Mechanical properties and nanostructure. In: 3rd International Conference NANOCON 2011. *Proceedings*. Tanger Ltd.: Brno, Czech Republic. 21-23. 09. 2011. P. 75-80.

HWANG, C. L.; CHANDRA, S. The use of rice husk in concrete. In: CHANDRA, S. (Ed.) *Waste materials used in concrete manufacturing*. Westwood, NJ: Noyes Publications, 1997, p. 184-234.

IBARRA, Y. S.; GAITERO, J. J.; ERKIZIA, E.; CAMPILLO. Atomic force microscopy and nanoindentation of cement pastes with nanotube dispersions. *Physica Status Solidi A*, v. 203, p. 1076-1081, 2006.

IIJIMA, S. Helicoidal microtubes of graphitic carbon. *Nature*, v. 354, p. 56-58, 1991.

JENNINGS, H. M.; THOMAS, J. J.; GEVRENOV, J. S.; CONSTANTINIDES, G.; ULM, F.-J. A multi-technique investigation of the nanoporosity of cement paste. *Cement and Concrete Research*, v. 37, p. 329-336, 2007.

JOLICOEUR, C.; SIMARD, M.-A. Chemical admixture-cement interactions: phenomenology and physico-chemical concepts. *Cement and Concrete Composites*, v. 20, p. 87-101, 1998.

JOZIĆ, D.; ZELIĆ, J. The effect of fly ash on cement hydration in aqueous suspensions. *Ceramics – Silikáty*, v. 50, p. 98-105, 2006.

KATHAYINI, H.; NAGARAJU, N.; FONSECA, A.; NAGY, J. B. Catalytic activity of Fe, Co and Fe/Co supported on Ca and Mg oxides, hydroxides and carbonates in the synthesis of carbon nanotubes. *Journal of Molecular Catalysis*, v. 223, p. 129-136, 2004.

KHASSIN, A. A.; YURIEVA, T. M.; ZAIKOVSKII, V. I.; PARMON, V. N. Effect of metallic cobalt particle size on occurrence of CO disproportionation – Role of fluidized metallic cobalt-carbon solution in carbon nanotube formation. *Reaction Kinetics and Catalysis Letters*, v. 64, p. 63-71, 1997.

KONSTA-GDOUTOS, M. S.; METAXA, Z. S.; SHAH, S. P. Multi-scale mechanical and fracture characteristics and early-age strain capacity of high performance carbon nanotube/cement nanocomposites. *Cement &Concrete Composites*, v. 32, p. 110-115, 2010a.

KONSTA-GDOUTOS, M. S.; METAXA, Z. S.; SHAH, S. P. Highly dispersed carbon nanotube reinforced cement based materials. *Cement and Concrete Research*, v. 40, p. 1052-1058, 2010b.

KUMAR, S.; KOLAY, P.; MALLA, S.; MISHRA, S. Effect of multiwalled carbon nanotubes on mechanical strength of cement paste. *Journal of Materials in Civil Engineering*, v. 24, p. 84-91, 2012.

LADEIRA,L. O.; SILVA, E. E.;DE OLIVEIRA, S.; LACERDA, R. G.; FERLAUTO, A. S.; ÁVILA E.; LOURENÇON, E. "Processo de síntese contínua e em larga escala de nanotubos de carbono sobre o clínquer de cimento e produtos nanoestruturados", Brazilian Patent, INPI 014080002727 (30.04.2008).

LI, F.; CHENG, M.; BAI, S.; SU, G.; DRESSELHAUS, M. S. Tensile strength of single-walled carbon nanotubes directly measured from their macroscopic ropes. *Applied Physics Letters*, v. 77, p. 3161-3163, 2000.

LI, G. Properties of high-volume fly ash concrete incorporating nano-SiO_2. *Cement and Concrete Research*, v. 34, p. 1043-1049, 2004.

LI, G. Y.; WANG, P. M.; ZHAO, X. Mechanical behaviour and microstructure of cement composites incorporating surface-treated multi-walled carbon nanotubes. *Carbon*, v. 43, p. 1239-1245, 2004.

LI, G. Y.; WANG, P. M.; ZHAO, X. Pressure-sensitive properties and microstructure of carbon nanotube reinforced cement composites. *Cement & Concrete Composites*, v. 29, p. 377-382, 2007.

LI, H.; XIAO, H.-G.; OU, J.-P. A study on mechanical and pressure-sensitive properties of cement mortar with nanophase materials. *Cement and Concrete Research*, v. 34, p. 435-438, 2004.

LI, Y.-Y.; HSIEH, C.-C. Synthesis of carbon nanotubes by combustion of a paraffin wax candle. *Micro & Nano Letters*, v. 2, p. 63-66, 2007.

LIU, Y.; GAO, L.; SUN, J. Noncovalent functionalization of carbon nanotubes with sodium lignosulfonate and subsequent quantum dot decoration. *Journal of Physical Chemistry C*, v. 111, p. 1223-1229, 2007.

LU, K. L.; LAGO, R. M.; CHEN, Y. K.; GREEN, M. L. H.; HARRIS, P. J. F.; TSANG, S. C. Mechanical damage of carbon nanotubes by ultrasound. *Carbon*, v. 34, p. 814-816, 1996.

LUO, J.; DUAN, Z.; LI, H. The influence of surfactants on the processing of multi-walled carbon nanotubes in reinforced cement matrix composites. *Physica Status Solidi A*, v. 206, p. 2783-2790, 2009.

MAKAR, J. M.; BEAUDOIN, J. J. Carbon nanotubes and their application in the construction industry. In: 1st International Symposium on Nanotechnology in Construction. *Proceedings*. Paisley, Scotland: Royal Society of Chemistry, 22-25 of June, 2003. p 331-341.

MAKAR, J. M.; CHAN, G. W. Growth of cement hydration products on single-walled carbon nanotubes. *Journal of American Ceramic Society*, v. 92, p. 1303-1310, 2009.

MAKAR, J.; MARGESON, J.; LUH, J. Carbon nanotube/cement composites – early results and potential applications. In: 3rd International Conference on Construction Materials:

Performance, Innovations and Structural Implications. Vancouver, BC, 22-24 of August 2005. p 1-10.

MALGAS, G. F.; ARENDSE, C. J.; CELE, N, P.; CUMMINGS, F. L. Effect of mixture ratios and nitrogen carrier gas flow rates on the morphology of carbon nanotube structures grown by CVD. *Journal of Materials Science*, v. 43, p. 1020-1025, 2008.

MEHTA, P. K. Global concrete industry sustainability. *Concrete International*, v. February 2009, p. 45-48, 2009.

MEHTA, P. K.; MONTEIRO, P. J. M. *Concreto: estrutura, propriedades e materiais*. 1st ed. São Paulo, SP: PINI. 573 p., 1994.

MELO, V. S. *Nanotecnologia aplicada ao concreto:* Efeito da mistura física de nanotubos de carbono em matrizes de cimento Portland. 2009. P. 146. Master's dissertation in civil engineering – School of Engineering, Federal University of Minas Gerais. Belo Horizonte.

MELO, V. S.; CALIXTO, J. M. F.; LADEIRA, L. O.; SILVA, A. P. Macro- and micro-characterization of mortars produced with carbon nanotubes. *ACI Materials Journal*, v. 108, p. 327-332, 2011.

METAXA, Z. S.; KONSTA-GDOUTOS, M. S.; SHAH, S. P. Carbon nanotube reinforced concrete. In: SOBOLEV, K. and TAHA, M. R. (Ed.) *Nanotechnology of Concrete: The Next Big Thing is Small.* Farmington Hills, MI: American Concrete Institute, p. 11-19, 2009.

MI, W.; LIN, J. Y.; MAO, Q.; LI, Y.; ZHANG, B. A study on the effect of carrier gas on the structure and morphology of carbon nanotubes prepared by pyrolysis of ferrocene and C_2H_2 mixture. *Journal of Natural Gas Chemistry*, v. 14, p. 151-155, 2005.

MONTHIOUX, M.; KUZNETSOV, V. L. Who should be given the credit for the discovery of carbon nanotubes? *Carbon*, v. 44, p. 1621-1623, 2006.

MOORE, V. C.; STRANO, M. S.; HAROZ, E. H.; HAUGE, R. H.; SMALLEY, R. E.; SCHMIDT, J.; TALMON, Y. Individually suspended single-walled carbon nanotubes in various surfactants. *Nano Letters*, v. 3, p. 1379-1382, 2003.

MORI, S.; SUZUKI M. Non-catalytic, low-temperature synthesis of carbon nanofibers by plasma-enhanced chemical vapor deposition. In: Kumar, A. (Ed.) *Nanofibers*. ISBN: 978-953-7619-86-2, InTech, p. 295-308, 2010.

MORSY, M. S.; ALSAYED, S. H.; AQEL, M. Hybrid effects of carbon nanotube and nano-clay on physico-mechanical properties of cement mortar. Construction and Building Materials, v. 25, p. 145-149, 2011.

MUDIMELA, P. R.; NASIBULINA, L. I.; NASIBULIN. A. G.; CWIRZEN, A.; VALKEAPÄÄ, M.; HABERMEHL-CWIRZEN, K.; MALM, J. E. M.; KARPPINEN, M. J.; PENTTALA, V.; KOLTSOVA, T. S.; TOLOCHKO, O. V.; KAUPPINEN, E. I. Synthesis of carbon nanotubes and nanofibers on silica and cement matrix materials. *Journal of Nanomaterials*, v. 2009, article ID 526128, 4 p, 2009. DOI: 10.1155/2009/526128.

MURR, L. E.; BANG, J. J.; ESQUIVEL, E. V.; GUERRERO, P. A.; LOPEZ, D. A. Carbon nanotubes, nanocrystal forms, and complex nanoparticles aggregates in common fuel-gas combustion sources and the ambient air. *Journal of Nanoparticle Research*, v. 6, p. 241–251, 2004.

MUSSO, S.; TULLIANI, J.-M.; FERRO, G.; TAGLIAFERRO, A. Influence of carbon nanotubes on the mechanical behaviour of cement composites. *Composites Science and Technology*, v. 69, p. 1985-1990, 2009.

NAEIMI, H.; MOHAJERI, A.; MORADI, L.; RASHIDI, A. M. Efficient and facile one pot carboxylation of multiwalled carbon nanotubes by using oxidation with ozone under mild conditions. *Applied Surface Science*, v. 256, p. 631-635, 2009.

NASIBULIN, A. G.; SHANDAKOV, S. D.; NASIBULINA, L. I.; CWIRZEN, A.; MUDIMELA, P. R.; HABERMEHL-CWIRZEN, K.; GRISHIN, D. A.; GAVRILOV, Y. V.; MALM, J. E. M.; TAPPER, U.; TIAN, Y.; PENTTALA, V.; KARPPINEN, M. J.; KAUPPINEN, E. I. A novel cement-based hybrid material. *New Journal of Physics*, v. 11, p. 1-11, 2009.

NATSUKI, T.; TANTRAKARN, K.; ENDO, M. Effects of carbon nanotubes structures on mechanical properties. *Applied Physics A*, v. 79, p. 117-124, 2004.

PELLENQ, R. J.-M.; LEQUEUX, N.; VAN DAMME, H. Engineering the bonding scheme in C-S-H: The iono-covalent framework. *Cement and Concrete Research*, v. 38, p. 159-174, 2008.

POURCHET, S.; COMPARET, C.; NONAT, A.; MAITRASSE, P. Influence of three types of superplaticizers on tricalciumaluminate hydration in the presence of gypsum. In: 8th CANMET/ACI International Conference on Superplasticizers and Other Chemical Admixtures in Concrete. Sorrento, Italy. 2006.

PUERTAS, F.; SANTOS, H.; PALACIOS, M.; MARTÍNEZ-RAMIREZ, S. Polycarboxylate superplasticizer admixtures: effect on hydration, microstructure and rheological behaviour in cement pastes, *Advances in Cement Research*, v. 17, p. 77-89, 2005.

QING, Y.; ZENAN, Z.; DEYU, K.; RONGSHEN, C. Influence of nano-SiO_2 addition on properties of hardened cement paste as compared with silica fume. *Construction and Building Materials*, v. 21, p. 539-545, 2007.

RAMACHANDRAN, V. S.; FELDMAN, R. F. Concrete science. In: RAMACHANDRAN, V. S. *Concrete Admixtures Handbook*: Properties, Science and Technology. 2nd ed. Park Ridge NJ, USA: Noyes Publications. 1996, p. 27.

RANJBARTOREH, A. R.; WANG, G. Molecular dynamic investigation of mechanical properties of armchair and zigzag double-walled carbon nanotubes under various loading conditions. *Physics Letters A*, v. 374, p. 969-974, 2010.

RICHARDSON, I. G. The calcium silicate hydrates. *Cement and Concrete Research*, v. 28, p. 137-158, 2008.

ROUAINIA, G.; DJEGHABA, K. Evaluation of Young's modulus of single walled carbon nanotube (SWNT) reinforced concrete composite. *Journal of Engineering and Applied Sciences*, v. 3, p. 504-515, 2008.

RÜMMELI, M. H.; KRAMBERGER, C.; SCHÄFFEL, F.; BOROWIAK-PALEN, E.; GEMMING, T.; RELLINGHAUS, B.; JOST, O.; LÖFFLER, M.; AYALA, P.; PICHLER, T.; KALENCZUK, R. J. Catalyst size dependencies for carbon nanotubes synthesis. *Physica Status Solidi B*, v. 244, p. 3911-3915, 2007.

SALVETAT, J.-P.; BONARD, J.-M.; THOMSON, N. H.; KULIK, A. J.; FORRÓ, L.; BENOIT, W.; ZUPPIROLI, L. Mechanical properties of carbon nanotubes, *Applied Physics A*, v. 69, p. 255-260, 1999.

SANCHEZ, F.; INCE, C. Microstructure and macroscopic properties of hybrid carbon fiber/silica fume cement composites. *Composites Science and Technology*, v. 69, p. 1310-1318, 2009.

SANCHEZ, F.; ZHANG, L. Molecular dynamics modeling of the interface between surface functionalized graphitic structures and calcium-silicate-hydrate: interaction energies, structure, and dynamics. *Journal of Colloid and Interface Science*, v. 323, p. 349-358, 2008.

SHAFFER, M. S. P.; FAN, X.; WINDLE, A. H. Dispersion and packing of carbon nanotubes. *Carbon*, v. 36, p. 1603-1612, 1998.

SKOOG, D. A.; LEARY, J. J. *Principles of instrumental analysis*. 4th ed. Fort Worth, TX: Saunders College Publishing. 700 p. 1992.

SING, K. S. W.; EVERETT, D. H.; HAUL, R.; MOSCOU, L.; PIEROTTI, R. A.; ROUQUÉROL, J.; SIEMIENIEWSKA T. Reporting physisorption data for gas/solid systems. *Pure and Applied Chemistry*, v. 57, p. 603-619, 1985.

SONGSASEN, A.; PAIRGREETHAVES, P. Preparation of carbon nanotubes by nickel catalyzed decomposition of liquefied petroleum gas (LPG). *Kasetsart Journal (Natural Science)*, v. 35, p. 354-359. 2001.

STRUBLE, L.; GODFREY, J. How sustainable is concrete? In: International Workshop on Sustainable Development and Concrete Technology, Beijing. Ames IA: Iowa State University, 20-21 of May 2004. p 201-211.

SULONG, A. B.; AZHARI, C. H.; ZULKIFLI, R.; OTHMAN, M. R.; PARK, J. A comparison of defects produced on oxidation of carbon nanotubes by acid and UV ozone treatment. *European Journal of Scientific Research*, v. 33, p. 295-304, 2009.

TANG, C.; BANDO, Y.; GOLBERG, D.; XU, F. Structure and nitrogen incorporation of carbon nanotubes synthesized by catalytic pyrolysis of dimethylformamide. *Carbon*, v. 42, p. 2625-2633, 2004.

ŢIPRIGAN, O.; KOÓS, A. A.; NEMES-INCZE, P. HORVÁTH, Z. E.; SÁRKÖZI, ZS.; SIMON, S.; DARABONT, A.; BÍRÓ, L. P. Obtaining bamboo-structured, multi-walled carbon nanotubes using the spray pyrolysis method. *Journal of Optoelectronics and Advanced Materials*, v. 9, p. 617-620, 2007.

TRIGUEIRO, J. P. C.; SILVA, G. G.; LAVALL, R. L.; FURTADO, C. A.; OLIVEIRA, S.; FERLAUTO, A. S.; LACERDA, R. G.; LADEIRA, L. O.; LIU, J.-W.; FROST, R. L.; GEORGE, G. A. Purity evaluation of carbon nanotube materials by thermogravimetric, TEM and SEM methods. *Journal of Nanoscience and Nanotechnology*, v. 7, p. 3477-3486, 2007.

UCHIKAWA, H.; SAWAKI, D.; HANEHARA, S. Influence of kind and added timing of organic admixture on the composition, structure and property of fresh cement paste. *Cement and Concrete Research*, v. 25, p. 353-364, 1995.

VESSELÉNYI, I.; NIESZ, K.; SISKA, A.; KÓNYA, Z.; HERNADI, K.; NAGY, J. B.; KIRICSI, I. Production of carbon nanotubes on different metal supported catalysts. *Reaction Kinetics and Catalysis Letters*, v. 74, p. 329-336, 2001.

VICAT, L. J. *Recherches expérimentales sur les chaux de construction, les bétons et les mortiers ordinaires*. Paris: Goujon. 97p., 1818.

WANG, Z.; ZHAO, J.; CUI, S. Chemical structures and adsorptive behaviors of superplasticizers on β-C_2S. *Journal of Wuhan University of Technology – Materials Science Edition*, v. 22, p. 337-340, 2007.

WORLD BUSINESS COUNCIL FOR SUSTAINABLE DEVELOPMENT – INTERNATIONAL ENERGY AGENCY (WBCSD-IEA). Cement technology roadmap 2009. ISBN: 978-3-940388-47-6.

XU, S. L.; GAO, L. L.; JIN, W. J. Production and mechanical properties of aligned multi-walled carbon nanotubes-M140 composites. *Science in China series E: Technological Sciences*, v. 52, p. 2119-2127, 2009.

XU, Y.; CHUNG, D. L. L. Carbon fiber reinforced cement improved by using silane-treated carbon fibers. *Cement and Concrete Research*, v. 29, p. 773-776, 1999.

YAKOVLEV, G.; KERIENĖ, J.; GAILIUS, A.; GIRNIENĖ, I. Cement based foam concrete reinforced by carbon nanotubes. *Materials Science (Medžiagotyra)*, v. 12, p. 147-151, 2006.

YASUI, A.; KAMIYA, Y.; SUGIYAMA, S.; ONO, S.; NODA, H.; ICHIKAWA, Y. Synthesis of carbon nanotubes on fly ashes by chemical vapor deposition processing. *IEEJ Transactions on Electrical and Electronic Engineering*, v. 4, p. 787-789, 2009.

YAZDANBAKHSH, A.; GRASLEY, Z. C.; TYSON, B.; ABU AL-RUB, R. K. Carbon nano filaments in cementitious materials: some issues on dispersion and interfacial bond. In: Nanotechnology of concrete: the next big thing is small, 2009.

YOSHIOKA, K.; SAKAI, E.; DAIMON, M.; KITAHARA, A. Role of steric hindrance in the performance of superplasticizers for concrete. *Journal of the American Ceramic Society*, v. 80, p. 2667-2671, 1997.

YOSHIOKA, K.; TAZAWA, E.; KAWAI, K.; ENOHATA, T. Adsorption characteristics of superplasticizers on cement component minerals. *Cement and Concrete Research*, v. 32, p. 1507-1513, 2002.

YU, M.-F.; LOURIE, O.; DYER, M.; MOLONI, K.; KELLY, T. F.; RUOFF, R. S. Strength and breaking mechanism of multiwalled carbon nanotubes under tensile load. *Science*, v. 287, p. 637-640, 2000.

YU, X.; KWON, E. A carbon nanotubes/cement composite with piezoresistive properties. *Smart Materials and Structures*, v. 18, o. 1-5, 2009.

ZHANG, T.; SHANG, S.; YIN, F.; AISHAH, A.; SALMIAH, A.; OOI, T. L. Adsorptive behavior of surfactants on surface of Portland cement. *Cement and Concrete Research*, v. 31, p. 1009-1015, 2001.

7

APPENDIX

APPENDIX 1

Characterization of ammonia functionalized CNTs

Introduction

When clinker or silica fume were used as catalyst support for CNT/CNF synthesis, the analysis methods for product characterization were limited. More detailed analysis such as Transmission electron microscopy (TEM) or Raman spectroscopy can only be performed on purified samples. The remove of clinker or silica fume needs a more complicated purification process than if magnesium oxide would be used as support. In order to characterize the alterations of the nanotube structure caused by the use of ammonia during the synthesis process, some investigations were done with CNTs grown on *MgO* catalyst support. The samples were purified by a method based on acid treatment and analyzed by TEM and Raman spectroscopy. It was supposed that the alteration of the nanotubes structure observed in the case of *MgO* support would be similar to that caused to CNTs/CNFs grown on clinker.

Transmission electron microscopy

As an electron beam hits a surface, different types of radiations are created that bring information about the sample. The beams that cross the sample are used to create transmission electron microscopy (TEM) images. In order to the electron beam be able to cross the surface, the acceleration voltage has to be higher than that used in SEM, and the sample has to be also thin enough. In the case of powder like samples it is possible to create suspensions and drop on a sample holder grid. TEM can give higher magnification images than SEM. TEM also provides information about the internal structure of the sample. (SKOOG and LEARY, 1992)

Raman spectroscopy

Raman effect is an inelastic light scattering resulting of the interaction between the incident light (photons) and the molecular vibrations (phonons) of the material. This process produces scattered light with higher or lower energy than the incident photon. The corresponding *phenomenae* are called Stokes and anti-Stokes effect.

One of the applications of this technique is the characterization of the degree of perfection of CNTs. A perfect graphite structure containing only sp^2 bonds has a unique, tangential mode of scattering that has Raman effect, corresponding to the G band. When

imperfections are present in the sample, another band appears: the D band, corresponding to the disorder of the structure. G' band is related to the D band at second order, but independent of the effects of disorder. The relationship between the intensities of D and G bands characterize how perfect the sample is. The higher the intensity of D band is with respect to the G band, the higher number of defects exists in the sample. In the case of CNTs, the positions of D and G bands are at approximately 1350 and 1582 cm^{-1} respectively. G' band is present at 2700 cm^{-1} (DRESSELHAUS *et al.*, 2005).

Ammonia treatment of CNTs grown on *MgO-FeO* catalyst

For the characterization of CNTs/CNFs prepared with ammonia in order to create amino functional groups an *MgO-FeO* catalyst mixture was prepared in the molar ratio of 1:4. This composition was chosen because of the ease of purification of the as-grown products that permits more detailed analysis.

The *MgO-FeO* catalyst was processed with and without ammonia. It was supposed, that the ammonia flow causes similar alterations in the structure of nanotubes grown on clinker to those of products grown on *MgO*. The synthesized products were purified in *HCl* solution and were analyzed by TEM, Raman spectroscopy and TGA.

TEM imaging was performed on purified samples of CNTs grown on *FeO-MgO* catalyst. As grown CNTs were placed in an oven at 430 °C for 30 minutes and then suspended in *HCl* solution by ultrasonic bath for 30 min. The samples were washed in distilled water until neutral pH was achieved. A suspension in absolute ethanol of the purified CNTs was prepared using an ultrasonic bath. One drop of the suspension was placed on the grid. Images were taken on a Tecnai SuperTwin FEI type instrument at the Center of Microscopy, UFMG.

Samples for Raman spectroscopy were purified using the same methodology as for TEM sample preparation. The purified CNTs were placed on a glass sample holder. The analysis was performed using an Olympus BX51 microscope equipped by a DeltaNu ExamineR 532 spectrometer in the Nanomaterials Laboratory of the UFMG.

TEM images show a modified, bamboo-like structure as the results of the ammonia treatment (Figure 7.1). At the same time, CNTs grown without ammonia present a higher quantity of defects. The mean diameter of unfunctionalized CNTs was 30.5 nm and of ammonia functionalized ones 28.4 nm (Figure 7.2).

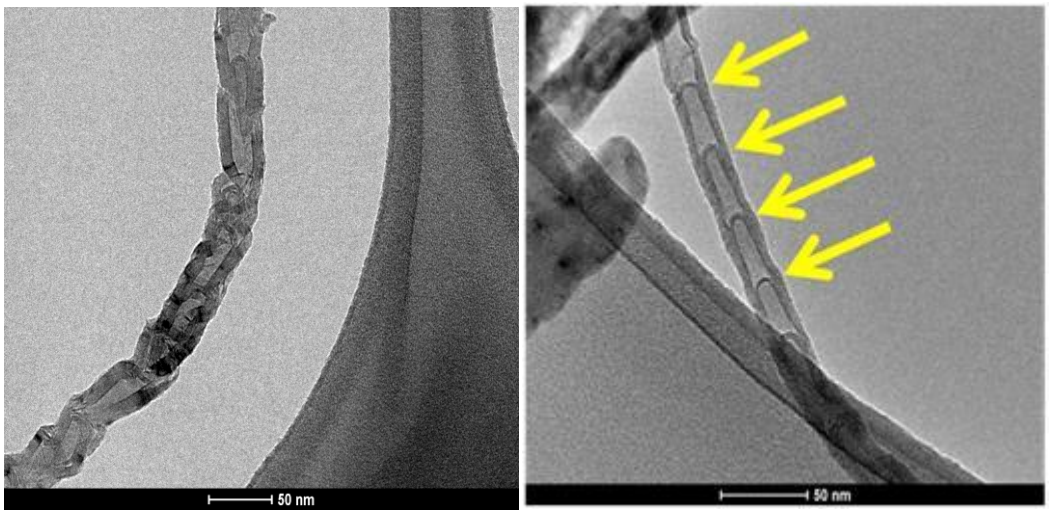

a) **b)**

Figure 7.1– Transmission electron micrograph of nanotubes grown on *MgO-FeO* catalyst a) without ammonia, b) with ammonia. Arrows indicate the bamboo-like structure.

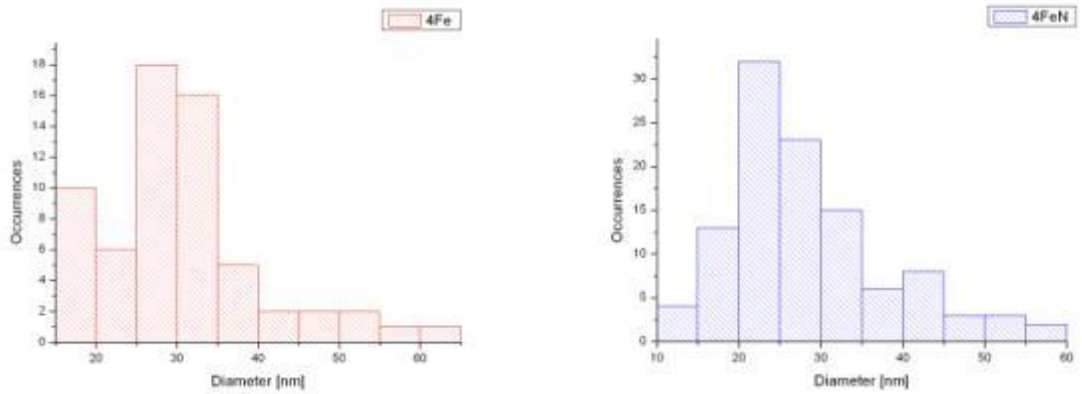

a) **b)**

Figure 7.2– Histograms of the diameters of CNTs grown on *MgO-FeO* catalyst measured on SEM images. **a)** without ammonia; **b)** with ammonia

The Raman spectra of purified CNTs grown on *MgO-FeO* catalyst had an I_D/I_G relation of 1.03 (Figure 7.3). The G' peak is also clearly visible. The nanotubes grown with ammonia had a reduced I_D/I_G ratio of 0.83 (Figure 7.4). This reduction suggests a CNT structures with higher quantity of perfect bonds between the carbon atoms. The peaks D and

G had a higher "valley" between them. This fact may be explained by a possibly higher quantity of amorphous carbon present in the case of CNTs synthesized with ammonia, which resisted the same purification treatment as in the case of CNTs grown without ammonia. The higher amount of amorphous carbon was also indicated by the disappearance of G' band in the background noise.

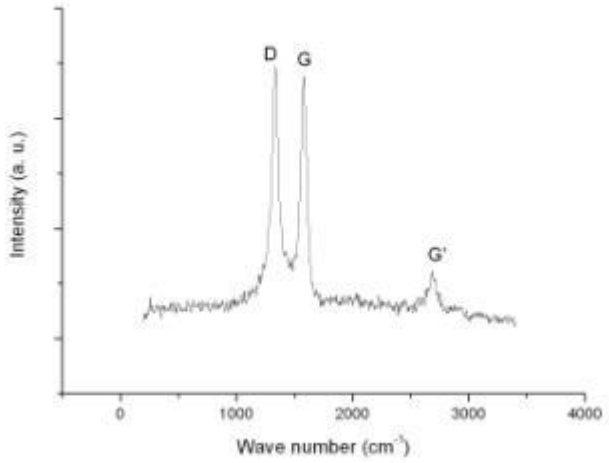

Figure 7.3 – Raman spectra of purified CNTs grown on *MgO-FeO* catalyst without ammonia. Intensity is represented with arbitrary units

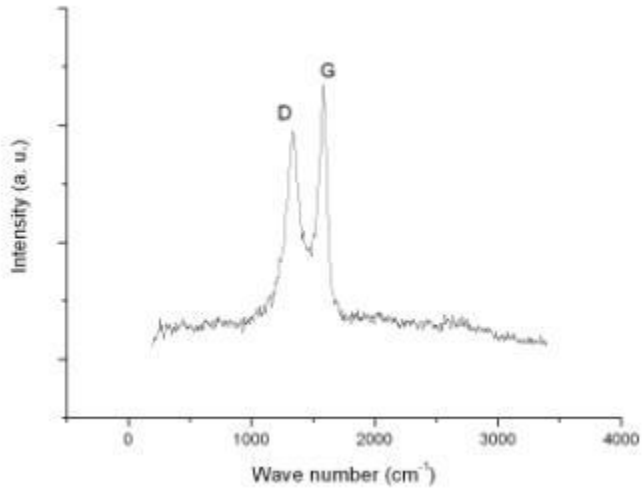

Figure 7.4 – Raman spectra of purified CNTs grown on *MgO-FeO* catalyst with ammonia. Intensity is represented with arbitrary units

The comparison of the TGA results of CNTs grown with and without ammonia on *MgO-FeO* catalyst shows a lower temperature mass loss peak for ammonia functionalized CNTs (Figures 7.5 and 7.6). The peak appears at 633 °C for untreated CNTs meanwhile functionalized CNTs show peak at 588 °C. The lower ignition temperature of functionalized CNTs may be caused by the smaller diameter of the CNTs, observed by TEM.

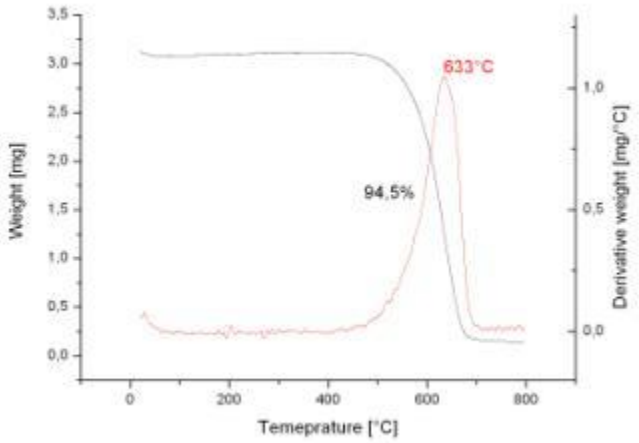

Figure 7.5– TGA and DTG curves of purified CNTs grown on *MgO-FeO* catalyst without ammonia. Black color represents TGA and red color represents DTG curves

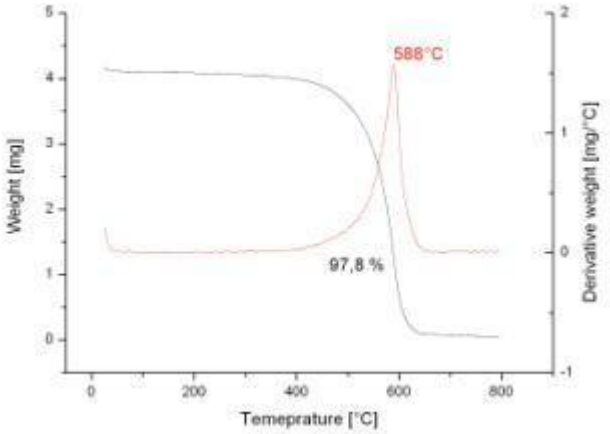

Figure 7.6 – TGA and DTG curves of purified CNTs grown on *MgO-FeO* catalyst with ammonia. Black color represents TGA and red color represents DTG curves

The results showed clearly some modifications of the products synthesized on *MgO-FeO* catalyst due to the injection of ammonia during the synthesis process. The functionalization method presented is simple with respect to other methods based on acids or microwave treatments. Also, the ammonia functionalization process occurs during the synthesis, which can shorten and simplify the production of amino-functionalized CNTs/CNFs in larger scale.

According to the presented results, the synthesis process including ammonia treatment was adapted to produce ammonia functionalized nano-structured clinker.

8

ANNEXES

ANNEX A – X-ray diffractometry analysis of raw materials

A.1 – Introduction

X-rays are electromagnetic radiation of wavelength between 5-25 nm. The X-rays are produced in X-ray tubes when electrons accelerated by high voltage hit the anode. The spectrum of the radiation is characteristic of the electrode metal material. The most common target (anode) materials are tungsten, copper, chromium, molybdenum, rhodium, iron or cobalt. When the X-ray radiation hits the sample material it suffers absorption and scattering. When the sample's atoms are ordered as they are in a crystal, diffraction takes place which is the interference among the X-rays scattered by the periodically placed atoms. The X-rays are only reflected from the sample when Bragg's law is satisfied:

$$sin\theta = \frac{n\lambda}{2d}, \qquad (A.1)$$

where θ is the angle of the incident radiation, n is an integer, λ is the wavelength of the radiation and d is the interplanar distance of the crystal. The interception of the diffracted beam gives information on the sample material qualitative composition and the size of crystallites.

The X-ray diffraction (XRD) instrument consists of an X-ray tube as source, a detector and a sample holder, all mounted on a goniometer that allows exposing the sample to the X-rays at different angles. The analysis of the sample consists of recording the intensity of the diffracted X-rays generally between 20 and 160° that will give peaks at certain angles. Each crystallous material has a typical X-ray diffraction pattern with peaks according to different angles. The comparison of the received XRD pattern with database patterns permits to identify the constituents of the sample. The resolution of the resulting intensity graph depends on the scanning speed of the detector (or source, or both, depending on the setup of the instrument). A lower scanning speed gives the position of each peak more precisely. (SKOOG and LEARY, 1992)

Besides phase identification, XRD can also be used to determine the average size of crystallites. In order to this, a typical peak has to be analyzed in more details. Crystals in the size range below 0.1 μm cause the broadening of the peaks described by the following equation of Scherrer:

$$B = \frac{0{,}9\lambda}{t\,cos\theta}, \qquad (A.2)$$

where B is the broadening of the peak in radians, λ is the wavelength of the characteristic X-ray radiation, t is the particle diameter and θ is the peak position in radians. All X-ray diffraction lines naturally have a breadth. The above equation refers to the broadening of such a peak. To allow the determination of the particle size, the measured breadth of the peak is to be compared with a near peak of a known, standard material with particle size above 0.1 μm. The pattern of such materials consists of sharp peaks. The real broadening of the peak due to particle size effect can be given by the following equation:

$$B^2 = B_M^2 - B_S^2, \qquad (A.3)$$

where B_M is the measured breadth of the line of the sample at half-maximum intensity and B_S is the measured breadth of the line of the standard at half-maximum intensity. (CULLITY, 1978)

According to the previously described facts, a higher scanning speed is to be employed on the possibly highest range of angles to identify the phases of a sample during the XRD analysis, while for particle size determination a low speed scanning of a specific peak is necessary to achieve higher resolution of that single region.

A.2 – Methodology

Sample preparation:

The powder samples were diluted in absolute ethanol and compacted in a glass sample holder with cavity of 20 mm × 20 mm.

Phase identification:

Scanning occurred using 0,1 °/step scanning speed. The obtained difractogram was compared with known standards of different iron crystals in order to identify the iron phase present in the sample.

Iron crystallite size measuring:

Scanning occurred using 0.02 °/step scanning speed on the highest peak of the iron phase identified. The same measurement was performed on silicon standard. The width of the peaks was measured at mid-height as well as the intensity. The mean crystallite diameter t was determined with the following equation:

$$t = \frac{0.9\,\lambda}{B\,cos\theta_B}, \qquad (A.4)$$

where λ is the characteristic wavelength of the X-ray tube, θ_B is the position of the peak and B is given by:

$$B = \sqrt{B_M^2 - B_S^2}, \qquad (A.5)$$

where B_M and B_S are the widths of the peaks at mid-height of the sample and the standard, in radians.

A.3 – X-ray diffractograms

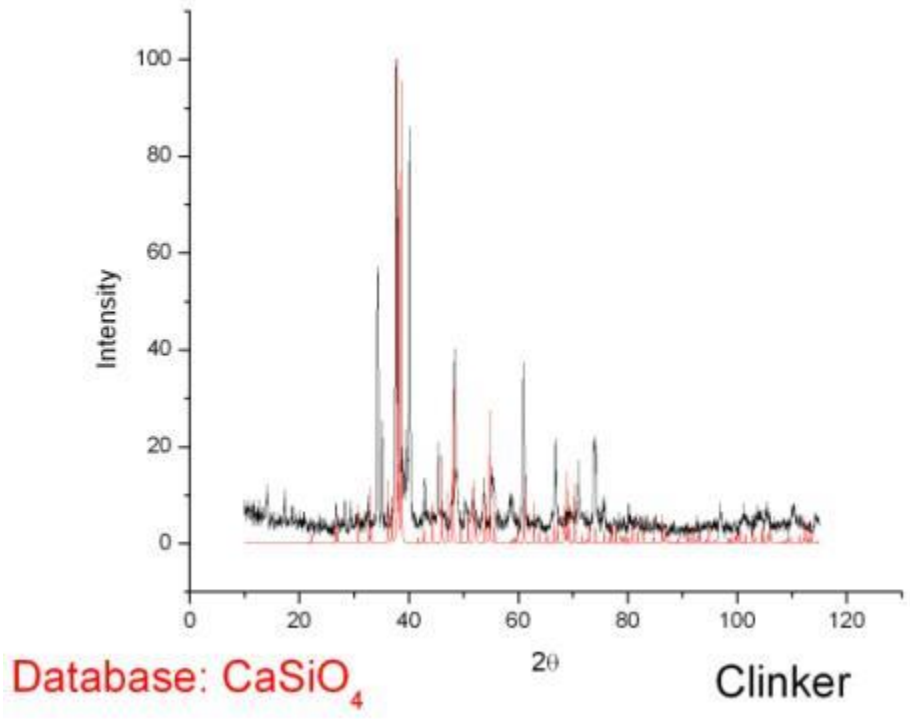

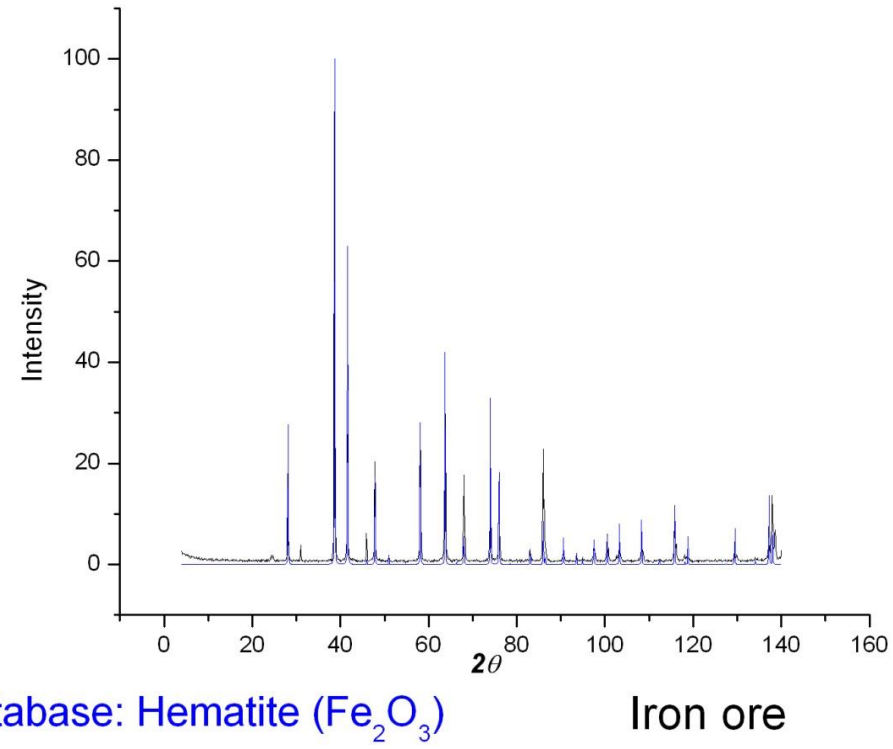

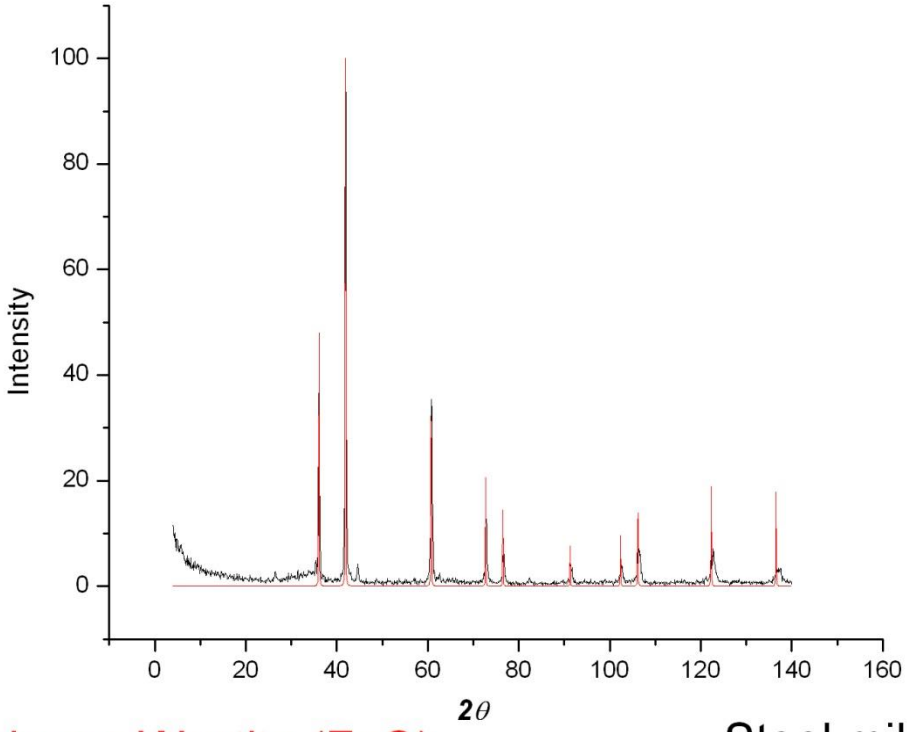

Database: Wustite (FeO)

Steel mill scale

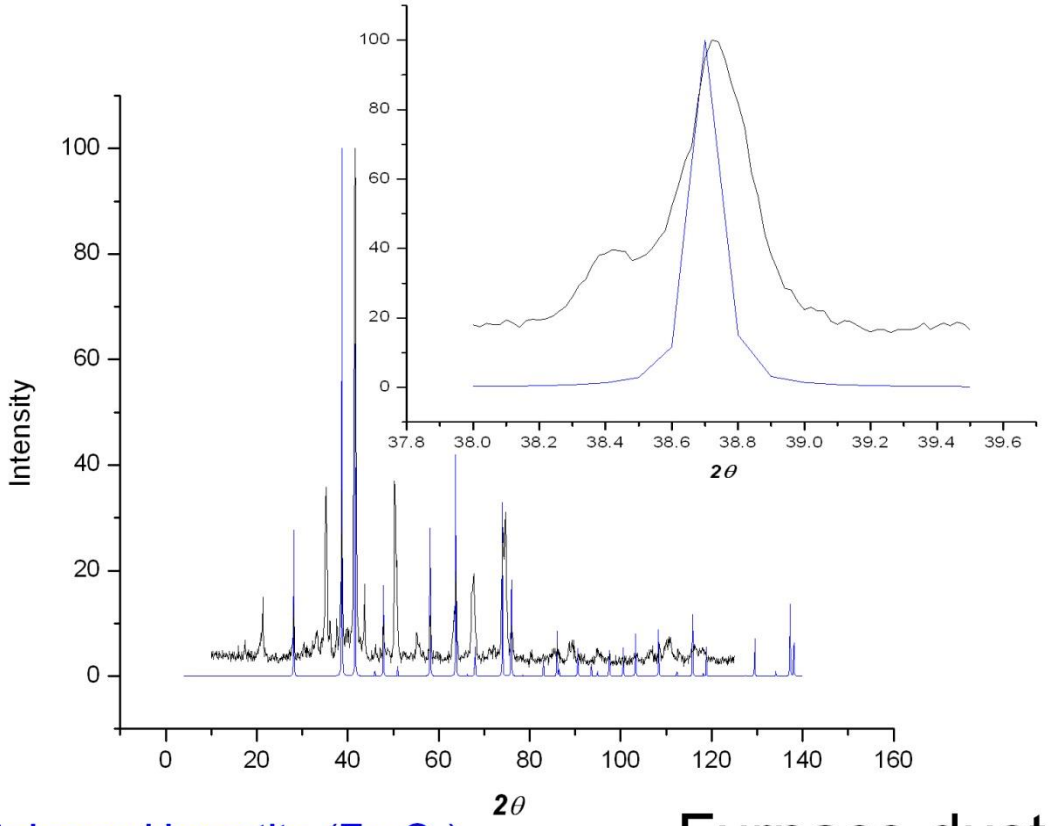

Database: Hematite (Fe_2O_3)

Furnace dust

Detailed diffractograms of the raw materials for Fe crystallite size determination by Scherrer method

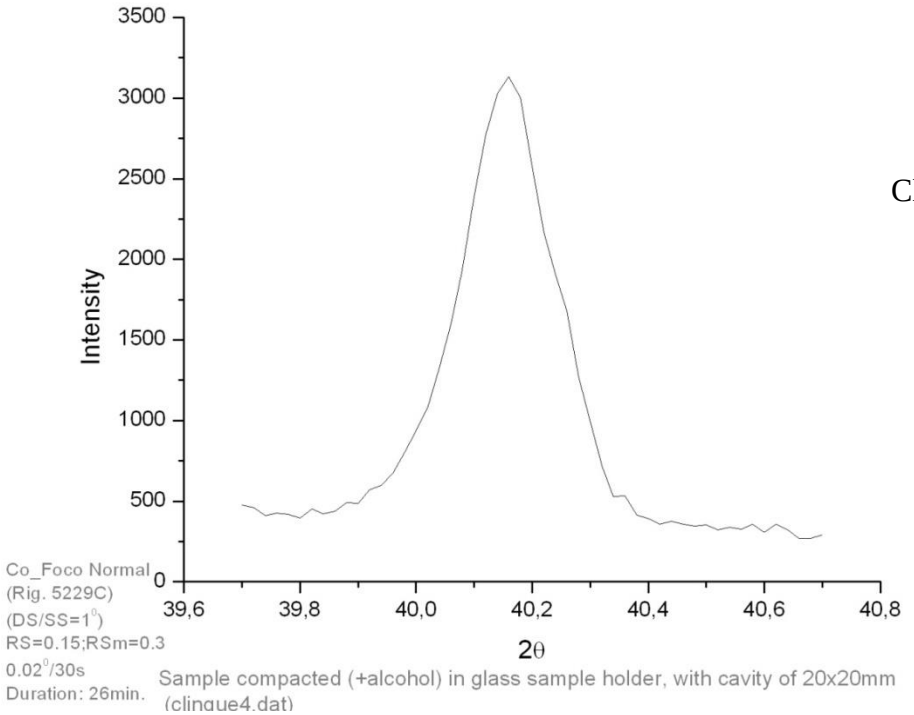

Clinker

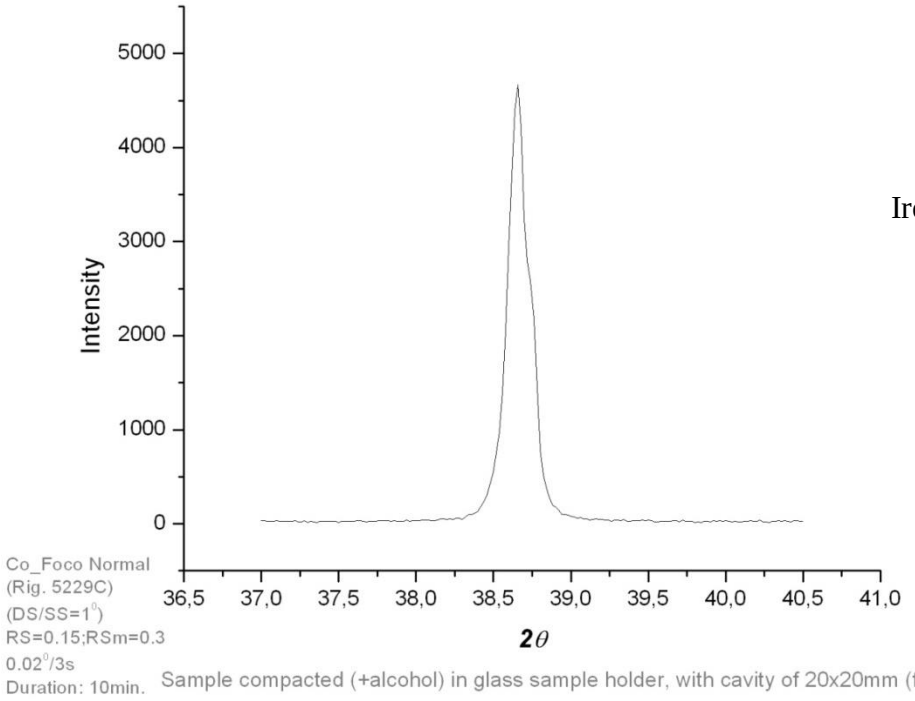

Iron ore

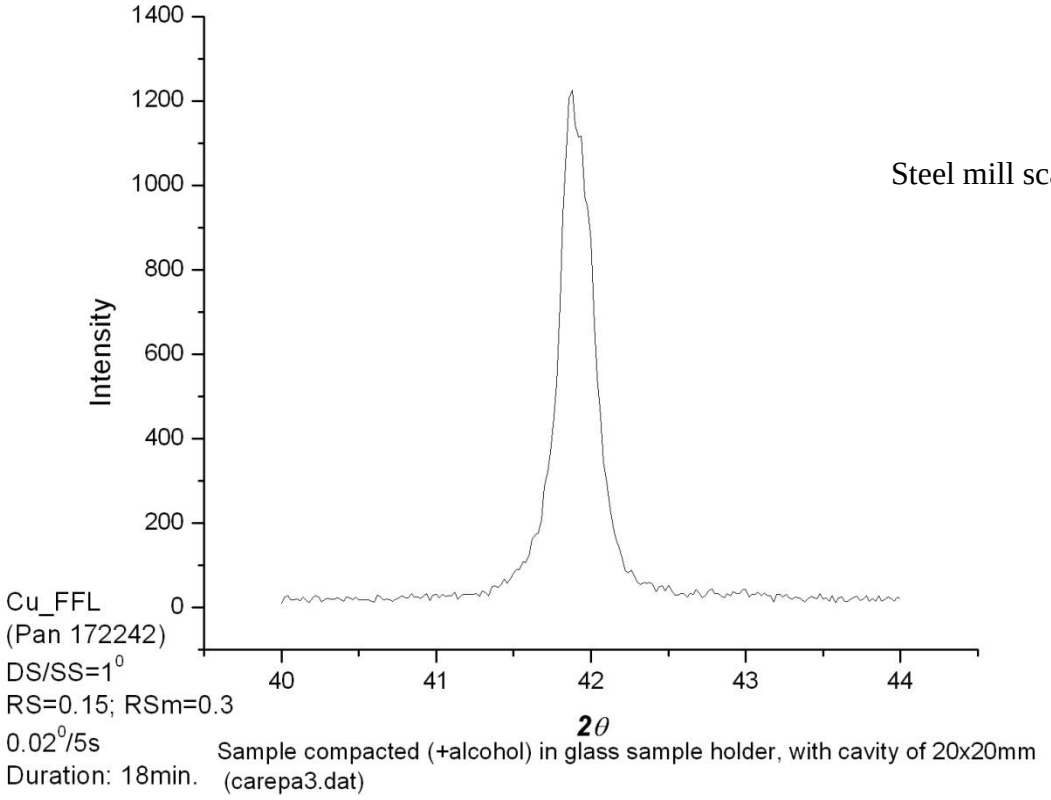
Steel mill scale
Intensity
1400
1200
1000
800
600
400
200
0
40
41
42
43
44
2θ
Cu_FFL
(Pan 172242)
DS/SS=1°
RS=0.15; RSm=0.3
0.02°/5s
Duration: 18min.
Sample compacted (+alcohol) in glass sample holder, with cavity of 20x20mm
(carepa3.dat)

ANNEX B – Detailed mechanical strength test results

Optimal nanotube/cement ratio

Identification	7 days flexural strength [MPa]	28 days flexural strength [MPa]
CL-NP	5.22 5.14 5.65 5.87 5.24 4.57	7.35 6.56 6.97 6.57 7.44 7.54
CL-NP-N05	6.07 6.19 6.84 5.29 6.63 6.76	7.34 6.89 6.83 7.22
CL-NP-N25	4.95 4.96 4.73 4.32 4.62 4.37	5.56 5.22 5.27 5.19 5.11 4.85
CL-NP-N50	4.40 4.43 4.34 4.13 4.31 4.90	6.47 5.94 5.14 6.05 5.80 5.20
CL-NP-N100	4.76 5.00 5.06 4.39 4.14 4.53	5.53 5.55 5.60 5.99 5.03 5.24
CL-NP-N125	4.23 4.40 4.81 4.55 5.57 4.99	6.93 5.86 6.63 5.70 5.86 5.47
CL-NP-N245	3.78 3.40 1.74 3.63	3.35 3.50 4.23

Legends:

CL-NP Reference mortar prepared with polynaphtalene and polycarboxylate admixtures

CL-NP-N05 Mortar with polynaphtalene and polycarboxylate admixtures containing 0.05 % clinker grown CNTs/CNFs

CL-NP-N10 Mortar with polynaphtalene and polycarboxylate admixtures containing 0.10 % clinker grown CNTs/CNFs

CL-NP-N25 Mortar with polynaphtalene and polycarboxylate admixtures containing 0.25 % clinker grown CNTs/CNFs

CL-NP-N50 Mortar with polynaphtalene and polycarboxylate admixtures containing 0.50 % clinker grown CNTs/CNFs

CL-NP-N100 Mortar with polynaphtalene and polycarboxylate admixtures containing 1.00 % clinker grown CNTs/CNFs

CL-NP-N125 Mortar with polynaphtalene and polycarboxylate admixtures containing 1.25 % clinker grown CNTs/CNFs

CL-NP-N245 Mortar with polynaphtalene and polycarboxylate admixtures containing 2.45 % clinker grown CNTs/CNFs

Chemical admixture comparison

Identification	7 days flexural strength [MPa]	28 days flexural strength [MPa]	28 days compressive strength [MPa]
CL-NP	6.84 6.39 7.14 7.76 6.96 7.61	7.85 7.89 7.32 8.63 7.76 8.51 7.09	41.2 33.0 34.7 40.7
CL-NP-N30	6.94 6.05 5.9 7.78 7.32 6.41	6.99 7.28 7.01 7.21 7.31 7.04 7.12	53.7 53.2 54.9 52.3
CL-LS	4.96 4.84 4.54 4.46	5.21 5.15 6.83 5.86 7.01	26.1 27.4 34.2 26.9
CL-LS-N30	4.10 6.11 6.15 6.38 5.82 6.50	7.07 6.59 6.85 6.97 7.10 6.57	56.0 54.6 55.0 51.7
CL-PL	2.80 3.51	4.19	28.9 32.1
CL-PL-N30	4.08 3.42 2.8 3.51 2.86 3.54	7.85 8.25 7.24 7.60 7.56 7.39 8.89 8.78	60.7 59.8 53.5 50.2
CL-SM	6.92 8.27 8.17 7.22 8.24 8.51	7.86 8.29 7.44 8.40 7.38 8.29 7.67 7.61	51.7 58.3
CL-SM-N30	8.26 7.91 8.88 8.30 7.21 8.54	8.41 8.63 7.39 7.38 8.28 7.98 7.75	31.5 28.0 41.7 42.8

Legends:

CL-NP	Reference mortar prepared with polynaphtalene and polycarboxylate admixtures
CL-NP-N30	Mortar with polynaphtalene and polycarboxylate admixtures containing 0.3 % clinker grown CNTs/CNFs
CL-LS	Reference mortar prepared with lignosulfonate based admixture
CL-LS-N30	Mortar with lignosulfonate based admixture containing 0.3 % clinker grown CNTs/CNFs
CL-PL	Reference mortar prepared with lignosulfonate and polysaccharide based admixture
CL-PL-N30	Mortar with lignosulfonate and polysaccharide based admixture containing 0.3 % clinker grown CNTs/CNFs
CL-SM	Reference mortar prepared with sulphonated melamine based admixture
CL-SM-N30	Mortar with sulphonated melamine based admixture containing 0.3 % clinker grown CNTs/CNFs

Effect of batching procedure

Identification	7 days compressive strength [MPa]	28 days compressive strength [MPa]
CL-LS05	40.1 41.0 41.0	48.8 49.5 48.1
CL-LS05-DM-N10	43.0 42.0 42.5	51.0 50.2 50.7
CL-LS05-WM-N10	42.4 41.6 42.0	48.9 48.7 48.1

Legends:

CL-LS05	Reference mortar prepared with lignosulfonate based admixture
CL-LS05-DM-N10	Mortar with lignosulfonate based admixture containing 0.1 % clinker grown CNTs/CNFs dry mixed with cement
CL-LS05-WM-N10	Mortar with lignosulfonate based admixture containing 0.1 % clinker grown CNTs/CNFs added with mixing water

Covalent functionalization: performance of ammonia functionalized nano-structured material

Identification	7 days flexural strength [MPa]	28 days flexural strength [MPa]
CL-NH-LP	4.02 4.10 3.82	3.77 3.11 3.74
CL-NH-LP-N10	3.73 2.54 3.50 2.21	2.46 2.85 2.78 2.09
CL-NH-LP-N30	3.86 4.23 3.86 4.87	2.65 3.64 3.82 3.74

Identification	7 days compressive strength [MPa]	28 days compressive strength [MPa]
CL-NH-LP	37.08 29.44 28.18	37.87 35.43 26.78
CL-NH-LP-N10	45.42 45.05 42.87 38.06	39.98 38.52 40.82
CL-NH-LP-N30	35.99 37.56 49.00 39.91	43.71 39.02 42.91

Legends:

CL-NH-LP Reference mortar prepared with lignosulfonate based admixture

CL-NH-LP-N10 Mortar prepared with lignosulfonate based admixture containing 0.1 % clinker grown, ammonia functionalized CNTs/CNFs

CL-NH-LP-N30 Mortar prepared with lignosulfonate based admixture containing 0.3 % clinker grown, ammonia functionalized CNTs/CNFs

Identification	7 days flexural strength [MPa]	28 days flexural strength [MPa]
SF-PVP	5.92 6.16 6.15 6.36	8.48 9.48 9.71 9.53 10.63
SF-PVP-N30	5.80 5.90 5.74 5.93	8.87 8.64 8.34 8.09 8.58
SF-LS	5.29 4.84 5.34 4.63	7.28 7.56 7.14 8.01 7.62
SF-LS-N30	4.97 5.01 4.73 4.84	7.91 8.66 8.54 8.02 8.03

Identification	7 days compressive strength [MPa]	28 days compressive strength [MPa]
SF-PVP	40.0 42.8 38.1 32.6	40.2 36.4 39.9 40.4 48.1
SF-PVP-N30	39.3 36.1 39.7 39.6	48.8 48.1 47.5 49.2 42.5
SF-LS	29.4 35.6 30.9 29.0	37.6 45.7 38.6 43.3 44.8
SF-LS-N30	35.6 41.1 32.2 40.7	59.6 55.9 61.1 57.9

Legends:

SF-PVP	Reference mortar prepared with polivinylpyrrolidone containing 10 % silica fume
SF-PVP-N30	Mortar prepared with polivinylpyrrolidone containing 0.3 % silica fume grown CNTs/CNFs and 10 % silica fume
SF-LS	Reference mortar prepared with lignosulfonate based admixture containing 10 % silica fume
SF-LS-N30	Mortar prepared with lignosulfonate based admixture containing 0.3 % silica fume grown CNTs/CNFs and 10 % silica fume

Covalent functionalization: hydrogen peroxide as functionalizing agent

Identification	10 days flexural strength [MPa]	28 days flexural strength [MPa]
CL-POX-LS	6.62	7.78
	6.73	7.73
	7.20	7.69
	6.56	7.16
CL-POX-LS-N30	7.44	8.66
	8.47	8.84
	7.33	7.76
	7.99	8.50

Identification	10 days compressive strength [MPa]	28 days compressive strength [MPa]
CL-POX-LS	28.6	31.4
	27.4	36.2
	23.7	35.7
	31.7	35.0
CL-POX-LS-N30	39.0	47.9
	25.4	36.0
	27.6	43.8
	35.3	46.6

Legends:

CL-POX-LS	Reference mortar prepared with lignosulfonate based admixture
CL-POX-LS-N30	Mortar prepared with lignosulfonate based admixture containing 0.3 % clinker grown, hydrogen peroxide functionalized CNTs/CNFs

ANNEX C Pore structure analysis results

C.1 – Gas adsorption porosimetry

Introduction

Gas adsorption porosimetry is known generally as BET, which stands for Stephen Brunauer, Paul Hugh Emmett and Ede Teller, the inventors of the theory of measuring the surface area of a porous material by the quantity of adsorbed gas molecules on its surface. The previously cleaned (outgassed) sample is placed in vacuum and slowly N_2 gas is injected in the recipient. The area occupied by an adsorbed nitrogen molecule is known (16.2 $Å^2$ that is 0.162 nm^2). When the molecules are adsorbed on the surface, they do not interfere in the atmospheric pressure, so the amount of injected nitrogen and the measured pressure will give information about the surface area (including open pores) and pore structure of the sample. The analysis can go on until the pressure of condensation of nitrogen is reached. As the adsorption is a reversible phenomenon, the desorption can also be performed decreasing the pressure. The whole process has to be effectuated at a constant temperature, generally 77 K (-196 °C). The results, called isotherms, are generally represented in a plot injected gas volume versus P/P_0 where P is the equilibrium pressure, P_0 is the saturation (condensation) pressure of nitrogen (Figure 8.1). In order to determine the specific surface area, the area of the adsorbed monolayer has to be divided by the mass of the sample. The forms of the isotherms give information whether the specific surface area can be determined by the BET model.

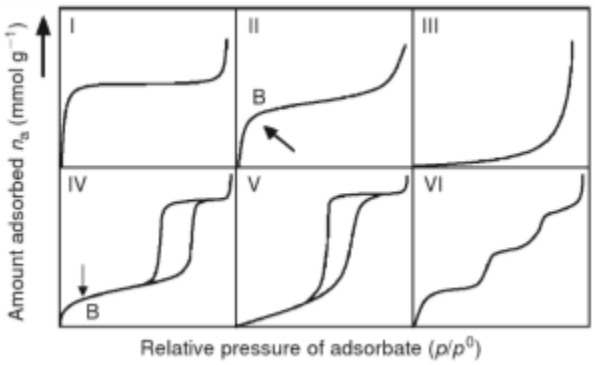

Figure 8.1– Classification of isotherms (I-VI) according to pore size and distribution, with the monolayer saturation point (B). II and IV follow BET model. Vertical axis represents gas volume and horizontal axis P/P_0 ratio. Source: Sing *et al.*(1985)

Closed pores are not included in the measurement as they are inaccessible for the nitrogen. Typical pore size ranges that can be investigated by gas adsorption porosimetry include micro- and meso pores from 1 nm, which is the physical limit for a nitrogen molecule. (SING *et al.*, 1985)

Sample preparation

Pieces of mortar specimens were cut with diamond saw. The specimens in all cases were those previously tested at 28 days of age. Mix proportions and other details are given in Table 8.1. The approximate size of the samples was 5 × 5 × 20 mm^3. The samples were dried at 60°C during one week. The samples were degasified after the drying process and analyzed on a Quantachrome Instruments Nova 2200 instrument.

Table 8.1 – Details of specimens analyzed by gas adsorption porosimetry and *He* pycnometry

Sample name	**CNT/CNF content* [%]**	**W/C ratio**
CPIII-CL-LS[1]	0	0.43
CPIII-CL-LS-N30[1,3]	0.3	0.43
CP-III-CL-POX-LS-N30[1,5]	0.3	0.43
CPV-CL-LS[2]	0	0.43
CPV-CL-LS-N30[2,3]	0.3	0.43
CPIII-SF-LS[1]	0	0.40
CPIII-SF-LS-N30[1,4]	0.3	0.40
CPIII-CL-NH-LP[1]	0	0.375
CPIII-CL-NH-LP-N10[1,6]	0.1	0.375
CPIII-CL-NH-LP-N30[1,6]	0.3	0.375

* – with respect to binder content
[1] – CP-III cement
[2] – CP-V cement
[3] – with nano-structured clinker
[4] –with nano-structured silica fume
[5] – with H_2O_2 treated nano-structured clinker
[6] – with ammonia treated nano-structured clinker

C.3 – BET results

Sample CPIII-CL-LS

Quantachrome Corporation
NOVA Enhanced Data Reduction Software Ver. 2.13
File Name = n262202.dat

Instrument	= NOVA-2200 Ver. 6.11		
User ID	= SERGIO	User Setup	= 66
Comments	= 3R PETER CIVIL UFMG		
Sample ID	= 2073	Sample Cell Number	= 31
Sample Weight	= 1.1844 g	Sample Volume	= 0.4781 cc
Sample Density	= 0.0000 g/cc		
Po Type	= Calculate	Po	= 706.30 mm Hg
Adsorbate	= Nitrogen	Bath Temperature	= 77.40 deg K
Adsorption Tolerance	= 0.0500 mm Hg	Desorption Tolerance	= 0.0500 mm Hg
Adsorption Equil Time	= 60 sec	Desorption Equil Time	= 60 sec
Adsorption Dwell Time	= 240 sec	Desorption Dwell Time	= 240 sec
Analysis Start Time	= Fri Jun 22 15:50:30 2012	Elapsed Time	= 237.10 Minutes.

Multi Point BET (Adsorption)

P/Po	BET Transform [1/{W[Po/P - 1]}]
0.049824	83.958995
0.101903	183.521390
0.153086	292.366692
0.203366	405.605038
0.252453	526.816145
0.302239	656.865002

Slope	=	2270.584342
Intercept	=	-44.034268
Correlation Coefficient	=	0.998416
BET C	=	-50.564031
Total Surface Area in Cell	=	1.8525 m^2
Specific Surface Area	=	1.5641 m^2/g

Quantachrome Corporation
NOVA Enhanced Data Reduction Software Ver. 2.13
File Name = n262202.dat

Instrument	= NOVA-2200 Ver. 6.11		
User ID	= SERGIO	User Setup	= 66
Comments	= 3R PETER CIVIL UFMG		
Sample ID	= 2073	Sample Cell Number	= 31
Sample Weight	= 1.1844 g	Sample Volume	= 0.4781 cc
Sample Density	= 0.0000 g/cc		
Po Type	= Calculate	Po	= 706.30 mm Hg
Adsorbate	= Nitrogen	Bath Temperature	= 77.40 deg K
Adsorption Tolerance	= 0.0500 mm Hg	Desorption Tolerance	= 0.0500 mm Hg
Adsorption Equil Time	= 60 sec	Desorption Equil Time	= 60 sec
Adsorption Dwell Time	= 240 sec	Desorption Dwell Time	= 240 sec
Analysis Start Time	= Fri Jun 22 15:50:30 2012	Elapsed Time	= 237.10 Minutes.

Single Point BET (Adsorption)

P/Po	Specific Surface Area [m^2/g]
0.302239	1.602388

Quantachrome Corporation
NOVA Enhanced Data Reduction Software Ver. 2.13
File Name = n262202.dat

Instrument	= NOVA-2200 Ver. 6.11		
User ID	= SERGIO	User Setup	= 66
Comments	= 3R PETER CIVIL UFMG		
Sample ID	= 2073	Sample Cell Number	= 31
Sample Weight	= 1.1844 g	Sample Volume	= 0.4781 cc
Sample Density	= 0.0000 g/cc		
Po Type	= Calculate	Po	= 706.30 mm Hg
Adsorbate	= Nitrogen	Bath Temperature	= 77.40 deg K
Adsorption Tolerance	= 0.0500 mm Hg	Desorption Tolerance	= 0.0500 mm Hg
Adsorption Equil Time	= 60 sec	Desorption Equil Time	= 60 sec
Adsorption Dwell Time	= 240 sec	Desorption Dwell Time	= 240 sec
Analysis Start Time	= Fri Jun 22 15:50:30 2012	Elapsed Time	= 237.10 Minutes.

BJH dV/d[logD] (Desorption)

Pore Diameter [Å]	Pore Area [m^2/g]	Pore Volume [cc/g] x 10e-3
806.627060	0.177926	3.587991
150.115039	0.979598	3.676309
86.469500	1.052015	2.274181
61.220585	1.275753	1.952558
46.332969	2.553382	2.957644
37.115088	21.238832	19.707028

Total Pore Volume is 0.00619 cc/g for
all pores of diameter smaller than 1414.811 Å.

Average pore diameter is 158.219 Å.

Quantachrome Corporation
NOVA Enhanced Data Reduction Software Ver. 2.13
File Name = n262202.dat

Instrument	= NOVA-2200 Ver. 6.11		
User ID	= SERGIO	User Setup	= 66
Comments	= 3R PETER CIVIL UFMG		
Sample ID	= 2073	Sample Cell Number	= 31
Sample Weight	= 1.1844 g	Sample Volume	= 0.4781 cc
Sample Density	= 0.0000 g/cc		
Po Type	= Calculate	Po	= 706.30 mm Hg
Adsorbate	= Nitrogen	Bath Temperature	= 77.40 deg K
Adsorption Tolerance	= 0.0500 mm Hg	Desorption Tolerance	= 0.0500 mm Hg
Adsorption Equil Time	= 60 sec	Desorption Equil Time	= 60 sec
Adsorption Dwell Time	= 240 sec	Desorption Dwell Time	= 240 sec
Analysis Start Time	= Fri Jun 22 15:50:30 2012	Elapsed Time	= 237.10 Minutes.

BJH dV/d[logD] (Desorption)

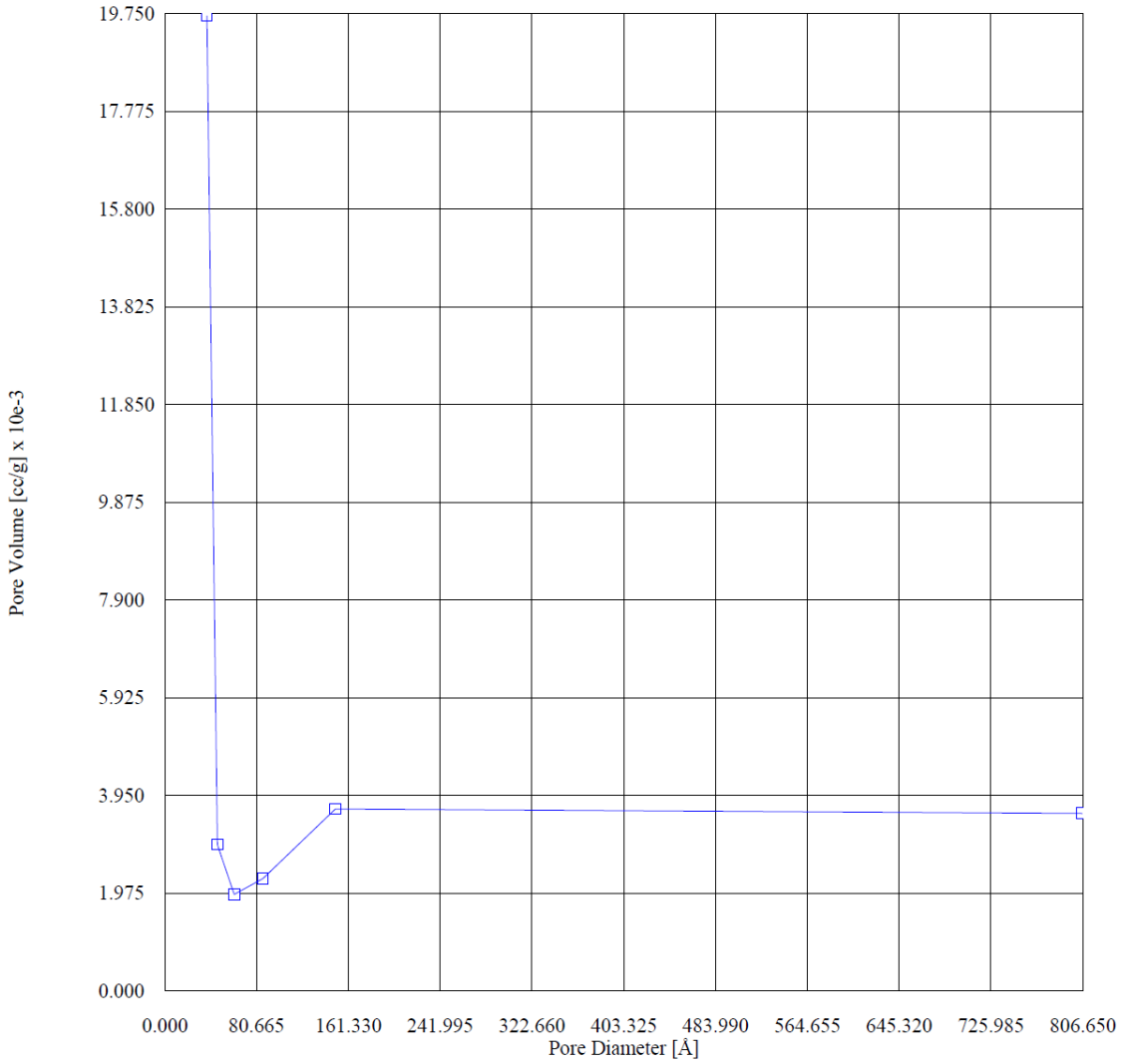

Quantachrome Corporation
NOVA Enhanced Data Reduction Software Ver. 2.13
File Name = n262202.dat

Instrument	= NOVA-2200 Ver. 6.11		
User ID	= SERGIO	User Setup	= 66
Comments	= 3R PETER CIVIL UFMG		
Sample ID	= 2073	Sample Cell Number	= 31
Sample Weight	= 1.1844 g	Sample Volume	= 0.4781 cc
Sample Density	= 0.0000 g/cc		
Po Type	= Calculate	Po	= 706.30 mm Hg
Adsorbate	= Nitrogen	Bath Temperature	= 77.40 deg K
Adsorption Tolerance	= 0.0500 mm Hg	Desorption Tolerance	= 0.0500 mm Hg
Adsorption Equil Time	= 60 sec	Desorption Equil Time	= 60 sec
Adsorption Dwell Time	= 240 sec	Desorption Dwell Time	= 240 sec
Analysis Start Time	= Fri Jun 22 15:50:30 2012	Elapsed Time	= 237.10 Minutes.

Isotherm (Adsorption/Desorption)

P/Po	Volume Adsorbed @STP [cc/g]
0.049824	0.499711
0.101903	0.494688
0.153086	0.494679
0.203366	0.503581
0.252453	0.512904
0.302239	0.527620
0.402008	0.574836
0.500903	0.636141
0.597384	0.717478
0.695330	1.001097
0.797992	1.139299
0.896265	1.478058
0.986092	4.005253
0.895528	2.145774
0.792342	1.598738
0.702089	1.419433
0.590654	1.281524
0.501351	1.165714
0.393083	0.563833
0.301867	0.509789
0.203510	0.480572
0.103893	0.476854

Quantachrome Corporation
NOVA Enhanced Data Reduction Software Ver. 2.13
File Name = n262202.dat

Instrument	= NOVA-2200 Ver. 6.11		
User ID	= SERGIO	User Setup	= 66
Comments	= 3R PETER CIVIL UFMG		
Sample ID	= 2073	Sample Cell Number	= 31
Sample Weight	= 1.1844 g	Sample Volume	= 0.4781 cc
Sample Density	= 0.0000 g/cc		
Po Type	= Calculate	Po	= 706.30 mm Hg
Adsorbate	= Nitrogen	Bath Temperature	= 77.40 deg K
Adsorption Tolerance	= 0.0500 mm Hg	Desorption Tolerance	= 0.0500 mm Hg
Adsorption Equil Time	= 60 sec	Desorption Equil Time	= 60 sec
Adsorption Dwell Time	= 240 sec	Desorption Dwell Time	= 240 sec
Analysis Start Time	= Fri Jun 22 15:50:30 2012	Elapsed Time	= 237.10 Minutes.

Isotherm (Adsorption/Desorption)

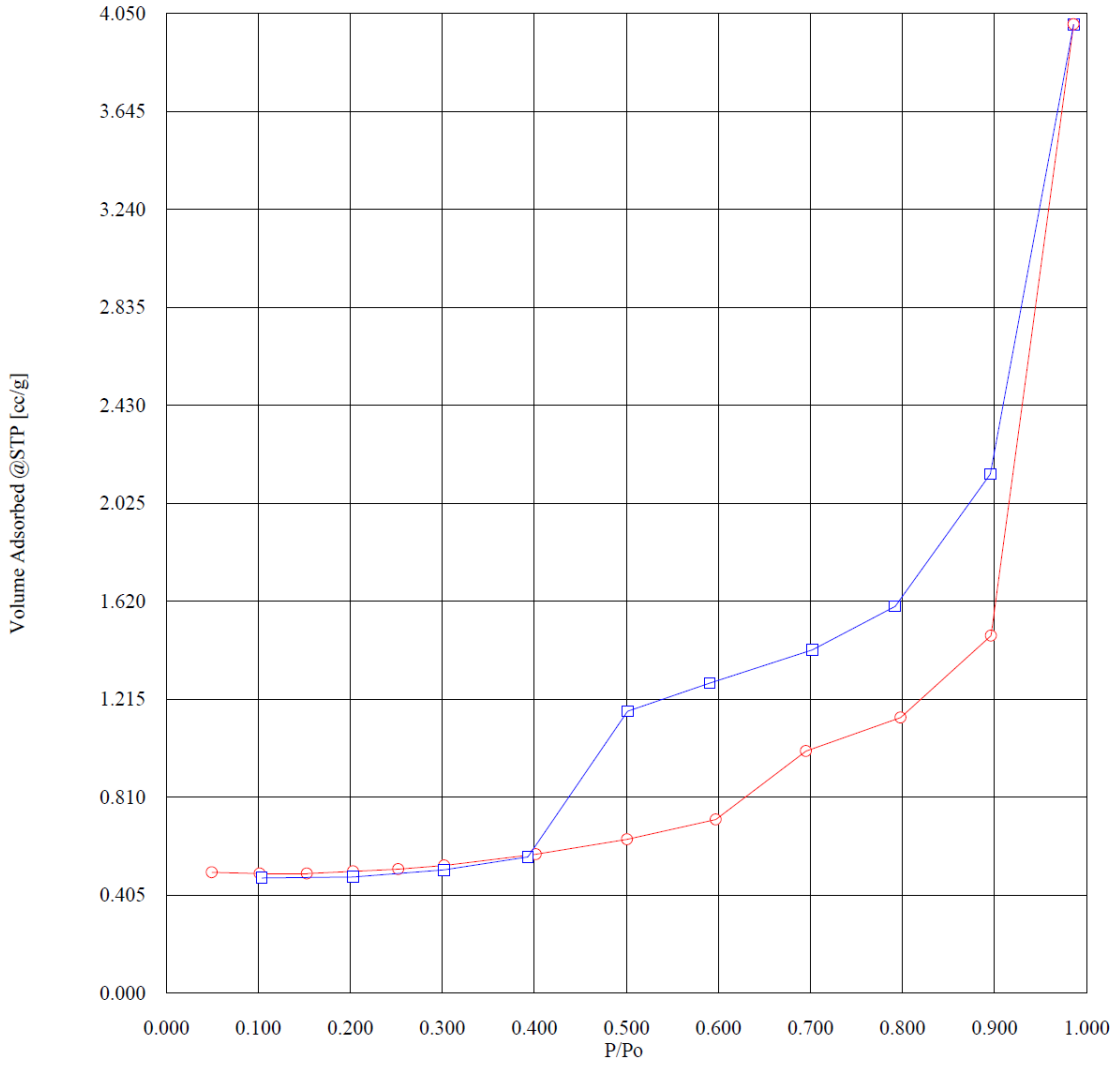

Red: adsorption

Blue desorption

Sample CPIII-CL-LS-N30

Quantachrome Corporation
NOVA Enhanced Data Reduction Software Ver. 2.13
File Name = n261501.dat

Instrument	= NOVA-2200 Ver. 6.11		
User ID	= SERGIO	User Setup	= 66
Comments	= 3N PETER CIVIL UFMG		
Sample ID	= 2064	Sample Cell Number	= 30
Sample Weight	= 1.2500 g	Sample Volume	= 0.4595 cc
Sample Density	= 0.0000 g/cc		
Po Type	= Calculate	Po	= 710.48 mm Hg
Adsorbate	= Nitrogen	Bath Temperature	= 77.40 deg K
Adsorption Tolerance	= 0.0500 mm Hg	Desorption Tolerance	= 0.0500 mm Hg
Adsorption Equil Time	= 60 sec	Desorption Equil Time	= 60 sec
Adsorption Dwell Time	= 240 sec	Desorption Dwell Time	= 240 sec
Analysis Start Time	= Fri Jun 15 08:03:36 2012	Elapsed Time	= 237.73 Minutes.

Multi Point BET (Adsorption)

P/Po	BET Transform [1/{W[Po/P - 1]}]
0.049440	76.143597
0.100624	157.095363
0.151181	238.920250
0.200832	316.494431
0.249781	392.527845
0.299205	470.511526

Slope	=	1578.414008
Intercept	=	-1.219530
Correlation Coefficient	=	0.999981
BET C	=	-1293.280515
Total Surface Area in Cell	=	2.7601 m^2
Specific Surface Area	=	2.2080 m^2/g

Quantachrome Corporation
NOVA Enhanced Data Reduction Software Ver. 2.13
File Name = n261501.dat

Instrument	= NOVA-2200 Ver. 6.11		
User ID	= SERGIO	User Setup	= 66
Comments	= 3N PETER CIVIL UFMG		
Sample ID	= 2064	Sample Cell Number	= 30
Sample Weight	= 1.2500 g	Sample Volume	= 0.4595 cc
Sample Density	= 0.0000 g/cc		
Po Type	= Calculate	Po	= 710.48 mm Hg
Adsorbate	= Nitrogen	Bath Temperature	= 77.40 deg K
Adsorption Tolerance	= 0.0500 mm Hg	Desorption Tolerance	= 0.0500 mm Hg
Adsorption Equil Time	= 60 sec	Desorption Equil Time	= 60 sec
Adsorption Dwell Time	= 240 sec	Desorption Dwell Time	= 240 sec
Analysis Start Time	= Fri Jun 15 08:03:36 2012	Elapsed Time	= 237.73 Minutes.

Single Point BET (Adsorption)

P/Po	Specific Surface Area [m^2/g]
0.299205	2.214582

Quantachrome Corporation
NOVA Enhanced Data Reduction Software Ver. 2.13
File Name = n261501.dat

Instrument	= NOVA-2200 Ver. 6.11		
User ID	= SERGIO	User Setup	= 66
Comments	= 3N PETER CIVIL UFMG		
Sample ID	= 2064	Sample Cell Number	= 30
Sample Weight	= 1.2500 g	Sample Volume	= 0.4595 cc
Sample Density	= 0.0000 g/cc		
Po Type	= Calculate	Po	= 710.48 mm Hg
Adsorbate	= Nitrogen	Bath Temperature	= 77.40 deg K
Adsorption Tolerance	= 0.0500 mm Hg	Desorption Tolerance	= 0.0500 mm Hg
Adsorption Equil Time	= 60 sec	Desorption Equil Time	= 60 sec
Adsorption Dwell Time	= 240 sec	Desorption Dwell Time	= 240 sec
Analysis Start Time	= Fri Jun 15 08:03:36 2012	Elapsed Time	= 237.73 Minutes.

BJH dV/d[logD] (Desorption)

Pore Diameter [Å]	Pore Area [m^2/g]	Pore Volume [cc/g] x 10e-3
816.695574	0.176390	3.601417
150.589628	1.271538	4.787012
86.938853	1.599089	3.475573
62.297711	2.070680	3.224966
46.850792	3.844860	4.503369
36.683532	20.847687	19.119169
30.068140	2.101111	1.579413
24.906483	0.508879	0.316860

Total Pore Volume is 0.00703 cc/g for
all pores of diameter smaller than 1434.594 Å.

Average pore diameter is 127.296 Å.

Quantachrome Corporation
NOVA Enhanced Data Reduction Software Ver. 2.13
File Name = n261501.dat

Instrument	= NOVA-2200 Ver. 6.11		
User ID	= SERGIO	User Setup	= 66
Comments	= 3N PETER CIVIL UFMG		
Sample ID	= 2064	Sample Cell Number	= 30
Sample Weight	= 1.2500 g	Sample Volume	= 0.4595 cc
Sample Density	= 0.0000 g/cc		
Po Type	= Calculate	Po	= 710.48 mm Hg
Adsorbate	= Nitrogen	Bath Temperature	= 77.40 deg K
Adsorption Tolerance	= 0.0500 mm Hg	Desorption Tolerance	= 0.0500 mm Hg
Adsorption Equil Time	= 60 sec	Desorption Equil Time	= 60 sec
Adsorption Dwell Time	= 240 sec	Desorption Dwell Time	= 240 sec
Analysis Start Time	= Fri Jun 15 08:03:36 2012	Elapsed Time	= 237.73 Minutes.

BJH dV/d[logD] (Desorption)

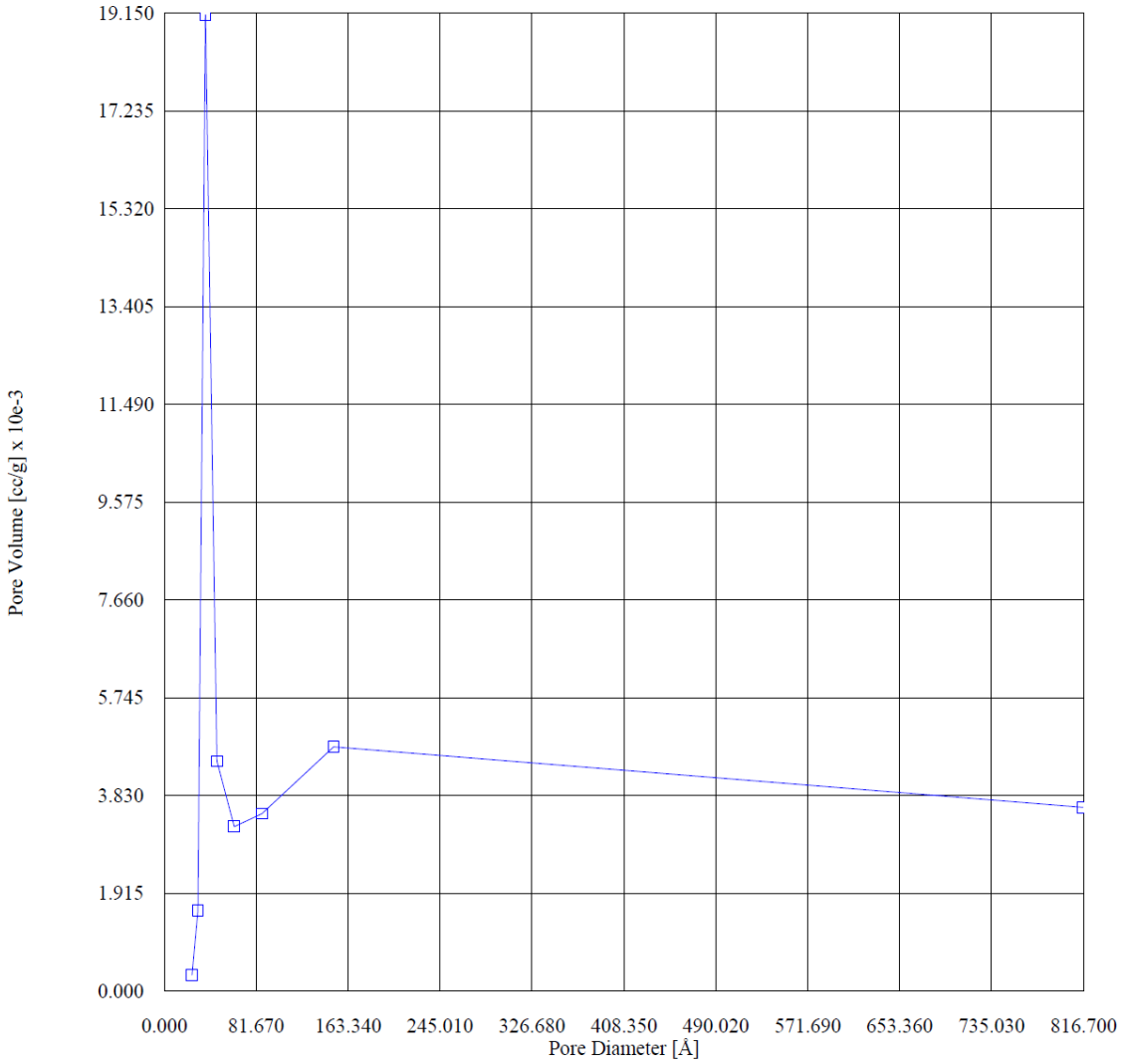

Quantachrome Corporation
NOVA Enhanced Data Reduction Software Ver. 2.13
File Name = n261501.dat

Instrument	= NOVA-2200 Ver. 6.11		
User ID	= SERGIO	User Setup	= 66
Comments	= 3N PETER CIVIL UFMG		
Sample ID	= 2064	Sample Cell Number	= 30
Sample Weight	= 1.2500 g	Sample Volume	= 0.4595 cc
Sample Density	= 0.0000 g/cc		
Po Type	= Calculate	Po	= 710.48 mm Hg
Adsorbate	= Nitrogen	Bath Temperature	= 77.40 deg K
Adsorption Tolerance	= 0.0500 mm Hg	Desorption Tolerance	= 0.0500 mm Hg
Adsorption Equil Time	= 60 sec	Desorption Equil Time	= 60 sec
Adsorption Dwell Time	= 240 sec	Desorption Dwell Time	= 240 sec
Analysis Start Time	= Fri Jun 15 08:03:36 2012	Elapsed Time	= 237.73 Minutes.

Isotherm (Adsorption/Desorption)

P/Po	Volume Adsorbed @STP [cc/g]
0.049440	0.546533
0.100624	0.569834
0.151181	0.596461
0.200832	0.635304
0.249781	0.678662
0.299205	0.726041
0.398100	0.843593
0.497485	0.974683
0.595292	1.135023
0.702734	1.327246
0.799454	1.539006
0.897118	1.999409
0.986287	4.549182
0.895721	2.669826
0.793572	1.969489
0.703512	1.705398
0.603885	1.510260
0.492910	1.294306
0.391765	0.742283
0.302158	0.635748
0.204977	0.546784
0.088377	0.482507

Quantachrome Corporation
NOVA Enhanced Data Reduction Software Ver. 2.13
File Name = n261501.dat

Instrument	= NOVA-2200 Ver. 6.11		
User ID	= SERGIO	User Setup	= 66
Comments	= 3N PETER CIVIL UFMG		
Sample ID	= 2064	Sample Cell Number	= 30
Sample Weight	= 1.2500 g	Sample Volume	= 0.4595 cc
Sample Density	= 0.0000 g/cc		
Po Type	= Calculate	Po	= 710.48 mm Hg
Adsorbate	= Nitrogen	Bath Temperature	= 77.40 deg K
Adsorption Tolerance	= 0.0500 mm Hg	Desorption Tolerance	= 0.0500 mm Hg
Adsorption Equil Time	= 60 sec	Desorption Equil Time	= 60 sec
Adsorption Dwell Time	= 240 sec	Desorption Dwell Time	= 240 sec
Analysis Start Time	= Fri Jun 15 08:03:36 2012	Elapsed Time	= 237.73 Minutes.

Isotherm (Adsorption/Desorption)

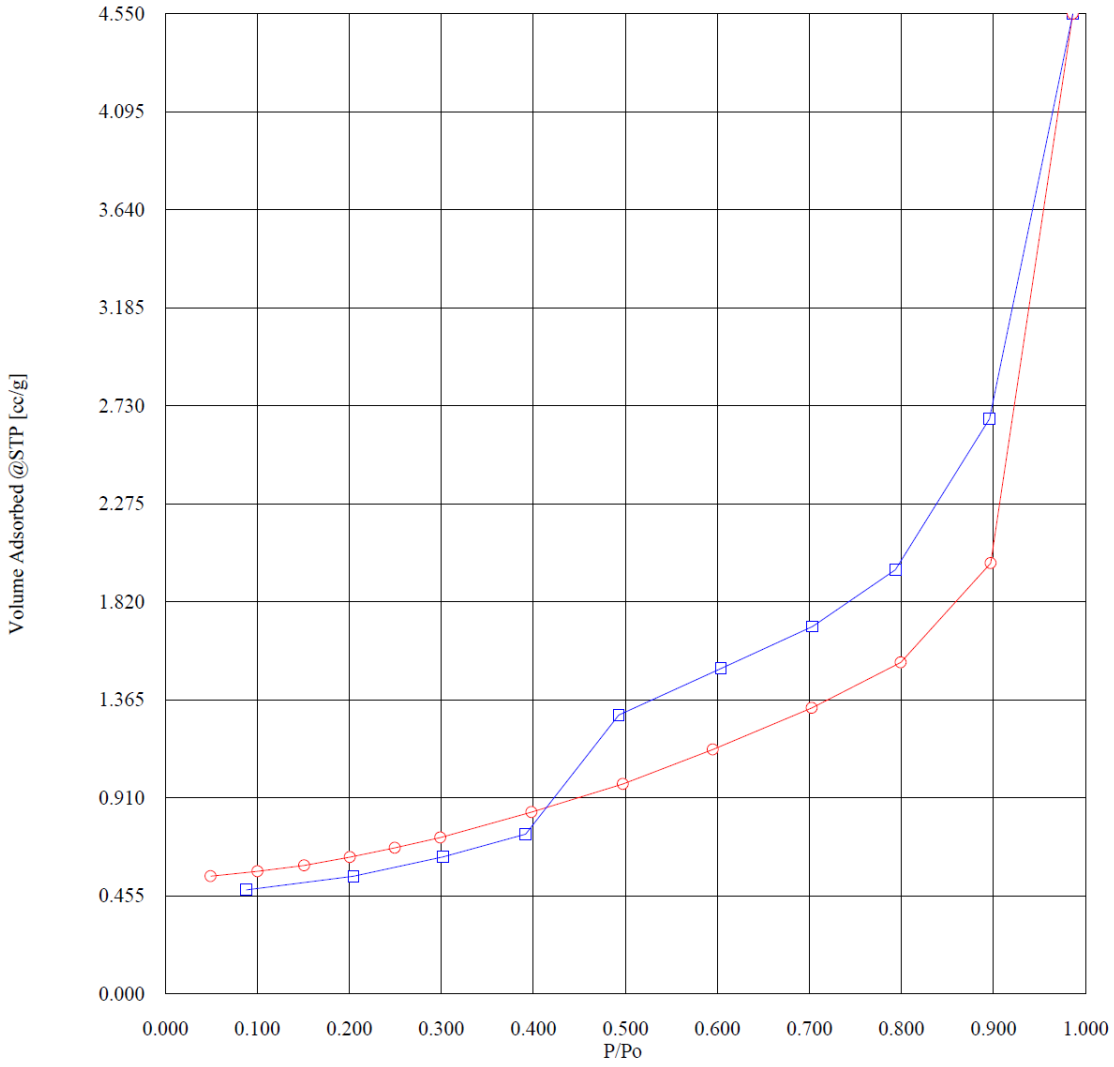

Red: adsorption

Blue desorption

Sample CPV-CL-LS

Quantachrome Corporation
NOVA Enhanced Data Reduction Software Ver. 2.13
File Name = n262502.dat

Instrument	= NOVA-2200 Ver. 6.11		
User ID	= SERGIO	User Setup	= 66
Comments	= 5R PETER CIVIL UFMG		
Sample ID	= 2074	Sample Cell Number	= 31
Sample Weight	= 1.3781 g	Sample Volume	= 0.5541 cc
Sample Density	= 0.0000 g/cc		
Po Type	= Calculate	Po	= 710.85 mm Hg
Adsorbate	= Nitrogen	Bath Temperature	= 77.40 deg K
Adsorption Tolerance	= 0.0500 mm Hg	Desorption Tolerance	= 0.0500 mm Hg
Adsorption Equil Time	= 60 sec	Desorption Equil Time	= 60 sec
Adsorption Dwell Time	= 240 sec	Desorption Dwell Time	= 240 sec
Analysis Start Time	= Mon Jun 25 10:06:46 2012	Elapsed Time	= 269.95 Minutes.

Multi Point BET (Adsorption)

P/Po	BET Transform [1/{W[Po/P - 1]}]
0.046833	85.595968
0.099764	188.408058
0.151842	299.413263
0.202621	411.118213
0.252284	528.738942
0.301978	653.102621

Slope	=	2224.089364
Intercept	=	-30.125603
Correlation Coefficient	=	0.999024
BET C	=	-72.827215
Total Surface Area in Cell	=	2.1875 m^2
Specific Surface Area	=	1.5873 m^2/g

Quantachrome Corporation
NOVA Enhanced Data Reduction Software Ver. 2.13
File Name = n262502.dat

Instrument	= NOVA-2200 Ver. 6.11		
User ID	= SERGIO	User Setup	= 66
Comments	= 5R PETER CIVIL UFMG		
Sample ID	= 2074	Sample Cell Number	= 31
Sample Weight	= 1.3781 g	Sample Volume	= 0.5541 cc
Sample Density	= 0.0000 g/cc		
Po Type	= Calculate	Po	= 710.85 mm Hg
Adsorbate	= Nitrogen	Bath Temperature	= 77.40 deg K
Adsorption Tolerance	= 0.0500 mm Hg	Desorption Tolerance	= 0.0500 mm Hg
Adsorption Equil Time	= 60 sec	Desorption Equil Time	= 60 sec
Adsorption Dwell Time	= 240 sec	Desorption Dwell Time	= 240 sec
Analysis Start Time	= Mon Jun 25 10:06:46 2012	Elapsed Time	= 269.95 Minutes.

Single Point BET (Adsorption)

P/Po	Specific Surface Area [m^2/g]
0.301978	1.610227

Quantachrome Corporation
NOVA Enhanced Data Reduction Software Ver. 2.13
File Name = n262502.dat

Instrument	= NOVA-2200 Ver. 6.11		
User ID	= SERGIO	User Setup	= 66
Comments	= 5R PETER CIVIL UFMG		
Sample ID	= 2074	Sample Cell Number	= 31
Sample Weight	= 1.3781 g	Sample Volume	= 0.5541 cc
Sample Density	= 0.0000 g/cc		
Po Type	= Calculate	Po	= 710.85 mm Hg
Adsorbate	= Nitrogen	Bath Temperature	= 77.40 deg K
Adsorption Tolerance	= 0.0500 mm Hg	Desorption Tolerance	= 0.0500 mm Hg
Adsorption Equil Time	= 60 sec	Desorption Equil Time	= 60 sec
Adsorption Dwell Time	= 240 sec	Desorption Dwell Time	= 240 sec
Analysis Start Time	= Mon Jun 25 10:06:46 2012	Elapsed Time	= 269.95 Minutes.

BJH dV/d[logD] (Desorption)

Pore Diameter [Å]	Pore Area [m^2/g]	Pore Volume [cc/g] x 10e-3
873.630618	0.152536	3.331500
152.353706	1.013285	3.859443
86.563061	1.086838	2.352000
62.384930	1.228532	1.916047
47.460946	2.218711	2.632554
37.076780	8.540168	7.916048

Total Pore Volume is 0.00556 cc/g for
all pores of diameter smaller than 1544.121 Å.

Average pore diameter is 140.196 Å.

Quantachrome Corporation
NOVA Enhanced Data Reduction Software Ver. 2.13
File Name = n262502.dat

Instrument	= NOVA-2200 Ver. 6.11		
User ID	= SERGIO	User Setup	= 66
Comments	= 5R PETER CIVIL UFMG		
Sample ID	= 2074	Sample Cell Number	= 31
Sample Weight	= 1.3781 g	Sample Volume	= 0.5541 cc
Sample Density	= 0.0000 g/cc		
Po Type	= Calculate	Po	= 710.85 mm Hg
Adsorbate	= Nitrogen	Bath Temperature	= 77.40 deg K
Adsorption Tolerance	= 0.0500 mm Hg	Desorption Tolerance	= 0.0500 mm Hg
Adsorption Equil Time	= 60 sec	Desorption Equil Time	= 60 sec
Adsorption Dwell Time	= 240 sec	Desorption Dwell Time	= 240 sec
Analysis Start Time	= Mon Jun 25 10:06:46 2012	Elapsed Time	= 269.95 Minutes.

BJH dV/d[logD] (Desorption)

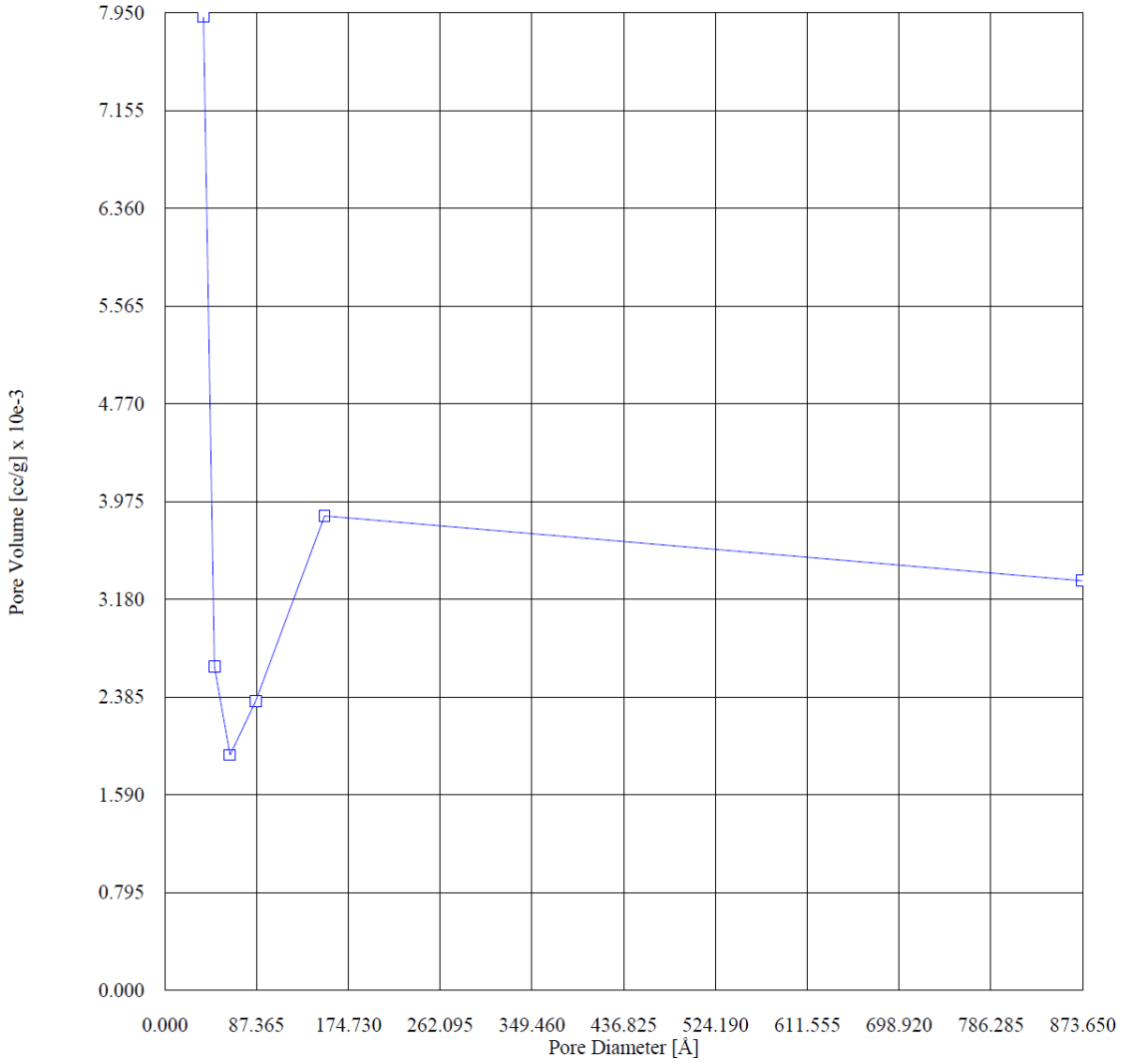

Quantachrome Corporation
NOVA Enhanced Data Reduction Software Ver. 2.13
File Name = n262502.dat

Instrument	= NOVA-2200 Ver. 6.11		
User ID	= SERGIO	User Setup	= 66
Comments	= 5R PETER CIVIL UFMG		
Sample ID	= 2074	Sample Cell Number	= 31
Sample Weight	= 1.3781 g	Sample Volume	= 0.5541 cc
Sample Density	= 0.0000 g/cc		
Po Type	= Calculate	Po	= 710.85 mm Hg
Adsorbate	= Nitrogen	Bath Temperature	= 77.40 deg K
Adsorption Tolerance	= 0.0500 mm Hg	Desorption Tolerance	= 0.0500 mm Hg
Adsorption Equil Time	= 60 sec	Desorption Equil Time	= 60 sec
Adsorption Dwell Time	= 240 sec	Desorption Dwell Time	= 240 sec
Analysis Start Time	= Mon Jun 25 10:06:46 2012	Elapsed Time	= 269.95 Minutes.

Isotherm (Adsorption/Desorption)

P/Po	Volume Adsorbed @STP [cc/g]
0.046833	0.459287
0.099764	0.470620
0.151842	0.478405
0.202621	0.494547
0.252284	0.510583
0.301978	0.530003
0.400926	0.577655
0.500199	0.641135
0.597322	0.732096
0.695199	0.861668
0.804343	1.033564
0.896130	1.360159
0.987276	3.601726
0.898024	1.810928
0.791884	1.216302
0.703772	1.035908
0.604672	0.912210
0.504916	0.790855
0.386905	0.504537
0.300317	0.463628
0.202636	0.432318
0.103348	0.421252

Quantachrome Corporation
NOVA Enhanced Data Reduction Software Ver. 2.13
File Name = n262502.dat

Instrument	= NOVA-2200 Ver. 6.11		
User ID	= SERGIO	User Setup	= 66
Comments	= 5R PETER CIVIL UFMG		
Sample ID	= 2074	Sample Cell Number	= 31
Sample Weight	= 1.3781 g	Sample Volume	= 0.5541 cc
Sample Density	= 0.0000 g/cc		
Po Type	= Calculate	Po	= 710.85 mm Hg
Adsorbate	= Nitrogen	Bath Temperature	= 77.40 deg K
Adsorption Tolerance	= 0.0500 mm Hg	Desorption Tolerance	= 0.0500 mm Hg
Adsorption Equil Time	= 60 sec	Desorption Equil Time	= 60 sec
Adsorption Dwell Time	= 240 sec	Desorption Dwell Time	= 240 sec
Analysis Start Time	= Mon Jun 25 10:06:46 2012	Elapsed Time	= 269.95 Minutes.

Isotherm (Adsorption/Desorption)

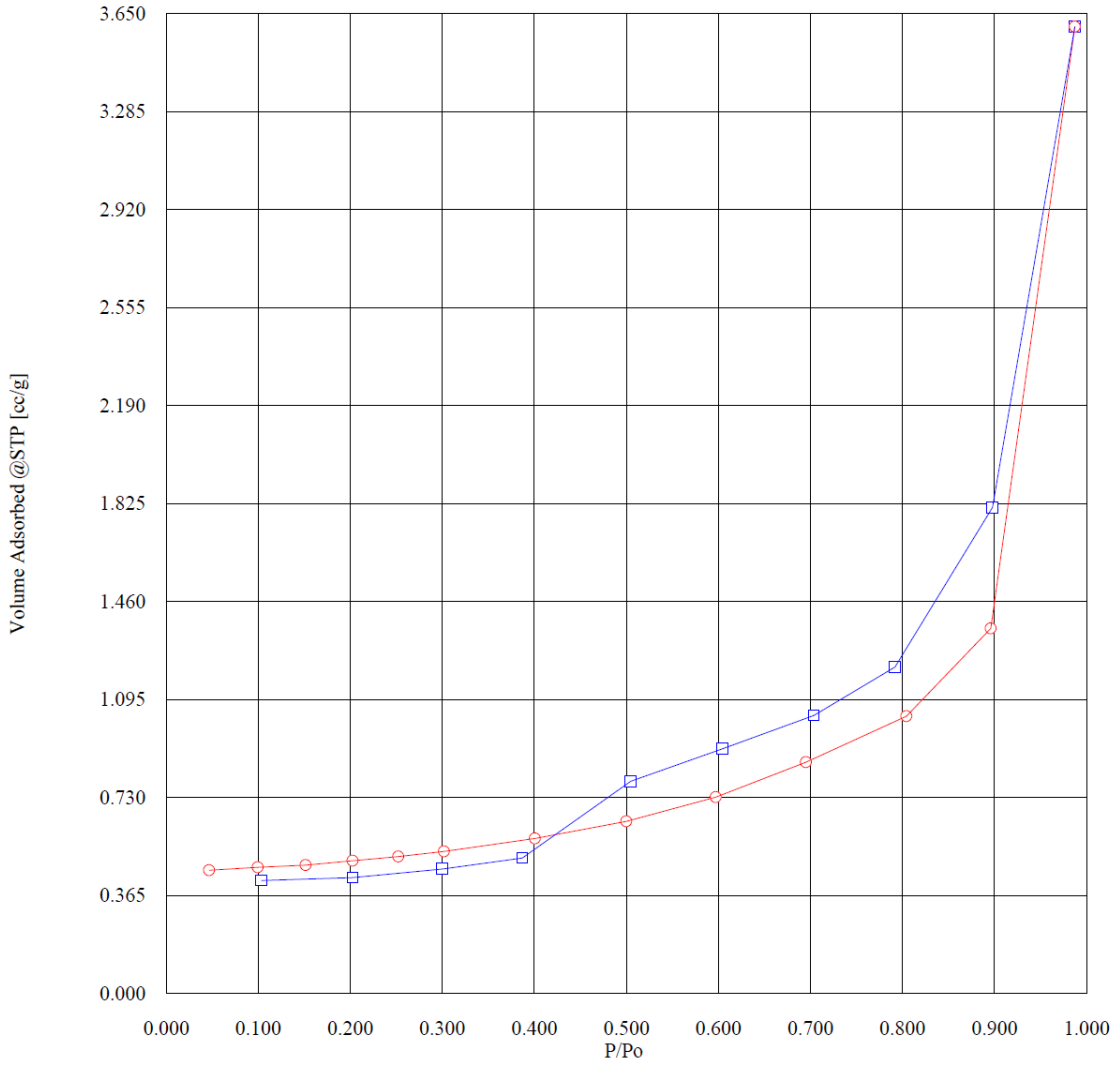

Red: adsorption

Blue desorption

Sample CPV CL-LS-N30

Quantachrome Corporation
NOVA Enhanced Data Reduction Software Ver. 2.13
File Name = n262201.dat

Instrument	= NOVA-2200 Ver. 6.11		
User ID	= SERGIO	User Setup	= 66
Comments	= 5N PETER CIVIL UFMG		
Sample ID	= 2072	Sample Cell Number	= 30
Sample Weight	= 1.3661 g	Sample Volume	= 0.5249 cc
Sample Density	= 0.0000 g/cc		
Po Type	= Calculate	Po	= 706.30 mm Hg
Adsorbate	= Nitrogen	Bath Temperature	= 77.40 deg K
Adsorption Tolerance	= 0.0500 mm Hg	Desorption Tolerance	= 0.0500 mm Hg
Adsorption Equil Time	= 60 sec	Desorption Equil Time	= 60 sec
Adsorption Dwell Time	= 240 sec	Desorption Dwell Time	= 240 sec
Analysis Start Time	= Fri Jun 22 15:50:30 2012	Elapsed Time	= 233.82 Minutes.

Multi Point BET (Adsorption)

P/Po	BET Transform [1/{W[Po/P - 1]}]
0.050052	88.074669
0.101713	186.106546
0.152524	286.895783
0.202135	382.931587
0.250683	477.611134
0.300112	578.409015

Slope	=	1958.980893
Intercept	=	-11.840885
Correlation Coefficient	=	0.999956
BET C	=	-164.442094
Total Surface Area in Cell	=	2.4433 m^2
Specific Surface Area	=	1.7885 m^2/g

Quantachrome Corporation
NOVA Enhanced Data Reduction Software Ver. 2.13
File Name = n262201.dat

Instrument	= NOVA-2200 Ver. 6.11		
User ID	= SERGIO	User Setup	= 66
Comments	= 5N PETER CIVIL UFMG		
Sample ID	= 2072	Sample Cell Number	= 30
Sample Weight	= 1.3661 g	Sample Volume	= 0.5249 cc
Sample Density	= 0.0000 g/cc		
Po Type	= Calculate	Po	= 706.30 mm Hg
Adsorbate	= Nitrogen	Bath Temperature	= 77.40 deg K
Adsorption Tolerance	= 0.0500 mm Hg	Desorption Tolerance	= 0.0500 mm Hg
Adsorption Equil Time	= 60 sec	Desorption Equil Time	= 60 sec
Adsorption Dwell Time	= 240 sec	Desorption Dwell Time	= 240 sec
Analysis Start Time	= Fri Jun 22 15:50:30 2012	Elapsed Time	= 233.82 Minutes.

Single Point BET (Adsorption)

P/Po	Specific Surface Area [m^2/g]
0.300112	1.806931

Quantachrome Corporation
NOVA Enhanced Data Reduction Software Ver. 2.13
File Name = n262201.dat

Instrument	= NOVA-2200 Ver. 6.11		
User ID	= SERGIO	User Setup	= 66
Comments	= 5N PETER CIVIL UFMG		
Sample ID	= 2072	Sample Cell Number	= 30
Sample Weight	= 1.3661 g	Sample Volume	= 0.5249 cc
Sample Density	= 0.0000 g/cc		
Po Type	= Calculate	Po	= 706.30 mm Hg
Adsorbate	= Nitrogen	Bath Temperature	= 77.40 deg K
Adsorption Tolerance	= 0.0500 mm Hg	Desorption Tolerance	= 0.0500 mm Hg
Adsorption Equil Time	= 60 sec	Desorption Equil Time	= 60 sec
Adsorption Dwell Time	= 240 sec	Desorption Dwell Time	= 240 sec
Analysis Start Time	= Fri Jun 22 15:50:30 2012	Elapsed Time	= 233.82 Minutes.

BJH dV/d[logD] (Desorption)

Pore Diameter [Å]	Pore Area [m^2/g]	Pore Volume [cc/g] x 10e-3
869.853614	0.127630	2.775478
159.129721	1.032483	4.107467
86.879559	1.180543	2.564126
61.453375	1.963690	3.016884
46.535504	4.505856	5.242057
37.109433	10.860937	10.076080
29.952850	1.961614	1.468898
24.882566	0.951736	0.592041

Total Pore Volume is 0.00571 cc/g for
all pores of diameter smaller than 1523.723 Å.

Average pore diameter is 127.680 Å.

Quantachrome Corporation
NOVA Enhanced Data Reduction Software Ver. 2.13
File Name = n262201.dat

Instrument	= NOVA-2200 Ver. 6.11		
User ID	= SERGIO	User Setup	= 66
Comments	= 5N PETER CIVIL UFMG		
Sample ID	= 2072	Sample Cell Number	= 30
Sample Weight	= 1.3661 g	Sample Volume	= 0.5249 cc
Sample Density	= 0.0000 g/cc		
Po Type	= Calculate	Po	= 706.30 mm Hg
Adsorbate	= Nitrogen	Bath Temperature	= 77.40 deg K
Adsorption Tolerance	= 0.0500 mm Hg	Desorption Tolerance	= 0.0500 mm Hg
Adsorption Equil Time	= 60 sec	Desorption Equil Time	= 60 sec
Adsorption Dwell Time	= 240 sec	Desorption Dwell Time	= 240 sec
Analysis Start Time	= Fri Jun 22 15:50:30 2012	Elapsed Time	= 233.82 Minutes.

BJH dV/d[logD] (Desorption)

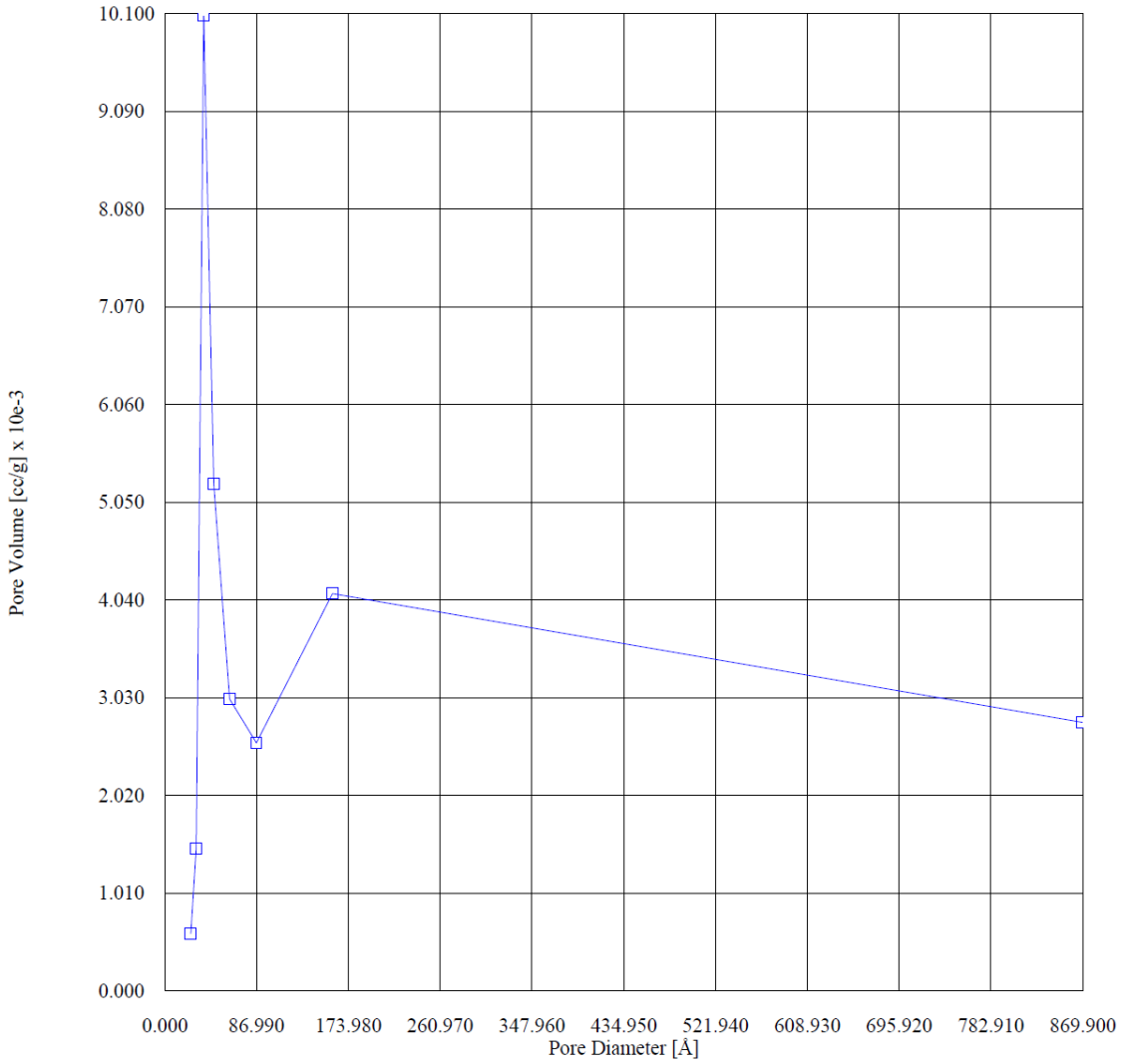

Quantachrome Corporation
NOVA Enhanced Data Reduction Software Ver. 2.13
File Name = n262201.dat

Instrument	= NOVA-2200 Ver. 6.11		
User ID	= SERGIO	User Setup	= 66
Comments	= 5N PETER CIVIL UFMG		
Sample ID	= 2072	Sample Cell Number	= 30
Sample Weight	= 1.3661 g	Sample Volume	= 0.5249 cc
Sample Density	= 0.0000 g/cc		
Po Type	= Calculate	Po	= 706.30 mm Hg
Adsorbate	= Nitrogen	Bath Temperature	= 77.40 deg K
Adsorption Tolerance	= 0.0500 mm Hg	Desorption Tolerance	= 0.0500 mm Hg
Adsorption Equil Time	= 60 sec	Desorption Equil Time	= 60 sec
Adsorption Dwell Time	= 240 sec	Desorption Dwell Time	= 240 sec
Analysis Start Time	= Fri Jun 22 15:50:30 2012	Elapsed Time	= 233.82 Minutes.

Isotherm (Adsorption/Desorption)

P/Po	Volume Adsorbed @STP [cc/g]
0.050052	0.478653
0.101713	0.486805
0.152524	0.501928
0.202135	0.529353
0.250683	0.560453
0.300112	0.593162
0.399182	0.672078
0.497174	0.762871
0.597543	0.885534
0.696393	1.043051
0.800993	1.446566
0.896470	1.789444
0.987102	3.695981
0.904286	2.261266
0.793352	1.577492
0.703464	1.378707
0.591657	1.182010
0.504253	0.997046
0.388838	0.640222
0.301502	0.558120
0.204725	0.485509
0.090268	0.431817

Quantachrome Corporation
NOVA Enhanced Data Reduction Software Ver. 2.13
File Name = n262201.dat

Instrument	= NOVA-2200 Ver. 6.11		
User ID	= SERGIO	User Setup	= 66
Comments	= 5N PETER CIVIL UFMG		
Sample ID	= 2072	Sample Cell Number	= 30
Sample Weight	= 1.3661 g	Sample Volume	= 0.5249 cc
Sample Density	= 0.0000 g/cc		
Po Type	= Calculate	Po	= 706.30 mm Hg
Adsorbate	= Nitrogen	Bath Temperature	= 77.40 deg K
Adsorption Tolerance	= 0.0500 mm Hg	Desorption Tolerance	= 0.0500 mm Hg
Adsorption Equil Time	= 60 sec	Desorption Equil Time	= 60 sec
Adsorption Dwell Time	= 240 sec	Desorption Dwell Time	= 240 sec
Analysis Start Time	= Fri Jun 22 15:50:30 2012	Elapsed Time	= 233.82 Minutes.

Isotherm (Adsorption/Desorption)

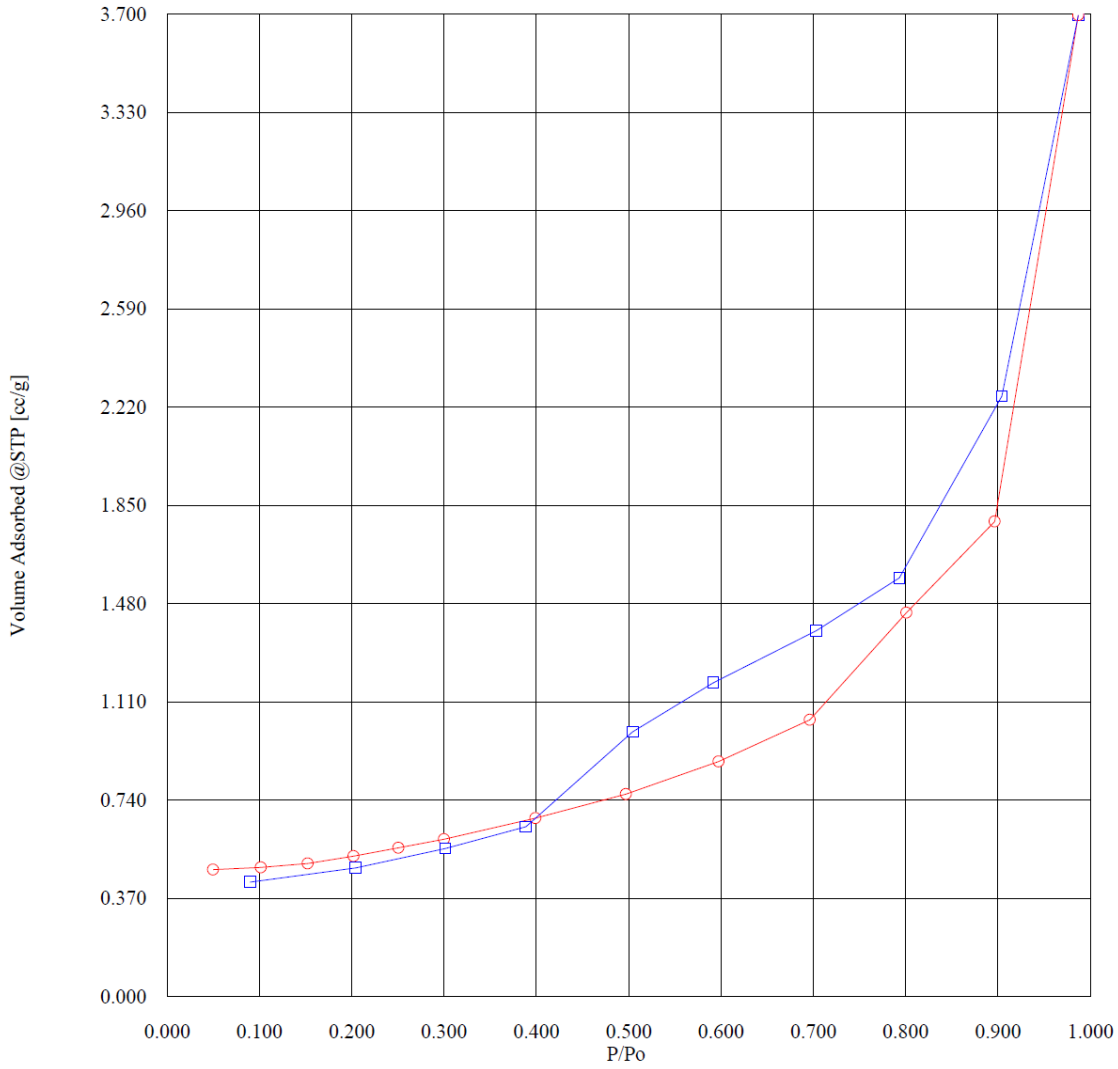

Red: adsorption

Blue desorption

SampleCPIII-SF-LS

Quantachrome Corporation
NOVA Enhanced Data Reduction Software Ver. 2.13
File Name = n262004.dat

Instrument	= NOVA-2200 Ver. 6.11		
User ID	= SERGIO	User Setup	= 66
Comments	= TMD PETER CIVIL UFMG		
Sample ID	= 2071	Sample Cell Number	= 31
Sample Weight	= 1.4524 g	Sample Volume	= 0.5893 cc
Sample Density	= 0.0000 g/cc		
Po Type	= Calculate	Po	= 705.18 mm Hg
Adsorbate	= Nitrogen	Bath Temperature	= 77.40 deg K
Adsorption Tolerance	= 0.0500 mm Hg	Desorption Tolerance	= 0.0500 mm Hg
Adsorption Equil Time	= 60 sec	Desorption Equil Time	= 60 sec
Adsorption Dwell Time	= 240 sec	Desorption Dwell Time	= 240 sec
Analysis Start Time	= Wed Jun 20 16:14:55 2012	Elapsed Time	= 272.50 Minutes.

Multi Point BET (Adsorption)

P/Po	BET Transform [1/{W[Po/P - 1]}]
0.054726	76.954673
0.103724	148.463645
0.153398	224.350914
0.202343	300.526302
0.251120	380.061233
0.299730	462.545211

Slope	=	1572.535742
Intercept	=	-13.652031
Correlation Coefficient	=	0.999649
BET C	=	-114.186943
Total Surface Area in Cell	=	3.2446 m^2
Specific Surface Area	=	2.2340 m^2/g

Quantachrome Corporation
NOVA Enhanced Data Reduction Software Ver. 2.13
File Name = n262004.dat

Instrument	= NOVA-2200 Ver. 6.11		
User ID	= SERGIO	User Setup	= 66
Comments	= TMD PETER CIVIL UFMG		
Sample ID	= 2071	Sample Cell Number	= 31
Sample Weight	= 1.4524 g	Sample Volume	= 0.5893 cc
Sample Density	= 0.0000 g/cc		
Po Type	= Calculate	Po	= 705.18 mm Hg
Adsorbate	= Nitrogen	Bath Temperature	= 77.40 deg K
Adsorption Tolerance	= 0.0500 mm Hg	Desorption Tolerance	= 0.0500 mm Hg
Adsorption Equil Time	= 60 sec	Desorption Equil Time	= 60 sec
Adsorption Dwell Time	= 240 sec	Desorption Dwell Time	= 240 sec
Analysis Start Time	= Wed Jun 20 16:14:55 2012	Elapsed Time	= 272.50 Minutes.

Single Point BET (Adsorption)

P/Po	Specific Surface Area [m^2/g]
0.299730	2.256676

Quantachrome Corporation
NOVA Enhanced Data Reduction Software Ver. 2.13
File Name = n262004.dat

Instrument	= NOVA-2200 Ver. 6.11		
User ID	= SERGIO	User Setup	= 66
Comments	= TMD PETER CIVIL UFMG		
Sample ID	= 2071	Sample Cell Number	= 31
Sample Weight	= 1.4524 g	Sample Volume	= 0.5893 cc
Sample Density	= 0.0000 g/cc		
Po Type	= Calculate	Po	= 705.18 mm Hg
Adsorbate	= Nitrogen	Bath Temperature	= 77.40 deg K
Adsorption Tolerance	= 0.0500 mm Hg	Desorption Tolerance	= 0.0500 mm Hg
Adsorption Equil Time	= 60 sec	Desorption Equil Time	= 60 sec
Adsorption Dwell Time	= 240 sec	Desorption Dwell Time	= 240 sec
Analysis Start Time	= Wed Jun 20 16:14:55 2012	Elapsed Time	= 272.50 Minutes.

BJH dV/d[logD] (Desorption)

Pore Diameter [Å]	Pore Area [m^2/g]	Pore Volume [cc/g] x 10e-3
811.035264	0.248990	5.048484
154.066258	2.090687	8.052610
85.820837	2.685226	5.761209
60.442924	3.310087	5.001784
46.132766	4.879565	5.627696
36.987597	33.363490	30.850884

Total Pore Volume is 0.00990 cc/g for
all pores of diameter smaller than 1416.405 Å.

Average pore diameter is 177.263 Å.

Quantachrome Corporation
NOVA Enhanced Data Reduction Software Ver. 2.13
File Name = n262004.dat

Instrument	= NOVA-2200 Ver. 6.11		
User ID	= SERGIO	User Setup	= 66
Comments	= TMD PETER CIVIL UFMG		
Sample ID	= 2071	Sample Cell Number	= 31
Sample Weight	= 1.4524 g	Sample Volume	= 0.5893 cc
Sample Density	= 0.0000 g/cc		
Po Type	= Calculate	Po	= 705.18 mm Hg
Adsorbate	= Nitrogen	Bath Temperature	= 77.40 deg K
Adsorption Tolerance	= 0.0500 mm Hg	Desorption Tolerance	= 0.0500 mm Hg
Adsorption Equil Time	= 60 sec	Desorption Equil Time	= 60 sec
Adsorption Dwell Time	= 240 sec	Desorption Dwell Time	= 240 sec
Analysis Start Time	= Wed Jun 20 16:14:55 2012	Elapsed Time	= 272.50 Minutes.

BJH dV/d[logD] (Desorption)

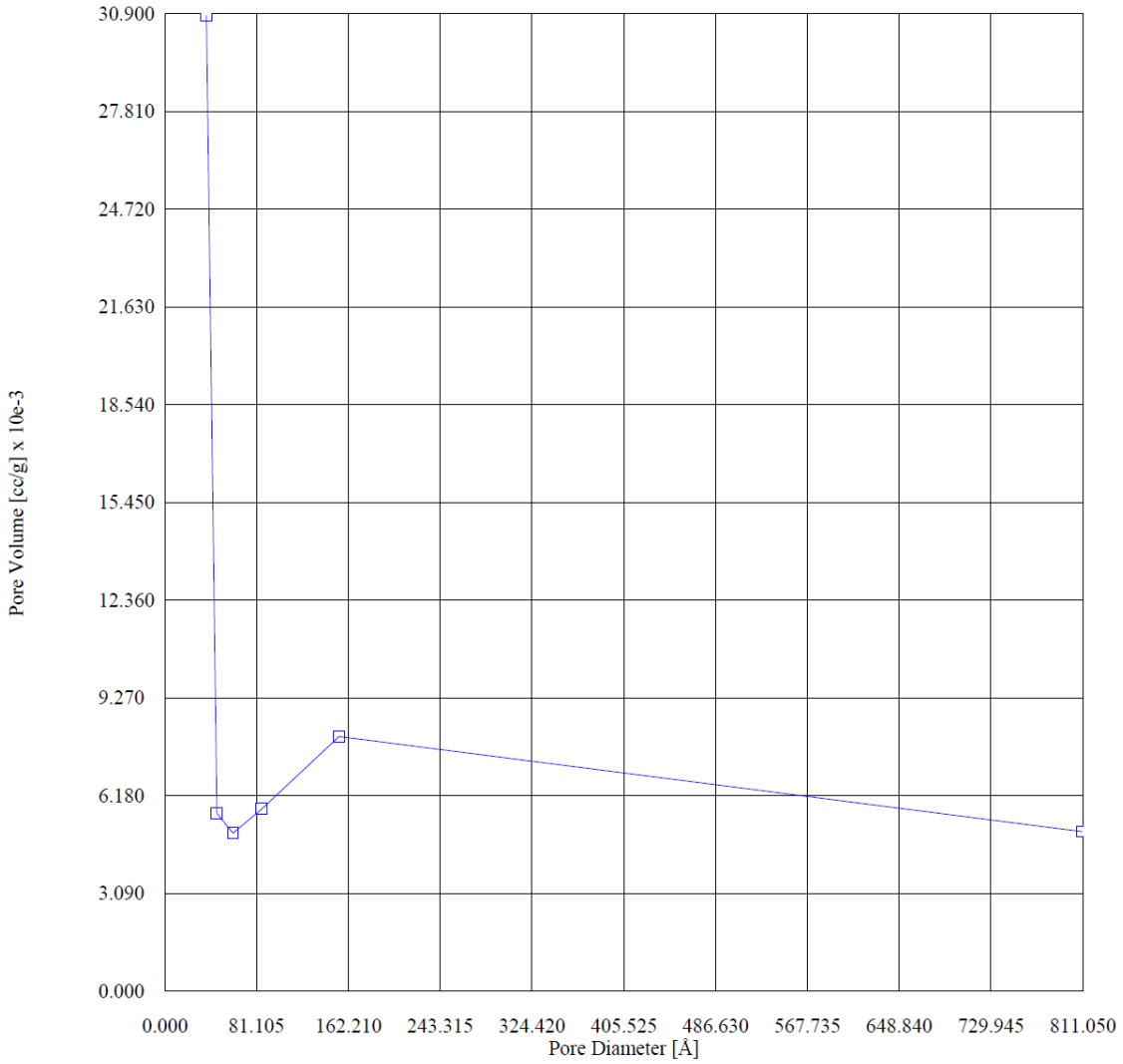

Quantachrome Corporation
NOVA Enhanced Data Reduction Software Ver. 2.13
File Name = n262004.dat

Instrument	= NOVA-2200 Ver. 6.11		
User ID	= SERGIO	User Setup	= 66
Comments	= TMD PETER CIVIL UFMG		
Sample ID	= 2071	Sample Cell Number	= 31
Sample Weight	= 1.4524 g	Sample Volume	= 0.5893 cc
Sample Density	= 0.0000 g/cc		
Po Type	= Calculate	Po	= 705.18 mm Hg
Adsorbate	= Nitrogen	Bath Temperature	= 77.40 deg K
Adsorption Tolerance	= 0.0500 mm Hg	Desorption Tolerance	= 0.0500 mm Hg
Adsorption Equil Time	= 60 sec	Desorption Equil Time	= 60 sec
Adsorption Dwell Time	= 240 sec	Desorption Dwell Time	= 240 sec
Analysis Start Time	= Wed Jun 20 16:14:55 2012	Elapsed Time	= 272.50 Minutes.

Isotherm (Adsorption/Desorption)

P/Po	Volume Adsorbed @STP [cc/g]
0.054726	0.601941
0.103724	0.623690
0.153398	0.646200
0.202343	0.675371
0.251120	0.705942
0.299730	0.740396
0.397733	0.826838
0.495310	0.931732
0.596180	1.070612
0.703312	1.267301
0.800882	1.544402
0.897713	2.314027
0.986108	6.409273
0.899318	3.840271
0.793746	2.603399
0.693651	2.126263
0.593807	1.828371
0.492388	1.570285
0.401453	0.770831
0.303434	0.679874
0.203910	0.620724
0.104279	0.581854

Quantachrome Corporation
NOVA Enhanced Data Reduction Software Ver. 2.13
File Name = n262004.dat

Instrument	= NOVA-2200 Ver. 6.11		
User ID	= SERGIO	User Setup	= 66
Comments	= TMD PETER CIVIL UFMG		
Sample ID	= 2071	Sample Cell Number	= 31
Sample Weight	= 1.4524 g	Sample Volume	= 0.5893 cc
Sample Density	= 0.0000 g/cc		
Po Type	= Calculate	Po	= 705.18 mm Hg
Adsorbate	= Nitrogen	Bath Temperature	= 77.40 deg K
Adsorption Tolerance	= 0.0500 mm Hg	Desorption Tolerance	= 0.0500 mm Hg
Adsorption Equil Time	= 60 sec	Desorption Equil Time	= 60 sec
Adsorption Dwell Time	= 240 sec	Desorption Dwell Time	= 240 sec
Analysis Start Time	= Wed Jun 20 16:14:55 2012	Elapsed Time	= 272.50 Minutes.

Isotherm (Adsorption/Desorption)

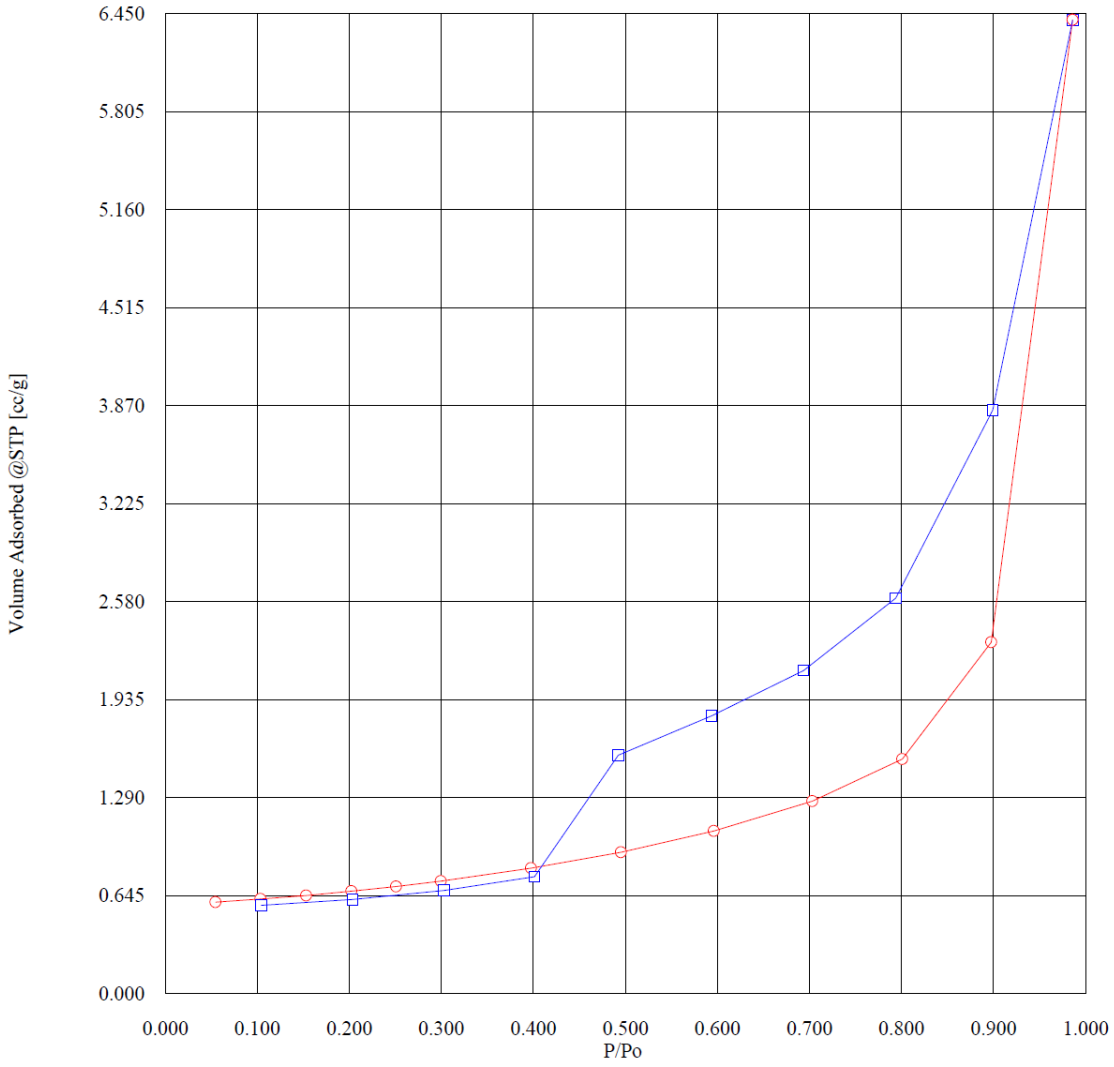

Red: adsorption

Blue desorption

SampleCPIII-SF-LS-N30

Quantachrome Corporation
NOVA Enhanced Data Reduction Software Ver. 2.13
File Name = n260801.dat

Instrument	= NOVA-2200 Ver. 6.11		
User ID	= SERGIO	User Setup	= 66
Comments	= TMN PETER ENG CIVIL		
Sample ID	= 2060	Sample Cell Number	= 30
Sample Weight	= 1.6062 g	Sample Volume	= 0.6416 cc
Sample Density	= 0.0000 g/cc		
Po Type	= Calculate	Po	= 707.56 mm Hg
Adsorbate	= Nitrogen	Bath Temperature	= 77.40 deg K
Adsorption Tolerance	= 0.0500 mm Hg	Desorption Tolerance	= 0.0500 mm Hg
Adsorption Equil Time	= 60 sec	Desorption Equil Time	= 60 sec
Adsorption Dwell Time	= 240 sec	Desorption Dwell Time	= 240 sec
Analysis Start Time	= Fri Jun 08 15:08:09 2012	Elapsed Time	= 268.25 Minutes.

Multi Point BET (Adsorption)

P/Po	BET Transform [1/{W[Po/P - 1]}]
0.052176	68.931554
0.101365	132.724986
0.150386	195.638366
0.198885	255.992265
0.247392	315.788523
0.296004	376.058538

Slope	=	1257.676494
Intercept	=	4.890536
Correlation Coefficient	=	0.999943
BET C	=	258.165380
Total Surface Area in Cell	=	4.4304 m^2
Specific Surface Area	=	2.7583 m^2/g

Quantachrome Corporation
NOVA Enhanced Data Reduction Software Ver. 2.13
File Name = n260801.dat

Instrument	= NOVA-2200 Ver. 6.11		
User ID	= SERGIO	User Setup	= 66
Comments	= TMN PETER ENG CIVIL		
Sample ID	= 2060	Sample Cell Number	= 30
Sample Weight	= 1.6062 g	Sample Volume	= 0.6416 cc
Sample Density	= 0.0000 g/cc		
Po Type	= Calculate	Po	= 707.56 mm Hg
Adsorbate	= Nitrogen	Bath Temperature	= 77.40 deg K
Adsorption Tolerance	= 0.0500 mm Hg	Desorption Tolerance	= 0.0500 mm Hg
Adsorption Equil Time	= 60 sec	Desorption Equil Time	= 60 sec
Adsorption Dwell Time	= 240 sec	Desorption Dwell Time	= 240 sec
Analysis Start Time	= Fri Jun 08 15:08:09 2012	Elapsed Time	= 268.25 Minutes.

Single Point BET (Adsorption)

P/Po	Specific Surface Area [m^2/g]
0.296004	2.741166

Quantachrome Corporation
NOVA Enhanced Data Reduction Software Ver. 2.13
File Name = n260801.dat

Instrument	= NOVA-2200 Ver. 6.11		
User ID	= SERGIO	User Setup	= 66
Comments	= TMN PETER ENG CIVIL		
Sample ID	= 2060	Sample Cell Number	= 30
Sample Weight	= 1.6062 g	Sample Volume	= 0.6416 cc
Sample Density	= 0.0000 g/cc		
Po Type	= Calculate	Po	= 707.56 mm Hg
Adsorbate	= Nitrogen	Bath Temperature	= 77.40 deg K
Adsorption Tolerance	= 0.0500 mm Hg	Desorption Tolerance	= 0.0500 mm Hg
Adsorption Equil Time	= 60 sec	Desorption Equil Time	= 60 sec
Adsorption Dwell Time	= 240 sec	Desorption Dwell Time	= 240 sec
Analysis Start Time	= Fri Jun 08 15:08:09 2012	Elapsed Time	= 268.25 Minutes.

BJH dV/d[logD] (Desorption)

Pore Diameter [Å]	Pore Area [m^2/g]	Pore Volume [cc/g] x 10e-3
836.022194	0.187920	3.927637
155.015669	1.888941	7.320386
84.972311	2.340452	4.971840
60.201670	3.300936	4.968047
46.010609	6.707254	7.715121
36.818599	43.387042	39.936253
30.208502	0.588767	0.444644

Total Pore Volume is 0.00972 cc/g for
all pores of diameter smaller than 1462.875 Å.

Average pore diameter is 140.914 Å.

Quantachrome Corporation
NOVA Enhanced Data Reduction Software Ver. 2.13
File Name = n260801.dat

Instrument	= NOVA-2200 Ver. 6.11		
User ID	= SERGIO	User Setup	= 66
Comments	= TMN PETER ENG CIVIL		
Sample ID	= 2060	Sample Cell Number	= 30
Sample Weight	= 1.6062 g	Sample Volume	= 0.6416 cc
Sample Density	= 0.0000 g/cc		
Po Type	= Calculate	Po	= 707.56 mm Hg
Adsorbate	= Nitrogen	Bath Temperature	= 77.40 deg K
Adsorption Tolerance	= 0.0500 mm Hg	Desorption Tolerance	= 0.0500 mm Hg
Adsorption Equil Time	= 60 sec	Desorption Equil Time	= 60 sec
Adsorption Dwell Time	= 240 sec	Desorption Dwell Time	= 240 sec
Analysis Start Time	= Fri Jun 08 15:08:09 2012	Elapsed Time	= 268.25 Minutes.

BJH dV/d[logD] (Desorption)

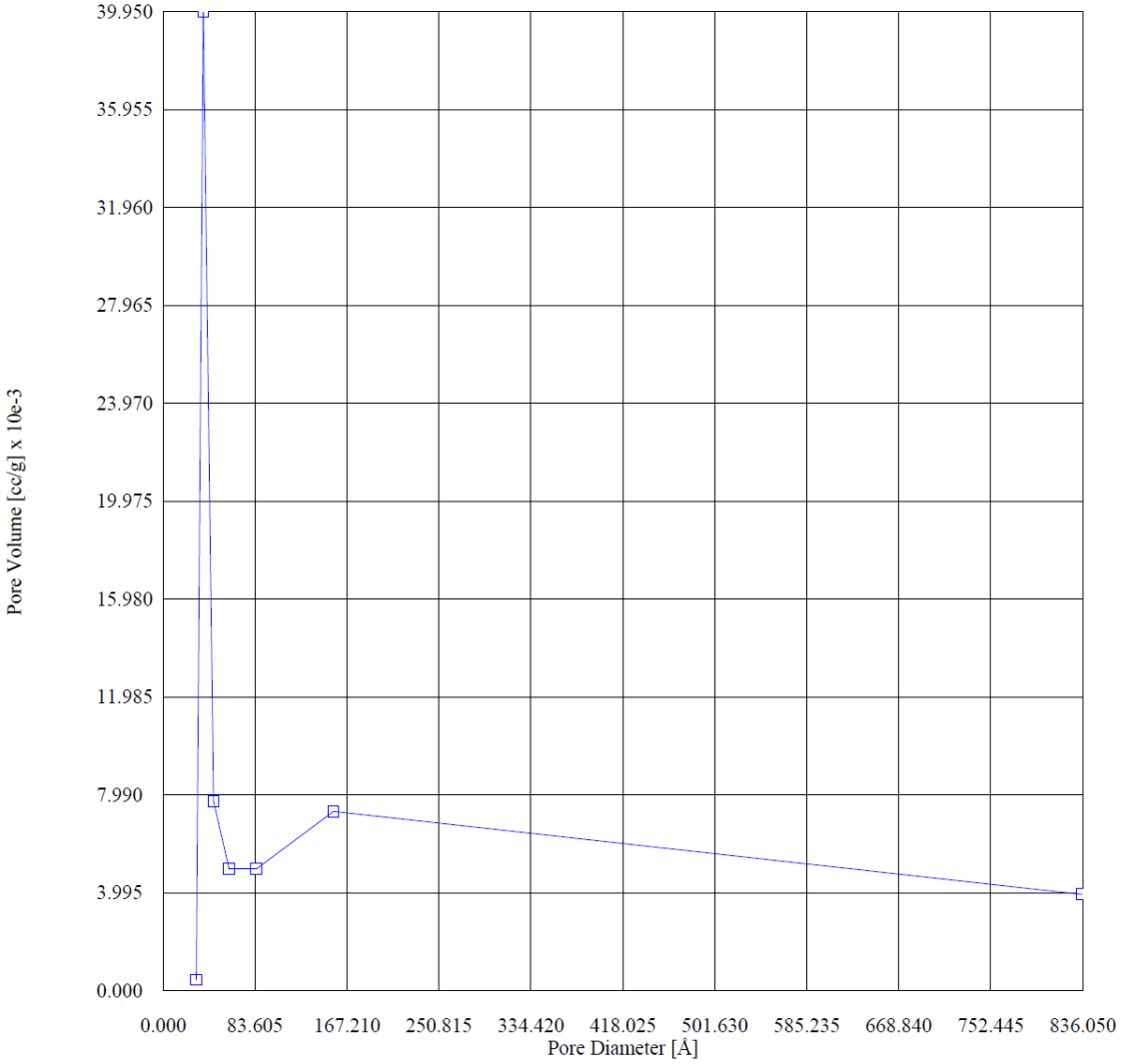

Quantachrome Corporation
NOVA Enhanced Data Reduction Software Ver. 2.13
File Name = n260801.dat

Instrument	= NOVA-2200 Ver. 6.11		
User ID	= SERGIO	User Setup	= 66
Comments	= TMN PETER ENG CIVIL		
Sample ID	= 2060	Sample Cell Number	= 30
Sample Weight	= 1.6062 g	Sample Volume	= 0.6416 cc
Sample Density	= 0.0000 g/cc		
Po Type	= Calculate	Po	= 707.56 mm Hg
Adsorbate	= Nitrogen	Bath Temperature	= 77.40 deg K
Adsorption Tolerance	= 0.0500 mm Hg	Desorption Tolerance	= 0.0500 mm Hg
Adsorption Equil Time	= 60 sec	Desorption Equil Time	= 60 sec
Adsorption Dwell Time	= 240 sec	Desorption Dwell Time	= 240 sec
Analysis Start Time	= Fri Jun 08 15:08:09 2012	Elapsed Time	= 268.25 Minutes.

Isotherm (Adsorption/Desorption)

P/Po	Volume Adsorbed @STP [cc/g]
0.052176	0.638965
0.101365	0.679991
0.150386	0.723914
0.198885	0.775952
0.247392	0.832862
0.296004	0.894593
0.396573	1.044834
0.500545	1.229418
0.600811	1.458584
0.700280	1.716297
0.798339	2.031030
0.895579	2.729741
0.986557	6.290807
0.901060	4.273085
0.790401	3.097688
0.693244	2.700599
0.590894	2.406514
0.493995	2.099244
0.394329	0.986268
0.304147	0.840853
0.188658	0.703667
0.103252	0.622861

Quantachrome Corporation
NOVA Enhanced Data Reduction Software Ver. 2.13
File Name = n260801.dat

Instrument	= NOVA-2200 Ver. 6.11		
User ID	= SERGIO	User Setup	= 66
Comments	= TMN PETER ENG CIVIL		
Sample ID	= 2060	Sample Cell Number	= 30
Sample Weight	= 1.6062 g	Sample Volume	= 0.6416 cc
Sample Density	= 0.0000 g/cc		
Po Type	= Calculate	Po	= 707.56 mm Hg
Adsorbate	= Nitrogen	Bath Temperature	= 77.40 deg K
Adsorption Tolerance	= 0.0500 mm Hg	Desorption Tolerance	= 0.0500 mm Hg
Adsorption Equil Time	= 60 sec	Desorption Equil Time	= 60 sec
Adsorption Dwell Time	= 240 sec	Desorption Dwell Time	= 240 sec
Analysis Start Time	= Fri Jun 08 15:08:09 2012	Elapsed Time	= 268.25 Minutes.

Isotherm (Adsorption/Desorption)

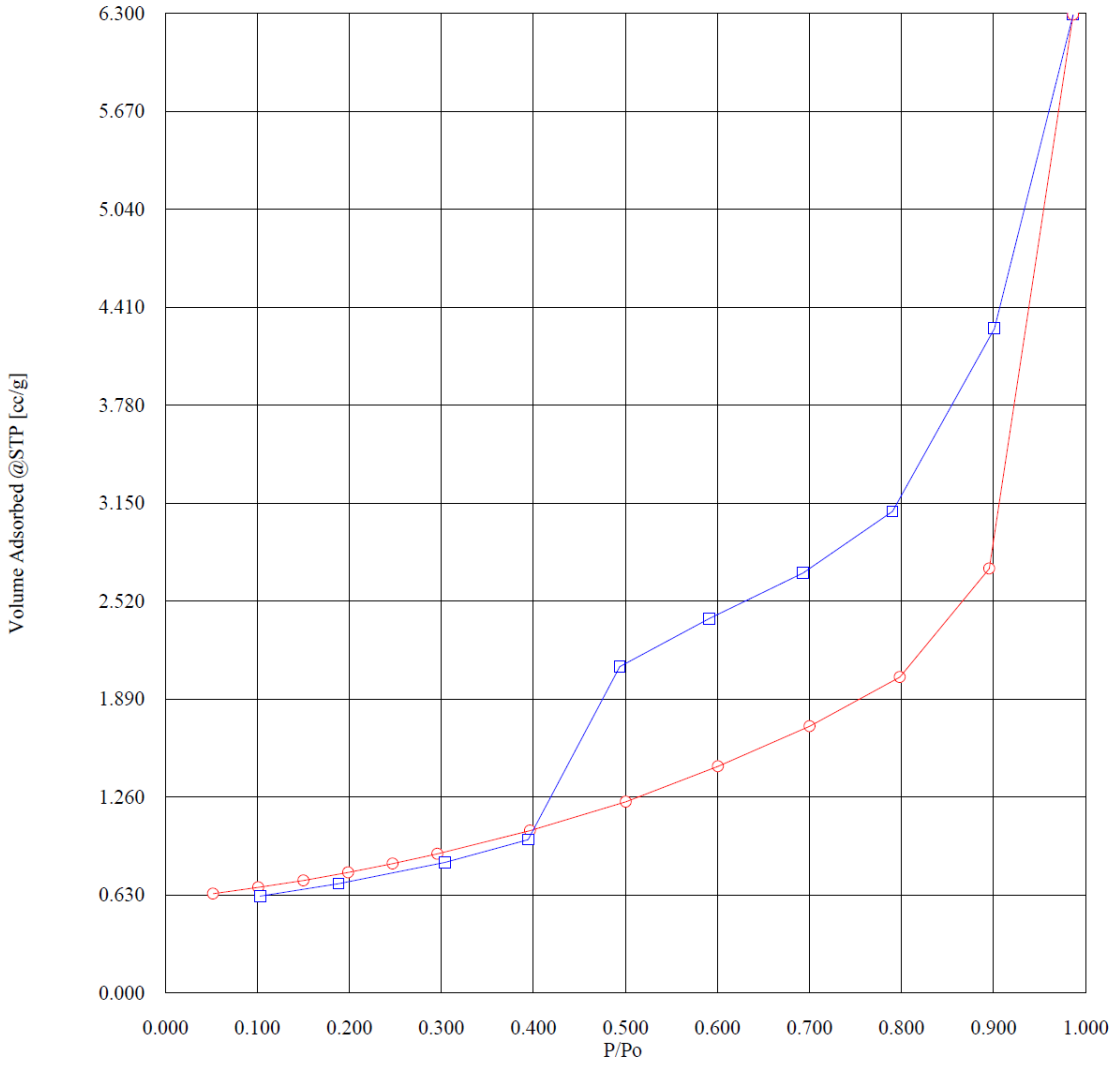

Red: adsorption

Blue desorption

SampleCPIII-POX-LS-N30

Quantachrome Corporation
NOVA Enhanced Data Reduction Software Ver. 2.13
File Name = n261502.dat

Instrument	= NOVA-2200 Ver. 6.11		
User ID	= SERGIO	User Setup	= 66
Comments	= 3PO PETER CIVIL UFMG		
Sample ID	= 2065	Sample Cell Number	= 31
Sample Weight	= 1.0847 g	Sample Volume	= 0.4151 cc
Sample Density	= 0.0000 g/cc		
Po Type	= Calculate	Po	= 710.48 mm Hg
Adsorbate	= Nitrogen	Bath Temperature	= 77.40 deg K
Adsorption Tolerance	= 0.0500 mm Hg	Desorption Tolerance	= 0.0500 mm Hg
Adsorption Equil Time	= 60 sec	Desorption Equil Time	= 60 sec
Adsorption Dwell Time	= 240 sec	Desorption Dwell Time	= 240 sec
Analysis Start Time	= Fri Jun 15 08:03:36 2012	Elapsed Time	= 241.45 Minutes.

Multi Point BET (Adsorption)

P/Po	BET Transform [1/{W[Po/P - 1]}]
0.047144	60.792829
0.099604	132.227413
0.151264	208.588345
0.201360	286.257084
0.250959	367.898431
0.300240	453.432135

Slope	=	1551.961044
Intercept	=	-20.208253
Correlation Coefficient	=	0.999079
BET C	=	-75.798377
Total Surface Area in Cell	=	2.4661 m^2
Specific Surface Area	=	2.2736 m^2/g

Quantachrome Corporation
NOVA Enhanced Data Reduction Software Ver. 2.13
File Name = n261502.dat

Instrument	= NOVA-2200 Ver. 6.11		
User ID	= SERGIO	User Setup	= 66
Comments	= 3PO PETER CIVIL UFMG		
Sample ID	= 2065	Sample Cell Number	= 31
Sample Weight	= 1.0847 g	Sample Volume	= 0.4151 cc
Sample Density	= 0.0000 g/cc		
Po Type	= Calculate	Po	= 710.48 mm Hg
Adsorbate	= Nitrogen	Bath Temperature	= 77.40 deg K
Adsorption Tolerance	= 0.0500 mm Hg	Desorption Tolerance	= 0.0500 mm Hg
Adsorption Equil Time	= 60 sec	Desorption Equil Time	= 60 sec
Adsorption Dwell Time	= 240 sec	Desorption Dwell Time	= 240 sec
Analysis Start Time	= Fri Jun 15 08:03:36 2012	Elapsed Time	= 241.45 Minutes.

Single Point BET (Adsorption)

P/Po	Specific Surface Area [m^2/g]
0.300240	2.305948

Quantachrome Corporation
NOVA Enhanced Data Reduction Software Ver. 2.13
File Name = n261502.dat

Instrument	= NOVA-2200 Ver. 6.11		
User ID	= SERGIO	User Setup	= 66
Comments	= 3PO PETER CIVIL UFMG		
Sample ID	= 2065	Sample Cell Number	= 31
Sample Weight	= 1.0847 g	Sample Volume	= 0.4151 cc
Sample Density	= 0.0000 g/cc		
Po Type	= Calculate	Po	= 710.48 mm Hg
Adsorbate	= Nitrogen	Bath Temperature	= 77.40 deg K
Adsorption Tolerance	= 0.0500 mm Hg	Desorption Tolerance	= 0.0500 mm Hg
Adsorption Equil Time	= 60 sec	Desorption Equil Time	= 60 sec
Adsorption Dwell Time	= 240 sec	Desorption Dwell Time	= 240 sec
Analysis Start Time	= Fri Jun 15 08:03:36 2012	Elapsed Time	= 241.45 Minutes.

BJH dV/d[logD] (Desorption)

Pore Diameter [Å]	Pore Area [m^2/g]	Pore Volume [cc/g] x 10e-3
829.003632	0.204905	4.246678
156.861596	1.645474	6.452792
87.595416	1.732654	3.794313
62.262133	1.857910	2.891936
46.783492	4.570045	5.345066
36.696575	23.150232	21.238355

Total Pore Volume is 0.00814 cc/g for
all pores of diameter smaller than 1447.926 Å.

Average pore diameter is 143.226 Å.

Quantachrome Corporation
NOVA Enhanced Data Reduction Software Ver. 2.13
File Name = n261502.dat

Instrument	= NOVA-2200 Ver. 6.11		
User ID	= SERGIO	User Setup	= 66
Comments	= 3PO PETER CIVIL UFMG		
Sample ID	= 2065	Sample Cell Number	= 31
Sample Weight	= 1.0847 g	Sample Volume	= 0.4151 cc
Sample Density	= 0.0000 g/cc		
Po Type	= Calculate	Po	= 710.48 mm Hg
Adsorbate	= Nitrogen	Bath Temperature	= 77.40 deg K
Adsorption Tolerance	= 0.0500 mm Hg	Desorption Tolerance	= 0.0500 mm Hg
Adsorption Equil Time	= 60 sec	Desorption Equil Time	= 60 sec
Adsorption Dwell Time	= 240 sec	Desorption Dwell Time	= 240 sec
Analysis Start Time	= Fri Jun 15 08:03:36 2012	Elapsed Time	= 241.45 Minutes.

BJH dV/d[logD] (Desorption)

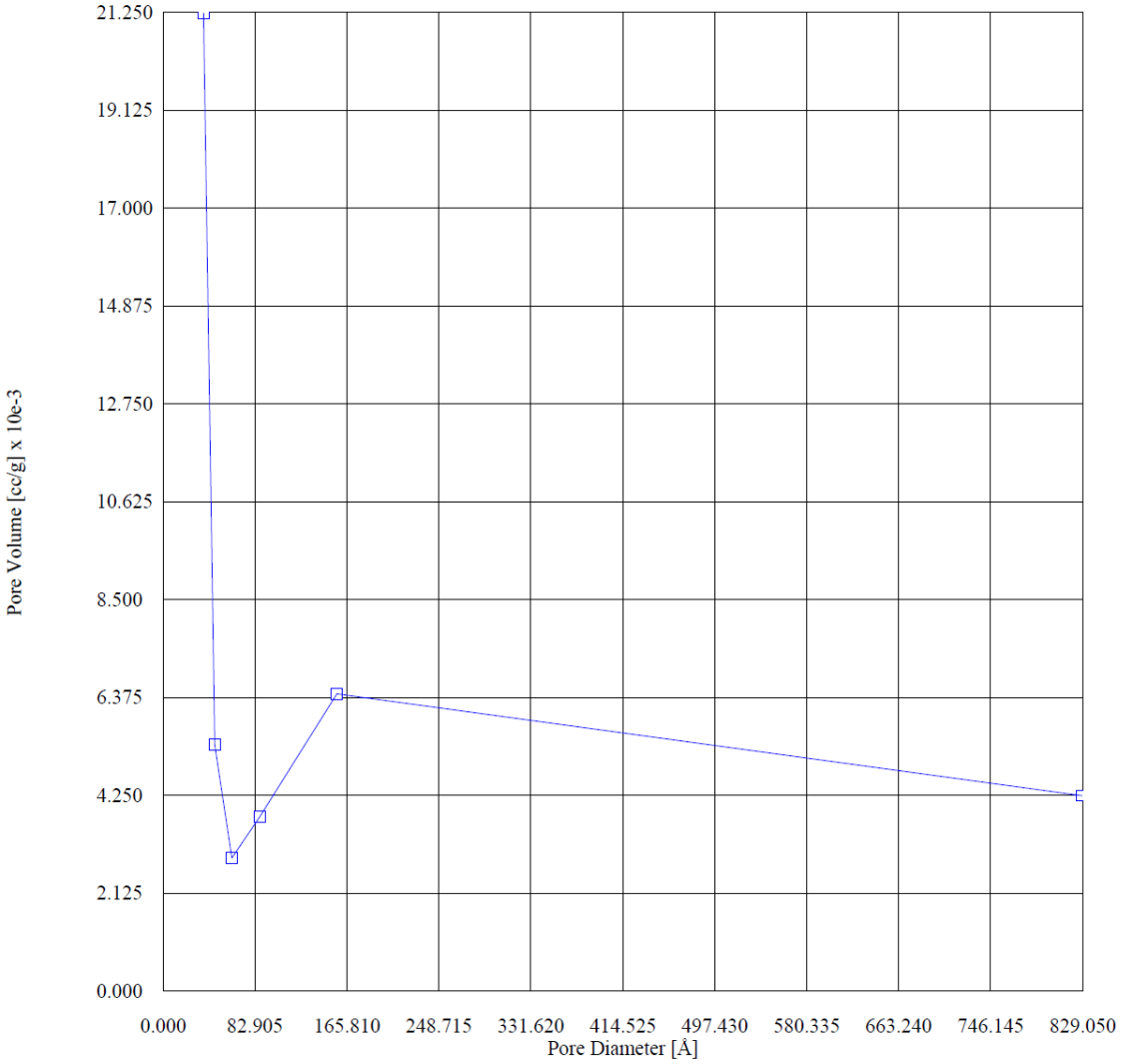

Quantachrome Corporation
NOVA Enhanced Data Reduction Software Ver. 2.13
File Name = n261502.dat

Instrument	= NOVA-2200 Ver. 6.11		
User ID	= SERGIO	User Setup	= 66
Comments	= 3PO PETER CIVIL UFMG		
Sample ID	= 2065	Sample Cell Number	= 31
Sample Weight	= 1.0847 g	Sample Volume	= 0.4151 cc
Sample Density	= 0.0000 g/cc		
Po Type	= Calculate	Po	= 710.48 mm Hg
Adsorbate	= Nitrogen	Bath Temperature	= 77.40 deg K
Adsorption Tolerance	= 0.0500 mm Hg	Desorption Tolerance	= 0.0500 mm Hg
Adsorption Equil Time	= 60 sec	Desorption Equil Time	= 60 sec
Adsorption Dwell Time	= 240 sec	Desorption Dwell Time	= 240 sec
Analysis Start Time	= Fri Jun 15 08:03:36 2012	Elapsed Time	= 241.45 Minutes.

Isotherm (Adsorption/Desorption)

P/Po	Volume Adsorbed @STP [cc/g]
0.047144	0.651185
0.099604	0.669386
0.151264	0.683637
0.201360	0.704726
0.250959	0.728655
0.300240	0.757113
0.398236	0.832403
0.496073	0.927259
0.595625	1.058792
0.695689	1.233928
0.798352	1.448205
0.895804	1.914069
0.986416	5.270335
0.901504	3.106499
0.796132	2.096472
0.703731	1.789557
0.603001	1.598102
0.492796	1.344785
0.392309	0.732757
0.302188	0.658354
0.204373	0.616327
0.104474	0.603002

Quantachrome Corporation
NOVA Enhanced Data Reduction Software Ver. 2.13
File Name = n261502.dat

Instrument	= NOVA-2200 Ver. 6.11		
User ID	= SERGIO	User Setup	= 66
Comments	= 3PO PETER CIVIL UFMG		
Sample ID	= 2065	Sample Cell Number	= 31
Sample Weight	= 1.0847 g	Sample Volume	= 0.4151 cc
Sample Density	= 0.0000 g/cc		
Po Type	= Calculate	Po	= 710.48 mm Hg
Adsorbate	= Nitrogen	Bath Temperature	= 77.40 deg K
Adsorption Tolerance	= 0.0500 mm Hg	Desorption Tolerance	= 0.0500 mm Hg
Adsorption Equil Time	= 60 sec	Desorption Equil Time	= 60 sec
Adsorption Dwell Time	= 240 sec	Desorption Dwell Time	= 240 sec
Analysis Start Time	= Fri Jun 15 08:03:36 2012	Elapsed Time	= 241.45 Minutes.

Isotherm (Adsorption/Desorption)

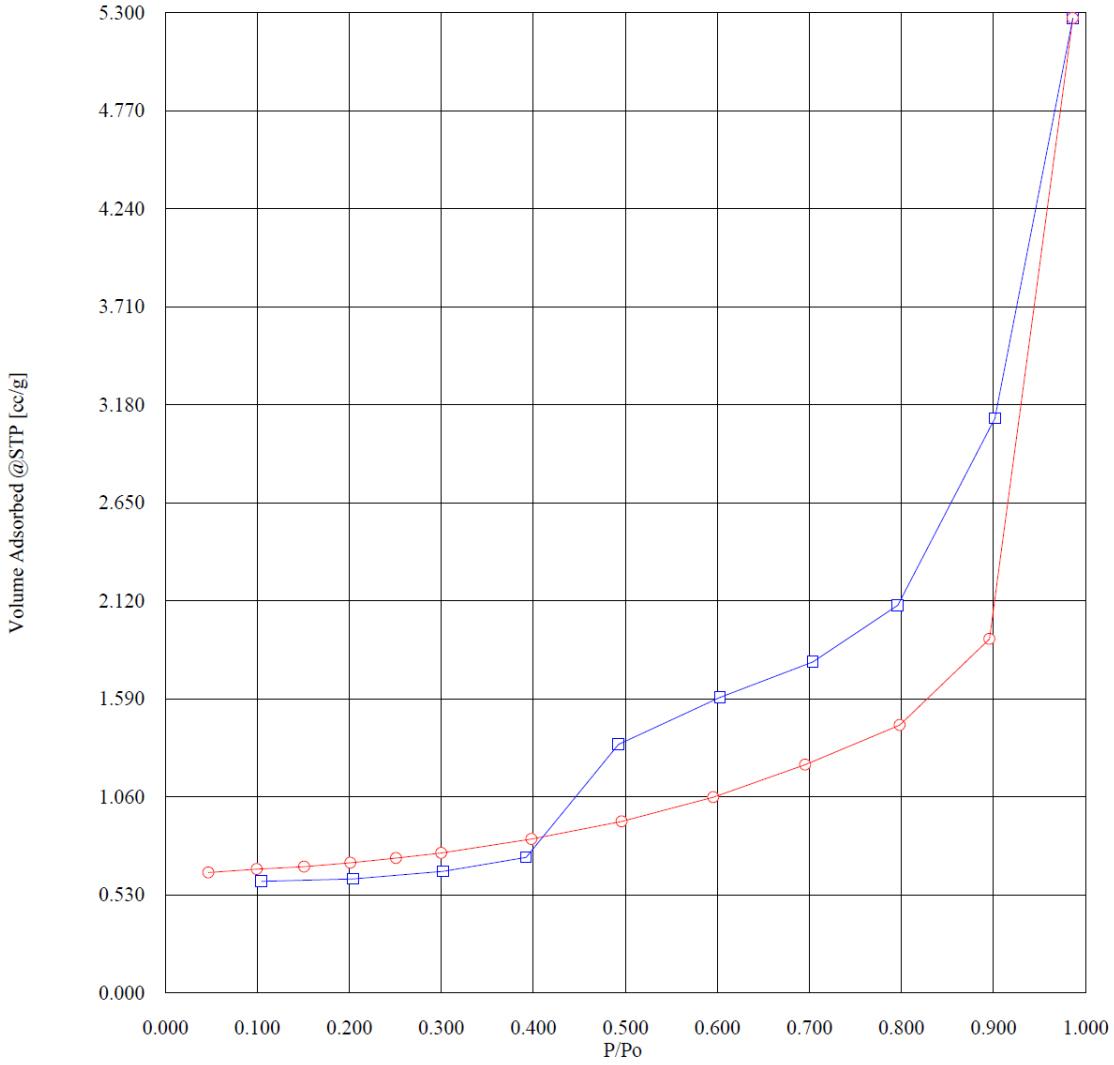

Red: adsorption

Blue desorption

Sample CPIII-CL-NH-LP

Quantachrome Corporation
NOVA Enhanced Data Reduction Software Ver. 2.13
File Name = n262003.dat

Instrument	= NOVA-2200 Ver. 6.11		
User ID	= SERGIO	User Setup	= 66
Comments	= R PETER CIVIL UFMG		
Sample ID	= 2070	Sample Cell Number	= 30
Sample Weight	= 1.1071 g	Sample Volume	= 0.4131 cc
Sample Density	= 0.0000 g/cc		
Po Type	= Calculate	Po	= 705.18 mm Hg
Adsorbate	= Nitrogen	Bath Temperature	= 77.40 deg K
Adsorption Tolerance	= 0.0500 mm Hg	Desorption Tolerance	= 0.0500 mm Hg
Adsorption Equil Time	= 60 sec	Desorption Equil Time	= 60 sec
Adsorption Dwell Time	= 240 sec	Desorption Dwell Time	= 240 sec
Analysis Start Time	= Wed Jun 20 16:14:55 2012	Elapsed Time	= 269.15 Minutes.

Multi Point BET (Adsorption)

P/Po	BET Transform [1/{W[Po/P - 1]}]
0.046092	84.937958
0.099053	187.155603
0.150629	290.142750
0.201042	386.577583
0.250717	479.550670
0.300140	575.179502

Slope	=	1928.948270
Intercept	=	-2.893670
Correlation Coefficient	=	0.999960
BET C	=	-665.609524
Total Surface Area in Cell	=	2.0018 m^2
Specific Surface Area	=	1.8081 m^2/g

Quantachrome Corporation
NOVA Enhanced Data Reduction Software Ver. 2.13
File Name = n262003.dat

Instrument	= NOVA-2200 Ver. 6.11		
User ID	= SERGIO	User Setup	= 66
Comments	= R PETER CIVIL UFMG		
Sample ID	= 2070	Sample Cell Number	= 30
Sample Weight	= 1.1071 g	Sample Volume	= 0.4131 cc
Sample Density	= 0.0000 g/cc		
Po Type	= Calculate	Po	= 705.18 mm Hg
Adsorbate	= Nitrogen	Bath Temperature	= 77.40 deg K
Adsorption Tolerance	= 0.0500 mm Hg	Desorption Tolerance	= 0.0500 mm Hg
Adsorption Equil Time	= 60 sec	Desorption Equil Time	= 60 sec
Adsorption Dwell Time	= 240 sec	Desorption Dwell Time	= 240 sec
Analysis Start Time	= Wed Jun 20 16:14:55 2012	Elapsed Time	= 269.15 Minutes.

Single Point BET (Adsorption)

P/Po	Specific Surface Area [m^2/g]
0.300140	1.817246

Quantachrome Corporation
NOVA Enhanced Data Reduction Software Ver. 2.13
File Name = n262003.dat

Instrument	= NOVA-2200 Ver. 6.11		
User ID	= SERGIO	User Setup	= 66
Comments	= R PETER CIVIL UFMG		
Sample ID	= 2070	Sample Cell Number	= 30
Sample Weight	= 1.1071 g	Sample Volume	= 0.4131 cc
Sample Density	= 0.0000 g/cc		
Po Type	= Calculate	Po	= 705.18 mm Hg
Adsorbate	= Nitrogen	Bath Temperature	= 77.40 deg K
Adsorption Tolerance	= 0.0500 mm Hg	Desorption Tolerance	= 0.0500 mm Hg
Adsorption Equil Time	= 60 sec	Desorption Equil Time	= 60 sec
Adsorption Dwell Time	= 240 sec	Desorption Dwell Time	= 240 sec
Analysis Start Time	= Wed Jun 20 16:14:55 2012	Elapsed Time	= 269.15 Minutes.

BJH dV/d[logD] (Desorption)

Pore Diameter [Å]	Pore Area [m^2/g]	Pore Volume [cc/g] x 10e-3
872.786625	0.157931	3.446007
158.082975	1.794845	7.093361
86.887872	1.527530	3.318096
60.813428	1.770193	2.691287
46.811877	3.323583	3.889578
36.536658	12.818156	11.708315
29.976331	1.174774	0.880385

Total Pore Volume is 0.00696 cc/g for
all pores of diameter smaller than 1534.679 Å.

Average pore diameter is 154.025 Å.

Quantachrome Corporation
NOVA Enhanced Data Reduction Software Ver. 2.13
File Name = n262003.dat

Instrument	= NOVA-2200 Ver. 6.11		
User ID	= SERGIO	User Setup	= 66
Comments	= R PETER CIVIL UFMG		
Sample ID	= 2070	Sample Cell Number	= 30
Sample Weight	= 1.1071 g	Sample Volume	= 0.4131 cc
Sample Density	= 0.0000 g/cc		
Po Type	= Calculate	Po	= 705.18 mm Hg
Adsorbate	= Nitrogen	Bath Temperature	= 77.40 deg K
Adsorption Tolerance	= 0.0500 mm Hg	Desorption Tolerance	= 0.0500 mm Hg
Adsorption Equil Time	= 60 sec	Desorption Equil Time	= 60 sec
Adsorption Dwell Time	= 240 sec	Desorption Dwell Time	= 240 sec
Analysis Start Time	= Wed Jun 20 16:14:55 2012	Elapsed Time	= 269.15 Minutes.

BJH dV/d[logD] (Desorption)

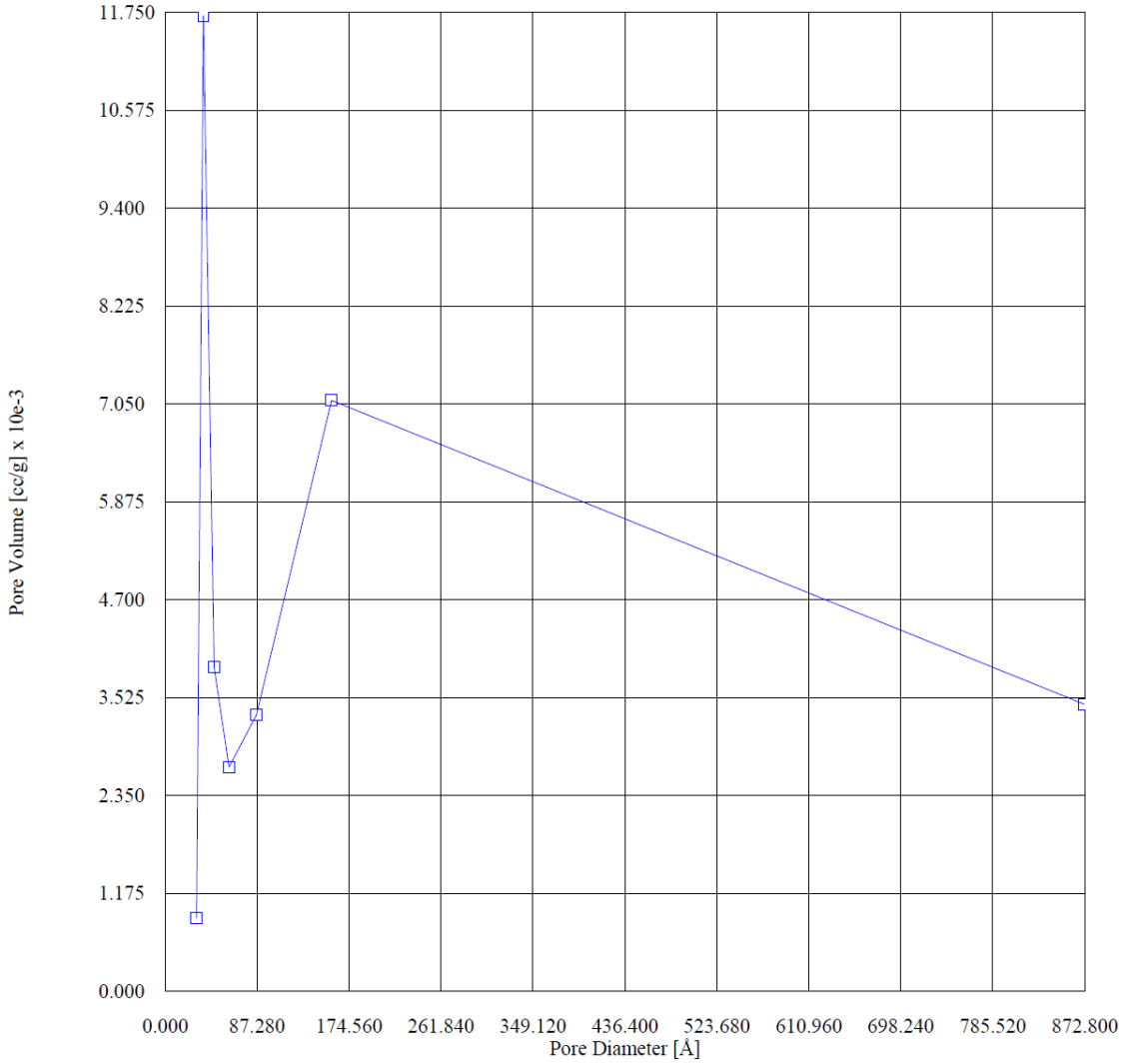

Quantachrome Corporation
NOVA Enhanced Data Reduction Software Ver. 2.13
File Name = n262003.dat

Instrument	= NOVA-2200 Ver. 6.11		
User ID	= SERGIO	User Setup	= 66
Comments	= R PETER CIVIL UFMG		
Sample ID	= 2070	Sample Cell Number	= 30
Sample Weight	= 1.1071 g	Sample Volume	= 0.4131 cc
Sample Density	= 0.0000 g/cc		
Po Type	= Calculate	Po	= 705.18 mm Hg
Adsorbate	= Nitrogen	Bath Temperature	= 77.40 deg K
Adsorption Tolerance	= 0.0500 mm Hg	Desorption Tolerance	= 0.0500 mm Hg
Adsorption Equil Time	= 60 sec	Desorption Equil Time	= 60 sec
Adsorption Dwell Time	= 240 sec	Desorption Dwell Time	= 240 sec
Analysis Start Time	= Wed Jun 20 16:14:55 2012	Elapsed Time	= 269.15 Minutes.

Isotherm (Adsorption/Desorption)

P/Po	Volume Adsorbed @STP [cc/g]
0.046092	0.455165
0.099053	0.470022
0.150629	0.489051
0.201042	0.520810
0.250717	0.558285
0.300140	0.596572
0.399322	0.690503
0.497227	0.797481
0.596827	0.947401
0.696131	1.129185
0.801429	1.376254
0.897781	1.850497
0.987196	4.507426
0.901897	2.696487
0.799352	1.613499
0.690684	1.294124
0.604046	1.142215
0.491795	0.941595
0.388863	0.577761
0.302331	0.500291
0.204982	0.433584
0.090426	0.388615

Quantachrome Corporation
NOVA Enhanced Data Reduction Software Ver. 2.13
File Name = n262003.dat

Instrument	= NOVA-2200 Ver. 6.11		
User ID	= SERGIO	User Setup	= 66
Comments	= R PETER CIVIL UFMG		
Sample ID	= 2070	Sample Cell Number	= 30
Sample Weight	= 1.1071 g	Sample Volume	= 0.4131 cc
Sample Density	= 0.0000 g/cc		
Po Type	= Calculate	Po	= 705.18 mm Hg
Adsorbate	= Nitrogen	Bath Temperature	= 77.40 deg K
Adsorption Tolerance	= 0.0500 mm Hg	Desorption Tolerance	= 0.0500 mm Hg
Adsorption Equil Time	= 60 sec	Desorption Equil Time	= 60 sec
Adsorption Dwell Time	= 240 sec	Desorption Dwell Time	= 240 sec
Analysis Start Time	= Wed Jun 20 16:14:55 2012	Elapsed Time	= 269.15 Minutes.

Isotherm (Adsorption/Desorption)

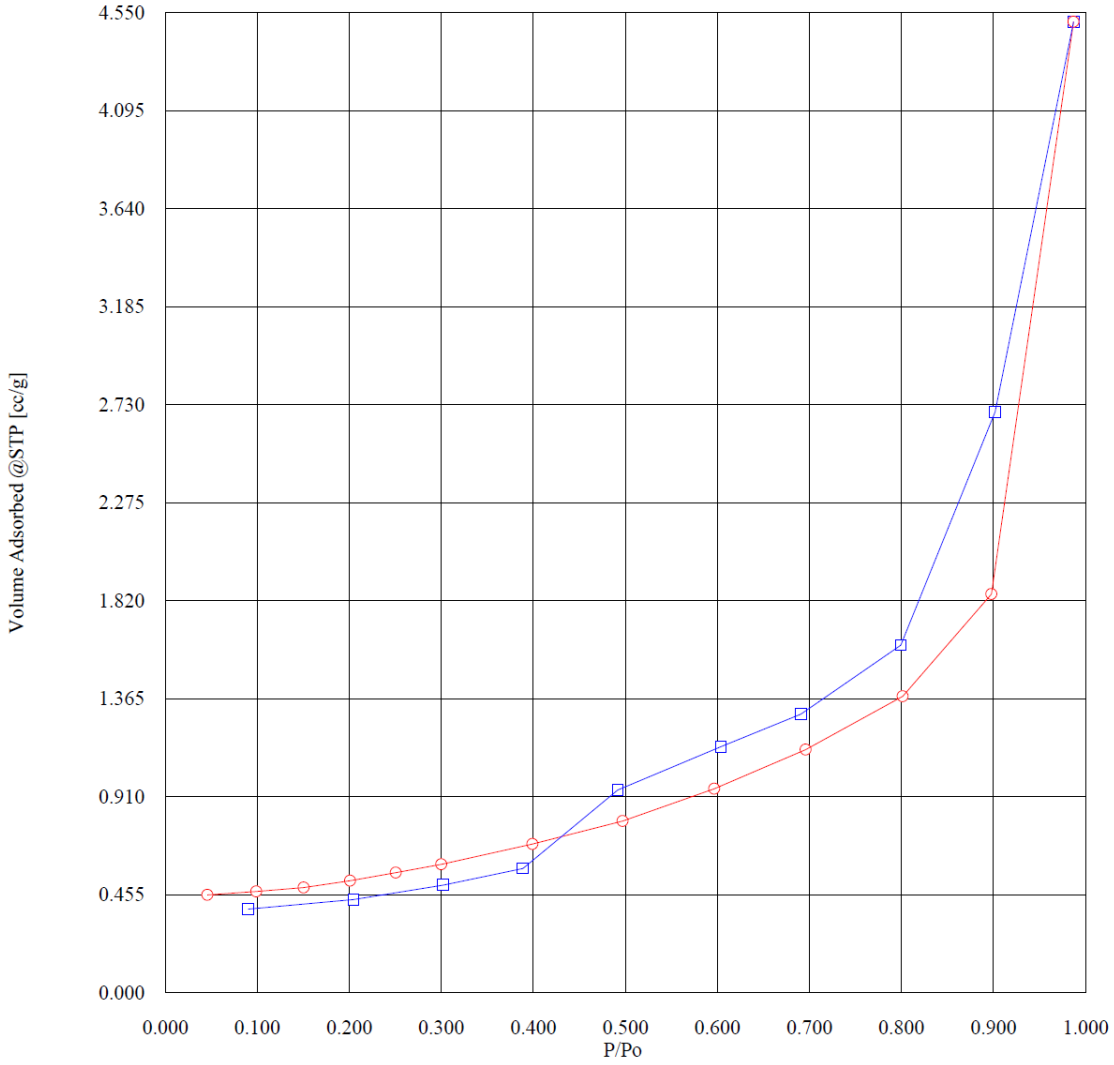

Red: adsorption

Blue desorption

Sample CPIII-CL-NH-LP-N10

Quantachrome Corporation
NOVA Enhanced Data Reduction Software Ver. 2.13
File Name = n261101.dat

Instrument	= NOVA-2200 Ver. 6.11		
User ID	= SERGIO	User Setup	= 66
Comments	= NNIT 01 PETER CIVIL UFMG		
Sample ID	= 2062	Sample Cell Number	= 30
Sample Weight	= 1.0506 g	Sample Volume	= 0.3972 cc
Sample Density	= 0.0000 g/cc		
Po Type	= Calculate	Po	= 708.56 mm Hg
Adsorbate	= Nitrogen	Bath Temperature	= 77.40 deg K
Adsorption Tolerance	= 0.0500 mm Hg	Desorption Tolerance	= 0.0500 mm Hg
Adsorption Equil Time	= 60 sec	Desorption Equil Time	= 60 sec
Adsorption Dwell Time	= 240 sec	Desorption Dwell Time	= 240 sec
Analysis Start Time	= Mon Jun 11 16:48:59 2012	Elapsed Time	= 217.20 Minutes.

Multi Point BET (Adsorption)

P/Po	BET Transform [1/{W[Po/P - 1]}]
0.045667	68.046900
0.098436	145.573530
0.149910	224.389427
0.199907	299.369641
0.249633	374.488366
0.299153	452.526665

Slope	=	1515.451165
Intercept	=	-2.629161
Correlation Coefficient	=	0.999958
BET C	=	-575.401088
Total Surface Area in Cell	=	2.4185 m^2
Specific Surface Area	=	2.3020 m^2/g

Quantachrome Corporation
NOVA Enhanced Data Reduction Software Ver. 2.13
File Name = n261101.dat

Instrument	= NOVA-2200 Ver. 6.11		
User ID	= SERGIO	User Setup	= 66
Comments	= NNIT 01 PETER CIVIL UFMG		
Sample ID	= 2062	Sample Cell Number	= 30
Sample Weight	= 1.0506 g	Sample Volume	= 0.3972 cc
Sample Density	= 0.0000 g/cc		
Po Type	= Calculate	Po	= 708.56 mm Hg
Adsorbate	= Nitrogen	Bath Temperature	= 77.40 deg K
Adsorption Tolerance	= 0.0500 mm Hg	Desorption Tolerance	= 0.0500 mm Hg
Adsorption Equil Time	= 60 sec	Desorption Equil Time	= 60 sec
Adsorption Dwell Time	= 240 sec	Desorption Dwell Time	= 240 sec
Analysis Start Time	= Mon Jun 11 16:48:59 2012	Elapsed Time	= 217.20 Minutes.

Single Point BET (Adsorption)

P/Po	Specific Surface Area [m^2/g]
0.299153	2.302197

Quantachrome Corporation
NOVA Enhanced Data Reduction Software Ver. 2.13
File Name = n261101.dat

Instrument	= NOVA-2200 Ver. 6.11		
User ID	= SERGIO	User Setup	= 66
Comments	= NNIT 01 PETER CIVIL UFMG		
Sample ID	= 2062	Sample Cell Number	= 30
Sample Weight	= 1.0506 g	Sample Volume	= 0.3972 cc
Sample Density	= 0.0000 g/cc		
Po Type	= Calculate	Po	= 708.56 mm Hg
Adsorbate	= Nitrogen	Bath Temperature	= 77.40 deg K
Adsorption Tolerance	= 0.0500 mm Hg	Desorption Tolerance	= 0.0500 mm Hg
Adsorption Equil Time	= 60 sec	Desorption Equil Time	= 60 sec
Adsorption Dwell Time	= 240 sec	Desorption Dwell Time	= 240 sec
Analysis Start Time	= Mon Jun 11 16:48:59 2012	Elapsed Time	= 217.20 Minutes.

BJH dV/d[logD] (Desorption)

Pore Diameter [Å]	Pore Area [m^2/g]	Pore Volume [cc/g] x 10e-3
846.721975	0.118184	2.501719
153.962297	1.836273	7.067920
87.594134	1.932476	4.231839
61.540906	1.843956	2.836968
46.717481	3.727735	4.353760
36.660670	14.508488	13.297272
30.117646	3.210101	2.417017
24.497522	0.727824	0.445747

Total Pore Volume is 0.00662 cc/g for
all pores of diameter smaller than 1490.545 Å.

Average pore diameter is 115.100 Å.

Quantachrome Corporation
NOVA Enhanced Data Reduction Software Ver. 2.13
File Name = n261101.dat

Instrument	= NOVA-2200 Ver. 6.11		
User ID	= SERGIO	User Setup	= 66
Comments	= NNIT 01 PETER CIVIL UFMG		
Sample ID	= 2062	Sample Cell Number	= 30
Sample Weight	= 1.0506 g	Sample Volume	= 0.3972 cc
Sample Density	= 0.0000 g/cc		
Po Type	= Calculate	Po	= 708.56 mm Hg
Adsorbate	= Nitrogen	Bath Temperature	= 77.40 deg K
Adsorption Tolerance	= 0.0500 mm Hg	Desorption Tolerance	= 0.0500 mm Hg
Adsorption Equil Time	= 60 sec	Desorption Equil Time	= 60 sec
Adsorption Dwell Time	= 240 sec	Desorption Dwell Time	= 240 sec
Analysis Start Time	= Mon Jun 11 16:48:59 2012	Elapsed Time	= 217.20 Minutes.

BJH dV/d[logD] (Desorption)

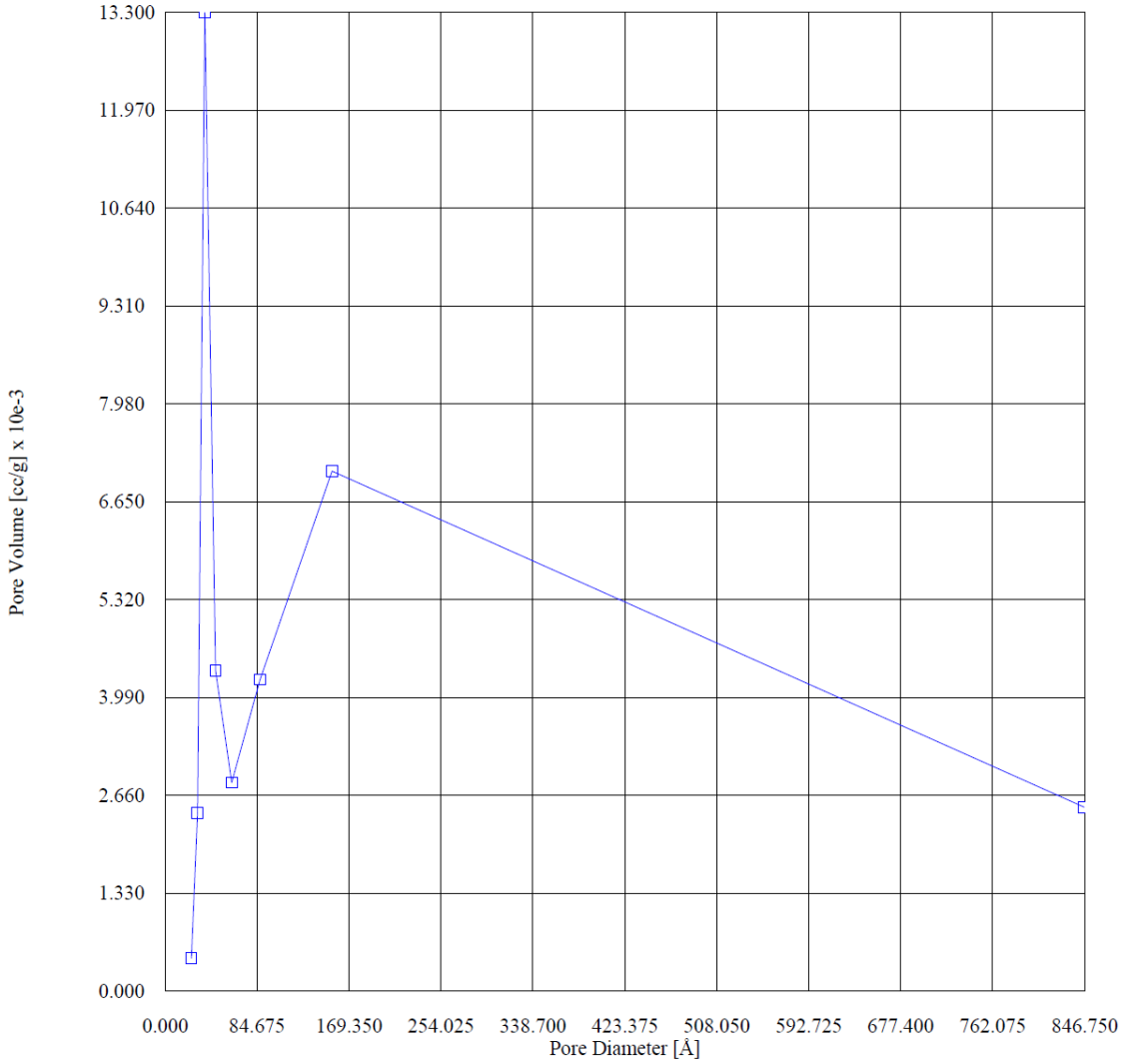

Quantachrome Corporation
NOVA Enhanced Data Reduction Software Ver. 2.13
File Name = n261101.dat

Instrument	= NOVA-2200 Ver. 6.11		
User ID	= SERGIO	User Setup	= 66
Comments	= NNIT 01 PETER CIVIL UFMG		
Sample ID	= 2062	Sample Cell Number	= 30
Sample Weight	= 1.0506 g	Sample Volume	= 0.3972 cc
Sample Density	= 0.0000 g/cc		
Po Type	= Calculate	Po	= 708.56 mm Hg
Adsorbate	= Nitrogen	Bath Temperature	= 77.40 deg K
Adsorption Tolerance	= 0.0500 mm Hg	Desorption Tolerance	= 0.0500 mm Hg
Adsorption Equil Time	= 60 sec	Desorption Equil Time	= 60 sec
Adsorption Dwell Time	= 240 sec	Desorption Dwell Time	= 240 sec
Analysis Start Time	= Mon Jun 11 16:48:59 2012	Elapsed Time	= 217.20 Minutes.

Isotherm (Adsorption/Desorption)

P/Po	Volume Adsorbed @STP [cc/g]
0.045667	0.562664
0.098436	0.600105
0.149910	0.628805
0.199907	0.667782
0.249633	0.710792
0.299153	0.754709
0.396968	0.864347
0.497198	0.997448
0.596384	1.167552
0.695697	1.363349
0.798857	1.630347
0.896135	2.105770
0.986811	4.288357
0.897899	2.968706
0.798873	1.959290
0.697923	1.596652
0.602599	1.420709
0.491959	1.205028
0.392365	0.809246
0.303234	0.695611
0.186500	0.594277
0.102933	0.543169

Quantachrome Corporation
NOVA Enhanced Data Reduction Software Ver. 2.13
File Name = n261101.dat

Instrument	= NOVA-2200 Ver. 6.11		
User ID	= SERGIO	User Setup	= 66
Comments	= NNIT 01 PETER CIVIL UFMG		
Sample ID	= 2062	Sample Cell Number	= 30
Sample Weight	= 1.0506 g	Sample Volume	= 0.3972 cc
Sample Density	= 0.0000 g/cc		
Po Type	= Calculate	Po	= 708.56 mm Hg
Adsorbate	= Nitrogen	Bath Temperature	= 77.40 deg K
Adsorption Tolerance	= 0.0500 mm Hg	Desorption Tolerance	= 0.0500 mm Hg
Adsorption Equil Time	= 60 sec	Desorption Equil Time	= 60 sec
Adsorption Dwell Time	= 240 sec	Desorption Dwell Time	= 240 sec
Analysis Start Time	= Mon Jun 11 16:48:59 2012	Elapsed Time	= 217.20 Minutes.

Isotherm (Adsorption/Desorption)

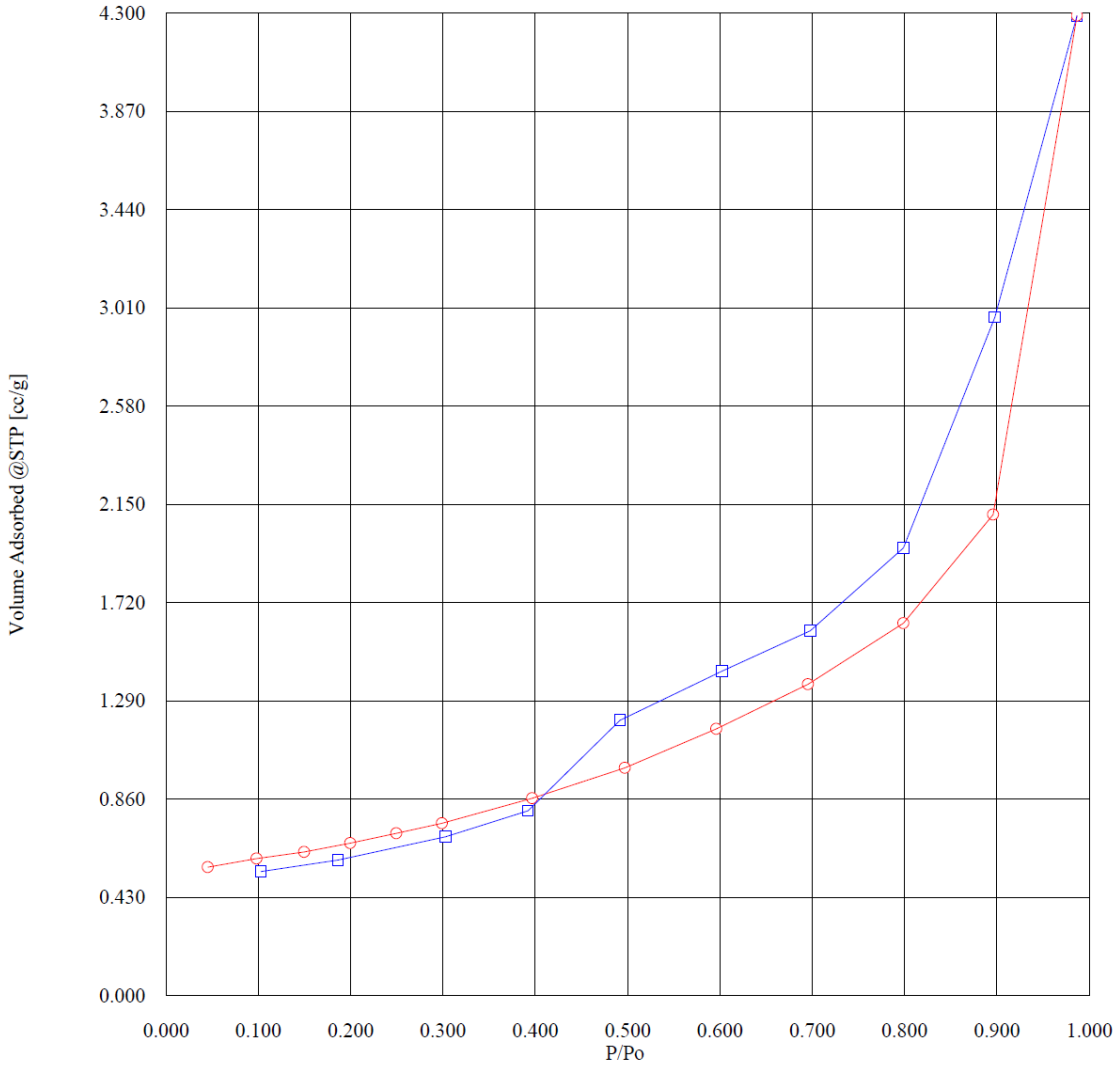

Red: adsorption

Blue desorption

SampleCPIII-CL-NH-LP-N30

Quantachrome Corporation
NOVA Enhanced Data Reduction Software Ver. 2.13
File Name = n260802.dat

Instrument	= NOVA-2200 Ver. 6.11		
User ID	= SERGIO	User Setup	= 66
Comments	= NNIT PETER ENG CIVIL		
Sample ID	= 2061	Sample Cell Number	= 31
Sample Weight	= 1.1853 g	Sample Volume	= 0.4780 cc
Sample Density	= 0.0000 g/cc		
Po Type	= Calculate	Po	= 707.56 mm Hg
Adsorbate	= Nitrogen	Bath Temperature	= 77.40 deg K
Adsorption Tolerance	= 0.0500 mm Hg	Desorption Tolerance	= 0.0500 mm Hg
Adsorption Equil Time	= 60 sec	Desorption Equil Time	= 60 sec
Adsorption Dwell Time	= 240 sec	Desorption Dwell Time	= 240 sec
Analysis Start Time	= Fri Jun 08 15:08:09 2012	Elapsed Time	= 272.95 Minutes.

Multi Point BET (Adsorption)

P/Po	BET Transform [1/{W[Po/P - 1]}]
0.050841	71.464585
0.101903	147.588946
0.152282	227.856949
0.201516	308.939480
0.251038	396.164482
0.300735	487.685956

Slope	=	1665.034362
Intercept	=	-20.405253
Correlation Coefficient	=	0.999267
BET C	=	-80.598321
Total Surface Area in Cell	=	2.5099 m^2
Specific Surface Area	=	2.1175 m^2/g

Quantachrome Corporation
NOVA Enhanced Data Reduction Software Ver. 2.13
File Name = n260802.dat

Instrument	= NOVA-2200 Ver. 6.11		
User ID	= SERGIO	User Setup	= 66
Comments	= NNIT PETER ENG CIVIL		
Sample ID	= 2061	Sample Cell Number	= 31
Sample Weight	= 1.1853 g	Sample Volume	= 0.4780 cc
Sample Density	= 0.0000 g/cc		
Po Type	= Calculate	Po	= 707.56 mm Hg
Adsorbate	= Nitrogen	Bath Temperature	= 77.40 deg K
Adsorption Tolerance	= 0.0500 mm Hg	Desorption Tolerance	= 0.0500 mm Hg
Adsorption Equil Time	= 60 sec	Desorption Equil Time	= 60 sec
Adsorption Dwell Time	= 240 sec	Desorption Dwell Time	= 240 sec
Analysis Start Time	= Fri Jun 08 15:08:09 2012	Elapsed Time	= 272.95 Minutes.

Single Point BET (Adsorption)

P/Po	Specific Surface Area [m^2/g]
0.300735	2.147519

Quantachrome Corporation
NOVA Enhanced Data Reduction Software Ver. 2.13
File Name = n260802.dat

Instrument	= NOVA-2200 Ver. 6.11		
User ID	= SERGIO	User Setup	= 66
Comments	= NNIT PETER ENG CIVIL		
Sample ID	= 2061	Sample Cell Number	= 31
Sample Weight	= 1.1853 g	Sample Volume	= 0.4780 cc
Sample Density	= 0.0000 g/cc		
Po Type	= Calculate	Po	= 707.56 mm Hg
Adsorbate	= Nitrogen	Bath Temperature	= 77.40 deg K
Adsorption Tolerance	= 0.0500 mm Hg	Desorption Tolerance	= 0.0500 mm Hg
Adsorption Equil Time	= 60 sec	Desorption Equil Time	= 60 sec
Adsorption Dwell Time	= 240 sec	Desorption Dwell Time	= 240 sec
Analysis Start Time	= Fri Jun 08 15:08:09 2012	Elapsed Time	= 272.95 Minutes.

BJH dV/d[logD] (Desorption)

Pore Diameter [Å]	Pore Area [m^2/g]	Pore Volume [cc/g] x 10e-3
761.110083	0.178255	3.391791
157.010389	1.915506	7.518860
87.735664	2.039748	4.473965
60.733734	1.676627	2.545696
47.225133	2.299541	2.714904
37.208125	14.852512	13.815853

Total Pore Volume is 0.00716 cc/g for
all pores of diameter smaller than 1315.017 Å.

Average pore diameter is 135.166 Å.

Quantachrome Corporation
NOVA Enhanced Data Reduction Software Ver. 2.13
File Name = n260802.dat

Instrument	= NOVA-2200 Ver. 6.11		
User ID	= SERGIO	User Setup	= 66
Comments	= NNIT PETER ENG CIVIL		
Sample ID	= 2061	Sample Cell Number	= 31
Sample Weight	= 1.1853 g	Sample Volume	= 0.4780 cc
Sample Density	= 0.0000 g/cc		
Po Type	= Calculate	Po	= 707.56 mm Hg
Adsorbate	= Nitrogen	Bath Temperature	= 77.40 deg K
Adsorption Tolerance	= 0.0500 mm Hg	Desorption Tolerance	= 0.0500 mm Hg
Adsorption Equil Time	= 60 sec	Desorption Equil Time	= 60 sec
Adsorption Dwell Time	= 240 sec	Desorption Dwell Time	= 240 sec
Analysis Start Time	= Fri Jun 08 15:08:09 2012	Elapsed Time	= 272.95 Minutes.

BJH dV/d[logD] (Desorption)

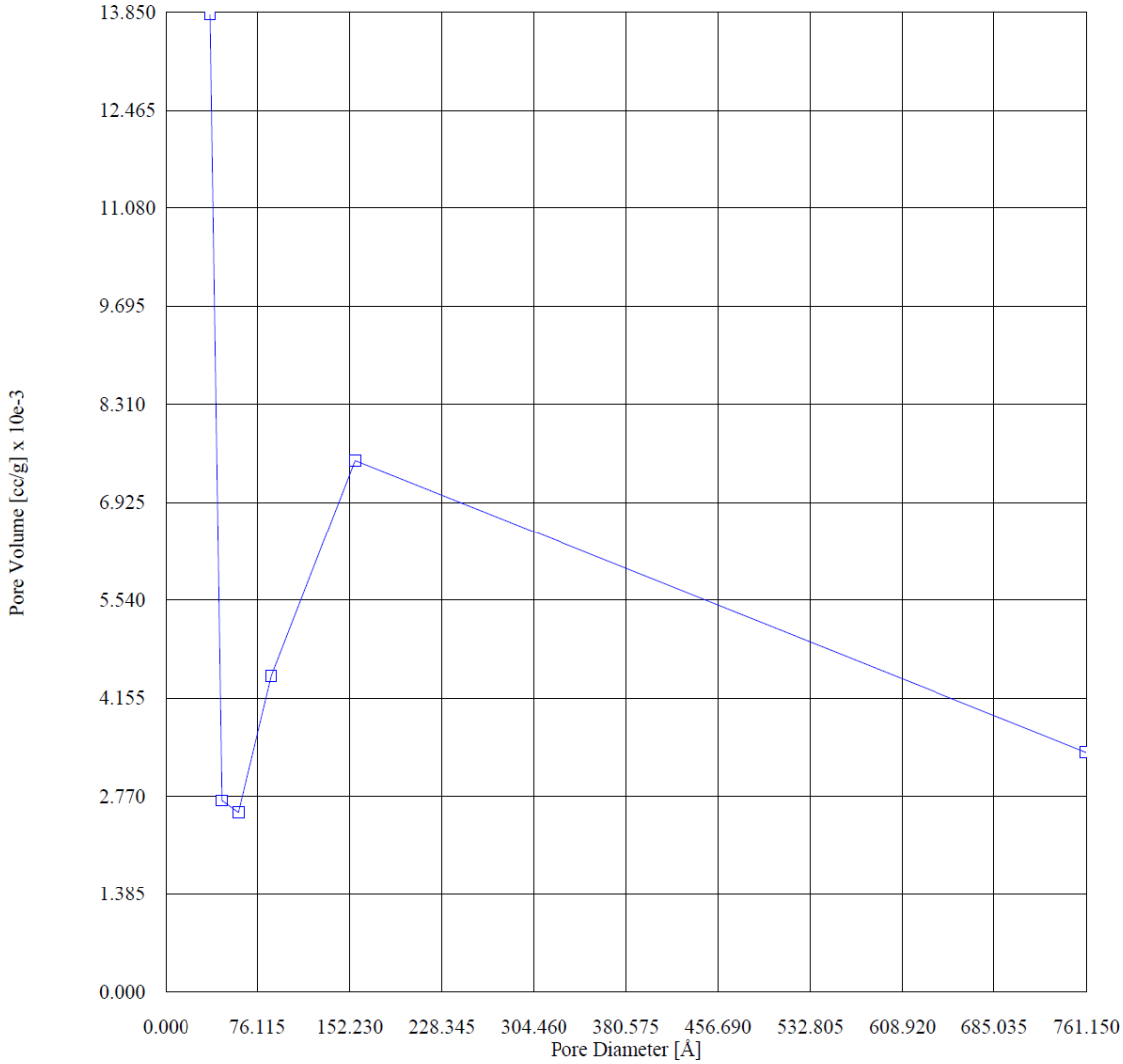

Quantachrome Corporation
NOVA Enhanced Data Reduction Software Ver. 2.13
File Name = n260802.dat

Instrument	= NOVA-2200 Ver. 6.11		
User ID	= SERGIO	User Setup	= 66
Comments	= NNIT PETER ENG CIVIL		
Sample ID	= 2061	Sample Cell Number	= 31
Sample Weight	= 1.1853 g	Sample Volume	= 0.4780 cc
Sample Density	= 0.0000 g/cc		
Po Type	= Calculate	Po	= 707.56 mm Hg
Adsorbate	= Nitrogen	Bath Temperature	= 77.40 deg K
Adsorption Tolerance	= 0.0500 mm Hg	Desorption Tolerance	= 0.0500 mm Hg
Adsorption Equil Time	= 60 sec	Desorption Equil Time	= 60 sec
Adsorption Dwell Time	= 240 sec	Desorption Dwell Time	= 240 sec
Analysis Start Time	= Fri Jun 08 15:08:09 2012	Elapsed Time	= 272.95 Minutes.

Isotherm (Adsorption/Desorption)

P/Po	Volume Adsorbed @STP [cc/g]
0.050841	0.599711
0.101903	0.615124
0.152282	0.630795
0.201516	0.653618
0.251038	0.676953
0.300735	0.705595
0.398066	0.771844
0.496702	0.868179
0.597725	1.003608
0.698187	1.185993
0.800537	1.441290
0.898051	1.997869
0.985018	4.632401
0.900090	2.986889
0.802319	1.896397
0.691349	1.471397
0.601849	1.315280
0.504124	1.174685
0.391986	0.707055
0.301554	0.642965
0.203904	0.600717
0.104875	0.572252

Quantachrome Corporation
NOVA Enhanced Data Reduction Software Ver. 2.13
File Name = n260802.dat

Instrument	= NOVA-2200 Ver. 6.11		
User ID	= SERGIO	User Setup	= 66
Comments	= NNIT PETER ENG CIVIL		
Sample ID	= 2061	Sample Cell Number	= 31
Sample Weight	= 1.1853 g	Sample Volume	= 0.4780 cc
Sample Density	= 0.0000 g/cc		
Po Type	= Calculate	Po	= 707.56 mm Hg
Adsorbate	= Nitrogen	Bath Temperature	= 77.40 deg K
Adsorption Tolerance	= 0.0500 mm Hg	Desorption Tolerance	= 0.0500 mm Hg
Adsorption Equil Time	= 60 sec	Desorption Equil Time	= 60 sec
Adsorption Dwell Time	= 240 sec	Desorption Dwell Time	= 240 sec
Analysis Start Time	= Fri Jun 08 15:08:09 2012	Elapsed Time	= 272.95 Minutes.

Isotherm (Adsorption/Desorption)

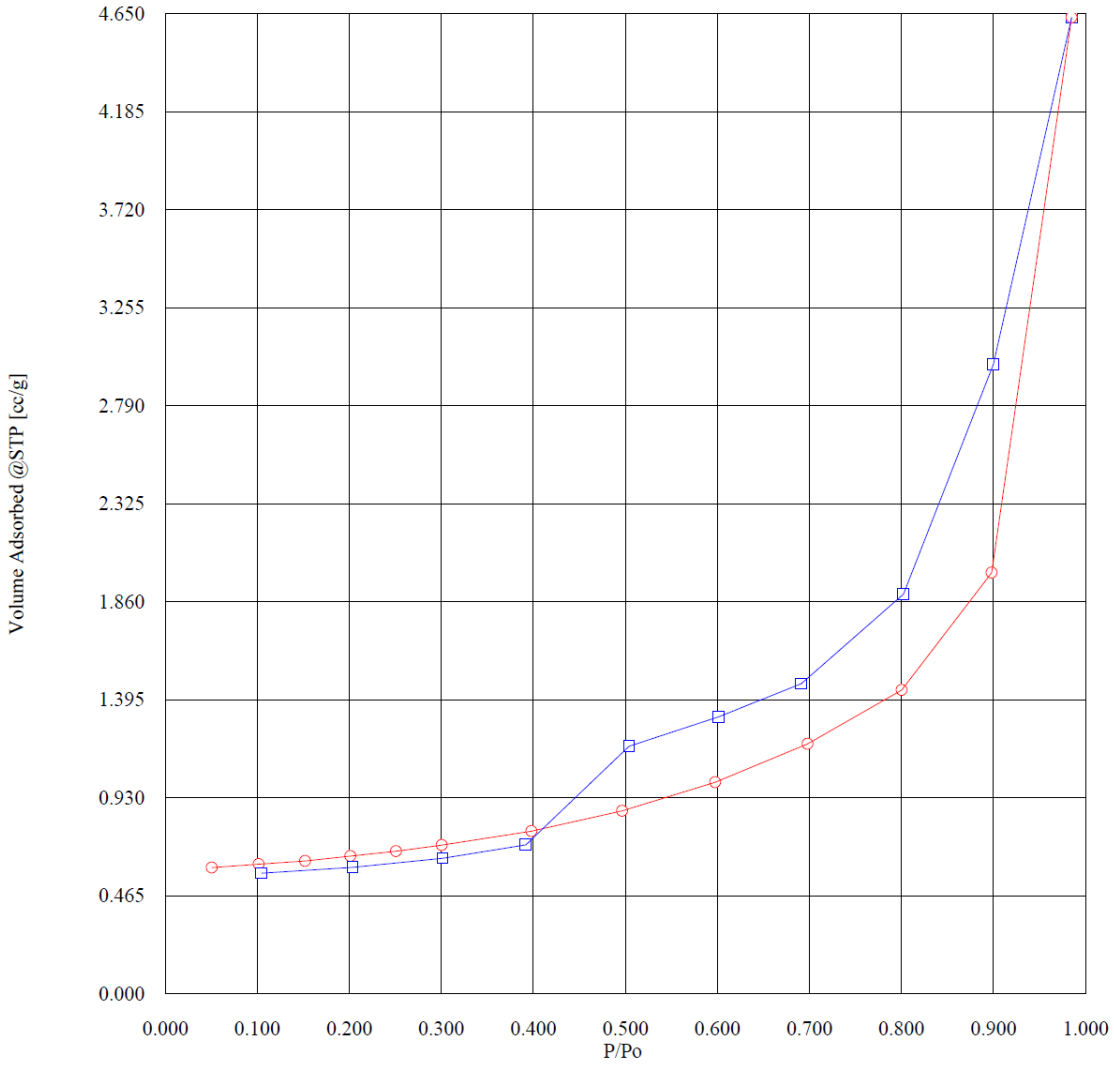

Red: adsorption

Blue desorption

C.3 – Helium pycnometry

Introduction

Helium pycnometry is used for measuring the density – or more accurately the volume – of a solid sample. A pycnometer consists of two chambers of known volume (one contains the sample) connected through a valve. One of the chambers is pressurized and the change of the pressure is registered after opening the valve. This pressure ratio with the known chamber volumes gives the sample volume. The density can be measured of the sample mass and the sample volume obtained. As the precision of the measurement depends of the ratio between the fine surface roughness of the sample and the atomic or molecular size of the used gas, the most convenient is to use helium. Besides the small size, the inertness of *He* gives also an advantage.

The sample should be previously cleaned and dried to avoid the interference of adsorption or vapor pressure. As pycnometry gives the volume inaccessible to the used gas, closed pores are included in the obtained sample volume. He pycnometry has approved to be useful to analyze pore structure of Portland cement mortars (AMARAL *et al.*, 2012).

Sample preparation

The same prepared for gas adsorption porosimetry were used for helium pycnometry investigations too. Measurements were performed using a Quantachrome Instruments Ultrapycnometer 1000 equipment.

C.4 – Helium pycnometry results

Sample CPIII-CL-LS

QUANTACHROME CORPORATION

Ultrapycnometer 1000 Version 2.4

Analysis Report

Sample & User Parameters	Analysis Parameters
Sample ID: 3R	Cell Size: Small
Weight: 1.1908 grams	V added - Small: 11.7443 cc
Analysis Temperature: 23.1 degC	V cell: 15.3780 cc
	Target Pressure: 14.0 psi
Date: 07-06-12	Equilibrium Time: Auto
Time: 16:34:56	Pulse Purge: 30 Pulses
User ID: SERGIO	Maximum runs: 20
	Number of Runs Averaged: 3

Results

Deviation Requested: 0.003 %	Deviation Achieved: +/- 0.0333 %
Average Volume: 0.4467 cc	Std. Dev.: 0.0003 cc
Average Density: 2.6656 g/cc	Std. Dev.: 0.0020 g/cc
Coefficient of variation: 0.0741 %	

Tabular Data

RUN	VOLUME (cc)	DENSITY (g/cc)
1	0.4617	2.5789
2	0.4497	2.6481
3	0.4440	2.6822
4	0.4422	2.6927
5	0.4425	2.6909
6	0.4421	2.6933
7	0.4416	2.6966
8	0.4419	2.6945
9	0.4446	2.6782
10	0.4427	2.6901
11	0.4447	2.6778
12	0.4429	2.6885
13	0.4457	2.6718
14	0.4453	2.6741
15	0.4450	2.6761
16	0.4456	2.6721
17	0.4456	2.6723
18	0.4463	2.6683
19	0.4468	2.6650
20	0.4471	2.6635

Sample CPIII-CL-LS-N30

QUANTACHROME CORPORATION

Ultrapycnometer 1000 Version 2.4

Analysis Report

Sample & User Parameters	Analysis Parameters
Sample ID: 3N	Cell Size: Small
Weight: 1.2671 grams	V added - Small: 11.7443 cc
Analysis Temperature: 23.4 degC	V cell: 15.3780 cc
	Target Pressure: 14.0 psi
Date: 06-29-12	Equilibrium Time: Auto
Time: 16:51:59	Pulse Purge: 30 Pulses
User ID: SERGIO	Maximum runs: 20
	Number of Runs Averaged: 3

Results

Deviation Requested: 0.003 %	Deviation Achieved: +/- 0.0562 %
Average Volume: 0.4774 cc	Std. Dev.: 0.0007 cc
Average Density: 2.6542 g/cc	Std. Dev.: 0.0036 g/cc
Coefficient of variation: 0.1363 %	

Tabular Data

RUN	VOLUME (cc)	DENSITY (g/cc)
1	0.5022	2.5229
2	0.4885	2.5936
3	0.4817	2.6306
4	0.4808	2.6355
5	0.4763	2.6604
6	0.4765	2.6594
7	0.4755	2.6649
8	0.4735	2.6761
9	0.4769	2.6569
10	0.4755	2.6647
11	0.4769	2.6567
12	0.4772	2.6554
13	0.4772	2.6552
14	0.4768	2.6576
15	0.4790	2.6454
16	0.4779	2.6516
17	0.4766	2.6585
18	0.4774	2.6543
19	0.4766	2.6586
20	0.4782	2.6497

Sample CPV-CL-LS

QUANTACHROME CORPORATION

Ultrapycnometer 1000 Version 2.4

Analysis Report

Sample & User Parameters	Analysis Parameters
Sample ID: 5R	Cell Size: Small
Weight: 1.3840 grams	V added - Small: 11.7443 cc
Analysis Temperature: 23.0 degC	V cell: 15.3780 cc
	Target Pressure: 14.0 psi
Date: 07-09-12	Equilibrium Time: Auto
Time: 07:39:59	Pulse Purge: 30 Pulses
User ID: SERGIO	Maximum runs: 20
	Number of Runs Averaged: 3

Results

Deviation Requested: 0.003 %	Deviation Achieved: +/- 0.0130 %
Average Volume: 0.5259 cc	Std. Dev.: 0.0001 cc
Average Density: 2.6316 g/cc	Std. Dev.: 0.0007 g/cc
Coefficient of variation: 0.0276 %	

Tabular Data

RUN	VOLUME (cc)	DENSITY (g/cc)
1	0.5456	2.5367
2	0.5326	2.5985
3	0.5280	2.6210
4	0.5231	2.6456
5	0.5233	2.6446
6	0.5229	2.6466
7	0.5215	2.6537
8	0.5211	2.6559
9	0.5244	2.6391
10	0.5244	2.6393
11	0.5232	2.6454
12	0.5237	2.6428
13	0.5235	2.6438
14	0.5254	2.6344
15	0.5241	2.6409
16	0.5250	2.6362
17	0.5240	2.6410
18	0.5258	2.6320
19	0.5261	2.6305
20	0.5258	2.6321

Sample CPV-CL-LS-N30

QUANTACHROME CORPORATION

Ultrapycnometer 1000 Version 2.4

Analysis Report

Sample & User Parameters	Analysis Parameters
Sample ID: 5N	Cell Size: Small
Weight: 1.3790 grams	V added - Small: 11.7443 cc
Analysis Temperature: 23.0 degC	V cell: 15.3780 cc
	Target Pressure: 14.0 psi
Date: 07-06-12	Equilibrium Time: Auto
Time: 17:33:03	Pulse Purge: 30 Pulses
User ID: SERGIO	Maximum runs: 20
	Number of Runs Averaged: 3

Results

Deviation Requested: 0.003 %	Deviation Achieved: +/- 0.1754 %
Average Volume: 0.5140 cc	Std. Dev.: 0.0019 cc
Average Density: 2.6828 g/cc	Std. Dev.: 0.0100 g/cc
Coefficient of variation: 0.3722 %	

Tabular Data

RUN	VOLUME (cc)	DENSITY (g/cc)
1	0.5334	2.5855
2	0.5159	2.6731
3	0.5133	2.6864
4	0.5090	2.7090
5	0.5084	2.7126
6	0.5072	2.7190
7	0.5073	2.7183
8	0.5054	2.7288
9	0.5093	2.7076
10	0.5094	2.7074
11	0.3902	3.5338
12	0.5077	2.7159
13	0.5094	2.7074
14	0.5104	2.7015
15	0.5113	2.6969
16	0.5074	2.7177
17	0.5157	2.6740
18	0.5126	2.6901
19	0.5127	2.6897
20	0.5167	2.6688

Sample CPIII-SF-LS

QUANTACHROME CORPORATION

Ultrapycnometer 1000 Version 2.4

Analysis Report

Sample & User Parameters	Analysis Parameters
Sample ID: TMU	Cell Size: Small
Weight: 1.4628 grams	V added - Small: 11.7443 cc
Analysis Temperature: 23.1 degC	V cell: 15.3780 cc
	Target Pressure: 14.0 psi
Date: 06-29-12	Equilibrium Time: Auto
Time: 10:32:53	Pulse Purge: 30 Pulses
User ID: SERGIO	Maximum runs: 20
	Number of Runs Averaged: 3

Results

Deviation Requested: 0.003 %	Deviation Achieved: +/- 0.0609 %
Average Volume: 0.5741 cc	Std. Dev.: 0.0008 cc
Average Density: 2.5481 g/cc	Std. Dev.: 0.0038 g/cc
Coefficient of variation: 0.1471 %	

Tabular Data

RUN	VOLUME (cc)	DENSITY (g/cc)
1	0.5940	2.4627
2	0.5836	2.5067
3	0.5775	2.5329
4	0.5756	2.5414
5	0.5740	2.5482
6	0.5737	2.5497
7	0.5731	2.5524
8	0.5744	2.5465
9	0.5731	2.5522
10	0.5739	2.5789
11	0.5727	2.5543
12	0.5739	2.5488
13	0.5734	2.5509
14	0.5730	2.5529
15	0.5727	2.5543
16	0.5746	2.5458
17	0.5740	2.5482
18	0.5741	2.5479
19	0.5751	2.5435
20	0.5730	2.5527

Sample CPIII-SF-LS-N30

QUANTACHROME CORPORATION

Ultrapycnometer 1000 Version 2.4

Analysis Report

Sample & User Parameters	Analysis Parameters
Sample ID: TMN	Cell Size: Small
Weight: 1.6305 grams	V added - Small: 11.7443 cc
Analysis Temperature: 23.0 degC	V cell: 15.3780 cc
	Target Pressure: 14.0 psi
Date: 06-29-12	Equilibrium Time: Auto
Time: 11:24:29	Pulse Purge: 30 Pulses
User ID: SERGIO	Maximum runs: 20
	Number of Runs Averaged: 3

Results

Deviation Requested: 0.003 %	Deviation Achieved: +/- 0.0765 %
Average Volume: 0.6249 cc	Std. Dev.: 0.0011 cc
Average Density: 2.6092 g/cc	Std. Dev.: 0.0045 g/cc
Coefficient of variation: 0.1723 %	

Tabular Data

RUN	VOLUME (cc)	DENSITY (g/cc)
1	0.6451	2.5277
2	0.6331	2.5759
3	0.6250	2.6086
4	0.6214	2.6241
5	0.6216	2.6232
6	0.6199	2.6304
7	0.6193	2.6327
8	0.6198	2.6305
9	0.6218	2.6224
10	0.6203	2.6284
11	0.6209	2.6262
12	0.6218	2.6223
13	0.6243	2.6116
14	0.6212	2.6249
15	0.6249	2.6092
16	0.6238	2.6138
17	0.6252	2.6081
18	0.6252	2.6081
19	0.6261	2.6044
20	0.6235	2.6152

Sample CPIII-CL-POX-LS-N30

QUANTACHROME CORPORATION

Ultrapycnometer 1000 Version 2.4

Analysis Report

Sample & User Parameters	Analysis Parameters
Sample ID: 3PO	Cell Size: Small
Weight: 1.1100 grams	V added - Small: 11.7443 cc
Analysis Temperature: 23.2 degC	V cell: 15.3780 cc
	Target Pressure: 14.0 psi
Date: 07-06-12	Equilibrium Time: Auto
Time: 15:41:51	Pulse Purge: 30 Pulses
User ID: SERGIO	Maximum runs: 20
	Number of Runs Averaged: 3

Results

Deviation Requested: 0.003 %	Deviation Achieved: +/- 0.0347 %
Average Volume: 0.4080 cc	Std. Dev.: 0.0003 cc
Average Density: 2.6958 g/cc	Std. Dev.: 0.0020 g/cc
Coefficient of variation: 0.0755 %	

Tabular Data

RUN	VOLUME (cc)	DENSITY (g/cc)
1	0.4204	2.6168
2	0.4060	2.7093
3	0.4023	2.7340
4	0.4004	2.7471
5	0.3993	2.7547
6	0.4004	2.7474
7	0.3979	2.7644
8	0.3997	2.7524
9	0.4029	2.7305
10	0.4025	2.7326
11	0.4025	2.7332
12	0.4063	2.7075
13	0.4050	2.7163
14	0.4059	2.7103
15	0.4087	2.6912
16	0.4068	2.7042
17	0.4116	2.6728
18	0.4077	2.6977
19	0.4079	2.6967
20	0.4085	2.6930

Sample CL-NH-LP

QUANTACHROME CORPORATION

Ultrapycnometer 1000 Version 2.4

Analysis Report

Sample & User Parameters	Analysis Parameters
Sample ID: R	Cell Size: Small
Weight: 1.1176 grams	V added - Small: 11.7443 cc
Analysis Temperature: 23.3 degC	V cell: 15.3780 cc
	Target Pressure: 14.0 psi
Date: 06-29-12	Equilibrium Time: Auto
Time: 16:00:09	Pulse Purge: 30 Pulses
User ID: SERGIO	Maximum runs: 20
	Number of Runs Averaged: 3

Results

Deviation Requested: 0.003 %	Deviation Achieved: +/- 0.0793 %
Average Volume: 0.4194 cc	Std. Dev.: 0.0007 cc
Average Density: 2.6645 g/cc	Std. Dev.: 0.0047 g/cc
Coefficient of variation: 0.1749 %	

Tabular Data

RUN	VOLUME (cc)	DENSITY (g/cc)
1	0.4402	2.5391
2	0.4287	2.6068
3	0.4204	2.6582
4	0.4210	2.6546
5	0.4207	2.6566
6	0.4170	2.6803
7	0.4163	2.6848
8	0.4178	2.6747
9	0.4165	2.6831
10	0.4160	2.6868
11	0.4176	2.6761
12	0.4166	2.6830
13	0.4169	2.6805
14	0.4181	2.6728
15	0.4185	2.6708
16	0.4195	2.6641
17	0.4162	2.6853
18	0.4187	2.6692
19	0.4204	2.6581
20	0.4192	2.6661

Sample CL-NH-LP-N10

QUANTACHROME CORPORATION

Ultrapycnometer 1000 Version 2.4

Analysis Report

Sample & User Parameters	Analysis Parameters
Sample ID: NNIT-01	Cell Size: Small
Weight: 1.0645 grams	V added - Small: 11.7443 cc
Analysis Temperature: 23.2 degC	V cell: 15.3780 cc
	Target Pressure: 14.0 psi
Date: 06-29-12	Equilibrium Time: Auto
Time: 15:08:26	Pulse Purge: 30 Pulses
User ID: SERGIO	Maximum runs: 20
	Number of Runs Averaged: 3

Results

Deviation Requested: 0.003 %	Deviation Achieved: +/- 0.0902 %
Average Volume: 0.3966 cc	Std. Dev.: 0.0008 cc
Average Density: 2.6842 g/cc	Std. Dev.: 0.0051 g/cc
Coefficient of variation: 0.1917 %	

Tabular Data

RUN	VOLUME (cc)	DENSITY (g/cc)
1	0.4108	2.5911
2	0.3973	2.6795
3	0.3917	2.7174
4	0.3872	2.7495
5	0.3896	2.7326
6	0.3894	2.7339
7	0.3907	2.7246
8	0.3908	2.7242
9	0.3903	2.7276
10	0.3903	2.7276
11	0.3921	2.7147
12	0.3916	2.7181
13	0.3929	2.7093
14	0.3939	2.7026
15	0.3939	2.7025
16	0.3936	2.7044
17	0.3943	2.6998
18	0.3977	2.6769
19	0.3960	2.6882
20	0.3961	2.6875

Sample CL-NH-LP-N30

QUANTACHROME CORPORATION

Ultrapycnometer 1000 Version 2.4

Analysis Report

Sample & User Parameters	Analysis Parameters
Sample ID: NNIT	Cell Size: Small
Weight: 1.2021 grams	V added - Small: 11.7443 cc
Analysis Temperature: 22.9 degC	V cell: 15.3780 cc
	Target Pressure: 14.0 psi
Date: 06-29-12	Equilibrium Time: Auto
Time: 12:17:13	Pulse Purge: 30 Pulses
User ID: SERGIO	Maximum runs: 20
	Number of Runs Averaged: 3

Results

Deviation Requested: 0.003 %	Deviation Achieved: +/- 0.0378 %
Average Volume: 0.4502 cc	Std. Dev.: 0.0004 cc
Average Density: 2.6701 g/cc	Std. Dev.: 0.0022 g/cc
Coefficient of variation: 0.0808 %	

Tabular Data

RUN	VOLUME (cc)	DENSITY (g/cc)
1	0.4666	2.5761
2	0.4544	2.6456
3	0.4512	2.6645
4	0.4478	2.6846
5	0.4476	2.6854
6	0.4458	2.6967
7	0.4495	2.6744
8	0.4500	2.6713
9	0.4470	2.6891
10	0.4475	2.6861
11	0.4487	2.6791
12	0.4489	2.6781
13	0.4472	2.6880
14	0.4493	2.6753
15	0.4480	2.6832
16	0.4499	2.6718
17	0.4497	2.6733
18	0.4499	2.6719
19	0.4500	2.6713
20	0.4507	2.6671

ANNEX D Publications

Poster presented at the 1º Encontro do INCT de Nanomateriais de Carbono, October 18-20, 2009, Niterói RJ

Síntese *in situ* de nanotubos de carbono de parede multipla em clínquer de cimento Portland

Péter Ludvig [1,2], Luiz O. Ladeira [2], José M. Calixto [1], Ivan C. P. Gaspar [1,2] e Valquiria S. Melo [1]

[1] Departamento de Engenharia de Estruturas – Escola de Engenharia – UFMG

[2] Laboratório de Nanomateriais – Departamento de Física – ICEx – UFMG

email: pludvig@ene-estrut.dout.ufmg.br, ladeira@fisica.ufmg.br, calixto@dees.ufmg.br

Introdução

Os nanotubos de carbono (NTC) são um dos materiais mais resistentes que existem. A incorporação deles em matrizes de cimento Portland pode melhorar significativamente as características mecânicas do material como a resistência (sobretudo em tração) e a dutilidade. Os desafios do nosso projeto são obter uma boa dispersão dos NTC no matriz, criar uma forte ligação entre os NTC e a matriz e viabilizar economicamente a produção deste nanocompósito. O primeiro e segundo problema podem ser resolvidos pela síntese *in situ* dos NTC em clínquer, o último pela produção contínua e pela utilização de resíduos industriais como matérias primas.

Metodologia

1. Síntese

Como suporte do catalisador foi usado o clínquer de cimento Portland. A análise por microssonda do clínquer mostra um teor de 3,08 % de Fe_2O_3. Como catalisador este teor de Fe e outras fontes adicionais de Fe foram usados. As outras fontes foram carepa de laminação de aço, minério de ferro não comercializável e lama vermelha. Catalisadores com diferentes teores de Fe adicional (de 0 % a 10 % em massa do suporte) foram preparados. Os NTC foram crescidos num processo CVD com 300 g de material às temperaturas entre 750 e 850 °C e com acetileno como fonte de carbono.

2. Testes de resistência

Com o compósito NTC-clínquer, corpos de prova (cps) de argamassa foram moldados contendo 0,3 % de NTC em relação ao teor de cimento. Diferentes aditivos comerciais de concreto foram utilizados. Testes de flexão em 3 pontos foram realizados aos 3, 7 e 28 dias (6 cps por idade) em barras de 25 x 25 x 150 mm e 80 mm de vão. Os testes de compressão foram realizados aos 28 dias em 4 cps de 40 x 40 x 40 mm.

Resultados e discussão

1. Síntese

Espectro Raman da amostra com 5 % de adição de carepa de laminação de aço. A relação I_G/I_D é aproximadamente igual a 1. Os NTC produzidos por este catalisador são de baixa qualidade, mas de rendimento alto (14,45 % da massa do produto).

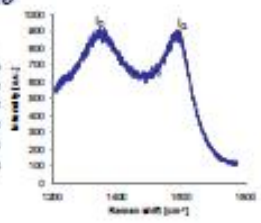

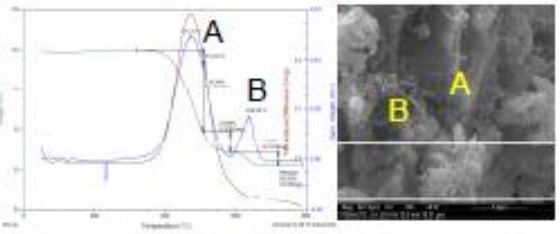

TG e imagem de MEV (aumento 7.000x) dos NTC crescidos no catalisador com 5 % de adição de carepa de laminação de aço. Podem ser diferenciados NTC *multiwall* mais finos e defeituosos (A) e NTC *multiwall* porém mais grossos (B).

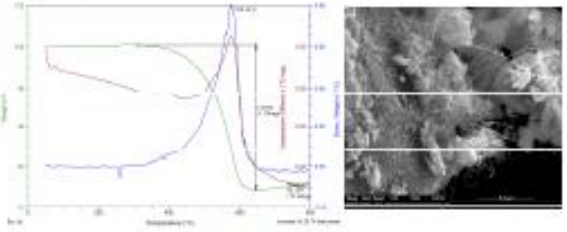

TG e imagem de MEV dos NTC sintetizados na amostra com 2,5 % de adição de carepa de laminação de aço. Os NTC são de melhor qualidade (temperatura de queima 576 °C) mas de menor rendimento (7,22 % da massa do produto).

2. Resistência mecânica

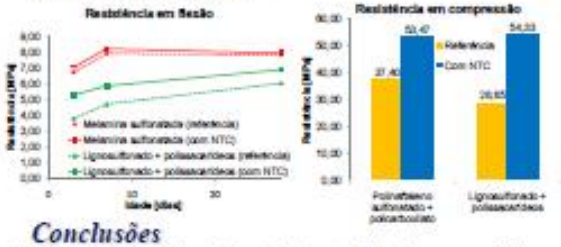

Conclusões

- Foi possível crescer NTC em clínquer de cimento Portland no processo CVD. A qualidade e a quantidade do produto foi variável em função dos catalisadores adicionais.
- Com um nanocompósito de argamassa contendo 0,3 % de NTC em massa do cimento foi possível obter até 14 % de aumento na resistência em flexão e até 90 % de aumento na resistência em compressão (traço lignosulfonado + polissacarídeos).
- As diferenças obtidas com traços de diferentes aditivos mostram, que a dispersão e a ligação dos NTC na matriz é fundamental para melhorar as características do compósito.
- Os NTC têm influência na velocidade de hidratação do cimento.

Mechanical behavior of Portland cement nanocomposites prepared by in-situ synthesis of carbon nanotubes and nanofibers

P. Ludvig[1,2], L. O. Ladeira[2], J. M. Calixto[1], I. C. P. Gaspar[1,2] and V. S. Melo[1]

(1) Department of Structural Engineering, Federal Univerity of Minas Gerais, Belo Horizonte, Brazil.
(2) Nanomaterials Laboratory, Department of Physics, Federal University of Minas Gerais, Belo Horizonte, Brazil.

The addition of carbon nanotubes (CNTs) to Portland cement may result in a composite with enhanced mechanical properties. A nanocomposite based on the simple physical mixture of CNTs and cement has already shown interesting results: 34 % gain in tensile strength [1]. The cost of such a composite is still high due to CNT price in the international market. Our group has already synthesized CNTs or carbon nanofibers (CNFs) directly on the clinker grains or other concrete-compatible materials. Using the process described in [2], the production of such composites can be economically more efficient and the dispersion issues of CNTs and CNFs in the cement matrix can be resolved.

CNTs and CNFs were grown directly on Portland cement clinker and silica fume by CVD. The quality (nanotube or fiber morphology) and quantity (carbon yield) of the product were influenced by the addition of iron particles in the form of industrial by-products such as steel mill scale and furnace dust. The product was characterized by SEM, TEM, Raman spectroscopy and TGA.

The fabrication of CNT-CNF and Portland cement composites involved functionalization methods based on acid, ozone and hydrogen peroxide treatment as well as the use of various commercially available surfactants. The in-situ synthesis facilitated the processing but limited the use of functionalization techniques as the support material (clinker) is sensitive to aggressive treatments.

Mechanical strength tests were performed on cement mortar specimens. Gains up to 89 % and 34 % were observed in compressive and in flexural strength respectively with the addition of only 0,3 % of CNTs/CNFs of the binder content. Functionalization and the use of surfactants influence significantly the mechanical behavior.

Keywords: carbon nanotubes, carbon nanofibers, Portland cement, composites

Work supported by FAPEMIG and Instituto Nacional de Tecnologia de Carbono/CNPq/MCT.

[1] Melo, V. S. "Nanotecnologia aplicada ao concreto: Efeito da mistura física de nanotubos de carbono em matrizes de cimento Portland" - Master's dissertation in Civil Engineering, School of Engineering, Federal University of Minas Gerais, Belo Horizonte, 2009.
[2] L. O. Ladeira, E. E. Silva, S. de Oliveira, R. G Lacerda, A. S. Ferlauto, E. Ávila and E. Lourençon, "Processo de síntese contínua e em larga escala de nanotubos de carbono sobre o clínquer de cimento e produtos nanoestruturados", Brazilian Patent, INPI 014080002727 (30.04.2008).

pludvig@eng-estrut.dout.ufmg.br, Laboratório de Nanomateriais, ICEx – Dep. Física – Sala 4149, Av. Antônio Carlos, 6627 – Pampulha – Belo Horizonte MG – CEP 31270-901

Paper published in Materials, v. 4, 575-584, 2011

Materials **2011**, *4*, 575-584; doi:10.3390/ma4030575

OPEN ACCESS

materials

ISSN 1996-1944

www.mdpi.com/journal/materials

Communication

Using Converter Dust to Produce Low Cost Cementitious Composites by *in situ* Carbon Nanotube and Nanofiber Synthesis

Péter Ludvig [1,2]*, José M. Calixto [1], Luiz O. Ladeira [2] and Ivan C.P. Gaspar [1]

[1] Department of Structural Engineering, Federal University of Minas Gerais/Av. Antônio Carlos, 6627, Pampulha, Belo Horizonte-MG, CEP 31.270-901, Brazil;
E-Mails: calixto@dees.ufmg.br (J.M.C.); ivgaspar@ufmg.br (I.C.P.G.)

[2] Nanomaterials Laboratory, Department of Physics, Federal University of Minas Gerais/Av. Antônio Carlos, 6627, Pampulha, Belo Horizonte-MG, CEP 31.270-901, Brazil;
E-Mail: ladeira@fisica.ufmg.br

* Author to whom correspondence should be addressed; E-Mail: pludvig@eng-estrut.dout.ufmg.br; Tel.: +55-31-3409-6644; Fax: +55-31-3409-5600.

Received: 13 January 2011; in revised form: 2 March 2011 / Accepted: 16 March 2011 / Published: 18 March 2011

Abstract: Carbon nanotubes (CNTs) and nanofibers (CNFs) were synthesized on clinker and silica fume particles in order to create a low cost cementitious nanostructured material. The synthesis was carried out by an *in situ* chemical vapor deposition (CVD) process using converter dust, an industrial byproduct, as iron precursor. The use of these materials reduces the cost, with the objective of application in large-scale nanostructured cement production. The resulting products were analyzed by scanning electron microscopy (SEM), transmission electron microscopy (TEM) and thermogravimetric analysis (TGA) and were found to be polydisperse in size and to have defective microstructure. Some enhancement in the mechanical behavior of cement mortars was observed due to the addition of these nano-size materials. The contribution of these CNTs/CNFs to the mechanical strength of mortar specimens is similar to that of high quality CNTs incorporated in mortars by physical mixture.

Keywords: cement; carbon nanotubes; composites; converter dust; *in situ* synthesis; CVD; compressive strength; flexural strength

1. Introduction

Portland cement concrete is the world's most consumed building material due to its good mechanical behavior, low cost and the global availability of raw materials. However, even after centuries of use of cement-based materials some serious problems still remain due to their low tensile strength. Carbon nanotubes (CNTs) and nanofibers (CNFs) have the potential to enhance the mechanical behavior of these composites as their tensile strength is one of the highest of the materials known today [1]. CNTs create links that limit the propagation and the opening of cracks at the submicron level. Some tentative studies have already been made to create such cement-CNT composites with a slight improvement of mechanical strength: up to 30–40% gain in compressive and/or flexural strength [2-6].

During the steel production process in a converter, the impurities included in the molten pig iron are removed by blowing high purity oxygen. The oxygen oxidizes the carbon and other impurities. The exhaust gas of the converter contains a high quantity of dust of iron oxide particles which are collected in a filter system. The material is accessible in great abundance in areas of steel production, as is the case of the state of Minas Gerais, Brazil. This dust represents a serious environmental problem as the large quantities created are mostly disposed in landfills. The composition and particle size of this dust is not controlled, but contains iron oxide particles with crystallite size below 100 nm, which is applicable to CNT synthesis.

Today the catalytic chemical vapor deposition (CVD) process has the biggest potential to be used for large-scale CNT production. The catalyst is normally composed of transition metal nanoparticles supported on a high surface area material that is stable under the synthesis conditions. Portland cement clinker and silica fume have high stability at typical CNT synthesis temperatures (between 700 and 1000 °C). Various catalyst compositions have already been used for CNT-CNF synthesis, including Portland cement [7] and silica fume impregnated with iron salts [8].

The aim of this work is to investigate the possibility of the use of converter dust (CD) as metal precursor for CNT-CNF *in situ* CVD synthesis on Portland cement clinker and silica fume, and to evaluate the mechanical strength of mortar specimens made with these nanostructured materials. Using high quality CNTs for cement composite production would raise costs with respect to the benefits in mechanical behavior. The CD as catalyst has significantly lower costs with respect to high purity metal salts or other transition metal precursors used for CNT synthesis. The use of the CD in the synthesis aims to reduce production costs and to contribute to reduce the amount of disposable industrial waste.

2. Experimental

2.1. Synthesis

Portland cement clinker was ground to the same fineness as cement. Silica fume (Silmix—Camargo Corrêa Metais SA) was used as received. Compositions of the synthesis supports are given in Table 1 and Table 2. The composition of Portland cement clinker was determined by wavelength dispersive X-ray spectrometry (WDS) microprobe analysis. The composition of silica fume was given by the manufacturer. CD was used as received, in a form of a brown, magnetic dust. Its chemical composition was determined by energy dispersive X-ray spectrometry (EDS) and is given in Table 3.

Table 1. Portland cement clinker chemical composition based on a wavelength dispersive X-ray spectrometry (WDS) microprobe investigation.

	MgO [%]	SO_3 [%]	MnO [%]	Al_2O_3 [%]	K_2O [%]	Fe_2O_3 [%]	SiO_2 [%]	CaO [%]
PC clinker	2.12	0.55	0.05	3.94	1.33	3.08	17.17	54.67

Table 2. Silica fume chemical composition, as obtained by the manufacturer.

	Fe_2O_3 [%]	CaO [%]	Al_2O_3 [%]	MgO [%]	Na_2O [%]	K_2O [%]	SiO_2 [%]	H_2O [%]
Silica fume	0.04	0.20	0.08	0.63	0.15	0.40	96.47	0.61

Table 3. Converter dust chemical composition, based on an energy dispersive X-ray spectrometry (EDS) investigation.

	C [%]	O [%]	Mg [%]	Si [%]	Ca [%]	Fe [%]
Converter dust	3.01	32.47	3.22	0.74	6.80	55.76

Catalysts were prepared by adding 2.5% Fe precursor to support materials with respect to mass and mixing in a ball mill during 24 hours. A CVD reactor was used for *in situ* CNT-CNF synthesis; it has a silicon carbide tube with a controllable temperature length of 50 cm. Thirty to three-hundred grams of the catalyst were placed in silicon carbide boats in the CVD reactor (Figure 1). The reaction temperature was chosen based on previous experiments; 850 °C for the clinker supported catalyst and 750 °C for the silica fume supported catalyst. The reactor zone was flushed by argon flux until the reaction temperature was reached. During the synthesis a mixture of argon (1500 sccm) and acetylene (500 sccm) flux was applied. After the synthesis process the argon flux was maintained until cooling to room temperature.

Figure 1. The CVD reactor used for *in situ* CNT/CNF synthesis on cementitious materials.

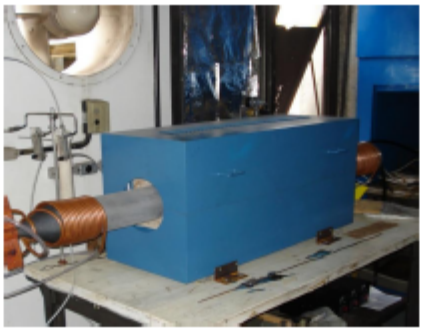

Synthesis products were characterized by scanning electron microscopy (SEM), transmission electron microscopy (TEM) and thermogravimetric analysis (TGA). A Quanta 200 FEG FEI

microscope was used for imaging the products using secondary electron detector. A Tecnai-G2-20-FEI TEM instrument was employed to identify CNTs and CNFs and to characterize CNT wall structure. Mean diameters of CNTs and CNFs were determined. TGA analysis was performed on a TA Instruments SDT-2960 equipment with 10 °C/min heat rate in air flow.

2.2. Mechanical Behavior

Cement mortars were mixed with 0 and 0.3% CNT-CNF content of the mass of binder, based on previous studies [9]. NST-C mortar was prepared with nanostructured clinker meanwhile NST-S mortar contained nanostructured silica fume. All mortars were made with 1:3 cement to aggregate proportion. The cement content was 530 kg/m^3. Equal amounts of sand of 0.15, 0.30, 0.60 and 1.20 mm in size were used, according to NBR7215 Brazilian standard [10]. Cement to water ratio was 0.40 in all cases. Brazilian CP-III-40 cement was used; it has a clinker content between 30 and 60% and blast furnace slag content between 35 and 70% [11]. To enhance workability of the mixture and to help CNT/CNF dispersion, a lignosulfonate based plasticizer was employed; 1.5% of cement content was used. Mortars REF-S and NST-S contained silica fume in 10% of the mass of binder. Details of mortar compositions are shown in Table 4.

Table 4. Mortar mix proportion.

Mortar	Composition (kg/m^3)	CNT/CNF content (kg/m^3)	W/C[b]	Plasticizer content (kg/m^3)
REF-C	530:0:1590[a]	0	0.4	7.95
NST-C	530:0:1590	1.59	0.4	7.95
REF-S	477:53:1590	0	0.4	7.95
NST-S	477:53:1590	1.59	0.4	7.95

[a]cement: silica fume: fine aggregates.
[b]water/cementitous material ratio.

The materials were mixed in a mortar blender. First the solid components were mixed together (cement, nanostructured material and sand) and mixing water was added subsequently. The plasticizer was added together with the water. Prismatic mortar specimens (40 mm × 40 mm × 160 mm in size) were cast in steel molds. After de-molding the specimens were kept in water until the day of testing. Tests were performed 7 and 28 days after casting, using a servo-hydraulic ram in a displacement controlled mode (0.5 mm/min). A three point bending test in a span of 100 mm was used to evaluate the flexural strength. Compressive tests were performed on the remaining ends of the specimens using 40 mm × 40 mm steel plates. The strength values were calculated as the mean of the results of four specimens tested at each age.

3. Results and Discussion

3.1. Synthesis

The rusty-brown catalyst powders turned black after the CVD process showing the deposit of carbon materials. The carbon deposit was formed mainly of fibrous products clearly seen on SEM

images (Figure 2). The images show that cement supported catalyst produced fibers with high diameter dispersion; meanwhile silica fume supported catalyst produced fibers with smaller diameter and less disperse in size. TEM images of the product revealed the presence of CNFs and highly defective CNTs (Figure 3). In the case of clinker supported material two characteristic carbon products were identified with diameters of 70–80 nm and 100–200 nm. Silica fume produced CNTs and CNFs with a diameter of 30–60 nm. The used raw materials were industrial byproducts and construction materials, with a low level of composition control in their production and consequently higher variability than other materials commonly used for CNT synthesis. This fact may explain such heterogeneity of CNFs and CNTs size and quality.

Figure 2. **(a)** Scanning electron microscopy (SEM) image of nanostructured clinker, at high magnification, of smaller diameter synthesis product; **(b)** SEM image of nanostructured clinker at low magnification. Polydispersion in diameter of the product can be observed; **(c)** SEM image of nanostructured silica fume at high magnification. Carbon nanotube (CNT) diameter is about 30–60 nm; **(d)** SEM image of nanostructured silica fume at low magnification shows nanotubes with lower diameter dispersion.

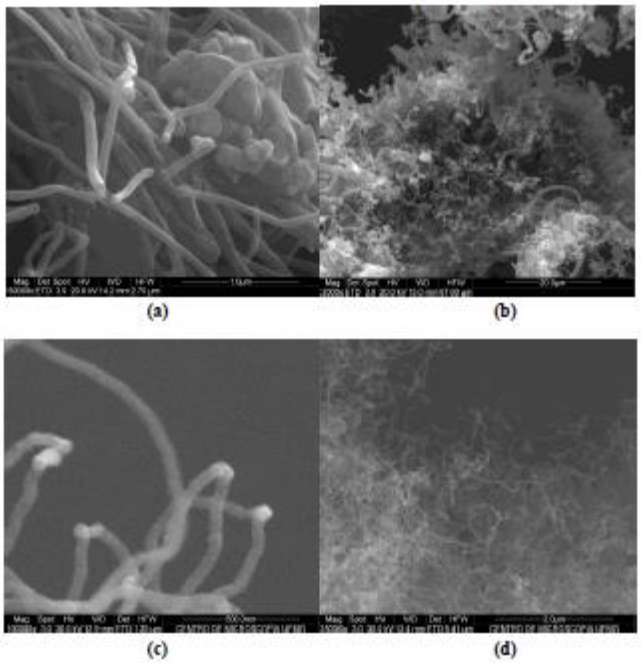

Figure 3. **(a)** Transmission electron microscopy (TEM) image of carbon nanotube (CNT) grown on silica fume at high magnification. The wall structure shows high level of imperfections; **(b)** TEM image of nanostructured silica fume at low magnification. Tubular and fibrous structures can be observed.

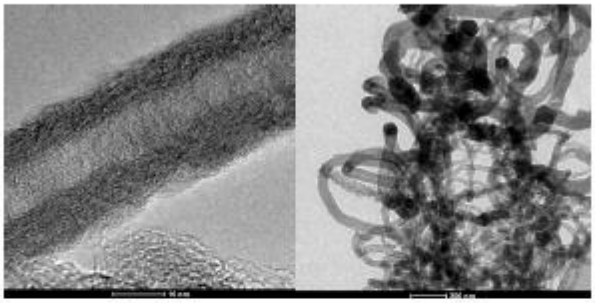

(a) (b)

The TGA analysis (Figure 4) of nano-structured clinker revealed two peaks of mass loss: the lower temperature peak (572 °C) may correspond to the thermally less stable CNFs, while the higher temperature peak (623 °C) may correspond to some higher perfection level fibers or CNTs. The total mass loss of the nanostructured material was 11.96%. The differential thermogram of silica fume supported material (Figure 5) also showed two peaks: the higher temperatures (615 and 666 °C) indicate CNFs and CNTs with higher level of structural perfection, as observed by Trigueiro *et al.* [12]. The total mass loss in the case of silica fume was 55.50%, which is significantly greater than for clinker. The higher surface area of silica fume and the relatively better control of its composition with respect to Portland cement clinker may explain this increase. Both samples had little mass loss below 400 °C indicating a highly pure product with low amorphous carbon content.

Figure 4. Thermogravimetric analysis (TGA) and DTGA diagrams of the nanostructured clinker with two clearly visible mass loss peaks.

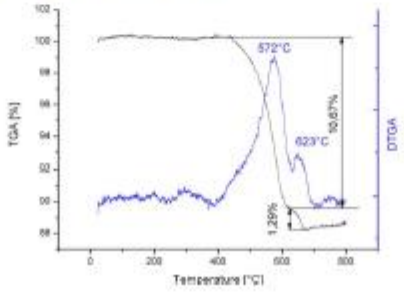

Figure 5. TGA and DTGA diagrams of the nanostructured silica fume with two mass loss peaks.

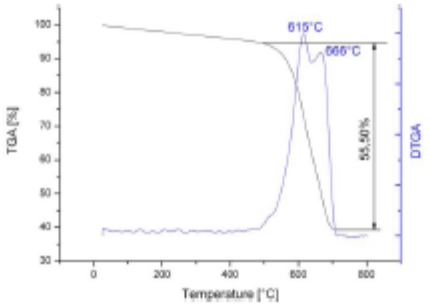

3.2. Mechanical Behavior

The results of the strength tests of the mortar specimens are shown in Figure 6. Both clinker based and silica fume based nanostructured composites had higher compressive and flexural strength than the reference specimens at 28 days. Mortar specimens made with nanostructured clinker had 14.1% higher flexural strength and 88.3% higher compressive strength than reference specimens at this age. These values were 8.7% and 39.6%, respectively, for mortars made with nanostructured silica fume. The positive effect of the incorporation of 10% silica fume on the mechanical strength of the mortars was observed after the comparison of the results of mortars REF-C and REF-S. Both compressive and flexural strength of REF-S specimens were higher at the investigated ages. Silica fume was finer than cement or aggregate; therefore its addition fills in pores present in cement mortars and concretes. At the same time, the addition of silica fume and CNTs/CNFs to the mortar caused an increase in the strengths with respect to the addition of silica fume alone. This fact shows the existence of a reinforcing effect of the *in situ* synthesized CNTs and CNFs.

For the mortars made with nanostructured clinker, the flexural strength gain at 7 days was higher than at 28 days. The small surface curvature radius nano-size CNTs and CNFs may act as nucleation sites for the formation of hydration products—as was reported earlier [13]—and may accelerate cement hardening. This could be the reason for the relatively smaller gain at 28 days. On the other hand, the same phenomenon was not observed in the case of nanostructured silica fume. There was no enhancement of the 7 day flexural strength; meanwhile at 28 days the nanostructured specimens showed 8.7% higher strength. Silica fume addition increases water demand due to the higher surface area they have. The refinement of particle size of the mortar due to silica fume addition may have affected the accelerator role of CNT/CNF addition.

Smaller gain both in compressive and in flexural strength was observed for mortars containing silica fume supported CNTs and CNFs than for nanostructured clinker. The CNTs and CNFs with apparently better structure and thus probably higher tensile strength grown on silica fume did not enhance the composites' strength to the same measure as the clinker supported ones.

Gain in compressive strength was in all cases higher than in flexural strength. The addition of CNTs and CNFs to the mortars had rather a micro filling and hydration catalyst effect than crack-bridging. This can be explained by the poor dispersion and adherence of the CNTs/CNFs in the cement matrix.

Figure 6. **(a)** Compressive strength of mortar specimens made with and without nanostructured clinker or silica fume at the age of 28 days; **(b)** Flexural strength of mortar specimens made with and without nanostructured clinker or silica fume at the ages of 7 and 28 days. Notes: REF-C—mortar without nanostructured material and without silica fume; NST-C—mortar made with nanostructured clinker; REF-S—reference mortar made with silica fume; NST-S—mortar made with nanostructured silica fume.

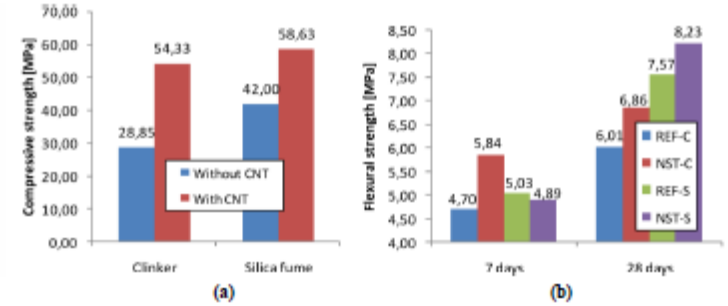

4. Conclusions

CNTs and CNFs were synthesized in a CVD process on catalysts prepared with the combination of Portland cement clinker as support and converter dust as iron precursor. These materials possess low purity, low control of composition and particle size and low cost with respect to other commonly used materials for CNT synthesis. The resulting products had a fibrous structure with high level of defects. Using silica fume as support, a higher carbon deposit level, and thinner and higher quality CNT and CNF structure was observed.

The reinforcing effect of these nanostructured materials was evaluated on cement mortar specimens. Some improvement in both compressive and flexural strength was observed: they do not differ from reported values obtained when using high quality nanotubes. Nanostructured clinker showed a larger gain in mechanical strength than nanostructured silica fume. Flexural strength enhancement remained lower than compressive strength, suggesting rather a micro filling and/or hydration acceleration effect than crack-bridging.

Acknowledgements

The authors would like to thank Camargo Corrêa Cimentos SA for the funds and materials provided during the investigations and Magnesita Refratários SA for the technical support to perform the mechanical tests. The authors would like to acknowledge the Center of Microscopy at the Federal

University of Minas Gerais (http://www.microscopia.ufmg.br) for providing the equipment and technical support for experiments involving electron microscopy. The authors would like to express their gratitude to Fapemig for the funds provided for their research project. Péter Ludvig and Ivan, C.P. Gaspar benefit of a Fapemig grant.

References

1. Salvetat, J.P.; Bonard, J.M.; Thomson, N.H.; Kulik, A.J.; Forró, L.; Benoit, W.; Zuppiroli, L. Mechanical properties of carbon nanotubes. *Appl. Phys. A* **1999**, *69*, 255-260.
2. Li, G.Y.; Wang, P.M.; Zhao, X. Mechanical behavior and microstructure of cement composites incorporating surface-treated multi-walled carbon nanotubes. *Carbon* **2005**, *43*, 1239-1245.
3. Makar, J.; Margeson, J.; Luh, J. Carbon nanotube/cement composites—Early results and potential applications. In *Proceedings of the 3rd International Conference on Construction Materials: Performance, Innovations and Structural Implications*, Vancouver, Canada, 22–24 August 2005; pp. 1-10.
4. Musso, S.; Tulliani, J.M.; Ferro, G.; Tagliaferro, A. Influence of carbon nanotubes structure on the mechanical behavior of cement composites. *Composites Sci. Technol.* **2009**, *69*, 1985-1990.
5. Nasibulin, A.G.; Shandakov, S.D.; Nasibulina, L.I.; Cwirzen, A.; Mudimela, P.R.; Habermehl-Cwirzen, K.; Grishin, D.A.; Gavrilov, Y.V.; Malm, J.E.M.; Tapper, U.; *et al*. A novel cement-based hybrid material. *New J. Phys.* **2009**, *11*, 1-11.
6. Konsta-Gdoutos, M.S.; Metaxa, Z.S.; Shah, S.P. Multi-scale mechanical and fracture characteristics and early-age strain capacity of high performance carbon nanotube/cement nanocomposites. *Cem. Concr. Res.* **2010**, *32*, 110-115.
7. Konsta-Gdoutos, M.S.; Metaxa, Z.S.; Shah, S.P. Highly dispersed carbon nanotube reinforced cement based materials. *Cem. Concr. Res.* **2010**, *40*, 1052-1059.
8. Mudimela, P.R.; Nasibulina, L.I.; Nasibulin, A.G.; Cwirzen, A.; Valkeapää, M.; Habermehl-Cwirzen, K.; Malm, J.E.M.; Karppinen, M.J.; Penttala, V.; Koltsova, T.S.; *et al*. Synthesis of carbon nanotubes and nanofibers on silica and cement matrix materials. *J. Nanomater.* **2009**, *526128*, 1-4.
9. Melo, V.S. *Nanotecnologia Aplicada ao Concreto: Efeito da Mistura Física de Nanotubos de Carbono em Matrizes de Cimento Portland*; MS Thesis, Federal University of Minas Gerais, Belo Horizonte, Brazil, 2009. Available online: http://www.pos.demc.ufmg.br/defesas/033.pdf (accessed on 13 January 2011).
10. Associação Brasileira de Normas Técnicas (ABNT). *NBR 7215: Cimento Portland—Determinação da Resistência à Compressão*; Associação Brasileira de Normas Técnicas: Rio de Janeiro, Brazil, 1996; p. 8.
11. Associação Brasileira de Normas Técnicas (ABNT). *NBR 5735: Cimento Portland de alto forno*. Associação Brasileira de Normas Técnicas: Rio de Janeiro, Brazil, 1991; p. 6.
12. Trigueiro, J.P.C.; Silva, G.G.; Lavall, R.L.; Furtado, C.A.; Oliveira, S.; Ferlauto, A.; Lacerda, R.G.; Ladeira, L.O.; Liu, J.W.; Frost, R.; *et al*. Purity evaluation of carbon nanotube materials by thermogravimetric, TEM and SEM methods. *J. Nanosci. Nanotechnol.* **2007**, *7*, 3477-3486.

13. Makar, J.M.; Chan, G.W. Growth of cement hydration products on single-walled carbon nanotubes. *J. Amer. Ceram. Soc.* **2009**, *92*, 1303-1310.

Oral presentation at the 7th Central European Congress on Concrete Engineering, September 22-23, 2011

TAILORING THE INNATE PROPERTIES OF PORTLAND CEMENT: THE APPLICATION OF CARBON NANOTUBES

Péter Ludvig[1,2], José Marcio Calixto[1],Luiz Orlando Ladeira[2]

[1] *Department of Structural Engineering, Federal University of Minas Gerais, Av. Antônio Carlos, 6627, Pampulha, Belo Horizonte-MG, CEP 31.270-901, Brazil*

[2] *Nanomaterials Laboratory, Department of Physics, Federal University of Minas Gerais, Av. Antônio Carlos, 6627, Pampulha, Belo Horizonte-MG, CEP 31.270-901, Brazil*

SUMMARY

Carbon nanotubes are a promising material to solve the low tensile strength and ductility of Portland cement based materials. Carbon nanotubes (CNTs) and nanofibers (CNFs) synthesized directly on cement clinker particles can also reduce production costs and help dispersion. Mortar specimens prepared with such nanostructured material were tested to determine tensile and compressive strength. The effects of different functionalizing agents were compared. Test results showed some enhancement of mechanical characteristics of Portland cement matrices made with CNT/CNF.

1. INTRODUCTION

Concrete made with Portland cement is the largest consumed construction material worldwide. Among the reasons for this fact are the availability of the raw materials and the excellent compressive behavior. On the other hand, tensile characteristics of cementitious materials are poor due to their low tensile strength and brittle behavior. In reinforced concrete, steel reinforcement bars are used to resist the tensile stresses. The distribution of cracks is more uniform and their width is reduced when small diameter steel rebars are used.

Recent investigations showed that the poor tensile behavior of cement based materials is partly due to macroscopic defects (pores) and partly to the innate properties of calcium silicate hydrate (C-S-H), the main constituent of hardened cement paste.

Carbon nanotubes (CNTs) are among the highest tensile strength materials known, up to 100 times higher than that of steel, yet only one hundredth of its density. Their tubular structure is composed of one or several graphene sheets rolled up in specific directions. The high tensile strength is due to the bond between carbon atoms that compose the CNTs which is the strongest link that exists. At the same time, the failure strain of CNTs can be as high as 15-20%. The typical dimensions of CNTs are between 2 and 50 nm in diameter and up to hundreds of microns in length, thus aspect ratios as high as 1:1,000,000 can be found.

These properties of CNTs make them a promising candidate to be incorporated in cementitious matrices in order to achieve a novel material with tailored characteristics: increased tensile strength and ductility. The length of CNTs is comparable to smaller cement grains and their diameter to C-S-H crystals. This size would allow a nano-scale distribution of tensile stresses with lower stress peaks, more crack bridging and smaller crack width at this nano-level. Several worldwide investigations have been conducted producing and testing

cementitious composites with CNT addition. Their results show some increase in tensile and compressive strength, as well as in the modulus of elasticity (Li *et al.*, 2005; Musso *et al.*, 2009; Konsta-Gdoutos *et al.*, 2010; Melo *et al.*, 2011). In all these studies employed physical mix of high quality CNT in cement matrices. CNTs with different types of functionalization were used in a content between 0.025 % to 0.75 % with respect to the cement weight.

The aim of this work is to present the results of Portland cement mortars made with *in situ* synthesized nanostructured clinker. The research group based at the Nanomaterials Laboratory at the Federal University of Minas Gerais (UFMG) developed a process to synthesize CNTs and carbon nanofibers (CNFs) directly on cement clinker particles which can reduce production costs and make processing and dispersion easier (Ladeira *et al.*, 2008). Since as-produced CNTs are highly hydrophobic, special surface treatment (functionalization) is necessary to allow the incorporation in water based composites like Portland cement mortar. The effects of different concrete admixtures as well as hydrogen peroxide as functionalizing agents on the mechanical behavior of mortars are compared.

2. METHODOLOGY

CNTs and CNFs were grown directly on cement clinker in a process described by Ludvig *et al.* (2011). Products were characterized by scanning electron microscopy (SEM). Mortar specimens of 40 x 40 x 160 mm^3 in size were cast using slag Portland cement, sand in equal amounts of four fractions (0.15 mm, 0.30 mm, 0.60 mm and 1.2 mm), water, plasticizer/superplasticizer and nanostrucutred clinker. Water to cement ratio was 0.4. Based on the results of Melo *et al.* (2011), the amount of CNTs and CNFs was 0.3 % with respect to cement weight. For untreated CNTs/CNFs the plasticizer served as a non-covalent functionalizing agent. Three different types of plasticizers/superplasticizers were employed: a combination of sulfonated polinaphtalene and policarboxylate (PP), lignosulfonate (LS) and sulfonated melamine (ME) based concrete admixtures. The mortar compositions are given in Tab. 1. Flexural tensile and compressive strength of the mortar beams were determined. These tests were performed at the age of 28 days.

Tab. 1 Mortar mix proportion

Composition (kg/m^3)	**CNT/CNF content (kg/m^3)**	**W/C [b]**	**Plasticizer content (kg/m^3)**
530 : 1590[a]	1.59	0.4	7.95

[a] – cement : fine aggregates

[b] – water/cement ratio

In an attempt to achieve better functionalization of the CNTs/CNFs, and thus a better link between nanotubes and the cement matrix, a hydrogen peroxide treatment was carried out on the synthesis products prior to casting. Some 80 ml of H_2O_2 was applied to 50 g of CNT-clinker composite. The preparation was dried at 105 °C immediately after the reaction stopped. The composition of mortars made with peroxide functionalized CNTs/CNFs was the same as the others, including lignosulfonate plasticizer.

3. RESULTS AND DISCUSSION

3.1 Synthesis

Typical synthesized products are shown on Fig. 1. The products had heterogeneous dimensions and morphology when compared to high quality CNTs. The products were well-distributed on the surface of clinker particles.

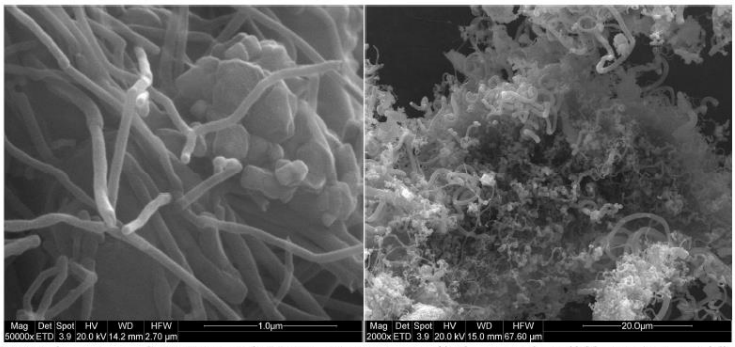

Fig. 1 SEM images of CNTs and CNFs grown on clinker under different magnifications

3.2 Mechanical behaviour

Tensile and compressive strength results of the test specimens are presented in Fig. 2. Compressive strength of mortars with CNTs showed more enhancement than flexural tensile strength. The mortar prepared with lignosulfonate plasticizer presented the best results, both in flexure and in compression, with 14 % gain in tensile and a 90 % gain in compressive strength. The addition of H_2O_2 treated CNTs to the mortar resulted in higher compressive and flexural tensile strengths with 33 % and 13 % gain at 28 days respectively.

Legends: PP – sulfonated polinaphtalene and policarboxylate surfactants;
LS – lignosulfonate plasticizer;
ME – sulfonated melamine plasticizer;
PO – hydrogen peroxide treated CNTs/CNFs with lignosulfonate plasticizer

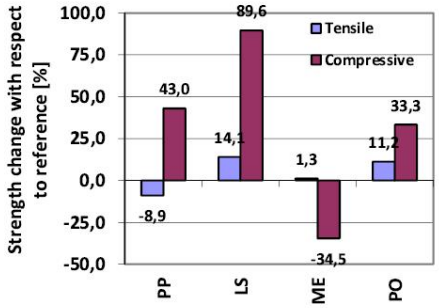

Fig. 2 Compressive and tensile strength results of mortar specimens at the age of 28 days.

Gain in compressive strength was in all cases higher than in flexural strength. The addition of CNTs and CNFs to the mortars had a micro filling and hydration catalyst effect rather than a

crack-bridging effect. This can be explained by the poor dispersion and adherence of the CNTs/CNFs in the cement matrix. At the same time, the high surface area CNTs and CNFs – if an adequate surface treatment is applied – may act as nucleating sites for cement hydration product formation, as it was observed by Makar and Chan (2009), resulting in a more complete hydration and thus in higher compressive strength.

4. CONCLUSIONS

CNTs and CNFs were synthesized in a CVD process on Portland cement clinker. The resulting products had a fibrous structure with high level of defects. The reinforcing effect of these nanostructured materials was evaluated on cement mortar specimens.CNT/CNF addition to the mortars affected the degree and speed of hydration of cement. Some improvements in both compressive and flexural strength were observed. Flexural strength enhancement remained lower than compressive strength, suggesting a micro filling and/or hydration catalizator effect rather than crack-bridging and fiber reinforcement.

5. ACKNOWLEDGEMENTS

The authors would like to express their gratitude to Intercement SA for providing materials and financial support and to INCT – Nanomateriais de Carbono for the funds provided for this research project. The authors would like to acknowledge the Center of Microscopy at the Federal University of Minas Gerais (http://www.microscopia.ufmg.br) for providing the equipment and technical support for experiments involving electron microscopy. Péter Ludvig was funded by a Fapemig Grant.

6. REFERENCES

Konsta-Gdoutos, M. S.; Metaxa, Z. S. and Shah, S. P. (2010) “Multi-scale mechanical and fracture characteristics and early-age strain capacity of high performance carbon nanotube/cement nanocomposites”, Cement & concrete composites, Vol. 32, 2010, pp. 110-115.

Ladeira, L. O.; Silva, E. E.; De Oliveira, S.; Lacerda, R. G.; Ferlauto, A. S.; Ávila E. and Lourençon, E. (2008) “Processo de síntese contínua e em larga escala de nanotubos de carbono sobre o clínquer de cimento e produtos nanoestruturados”, Brazilian Patent, INPI 014080002727 (30.04.2008).

Li, G.Y.; Wang, P.M. and Zhao, X. (2005), „Mechanical behavior and microstructure of cement composites incorporating surface-treated multi-walled carbon nanotubes”, Carbon, Vol. 43, 2005, pp. 1239-1245.

Ludvig, P.; Calixto, J. M.; Ladeira, L. O. and Gaspar, I. C. P. (2011), “Using Converter Dust to Produce Low Cost Cementitious Composites by *in situ* Carbon Nanotube and Nanofiber Synthesis”, Materials, Vol. 4, 2011, pp. 575-584.

Makar, J.M. and Chan, G.W. (2009) “Growth of cement hydration products on single-walled carbon nanotubes”, J. Amer. Ceram. Soc. Vol. 92, 2009, pp. 1303-1310.

Melo, V. S.; Calixto, J. M.; Ladeira, L. O. and Silva, A. P. (2011), “Macro- and Micro-Characterization of Mortars Produced with Carbon Nanotubes”, ACI Materials Journal, Vol. 108, No. 3, May-June 2011, pp. 327-332.

Musso, S.; Tulliani, J.-M.; Ferro, G. and Tagliaferro, A. (2009), “Influence of carbon nanotubes on the mechanical behavior of cement composites”, Composites science and technology, Vol. 69, 2009, pp. 1985-1990.